SOIL EROSION AND SEDIMENT YIELD IN TROPICAL MOUNTAINOUS WATERSHED OF NORTHWEST THAILAND: THE SPATIAL RISK ASSESSMENTS UNDER LAND USE AND RAINFALL CHANGES

by

SUKHO SEMMAHASAK

A thesis submitted to the University of Birmingham for the degree of
DOCTOR OF PHILOSOPHY

School of Geography, Earth and Environmental Sciences
College of Life and Environmental Sciences
University of Birmingham
August 2014

ABSTRACT

Soil erosion is a serious threat to sustainability of cultivation in many parts of the world. In most tropical mountainous watersheds of northwest Thailand, very high rainfall erosivity occurs (especially in the rainy season) together with increasing encroachment of agricultural activities on steeply sloping land are hypothesised as the major causes of soil erosion and land degradation. However, the specific factors and processes that cause soil erosion are poorly understood. Thus, the Mae Rim watershed was chosen as a case study for this thesis: (1) to investigate the key controlling factors that interact to generate high soil erosion rate and (2) to assess the spatial soil erosion risk and sediment yield under changing climate and land use by applying a novel GIS-based method. The gross soil erosion in each watershed cell was estimated using the Revised Universal Soil Loss Equation (RUSLE) by thoroughly determining its various model parameters. RUSLE results showed mean annual soil loss rate of 31 tonnes ha^{-1} yr^{-1}, while the mean annual suspended sediment yield (SSY) predicted by using an innovative approach RUSLE-SISDR (i.e., RUSLE in conjunction with Spatial Interpolation of Sediment Delivery Ratio) was 7.4 tonnes ha^{-1} yr^{-1}, implying only slightly overestimate in prediction (2%) when compared to the actual measured SSY (7.29 tonnes ha^{-1} yr^{-1}). From the results of the spatial analysis between controlling factors and soil erosion, bare land, field crop land and high steep slope were linked to extreme soil erosion (erosive magnitude > 150 tonnes ha^{-1} yr^{-1}). With respect to soil erosion under scenarios of land use and rainfall change, it was revealed that the conversion from deciduous forest to field crop area has very serious implications for soil erosion in the Mae Rim watershed. Indeed, transition from forest to agriculture may lead to erosion increase despite reduced rainfall. The results obtained from analysing scenario sensitivities identify synergistic effects on soil erosion hazard if bare land, field crop land and rainfall erosivity are increased simultaneously in the future.

ACKNOWLEDGEMENTS

A PhD thesis often appears a solitary undertaking. However, it is impossible to maintain the degree of focus and dedication required for its completion without the help and support of many people.

First and foremost, I would like to express my deepest gratitude to both supervisors, Professor Damian Lawler and Professor David Hannah for their constructive critiques, scientific and innovative advices, as well as useful recommendations throughout my doctoral research. Without their constant support and timely help, this thesis would not have been made possible.

I wish also to acknowledge the Chiang Mai Rajabhat University in Thailand and School of Geography, Earth and Environmental Sciences, respectively, for the financial support during the last three years and for the opportunity to do my research at the University of Birmingham. I am thankful to Gretchel Coldicott for being very kind and willing to help in any way possible. Also, many thanks to all staff and doctoral researchers in the Water Science research group, especially Isaac Aidoo, who as a good friend, always dedicated his time to read parts of my thesis.

I would again like to thank my friends and colleagues, Dr Nakarin Chaikaew, Choosit Choochat, Wirapol Chaowaluck, Att Atchariyamontree and Poom Sartsin for their assistance during the collection of field data in the northwest Thailand watersheds. Special thanks also to Preecha Yamyuen and staff member from the Royal Irrigation Department of Thailand for kindly supporting me with the *suspended sediment dataset* and other hydrological information for study area.

Last but not least, I would like to thank my big family: Ruengrong, Sawitree, Tawatchai, Sowarat, Pachimaporn, Paisarn, Worrapan and Pannawit. They were always supporting and encouraging me with their best wishes. Finally, I would like to thank my wife, Chutiwalanch (Noon), for her understanding and faithful support as well as her patience and unconditional love. Thank you!

TABLE OF CONTENTS

LIST OF ILLUSTRATIONS

Page

LIST OF TABLES

LIST OF ABBREVIATIONS/ ACRONYMS

A	Mean annual soil loss per unit area
C	Cover management or land cover factor
DBA	Drainage Basin Area
DEM	Digital Elevation Model
ETM+	Enhanced Thematic Mapper Plus
FCC	False Colour Composite
GIS	Geographical Information System
GPS	Global Positioning System
ha	hectare (1 ha = 0.01 square kilometre)
K	Soil erodibility factor
K_{TC}	Transport Capacity Coefficient
Lat	Latitude
LDD	Land Development Department
Long	Longitude
LS	Slope length and steepness factor
m a.s.l.	Metre above sea level
MFI	Modified Fournier Index
NIR	Near-Infrared Band
NSME	Nash and Sutcliffe's Model Efficiency
NW	North West
P	Conservation support practice factor
p-value	Statistical significance
Q	River discharge

R	Rainfall-runoff erosivity factor
r	Correlation coefficient
r^2	Correlation of determination
RID	Royal Irrigation Department
RRMSE	Relative Root Mean Square Error
RS	Remote Sensing
RUSLE-SISDR	Revised Universal Soil Loss Equation in conjunction with the Spatial Interpolation of Sediment Delivery Ratio
RUSLE-STC	Revised Universal Soil Loss Equation in conjunction with the Sediment Transport Capacity
SDR	Sediment Delivery Ratio
SE	Soil erosion
SEA	Southeast Asian
SISDR	Spatial Interpolation of Sediment Delivery Ratio
SSC	Suspended Sediment Concentration
SSL	Suspended Sediment Load
SSY	Suspended sediment yield
STC	Sediment Transport Capacity
SWIR	Shortwave-Infrared Band
TM	Thematic Mapper
USLE/RUSLE	Universal Soil Loss Equation/ Revised Universal Soil Loss Equation
UTM	Universal Transverse Mercator
WGS84	World Geodetic System 1984

CHAPTER 1: INTRODUCTION

1.1 Global soil erosion issues

Land degradation is a global environmental crisis, threatening agricultural areas at an alarming rate. Global societies of people are significantly aware of the crisis alongside energy and global warming problems, because it has a direct impact on food production for humans. Land degradation occurs when natural or human-induced processes decrease the ability of land to support crops, livestock and organisms. One type of land degradation is 'soil erosion' (Miller, 2006). Among the human-induced causes of soil degradation, Bridges and Oldeman (1999) (cited in Yang *et al*., 2003, p. 2913) stated that soil erosion by water is the most common type, causing approximately 55% of total global soil loss. According to 2000 studies conducted by the Consultative Group on International Agricultural Research, soil erosion and degradation had reduced food production on 16% of the world's cropland (Pimentel, 1993). Moreover, the current rate of agricultural land degradation worldwide by soil erosion and other factors was found to be leading to an irreversible loss in productivity, ranging from 6 to 10 million hectares of fertile land a year (Pimentel, 2006).

The problem of population growth causes an increasing demand for food and crop land. As a consequence, forest, soil and water resources have been exploited wastefully. Soil and land resources are a cause of concern, especially in countries where major revenue is based on agricultural products, such as in Southeast Asian (SEA) countries. Most farmers living on marginal land or

mountainous areas in the SEA region still lack knowledge on suitable soil conservation means. As a result, they thus have to face the inevitable soil erosion problem in their land. This is consistent with Yang *et al*. (2003) who studied the trends of global land use and climate change between 1900 and 2090 using the Revised Universal Soil Loss (RUSLE) model. They also point out that Southeast Asia is the region most seriously affected by soil erosion in the world, as a result of the trend of comparative outcomes from selected countries (Table 1.1), showing that Thailand has the highest predicted rate of soil erosion in the 2090s with the mean value of 17.3 tonnes ha^{-1} $year^{-1}$ (Yang *et al.,* 2003).

Table 1.1 Mean value of potential soil erosion in each region (unit: tonnes ha^{-1} $year^{-1}$)

Region	1900*s*	1910*s*	1920*s*	1930*s*	1940*s*	1950*s*	1960*s*	1970*s*	1980*s*	2090*s*
Whole world	8.7	8.9	8.9	9.3	9.3	9.7	9.9	10.1	10.2	11.6
Continents										
Africa	3.8	3.7	3.8	3.9	3.8	4.2	4.5	4.5	4.5	6.0
Asia	10.4	10.8	10.8	11.2	11.3	11.8	12.0	12.0	12.2	14.4
Australia	2.4	2.4	2.5	2.4	2.7	2.7	2.8	3.1	3.0	4.1
Europe	10.7	11.4	11.2	11.6	10.7	11.5	11.6	11.6	11.1	8.9
North America	6.8	6.8	6.9	7.5	7.9	8.3	8.8	8.9	9.3	10.0
South America	6.1	6.3	6.4	6.8	7.0	7.0	7.2	8.2	8.5	10.3
Selected countries										
United States	7.5	7.5	7.3	7.3	7.7	7.0	7.2	7.1	6.9	7.6
Brazil	2.1	2.1	2.3	2.3	2.5	2.5	3.0	3.8	4.3	4.9
China	14.9	15.6	14.9	15.1	15.0	15.0	15.0	14.9	14.7	14.2
India	14.3	15.1	15.3	16.2	16.6	17.1	16.6	16.8	16.8	15.5
Thailand	5.5	5.8	6.5	7.8	9.0	10.4	12.2	13.4	14.1	17.3

(Source: Modified from Yang *et al.*, 2003, p. 2922)

1.2 Global awareness of soil erosion

Soil erosion by water depends not just on anthropogenic factors, but also on physiographical factors (e.g., rainstorm intensity, runoff, topography and soil texture) are also important. Not surprisingly, the significance of this issue (soil erosion by water) has prompted numerous studies around the world. Several techniques are adopted for assessing soil erosion, ranging in size from small field plots to regional scale, which include: the application of Caesium-137 (^{137}Cs) (Fornes *et al.*, 2005); use of a sediment tracer technique 'fingerprint' (Russell *et al.,* 2001; Walling, 2005); adoption of an erosion pin technique, 'the Photo-Electric Erosion Pin (PEEP)', for monitoring soil erosion and deposition of channel bank (Lawler *et al.,* 2001; Lawler, 2008); employing the method of a sediment rating curve (Old *et al.,* 2005; Sivakumar and Wallender, 2005; Mano *et al.,* 2009; Marttila and Kløve, 2010); and applying various modelling for soil erosion assessment (Morgan, 2001; Fentie *et al.,* 2002; Renschler and Harbor, 2002; Vigiak *et al.,* 2005; Van Rompaey *et al.,* 2005; Chen *et al.,* 2006; Irvem *et al.,* 2007; Cebecauer and Hofierka, 2008; Pelacani *et al.,* 2008; Pistocchi, 2008; Licciardello *et al.,* 2009; Wilkinson *et al.,* 2009; Wainwright and Millington, 2010).

Over the last few decades, adoption of numerical modelling for soil erosion assessment seems to have received a good response from worldwide researchers. Firstly, model application can assist the authors to better understand and connect the processes of sediment production, routing delivery and downstream yield (Ding and Richards, 2009). Besides, integration of the

models with Geographical Information System (GIS) techniques will be able to depict the spatial processes of soil erosion sources within the specific catchment of interest. Secondly, adoption of numerical modelling is likely to be worthwhile in terms of time and cost saving when applying to a large catchment (>100 Km^2), compared to other techniques such as ^{137}Cs, sediment tracer fingerprint and PEEP (Boardman, 2006). In addition, the sediment rating curve method may result in problems of inaccurate prediction owing to an inability to elucidate the dynamics of suspended transport within the watershed, unless the sediment deposition can be ignored or the drainage area is too small (Gao, 2008). The other problems are, moreover, the qualities of the sediment collection methods (i.e., infrequent sampling strategies [1–2 times a month]) and sampling devices; such limitations are normally found in the developing countries.

1.3 RUSLE application: Spatial consideration and criticism

Many recent soil erosion studies have focused on up-scaling sites, for example watershed to regional scales, as well as increasing demands for erosion model application (De Jong *et al.,* 1999) with the main purpose that responds to the national or international conservation by focusing on sustainable soil management. Consequently, the selections of soil erosion modelling methods that suitable for a variety of contexts in each country are necessary. So far, empirical modelling such as the Universal Soil Loss Equation (USLE) and its revised versions, RUSLE/RUSLE2 are still the most popular in practice and in scientific research (e.g., Millward and Mersey, 1999; Wang *et al.* 2001; Lin *et*

al., 2002; Angima *et al.,* 2003; Amore *et al.,* 2004; Cohen *et al.,* 2005; De Asis *et al.,* 2007; Irvem *et al.,* 2007; Royall, 2007; Cebecauer and Hofierka, 2008; Shamshad *et al.,* 2008; Beskow *et al.,* 2009; Rahman *et al.,* 2009; Terranova *et al.,* 2009; Meusberger *et al.,* 2010). The USLE/RUSLE is an empirical model developed from analysis of more than 10,000 plot-years of runoff and soil loss data from small plots scattered through the eastern part of the USA (Wischmeier and Smith, 1978). It has been used for soil loss predictions by considering key controlling factors, e.g., rainfall erosivity, slope length and slope steepness, soil erodibility, vegetation cover and conservation support practice, which can be expressed as equation [4.1] (see more details in Section 4.2.1). Although its development is based on data from the USA, much work is now being done all over the world to adapt RUSLE to suit local conditions (Aksoy and Kavvas, 2005; Dubber and Hedbom, 2008) due to the fact that:

(i) USLE/RUSLE is simple to implement (Van Rompaey *et al.,* 2001; Gao, 2008). Thus, it can be applied in areas of limited data, especially in developing countries, and can also be easily adapted to enable its application to various spatial scales and some regional sites in other environmental conditions when used with GIS (Zhou *et al.,* 2008).

(ii) USLE/RUSLE is proven to be a useful tool for displaying the spatial variation of soil erosion risk from the watershed up to the basin scales. For example, Cohen *et al.* (2005) and Irvem *et al.* (2007) used an old version, USLE, for assessing spatial erosion risk in a Kenyan watershed and Seyhan River Basin in Turkey, respectively. Meanwhile, the new version, RUSLE, has been applied by Zhou *et al.* (2008) and Bazzoffi (2009) to generate spatially

distributed soil erosion risk scenarios in a mountainous watershed in China, and Italy, respectively, for studying the effect of vegetation cover on soil erosion.

(iii) Some literature shows the ability of the USLE/RUSLE to make reasonable soil loss and sediment yield predictions (Lin *et al.,* 2002; Mutua *et al.,* 2006; Jain *et al.,* 2009; Hui *et al.,* 2010). In research by Lin *et al.* (2002), for instance, they estimated watershed erosion in Upland Dafuko Creek,Taiwan by using a simple method for automated spatial distribution extraction for overland flows in conjunction with USLE. Their results showed reasonable annual erosion depth values ranging from 2.2 to 2.7 mm, close to the 2.6 mm average annual deposition depth in the topsoil at the main Peikang Creek watershed. Also, Mutua *et al*. (2006) developed a hill slope sediment delivery distributed (HSDD) model for estimating sediment delivery ratio (SDR) on a cell by cell basis, using the concept of runoff travel time as a function of catchment characteristics, in conjunction with RUSLE. As a result, the coefficient of determination (r^2) = 0.82 illustrated a fairly good relationship between the predicted and observed sediment yields (Figure 1.1). Similar to Jain *et al.* (2009), they used the sediment outflow map and USLE to identify the sediment source and sink areas in the Himalayan Chaukhutia watershed (India). In comparison of the observed and estimated sediment yield, it showed a satisfactory prediction of annual sediment outflow with less than ±40% error (Figure 1.2). In addition, Hui *et al.* (2010) developed a spatial-varied SDR module in conjunction with USLE for assessment of soil erosion and sediment yield in the Liao watershed, China. The results showed sediment yield prediction as 1.32 million tonnes yr^{-1}, which is 20% higher than the measured

yield value. The average deviation of the USLE was less than 20%, and the estimated soil erosion was of acceptable accuracy.

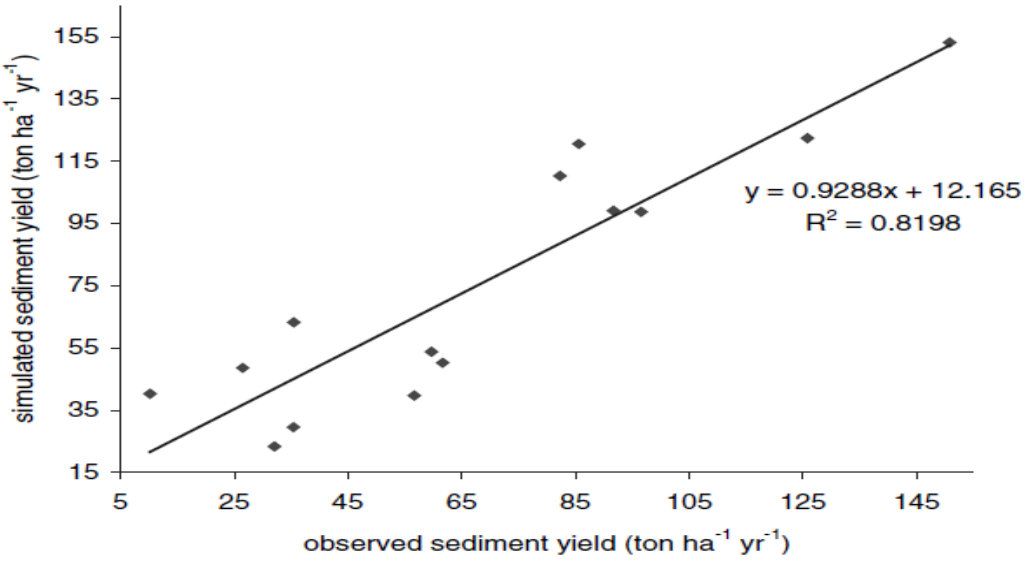

Figure 1.1 Comparisons between simulated and observed sediment yield in the Masinga catchment, Kenya (Source: Mutua *et al.,* 2006).

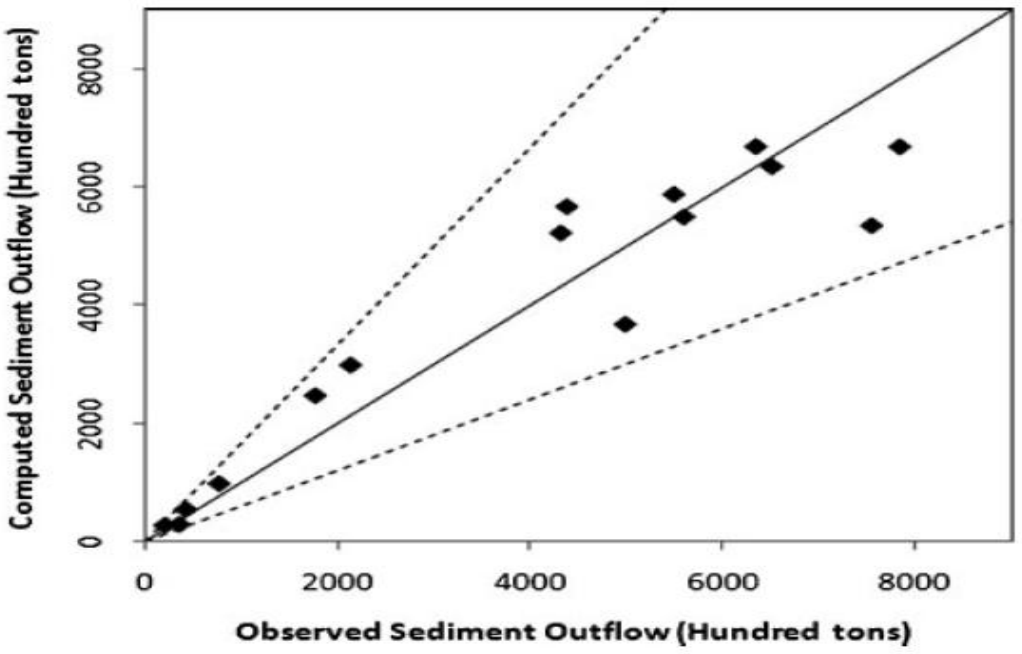

Figure 1.2 Scatter plot of annual values of computed and observed sediment outflow in the Himalayan Chuakhutia catchment, India (Source: Jain *et al*., 2009).

(iv) Some papers illustrate that the USLE/RUSLE has performed its model efficiency more plausibly than some physically based models like Water Erosion Prediction Project (WEPP) and Pan-European Soil Erosion Risk Assessment (PESERA). For example, Tiwari *et al.* (2000) plotted 1600 years of natural runoff plot data for verification and validation of USLE, RUSLE and WEPP. In particular, for consideration of individual annual erosion values, Nash and Sutcliffe's model efficiently calculated the results as 0.58, 0.60 and 0.4 for USLE, RUSLE and WEPP, respectively (Table 1.2). Therefore, it could be concluded that USLE and RUSLE performed similarly and better than WEPP (Kinnell, 2010; Gover, 2011).

Table 1.2 Summary statistics for annual value of soil loss estimated by USLE, RUSLE and WEPP

Parameter	**USLE**	**RUSLE**	**WEPP**
Soil loss			
Avg. estimated soil loss (Kg/m^2)	3.51	3.51	3.51
Avg. estimated soil loss (Kg/m^2)	3.22	3.22	3.29
Avg. magnitude of error (Kg/m^2)	2.13	2.00	2.73
Regression results			
Slope	0.59	0.51	0.53
Intercept	1.16	1.45	1.42
Correlation coefficient	0.58	0.62	0.43
Model efficiency	**0.58**	**0.60**	**0.40**

(Source: Modified from Tiwari *et al.*, 2000, p.1132).

Furthermore, Meusburger *et al.* (2010) compared soil erosion predictions by using USLE and PESERA in an alpine catchment. The Spearman correlation was used to compare modelled soil erosion estimates with the Caesium-137 activity. Their results showed that the magnitude of erosion estimates in USLE model seems more plausible than PESERA, despite both models underestimating the ^{137}Cs-derived soil erosion estimated in all runs (Table 1.3).

Table 1.3 Comparison between mean (nine slopes) ^{137}Cs-derived soil erosion rates and mean estimates (tonnes ha^{-1} yr^{-1}) of USLE and PESERA for four different model runs with measured data at plot scale, 100% [1]FVC, 0% FVC and [2]LSU-derived FVC.

Model	Cs-137 erosion estimate	Measured data	100% FVC	0% FVC	LSU-derived FVC
USLE	20.1 ± 5.8	9.60	1.40	201.6	11.40
PESERA	20.1 ± 5.8	0.37	0.05	2.9	0.38

[1]FVC is a fractional vegetation cover map; [2]LSU is linear spectral unmixing

(Source**:** Modified from Meusburger *et al.*, 2010, p.214).

Use of RUSLE to predict annual soil loss rate can be found in various study sites, ranging from field plot or tillage, and (small) catchment, up to basin scales. For example:

(i) At field plot scale, Fernández *et al.* (2010) used RUSLE to predict soil erosion in Verín and Soutelo experimental plots, northwest Spain (50 x 10 m^2 each). Their results overestimated the observed erosion rates, however, when the R and C factors obtained by RUSLE were multiplied by 0.7 and 0.865, respectively, the efficiency of the model improved.

(ii) At the small catchment scale, particularly in the research of Shi *et al.* (2004), RUSLE is used to estimate annual average soil loss rates. The predicted results, approximately 26 tonnes ha^{-1} yr^{-1} and 52 tonnes ha^{-1} yr^{-1}, are found on flat agricultural land and cultivated sloping land, respectively, over the entire catchment (Three Gorge Area) in China.

(iii) At basin scale, Irvem *et al*. (2006) adopt the original version of USLE to predict soil loss over the Seyhan River Basin in Turkey. Their predicted results show an average annual soil loss as 16.38 tonnes ha^{-1} yr^{-1} as well as finding annual soil loss of more than 200 tonnes ha^{-1} yr^{-1} at the pixel level in the southern region of the basin. Interestingly, the RUSLE model has been applied for global-scale studies as well (Nam *et al.,* 2003; Yang *et al.,* 2003).

On the other hand, there are several limitations of RUSLE:

(i) RUSLE does not consider runoff explicitly. Kinnell (2010) indicates that one problem with this model is that there is no direct consideration of runoff even though erosion depends on sediment being discharged with the flow, which varies with runoff and sediment concentration. As a result, systematic errors in the prediction of event erosion emerged.

(ii) RUSLE does not provide capacity to account for deposition taking place as well as gullies and bank erosion or mass movements for prediction of sediment yield at the basin scale (De Vente *et al.*, 2005).

(iii) RUSLE was initially applied for predicting soil loss and improving erosion-control practice on the farm field level in USA; if applied in different geographical areas at the larger levels, some limitations need to be taken into

consideration. Thus, the predicted value of soil loss should not be taken absolutely, but only be applied when comparing (Terranova *et al.,* 2009; Kinnell, 2008, 2010).

(iv) RUSLE is not designed to predict soil losses in the short term. Whenever such a model is applied to determine soil loss on annual and event time scales, the model's performance tends to over-predict small annual soil losses and under-predict large annual soil losses (Riesse *et al.*, 1993; Tiwari *et al,* 2000; Kinnell, 2010).

1.3.1 Model selection

Thus far there have been no numerical modelling methods that have been clearly proven to accurately predict soil erosion and/or sediment yield on a large catchment scale. As noted previously (see Table 1.2 and 1.3 in Section 1.3), WEPP and PESERA, which are physically based models based on the solution of fundamental physical equations, are less accurate in estimating soil loss than either USLE or RUSLE modelling (Tiwari *et al*., 2000; Meusburger *et al*., 2010). Likewise, a more detailed, physically-based model like European Soil Erosion Model (EUROSEM), a dynamic model using mathematical expressions to represent the processes of erosion that take place over a single event (Quinton *et al*., 2011), similarly demands a large amount of data (Karydas *et al*., 2009). Such models require data on, for instance, soil-water content with depth, rill and inter-rill erodibilities; soil shear strength; soil cohesion; soil surface roughness; soil bulk density, subsurface interflow of water, plant density and evapotranspiration rates (Nearing, 2004; Morgan, 2011). As noted by Merritt *et*

al. (2003) and Quinton *et al.* (2011), the main weaknesses of physically-based models are that a large amount of data is required, which is almost impossible on a large scale. De Vente and Poesen (2005) state that an application of a purely physically-based model, integrating all sediment producing processes at the watershed or regional scale, is not foreseeable in the near future due to insufficient systematic knowledge to describe all relations and feedback in the physical equations and data requirements. Similar to the view of Renscher and Harbor (2002), the process understanding enclosed by physically based models has not generally been demonstrated to match measurements across large landscapes. Consequently, as mentioned above, the physically-based models do not seem to be a good choice for this study, especially when applied in large areas (excepting the PESERA that can be applied on a regional scale, i.e., European scale); moreover, they are often too complex to be used as operational tools.

Recently, a number of new landscape evolution and digital elevation-based soil erosion models have been developed (Hancock, 2009). One such model, the Cellular Automation Evolutionary Slope and River (CAESAR), is capable of reasonably assessing and simulating the spatially eroded sediment fluxes at the field plot, and is also designed and parameterised to simulate much larger areas on a coarser scale (Coulthard *et al.,* 2012). Unlike other physically based models, the CAESAR is less demanding in terms of variable data inputs. According to Hancock *et al.* (2012), the main data sources required for running the CAESAR model are hillslope sediment particle size and soil creep data, rainfall data (mm/hr), and catchment digital elevation models. Nevertheless,

some specific input parameters of the CAESAR may be difficult to acquire for several reasons. First, soil particle size and soil creep data can be obtained from the soil pits dug (Hancock, 2009; Hancock *et al.,* 2010), and soil particles are not homogenous (Coulthard *et al*., 2012). Therefore, studies on a larger scale may require more time and cost to be conducted thoroughly and they probably would be difficult or impossible to carry out manually. Second, long-term hourly rainfall data is quite difficult to obtain because it is not available everywhere. In Thailand, for instance, recorded statistical data regarding long-term hourly rainfall are still scarce and incomplete in some local areas, especially in remote rural and mountainous areas. In addition to the problems of data acquisition as mentioned, there are other weaknesses of the CAESAR model. First, there is no consideration of the spatial distribution of vegetation cover types that probably respond to the spatial variability of rainfall and runoff in the CAESAR model (Hancock, 2012). Therefore, errors and uncertainties may subsequently occur in both prediction and simulation when applying the CAESAR model. Another weakness is the complexity of its computations. According to Hancock *et al.* (2010), the CAESAR model has a more sophisticated representation of hydraulics and sediment transport, which requires considerably more calculations. Thus, if the model computations deal with a large amount of input data or a series of events, the results or scenarios obtained from the model will be achieved at the expense of longer run times.

Regarding Agent-Based Models (ABMs) introduced by Wainwright and Millington (2010), they are likely to be more complex than the physically-based

models when the interactions of human behaviour on geomorphological processes need to be assessed (Figure 1.3) (Lawler and Fairchild, 2010). However, they may be very difficult to apply in areas where there are more complex society relationships with the land, such as in many developing countries.

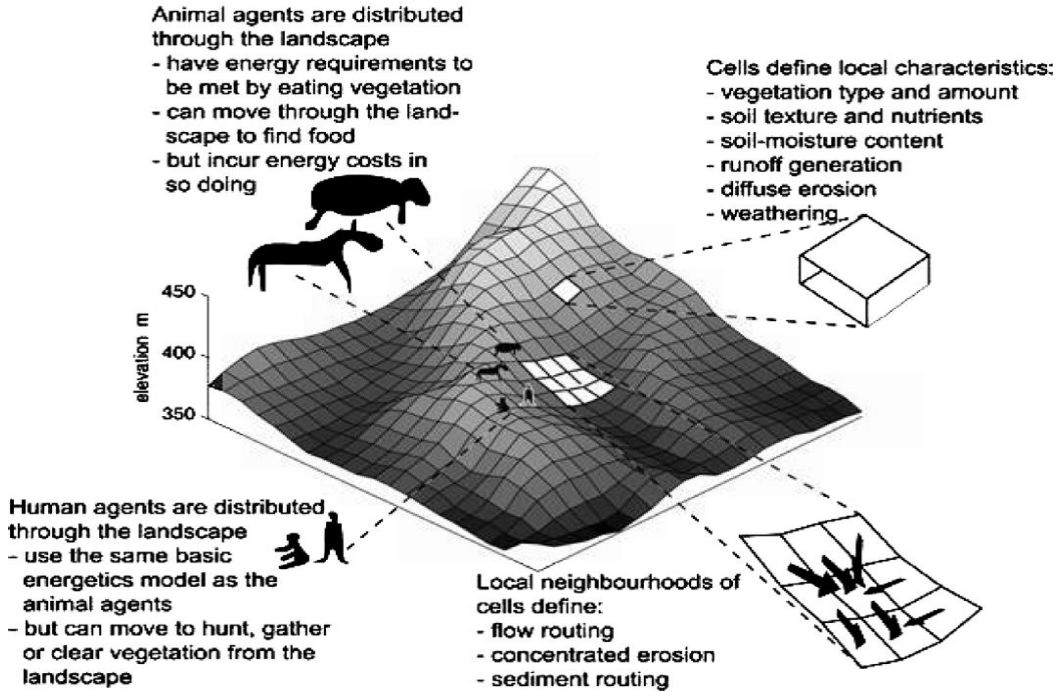

Figure 1.3 General structure of agent-based model (Source: Wainwright, 2008).

When considering strengths and weaknesses of the model types as exemplified above, it seems reasonable to say that the simpler model, i.e., RUSLE, would be the best option to apply in areas of insufficient data. Because of the relative simplicity of data required for the RUSLE model as well as the potential for assessing soil erosion when applied on a large watershed scale, the RUSLE is preferable to other models (e.g., WEPP, PESERA, EUROSEM, CAESAR, and ABM)**.** Importantly, in many situations, decision makers and stakeholders are

more interested in the spatial variation of soil erosion risk than in absolute values of soil loss. Thus, the ability of the RUSLE model in combination with remote sensing and GIS can serve as previously mentioned by providing a potential risk map of spatially eroded soil (e.g., Lu *et al.*, 2004; Bazzoffi, 2009). All in all, in the context described above, the RUSLE model is selected for this research for the reasons outlined.

1.4 Adoption of SDR and STC concepts in conjunction with RUSLE

At the watershed scale, using RUSLE alone cannot predict sediment yield. The sediment delivery ratio (SDR) concept is the ratio of the specific suspended sediment yield (SSY) at the downstream point of interest (watershed outlet) or a specific channel cross-section to gross erosion rates in the whole watershed (see Section 5.2.3). Also, it is widely adopted in conjunction with RUSLE for estimating sediment yield on various spatial scales (Lin *et al.,* 2002; Amor *et al.,* 2004; Lim *et al.,* 2005; Mutua *et al.,* 2006; Ricker *et al.,* 2008). However, the SDR concept is still challenging (Kinnell, 2008; Ding and Richards, 2009) because the gross erosion is not only at least as difficult to predict as sediment yield, but there is also even more uncertainty in the ratio (Lane *et al*., 1997; De Vente *et al.,* 2007). In addition, Ding and Richards (2009) have argued that the SDR deals with watershed as lumped, and it does not consider the spatial variation in sediment delivery processes within the watershed (Van Rompaey *et al.,* 2001; Alatorre *et al.,* 2010).

Consequently, using the sediment transport capacity (STC) concept is likely to be a better way than the SDR due to its ability to demonstrate the movement of soil material down a slope to downstream. Huang *et al.* (1999, p. 503) defined the STC as 'the maximum amount of sediment that a flow can carry, is the basic concept in determining detachment and deposition processes in current process-based erosion models'. The STC is also 'used to represent the potential sediment flux and as a basis for scaling actual erosion rates' (Prosser and Rustomji, 2000, p. 180). Additionally, the concept of STC is commonly used in modelling sediment movement via overland flow and in channel transport models (Merritt *et al.,* 2003). Kinnell (2008) stated that models considering the concept of STC are preferred to those using SDRs as the STC concept considers the deposition; ignorance of deposition on a concave slope at watershed scale may result in overestimation sediment value.

However, the STC concept is not new; Meyer and Wischmeier (1969) (cited in Morgan and Nearing, 2011, p. 11) conceptualise soil erosion as a two-phase process, consisting of the processes of detachment and sediment transport capacity of overland flow with regard to the movement of soil particles down a slope (Figure 1.4). In addition, existing modelling methods such as Agricultural Non-Point Source (AGNPS), Areal Non point Source Watershed Environment Response Simulation (ANSWERS) and Morgan, Morgan and Finney (MMF) adopt this Meyer-Wischmeier approach to describe the process of erosion as well as to estimate sediment delivery when deposition occurs because of changes in slope gradient (Kinnell, 2008, 2010).

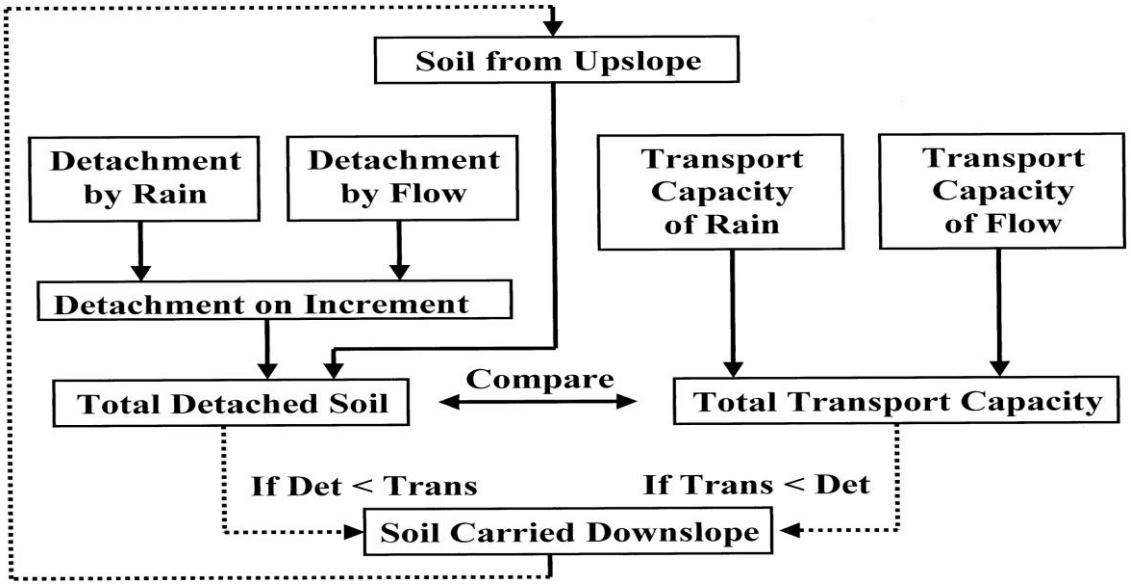

Figure 1.4 The Meyer-Wischmeier approach: a conceptual framework of soil erosion by water process (Source: Kinnell, 2010).

Although the STC is being used increasingly, the SDR approach still has been consistently used in order to describe the distributed processes like the STC approach. As detailed in Hui *et al.* (2010), a 'spatially distributed SDR' module was developed to account for soil erosion and deposition dealing in conjunction with USLE. They found the sediment yield prediction at the outlet was acceptable and the average deviation of the USLE model was less than 0.2 as asserted by Bingner *et al.* (1989) (cited in Hui *et al*. 2010, p. 949).

1.4.1 Research gap I

From the literature reviewed above, it is still not clear whether the STC or the spatially distributed SDR concept is best. Especially in conjunction with RUSLE and applied in the context of the tropical mountainous watersheds in Northwest Thailand, which concept will be most suitable for estimating soil loss and

sediment yield in such area better? Hence, this research has introduced the novelty of SDR deriving from interpolation of the spatially distributed SDR along the main stream of the watershed, named 'Spatial Interpolation of SDR (SISDR)'. In short, both concepts of RUSLE-STC and RUSLE-SISDR have been applied in this research to estimate soil erosion and sediment yield in a selected watershed of Northwest Thailand. Moreover, the computed suspended sediment yields obtained from both model concepts have also been verified with the actual measure of suspended sediment yield for comparing the model's efficiency and performance between them.

1.5 Significance of soil erosion problem in Northwest Thailand

The problems of soil erosion by water in the SEA region include: on-site effects caused by deforestation resulting in soil erosion potential, soil nutrient loss, and reducing the quality of forest. These are considerable problems in mountainous areas (Sangchyoswat, 1998). Increasing pressure on upland and highland areas in Southeast Asia is quite complex, but it is at least partly a response to the demands of a growing population and the transformation of subsistence communities to market economies. This has led to more intensive cultivation of marginal sloping lands and the breakdown of the stability of traditional shifting cultivation. Fallow periods have shortened and lands are being increasingly cultivated before soil recovery is complete (Pahlman, 1991; Scoccimarro, *et al.,* 1999; Fukushima *et al.*, 2008).

In Thailand, one of the most devastating consequences of intensified farming on the uplands is soil degradation. Upland soils tend to be of moderate to low fertility and highly susceptible to soil erosion. About 17.4 million ha or 34% of the cultivated area is classified as vulnerable to soil erosion, especially in the more rugged terrain of the eastern and northern regions (GMS Environment Operations Centre, 2007). Due to growth in the population and economy of Thailand, the demand for lands for uses such as farmlands, has continuously increased. Lack of legal enforcement has led to natural forest being encroached upon and use of lands that are not suitable environmentally for the expansion of agricultural activities. After over four decades of development coupled with population growth of majority and minority ethnic groups, the region has witnessed evident changes to its physical landscape. For example, forest cover declined from 53.3% in 1961 to 25.3% in 1998 in addition to the urban expansion and the conversion of forest to agriculture)GMS Environment Operations Centre, 2005(. These changes have ultimately brought about more serious problems of soil erosion. As Morgan (2005, p.1) remarked: 'on agricultural land where the redistribution of soil within a field, the loss of soil from a field, the breakdown of soil structure and the decline in organic matter and nutrients result in a reduction of cultivable soil depth and decline in soil fertility'.

Northwest Thailand has encountered a serious soil erosion problem, because of steep slopes, high rainfall and increasing swidden cultivation by hill tribes (Scoccimarro, *et al.,* 1999; Fukushima *et al.*, 2008). It is thought by some that

the activities of these tribes can exacerbate soil erosion and increase the flux of sediment into rivers, floodplains and reservoirs. Additionally, some watersheds in northwest Thailand have produced very high suspended sediment yields bigger than 20,000 tonnes km^{-2} yr^{-1}, according to a yearly report from the Royal Irrigation Department (2011) of Thailand.

1.5.1 Research gap II

At a higher suspended sediment yield in the northwest Thailand watersheds which had been recorded by the Royal Irrigation Department of Thailand, it can be assumed that the watersheds in the northwest Thailand are potentially significant generating sources of sediment fluxes, flowing into the channel downstream. Moreover, the spatial contexts such as changing land use and climate in northwest Thailand may have contributed to generating the high sediment problem. However, it is still unclear how the key controls (e.g., soil properties, slope angle distributions, vegetation cover, land management practices, precipitation regime) interact to produce such high soil erosion rates. Besides, research on soil erosion impacted by rainfall and land use changes in northwest Thailand is very rare. Hence, this research has studied the spatiotemporal changes in land use and rainfall erosivity affecting or relating to soil erosion over the entire watershed. Sensitivity analysis has been taken into account for investigating the key correlative factors controlling the soil erosion generation in a watershed of northwest Thailand.

1.6 Aims and objectives of research

To address research gap I (Section 1.4.1) and research gap II (Section 1.5.1), the overall challenges and aims of this thesis are to apply RUSLE-GIS-based modelling to predict soil erosion and sediment yield in space and time. In addition, spatial soil loss with high (critical) rates in the study area (Mae Rim watershed) have been identified and mapped in order to assist and guide decision makers and stakeholders to plan and establish the most appropriate strategies for minimising soil erosion. Hence, a proposed guide to soil conservation and control measures based on this research is anticipated to be helpful in promoting sustainable soil management practices for farmers and stakeholders in the tropical mountainous watershed of NW Thailand who still face problems of soil erosion by water on their farmlands.

I. Identify the spatial variation of soil erosion risk and the key controls which interact to generate the extremely high soil erosion rates in the study area. This work could help as an evaluation tool to plan for future appropriate land use planning

II. Compare and verify the sediment yield predictions, derived from RUSLE-GIS-based modelling in conjunction with two different approaches of Sediment Transport Capacity (STC) and Spatial Interpolation of Sediment Delivery Ratio (SISDR).

III. Assess the sensitivity of soil erosion to scenarios of land use and climate change on soil erosion in the study area.

In this thesis, the quantitative empirical model (i.e., Revised Universal Soil Loss Equation) has been applied by integrating with a Geographical Information System (GIS) and remote sensing approaches to predict soil erosion rates and sediment yield, and these should act as scenarios to help decision makers and stakeholders to plan the most appropriate pattern of watershed management.

1.7 Structure of the thesis

This thesis is organised into seven chapters (Figure 1.5):

Chapter one is a general introduction, which includes: global soil erosion issues, global awareness of soil erosion, RUSLE application: spatial consideration and criticism, adoptions of SDR and STC concepts in conjunction with RUSLE for sediment yield prediction, significance of soil erosion problem in the northwest of Thailand, and research aims and objectives.

Chapter two deals with the general literature background for the thesis regarding soil erosion processes and soil erosion models and criticisms.

Chapter three describes the physical characteristics of the study area. It also briefly provides the material used, general methods and fieldwork data collection.

Chapter four analyses controlling factors, by using a RUSLE-GIS-based model, to estimate mean annual soil erosion rate and also generate the spatial variation of soil erosion risk map in the study area. It also details how to evaluate each controlling factor in the RUSLE process, and identifies the key controls interacting with the extremely severe soil erosion risk.

Chapter five provides an analysis of suspended sediment fluxes and yields in eight watersheds of northwest Thailand using the sediment rating curve methods. It also contains a prediction of suspended sediment yield predictions as well as a verification of the model's efficiency and performance as a result of applying two different approaches of RUSLE-STC and RUSLE-SISDR.

Chapter six examines the potential effects of changes in land use and rainfall erosivity on soil erosion in the study area. It also provides the testing of sensitivity analysis of soil erosion scenarios under various assumed conditions by altering rainfall and vegetation cover factors in the RUSLE model.

Chapter seven is the conclusions of the thesis's key findings, significant contributions to watershed soil erosion studies, including recommendations and future research needs.

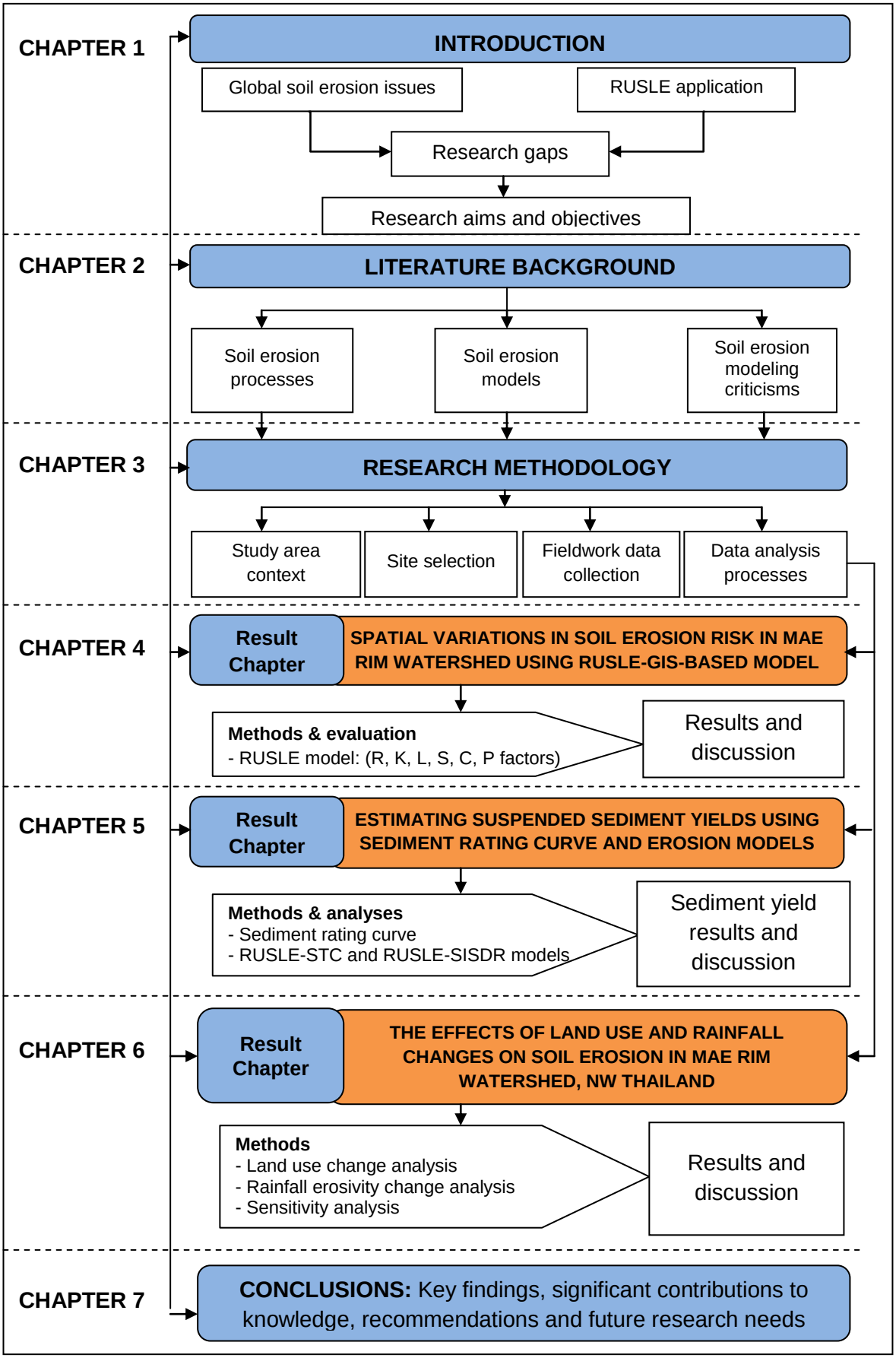

Figure 1.5 Schematic diagram of the thesis structure

CHAPTER 2: LITERATURE BACKGROUND

2.1 Introduction

This chapter provides an overview of the background literature on soil erosion processes before providing a review of soil erosion model classifications is presented and critically evaluated. Finally, the concepts of environmental risk assessment are elucidated.

2.2 Soil erosion processes

Erosion is the process whereby earth or rock material is loosened or dissolved and removed from any part of the earth's surface. Whereas weathering involves only the breakdown of rock, erosion additionally entails the detachment and transport of weathered material from one location to another, denuding the earth's surface and delivering sediment to the fluvial system. Erosion rates are frequently measured on small fractional-hectare plots. The landscape and associated fluvial transport system may be divided into zones where either erosive or depositional processes dominate. Erosion processes predominate in mountainous environments, while deposition predominates on floodplains, although both erosion and depositional processes occur simultaneously in virtually all environments. Thus, materials eroded from mountain slopes may be deposited in valleys and floodplain deposits are eroded by stream channels (Morris and Fan, 1997).

Soil erosion may be classified according to the erosive agent (water and wind), the erosion site (splash, sheet, rill, gully and channel) or the erosive process (e.g., raindrop, channel, mass wasting) (Morgan, 1991; Chankao; 1996; Tangtham, 2002). Figure 2.1 explains the mechanism of soil erosion processes; at the first stage, splash erosion initially takes place when the falling raindrops hit bare soil dislodging soil particles. Once the rainfall amount accumulating on the land surface exceeds the infiltration capacity of the soil, surface runoff or overland flow is generated. The dislodged or loosened soil particles will then be removed by surface runoff in a thin layer, flowing down to a point of deposition (called sheet erosion). While sheet erosion is difficult to see due to the fact that water does not cut any channel when carrying away soil particles, rill erosion leaves visible scouring on the landscape. Rill erosion is formed when runoff from sheet erosion begins cutting small, separate channels as it travels a downward slope. Gully erosion is an advanced stage of rill erosion, it occurs when the water in rill concentrates to form larger channels. Unlike rill erosion, the gully cannot be removed by normal cultivation methods (Poesen *et al*., 2003; Aksoy and Kavvas, 2005; Morgan, 2005). Gully erosion and channel erosion may refer to either the gradual or the massive erosion of the beds and banks of gullies and stream channels. Mass wasting refers to erosion associated with slope failures, including landslides and similar slope movements. Wind erosion refers to movement of soil particles by wind. Wind erosion may be important in arid or semiarid regions as an agent that can transport sediment from ridges into depressions from which it can subsequently be transport by runoff (Rooseboom, 1992).

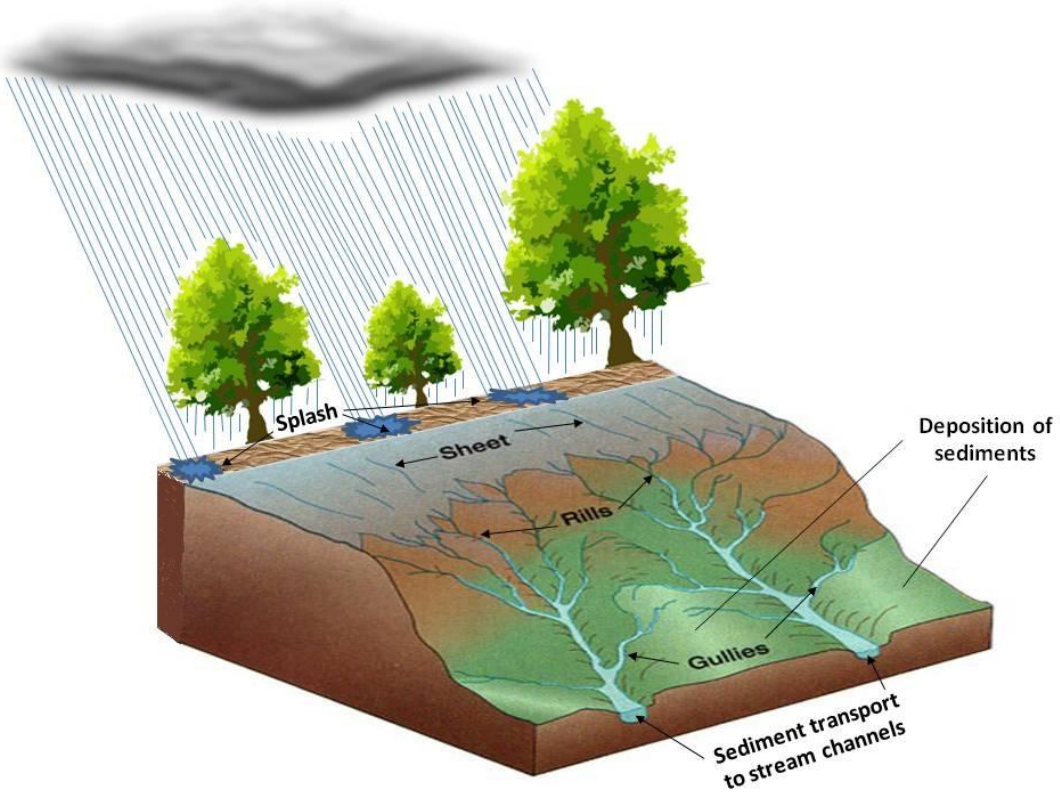

Figure 2.1 Schematic diagram of soil erosion processes

Furthermore, De Vente *et al.* (2008) briefly concluded the description of soil erosion processes by distinguishing between soil erosion, deposition and sediment yield (Figure 2.2). Buss *et al.* (2009) also illustrated a holistic drainage basin context and nested spatial scales, with particular reference to sediment supply (Figure 2.3). Soil erosion is a common natural phenomenon regardless of geographical aspects of the land. This is, however, due to various natural factors exerting their influences over the erosion. With regard to sediment yield, it refers to the part of eroded material, normally originating from soil erosion processes, which is conveyed to the outlet of watershed (De Vente *et al.,* 2008).

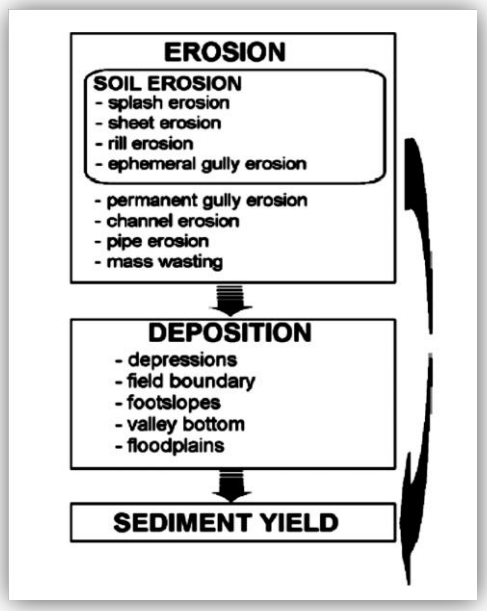

Figure 2.2 The distinction between erosion, soil erosion, deposition and sediment yield (Source: De Vente *et al.,* 2008).

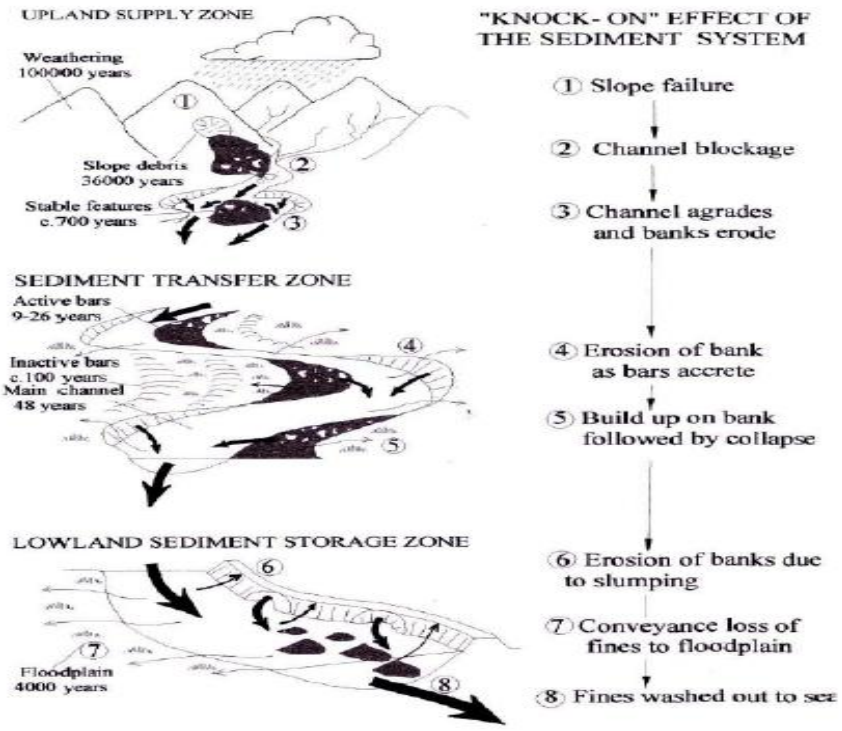

Figure 2.3 Sediment supplies and connections in a catchment context. (Source: Buss *et al.,* 2009)

Moreover, Baver (1965) (cited in Tangtham, 2002, p. 18) summarized erosion in the following function:

$$Erosion = f\ (C, T, V, S, H) \qquad [2.1]$$

Where: *C* = Climate; *T* = Topography; *V* = Vegetation cover; *S* = Soil properties, and *H* = Human activities

• *Climate factors* play an important role in soil erosion. They include rainfall and temperature changes. Rain is considered the most important factor because rain drops are both initial energy causing soil particles to disintegrate and an agent of surface runoff as well as soil particle movements. Temperature changes between day and night or during seasonal transitions affecting soil structure, lessening soil particle gravitation.

• *Topography factors* include slope and slope length, affecting the velocity of soil erosion. The higher the slope, the more ferocious erosion becomes. Slope length is directly related to soil quantity being eroded.

• *Vegetation cover* reduces raindrop impact. The tree canopy shores up the rain and slowly releases the water to the ground by means of throughfall and stemflow. Moreover, the canopy facilitates micro-organism activities providing food and energy as well as reducing surface flow.

• *Soil properties* affecting erosion are divided into two types: properties toward infiltration rate and permeability, and properties against detachment, abrasion and transportation forces of underground water and soil surface.

• *Human activities* play a crucial part in soil erosion. Some of the activities include deforestation, forest clearing for agriculture, forest fires for hunting, livestock over-farming, incorrect agriculture, and road and residence building. These activities are extremely difficult to solve or modify because they depend on people's education and individual conscience.

Soil erosion predictions can be undertaken by various means, depending on the objectives of those predictions. For instance, they may be used to incorporate environmental impact prevention plans or to assess future negative impacts on agricultural production due to loss of soil surface. Utilizing a mathematical model to assess and predict soil erosion is a way to reduce time and budget of an investigation when it is done in a large-scale area. Furthermore, results of the prediction are accurate to a certain extent. However, the model requires a large amount of data for analysis (Tangtham, 2002).

2.3 Soil erosion models

During the last decade, large numbers of erosion and sediment transport models have played important roles in predicting soil loss and/or sediment yield. There are many different soil erosion models with different degrees of simplification, from the simple to complex. According to Terranova *et al.* (2009), soil erosion models can be divided into three categories:

2.3.1 Qualitative models – based on the direct observation of soil degradation phenomena, remote sensing or aerial photo interpretation, and the construction of geomorphological maps. These models use satellite imagery or aerial photos, applying them to direct detection of the active soil erosion and the erosive consequences (Vrieling, 2006; Rahman *et al.*, 2009). Although the qualitative model based on remote sensing methods can be rather time-consuming or costly due to long-term field measurements and detailed field surveys, it beneficially provides the new potentialities of data particularly for: (i) the automatic detection of gullies; (ii) the accurate assessment of aging in vegetation cover in different environments; (iii) the spatiotemporal evaluation of rainfall characteristics; and, (iv) the accurate mapping of soil properties and soil moisture in a wide range of environments (Vrieling, 2006).

2.3.2 Semi-quantitative models – the simple models, based on scoring factors or expert judgements, which can be applied in complex climatic conditions and can cover a wide variability of the explanatory variables in a relatively short time span (Sonneveld *et al*., 2011). Examples of the semi-quantitative models are

CSSM – the Coleman and Scatena Scoring Model (Coleman and Scatena, 1986), PSIAC – Pacific Southwest Inter-agency Committee (De Vente and Poesen, 2005; Tangestani, 2006), FSM – Factorial Scoring Model (Verstraeten *et al.*, 2003), EHU – Erosion Hazard Unit (Chakela and Stocking, 1988), GLASOD – Global Assessment of Soil Degradation (Oldeman *et al.,* 1991; Sonneveld and Dent, 2009), EPM – Erosion Potential Method (Tangestani, 2006), ERU – Erosion Response Units (Bou Kheir *et al.*, 2006) and SPADS – Spatially Distributed Scoring Model (De Vente *et al.*, 2008).

2.3.3 Quantitative models – based on the parameterisation of several factors. The complexity of these models depends on the greater amount of factors considered and on the complexity of each single factor. Typically, they can be divided into three groups:

(a) Empirically based models. Most of these models have been developed based on field observations in specific environmental contexts to which the model was applied (Terranova *et al*., 2009). Moreover, the parameter values in empirically based models may be derived by calibration, but are more often transferred from calibration at experimental sites (Merritt *et al*., 2003). The (R)USLE – (Revised) Universal Soil Loss Equation (Renard *et al.,* 2011), and the SEDD – Sediment Delivery Distributed (Ferro and Porto, 2000) are such models that are more often used rather than the complex models, in particular for identifying soil erosion source and nutrient generation as a first step,

especially operated in situations with insufficient data and parameter inputs (Merritt *et al*., 2003).

(b) Physically based models. These models are the most complex and strict mathematical relationships. They are commented on by Bhattarai and Dutta (2007, p. 1636) that 'these models are the synthesis of individual components that affect the erosion process and it is argued that they are highly capable of assessing both the spatial and temporal variability of the natural erosion processes'. The physically based models include WEPP – Water Erosion Prediction Project (Laften *et al.*, 1991; Amore *et al.*, 2004; Baigorria and Romero, 2007), PESERA – Pan European Soil Erosion Risk Assessment (Kirkby *et al*., 2008; Licciardello *et al.*, 2009), KINEROS – Kinematic Erosion Simulation (Martínez-Carreras, 2007), EUROSEM – European Soil Erosion Model (Quinton *et al*., 2011) and LISEM – Limburg Soil Erosion Model (Hessel *et al*., 2011).

(c) *Conceptually based models.* These models lie between the empirically based and the physically based models, and display a partial representation of the hydrological sediment yield processes (Karnoven *et al*., 1999). They take into account the physical processes governing erosion by water through empirical relationships among the involved variables (Terranova *et al.,* 2009). The conceptually based models include SWAT – Soil and Water Assessment Tool (Shen *et al.,* 2009), AGNPS – Agricultural Non-Point Source (Young *et al*., 1989; Rode and Fredo, 1999; Walling *et al.,* 2003), SEMMED – Soil Erosion

Model for Mediterranean Area (De Jong *et al.*, 1999), and MMF – Morgan, Morgan and Finney (Morgan, 2001; Vigiak *et al*., 2005; Morgan and Duzant, 2008).

2.4 Criticisms of soil erosion modelling

Although the physically based model has apparently been more reliable and accurate due to relying on mathematical equations to describe various hydrological and sediment processes both on hill slopes and in channels (Gao, 2008; Kinnell, 2010), the empirically based model, in particular, the RUSLE, is still popular today. This is due to its simplicity and extensive database (Charlton, 2008). Fu *et al.* (2010) ascribed that the physically based model always requires estimation and calibration of more parameters than the empirically based model. Besides the requirement of large computation power, the physically based model needs to develop input databases that describe appropriately the spatial variability of model variables, as well as to implement an adequate monitoring strategy that would allow for variable and parameter calibration. Moreover, De Vente and Poesen (2005) remarked that the physically based model may not have extrapolation problems as they are built on physical laws. In contrast, an application of a pure physically based model that integrates all sediment producing processes over the basin or at a large scale is not foreseen in the near future due to insufficient systematic knowledge to describe all relations and feedbacks in physical equations and the huge data requirements. Similar to Renscher and Harbor (2002) and Wilkinson *et al.* (2009), the

physically based model is more complex; understanding of the process has not generally been demonstrated to match measurements across large landscapes.

Soil erosion studies with applications in soil erosion modelling span a wide range of spatial scales: (i) the simple plot for scientific study; (ii) the field scale for the interest of the single farmer; (iii) the catchment scale for community level issues; and (iv) the watershed/ basin/ regional/ national scales for policy maker interests (Kirkby *et al.*, 1996; Amore *et al.*, 2004). Surprisingly, the empirically based models like RUSLE are still used to estimate the mean annual soil loss rates over large areas (i.e., from the levels of watershed to regional) despite some limits buried in the concept itself (see Section 1.3). For instance, Sidorchuk (2002) (cited in Sidorchuk, 2009, p. 3) employed RUSLE to calculate soil loss from the national territory of New Zealand. His results showed the reasonable prediction of soil loss when compared with sediment yields from the rivers. Moreover, Beskow *et al.* (2009) applied USLE with GIS to estimate potential soil loss from the Grande River Basin in Brazil, covering approximately 6,273 km^2. Their results represented acceptable precision and allowed for identification of the most susceptible areas to water erosion.

In other aspects, the RUSLE model has also been used in different ways, for example, Shamshad *et al.* (2008) adjusted the R-factor in the RUSLE model for preparing an appropriate map of rainfall erosivity in Palau Penang in Peninsular Malaysia. Three independent variables, such as storm rainfall and duration; monthly rainfall for days with rainfall ≥ 10 mm ($rain_{10}$) and monthly number of

days with rainfall ≥ 10 mm ($days_{10}$); and Fournier index, were employed to estimate the monthly rainfall erosivity (EI_{30}) values. Their results illustrated that the Fournier index approach was the best with the least percentage error (PE) and root mean square error (RMSE) values compared to the models from the other two approaches. Besides, Terranova *et al.* (2009) used RUSLE and GIS to generate soil erosion risk scenarios in Calabria (southern Italy). Their various scenarios consisted of the present scenario; the project scenario; the scenario with forest fires and the mean values of the erosivity factor; and the scenario with forest fires and the highest values of the erosivity factor. They suggested that comparison of the various scenarios of soil erosion by water can be a very useful tool in the definition of prevention and control measures to reduce environmental hazards and their related costs.

As mentioned above, RUSLE has not only proved to be a useful tool for determining erosion hazards at the region scale (Zhou *et al.*, 2008; Bazzoffi, 2009), but it also has the potential to estimate sediment source and sediment yield at acceptable levels (although it may involve misapplication and misconception in its use) (see also Govers, 2011).

There is generally no best modelling method for all applications (Merritt *et al.,* 2003) and some contradictions between modellers still exist (e.g., Kinnnell, 2008 against Parsons *et al*., 2008; Smith *et al.,* 2010 against Wainwright *et al*., 2010). Meanwhile, the semi-quantitative models have emerged as an alternative model, particularly for reducing the limitations of the sediment yield

estimations at the watershed scale. Boardman (2006, p.79) noted that 'semi-quantitative methods have been advocated and an expert-system approach based on field monitoring of erosion can also be an effective tool.' In addition, De Vente and Poesen (2005) argued that the semi-quantitative models based on expert judgements may be the most suitable to apply for mapping soil erosion risk. Le Bissonais *et al.* (2001), for example, adopted the Coordination of Information on the Environment (CORINE) for the evaluation of erosion risk at the national scale in France, while Nigel and Rughooputh (2010) used the newly created semi-quantitative model, MauSERM (Moritius Soil Erosion Risk Mapping), to produce monthly soil erosion risk figures for mainland Muaritius. Bou Kheir *et al.* (2006) also used semi-quantitative methods to produce a regional soil erosion risk map in Lebanon.

However, some research has revealed that the semi-quantitative methods can also predict sediment yield. According to De Vente *et al.* (2005), their findings showed that semi-quantitative approaches provided fairly accurate and reliable estimates of area-specific sediment yield, ranging from small to medium sized basins in Spain. Additionally, Tangestani (2006) has adopted EPM and PSIAC models to predict sediment yield in the semi-arid environment of the Afzar catchment in Iran. He compared predicted soil erosion and sediment yield with field observations and the Global Assessment of Soil Degradation (GLASOD) map. His results showed that the PSIAC model is more reliable than EPM model after implementing field verification. In cases where database layers are

limited however, the EPM model could potentially be used for rapid assessment and mapping of soil erosion risk (Tangestani, 2006).

In conclusion, scientists have been challenged to research and develop models for achieving the accurate prediction of soil erosion and sediment yield. Even though USLE and RUSLE models are often criticised by Kinnell (2005, 2008, 2010), the physically based models still have limits in estimating soil erosion, when applied to larger scales. The complexity and limitations of the variables used in their equation are likely to be unpopular in adoption of planning and managing soil and water resources at national level. In particular, developing countries often have insufficient data to support physically based models. Thus, we should not be disappointed by unsatisfactory results predicted from the these models because 'at this stage models are still developing and unsatisfactory results may indicate which aspects of models are most in need of further development' (Boardman, 2006, p. 77). This is consistent with Parsons *et al.* (2008) who noted that 'we do not wish to denigrate the achievement of the USLE' (Parsons *et al.,* 2008, p. 1630). Clearly, all models have fundamental limitations in predictions. However, the capabilities of each model can be adapted to the different tasks at appropriate scales as De Vente and Poesen (2005) have tried to compare the different model types with respect to the different time and space scales (Figure 2.4). Geographical information system (GIS) and remote sensing techniques are useful tools for soil erosion models, as they permit an analysis of soil erosion estimation and its spatial distribution

feasible with reasonable costs and better accuracy in larger areas (Lu *et al.,* 2004).

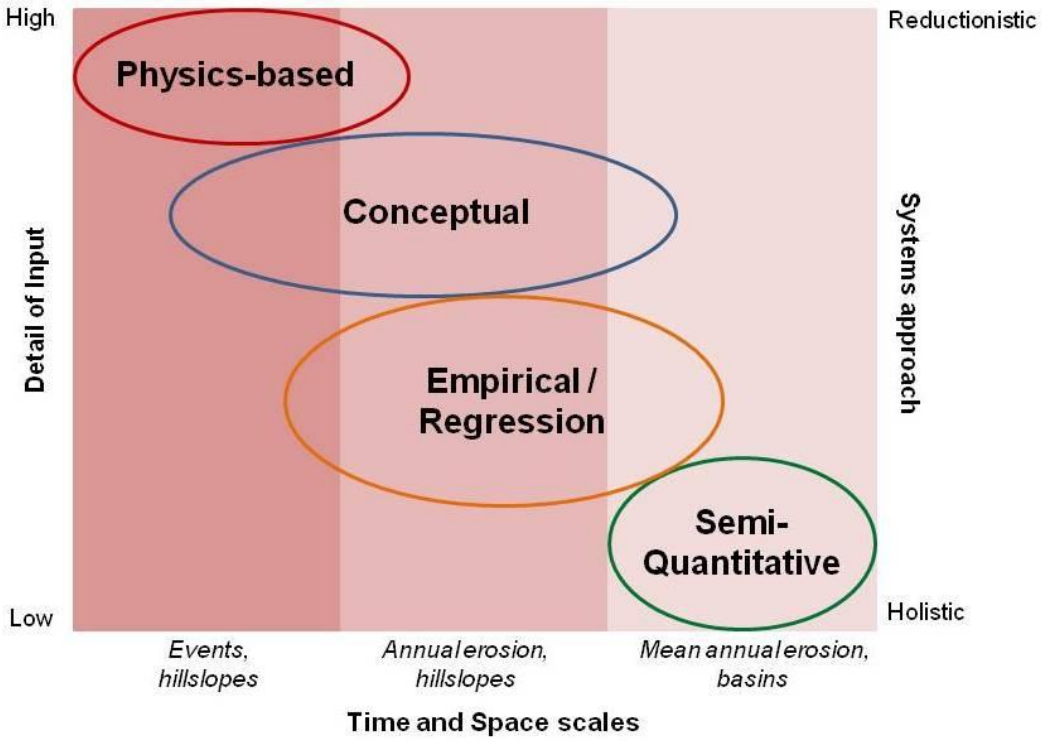

Figure 2.4 Comparison of model types with respect to scale, input requirements and kind of output. (Source: Modified from De Vente and Poesen, 2005, p.119)

2.5 Chapter summary

This chapter has reviewed the literature providing a summary of the current knowledge on soil erosion processes, to underpin understanding the different processes and forms of erosion and deposition that occur by running water. The description of different forms and processes of soil erosion and deposition assists to identify which of these processes are most significant in contributing sediment in a catchment. In addition, the different types of soil erosion models have been discussed in detail. Also, comparisons of several model types with

respect to advantages, limitations, time and space scales have been criticised and provided rationales for documenting why an empirically based model (e.g., RUSLE) has been widely used and successfully, rather than other model types, in terms of soil erosion prediction at watershed scale. The next chapter presents the research design and describes the fieldwork data collection in detail and overarching methods used in the thesis.

CHAPTER 3: RESEARCH METHODOLOGY

3.1 Introduction

This chapter gives an overview of the physical characteristics of the study area, fieldwork data collection and data analysis processes. The elaborated step-by-step methods and materials used for generating, processing and analysing data are provided in each results chapter (i.e., Chapters 4 to 6), while this chapter provides the overarching philosophy and approach behind the thesis research design.

3.2 Study area context

This thesis studies the assessment of soil erosion and sediment yield in the watersheds of northwest Thailand. Such areas are situated in tropical Asia which is most concerned with the problems of soil erosion as a result of human-induced process (Chang, 1993; Yang *et al.,* 2003). Because northwest Thailand is a highly mountainous terrain alternating with narrow plains (about 10% of the total area of northern Thailand), the cultivation in lowland areas or on floodplains is out of balance with an increasing population. Consequently, people in the lowlands need to encroach into the uplands to increase their farms and products (Valentin *et al.,* 2008). Meanwhile, on the upland area above 600 m a.s.l., mostly minority hill tribe groups (e.g., Kmong, Karen, Lua, Mian, Akha, Lahu and Lisu) and some local Thai people have occupied the land for settlement (Figure 3.1)

Considering the lowland and upland characteristics in the northern region of Thailand, according to Suraswadi *et al*. (2005), the lowland zone is typically located below 600 m a.s.l. It contains low foothills surrounding the plains which are often closely incorporated in the lowland agricultural and settlement systems. The upland zone, which includes mid- and high-altitude areas, is located beyond these foothills at about 600 m and above. It consists of diverse landscape such as high mountain peaks and ridges, mountain slopes and intermountain valleys with hill-slope cultivations and irrigated rice terraces (Forsyth and Walker, 2008).

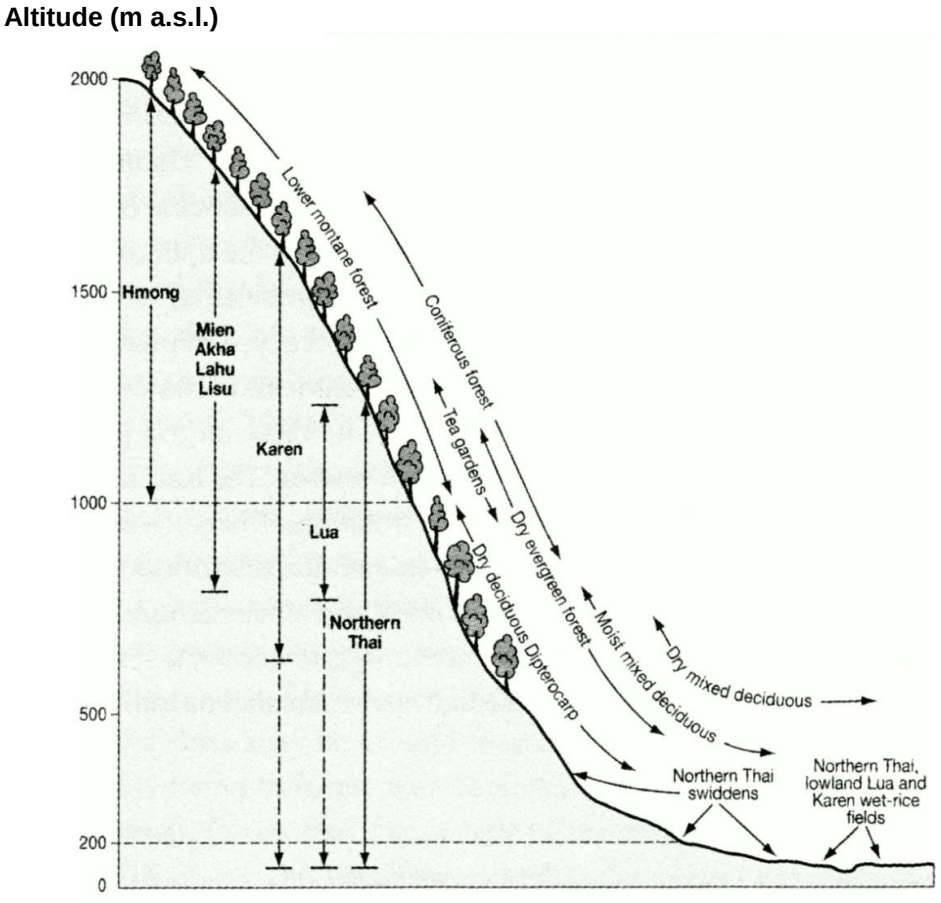

Figure 3.1 Ethnic groups and elevation relation in North-western Thailand

(Source: Forsyth and Walker, 2008)

After a combination of farmer initiatives and intervention by agricultural development schemes in the late 1970, opium cultivation in mountainous areas was replaced by introducing alternative cash crops such as vegetables (e.g., cabbage and lettuce) and fruit trees (e.g., peach, persimmon and apple) (Williamson, 2006). Soil erosion was exacerbated as a result of commercialisation encouraging more land clearing and more intensive land use on currently cleared land (Ziegler *et al*., 2009). Despite monitoring and advising of natural resource conservation by government agencies, such as the Land Development Department (LDD), the Royal Irrigation Department (RID) and the Royal Forestry Department (RFD), the problems of natural resource depletion have not been removed or relieved in any way, particularly in soil erosion problems.

Given the background mentioned above, it illustrates that soil erosion still acts as a major environmental problem in north-western Thailand, particularly in Chiang Mai, which is the largest city and has the most varied cultures in the north-western region; it is located on the Upper Ping River Basin, with a size of about 23,000 km^2. The region includes the significant sub-watersheds, such as the upper, second, and third parts of Mae Ping, Mae Taeng, Mae Kuang, Mae Chaem, Mae Rim, Mae Klang, Mae Ngad, Mae Khan and Mae Wang watersheds (Figure 3.2).

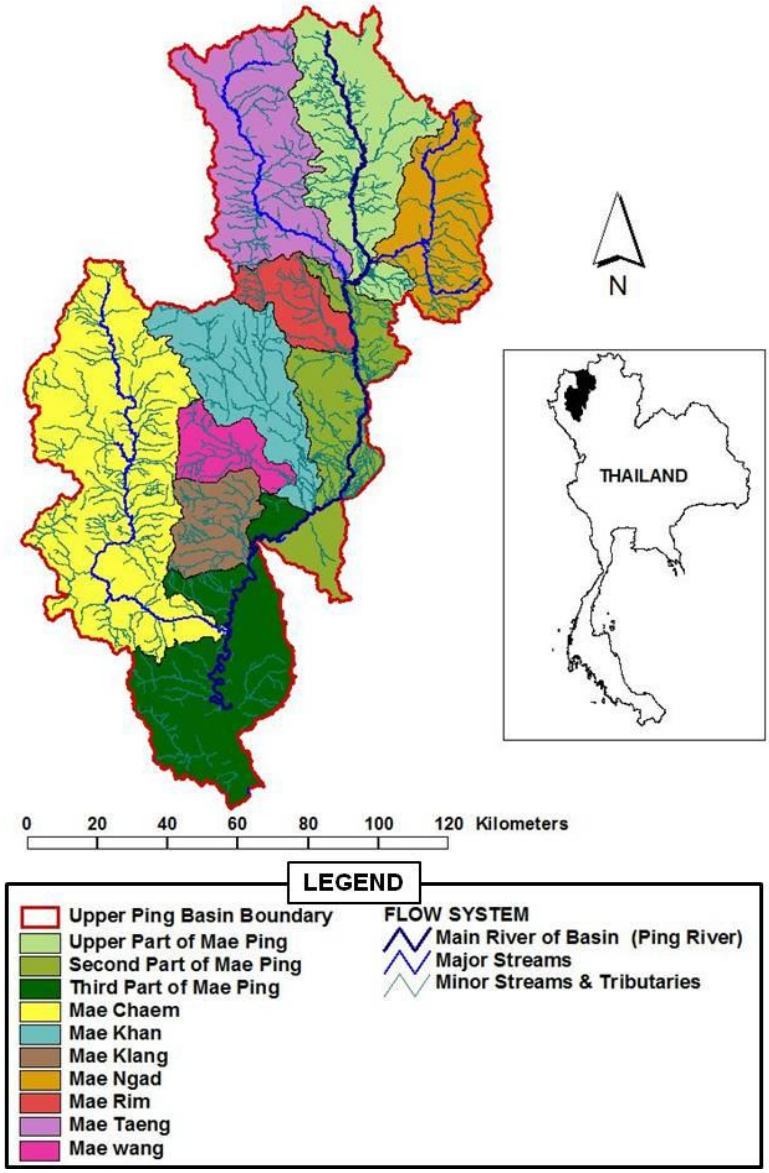

Figure 3.2 Upper Ping River Basin with sub-basins.

3.3 Site selection

Within the Upper Ping River Basin, the '*Mae Rim watershed'* is selected as the case study area for the thesis. Although this site does not appear to have the highest amount of suspended sediment yield according to the original information from the Royal Irrigation Department (2011) (Table 3.1), the time period of SSY samplings at gauging station P21 has been longer than 10 years.

This is particularly useful for further implementing calibration of the values predicted from the erosion model application. The other remarkable features of the Mae Rim watershed are: (a) the suspended sediment concentration data and flow gauging station are available until now; (b) its area covers all the lowland, upland and mountainous areas to represent the different land use patterns and cropping systems; (c) there are several minority groups or hill tribes living in the area, which might affect soil erosion, particularly on the upland slope areas by their intensification of traditional agriculture, i.e., shifting cultivation or slash-and-burn techniques; and, (d) drainage area is not too large (515 km^2). It is therefore appropriate for effectively conducting the fieldwork survey and data collection within the limited time and budget.

Table 3.1 Original report of suspended sediment yields in watersheds of Upper Ping River Basin.

Station Code	Gauge name	River	Available from	Mean annual sediment yield (SSY) (100 tonnes km^{-2} yr^{-1})	Drainage Area (km^2)
P1	Nawarat Bridge	Mae Ping	1993 – present	51.73	6,355
P73	Ban Sop Soi		2001 – 2007	45.53	16,815
P75	Ban Cholae		2001 – present	35.79	3,090
P4A	Ban Mae Taeng	Mae Taeng	1992 – present	52.97	1,902
P65	Ban Muang Pok		1992 – 2000	145.56	240
P70	Ban Huai Due		1995 – 2000	241.45	182
P14	Ta Kham Bridge	Mae Chaem	1968 – 2005	192.8	3,927
P21	Ban Rim Tai	Mae Rim	2001 – present	42.69	515
P24A	Pracha Uthit Bridge	Mae Klang	1997 – 2001	48.45	611
P56A	Ban Rom Klao	Mae Ngad	2000 – present	51	1,309
P71	Ban Klang	Mae Khan	n/a		1,299
P82	Ban Sob Win	Mae Wang	2006 – present	17,541.55	389
P84	Ban Pan Ton		2006 – present	1,064.50	493

(Source: Original information from the Royal Irrigation Department (RID), Thailand).

3.4 Mae Rim watershed

Figure 3.3 Mae Rim River (at UTM-X: 488677, UTM-Y: 2099859; altitude: 340 m a.s.l.) (Source: Field survey, taken on 27 August 2010).

3.4.1 Location – The Mae Rim watershed is one of 13 catchments in the Upper Ping River Basin. About 46 kilometres length of *Mae Rim River* (Figure 3.3) is contained in a drainage area of 515 square kilometres, flowing from the northwest to southeast and joins the *Mae Ping River* at *Ban Sob Rim* village. The watershed is located in the northwest of Chiang Mai City (the regional centre of northern Thailand) between the latitudes of 18º54´36´´ to 19º10´48´´ N and the longitudes of 98º38´24´´ to 98º58´48´´ E. The elevation is typically around 300 to 1,800 m a.s.l. (Figure 3.4).

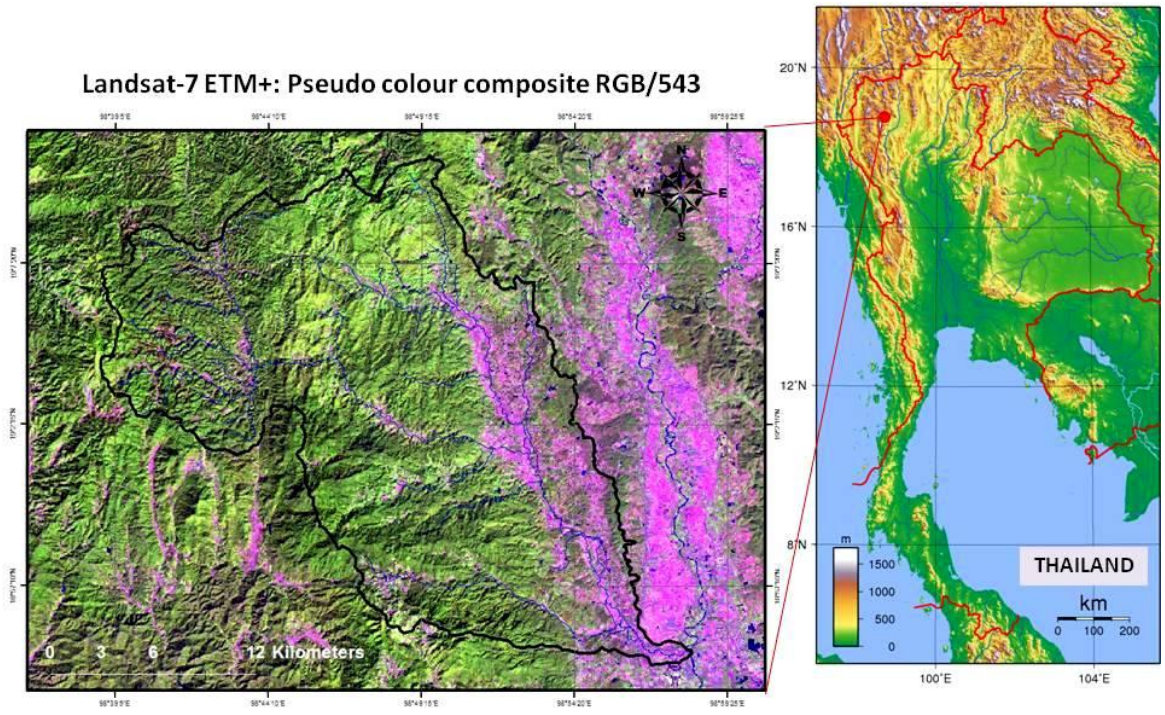

Figure 3.4 The study area of the Mae Rim watershed. (Source: Landsat-7 ETM+ satellite imagery from the Geo-Informatics and Space Technology Development Agency (GISTDA) of Thailand; Topographical map of Thailand from Sadalmelik, 2007).

3.4.2 Climate and Hydrology – The climatic condition of the Mae Rim watershed is characterised by the monsoon, which creates three distinct seasons: cool–dry (November–February), hot–dry (March–May), and rainy (June–October). During mid-May and mid-October, the southwest monsoon usually blows in from the Indian Ocean. Consequently, the rainfall is generally heaviest in August with an average precipitation of 230 mm for that month alone. From mid-October to February, the northeast monsoon brings cooler temperatures and generally less humidity and less chance of rainfall for most of northern Thailand. The average monthly maximum temperature in the study

area is 36ºC in April whereas the average monthly minimum temperature is 14ºC in January (Figure 3.5).

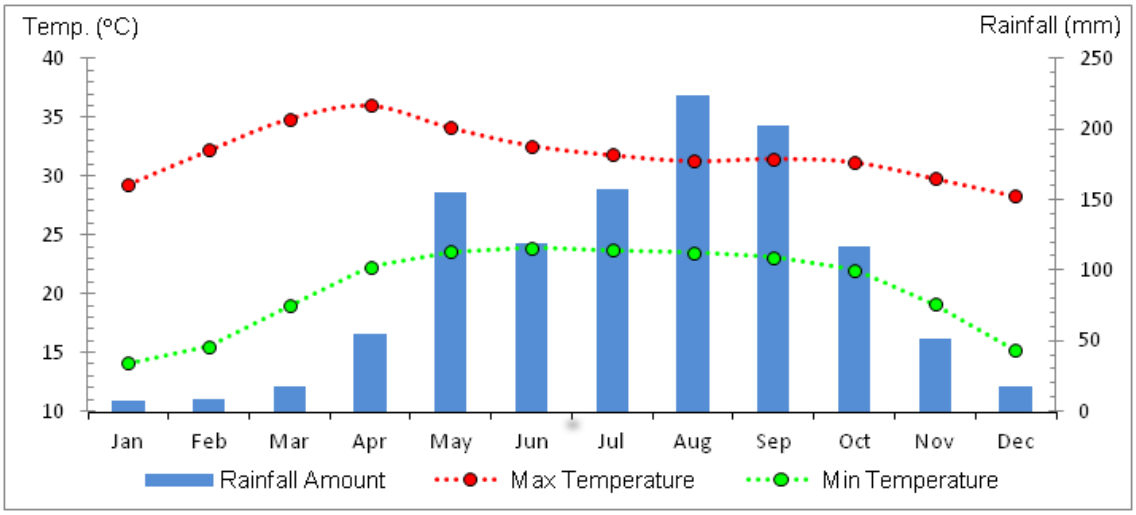

Figure 3.5 The average temperature and rainfall amounts for the 30-year period 1970–2000 in the Mae Rim watershed (Source: Climatological data from the Thai Meteorological Department).

The hydrological data of Mae Rim watershed was provided by the Royal Irrigation Department, which illustrates that the average water volume for each month of Mae Rim River, which has been measured at gauging station P21 between 1989 and 2009, is at its lowest (2 Mm^3) in April, but then grows steadily from May to August, typically peaking at amount of 32 Mm^3 in September and declining again from October to March (Figure 3.6).

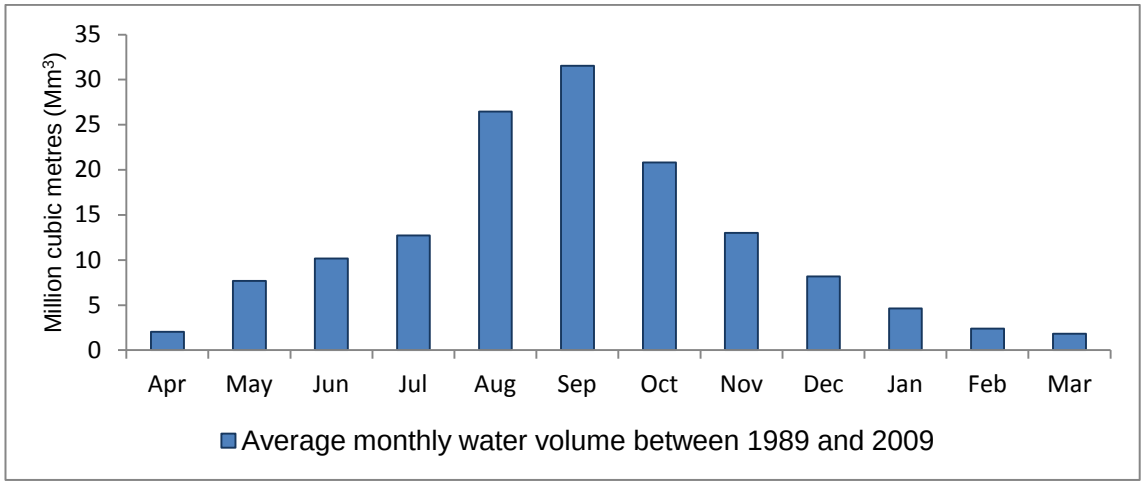

Figure 3.6 The average monthly water volume for the 20-year period (1989–2009) of the Mae Rim River. (Source: Hydrological data from Royal Irrigation Department (RID), Thailand).

3.4.3 Soil – Soil in ravines and creeks of the Mae Rim watershed is a grey sandy loam, which is hygroscopic, so has the ability to absorb the water. The soil in the mountainous area covered by the most hill evergreen forest is a reddish brown lateritic soil, which has moderate acidity, richness of organic matter, low utilisation of phosphorus and potassium, and low soil retention (Rerkasem and Rerkasem, 1995). Soil structure is a rectangular box and medium grain size; while soil depth ranges from 100–240 cm. Downings from the hillside areas are mostly lateritic soil which is a rusty-red in colour because of iron oxides and low fertilisation. For the floodplains, it is composed of numerous gravels on the surface, which are easily eroded by stream flow (Rhodes et al., 2005).

3.5 Fieldwork data collection

The fieldwork data collection was conducted during June and September in 2010 (i.e., four months before analysing GIS modelling). Data obtained from the fieldwork were primary and secondary data. The primary data collection, which started from early July to the end of September, involved ground truth survey; many types of equipments (e.g., GPS, topographical maps, camera, compass and tape measure) were employed for reaching, getting and recording the points of interest in the actual field. In terms of the secondary data (e.g., daily and monthly rainfall, suspended sediment fluxes and river discharges, digital soil maps and Landsat satellite imageries), most of them were obtained during June 2010 from Thai government agencies (Table 3.2).

Table 3.2 The secondary data collected from the Thai government agencies

Data	Spatial resolution/ Map scale	Obtained from
1. Satellite imageries		The Geo-Informatics and Space Technology Development Agency (GISTDA)
1.1 Landsat-5 TM, 1989	30 x 30 m	
1.2 Landsat-7 ETM+, 2009	30 x 30 m	
2. Topographical maps L7018, Map sheets: 4646 I, 4747 II and 4747 III	1: 50,000	The Royal Thai Survey Department (RTSD)
3. Digital soil map	1: 50,000	The Land Development Department (LDD)
4. Daily/ Monthly rainfall	n/a	Thai Meteorological Department (TMD)
5. Hydrological data: (river discharge, suspended sediment concentrations and suspended sediment loads)	n/a	The Royal Irrigation Department (RID)

3.5.1 Data collection based on remote sensing method

Fieldwork data collection based on remote sensing method was conducted in order to collect training data for classification and to identify land use/cover types for reference pixels to be used for accuracy assessment of the output classification (Jones and Vaughan, 2010). Before visiting the fieldwork location, however, the multispectral images of Landsat-7 ETM+ (captured in July 2009) had necessarily been rectified in order to eliminate an inherent distortion of satellite imagery (Gao, 2009). The *'Image mapping rectification'* technique was employed for that. This technique normally involves selecting ground control point (GCP) image pixel coordinates (row and column) with their map coordinate counterparts. The coordinates of easily identifiable features (e.g., road junctions) as grid references or as northings and eastings in Universal Transverse Mercator (UTM) map projection were input into the image processing package together with the location of the corresponding image pixel, and the image is suitably warped to the map coordinates (Jones and Vaughan, 2010). In addition, the other steps that were necessarily manipulated for the processes of acquiring accurate results based on remote sensing method include:

I. Colour composites – the rectified multispectral image bands were subsequently combined as a *'False Colour Composite'* (FCC) image using the conventional three-colour display system. In this study, three of the image bands were extracted from the raw image for their ability to discriminate and detect characteristics or spectral reflectance of earth surface materials (e.g., vegetation, soil and water) (Figure 3.7). Such bands include:

B3 or *'visible red band'* (wavelength is 0.63–0.69 µm) which was replaced in the blue frame buffer memory because the water bodies, especially turbid river water, can positively reflect in the visible red band (Hellweger *et al*., 2004; Fang-Fang *et al*., 2011);

B4 or *'near-infrared band (NIR)*' (wavelength is 0.76–0.90 µm), which was displayed on the red frame buffer memory due to the fact that most vegetation reflectance is normally low in the visible spectrum as a result of chlorophyll absorption, but high reflectance in the NIR (Lillesand and Kiefer, 2002);

B5 or *'shortwave-infrared band (SWIR)'* (wavelength is 1.55–1.75 µm), which was replaced in the green frame buffer memory because the (bare) soil shows a higher reflectance in the SWIR (Rahman *et al.,* 2004). The processes of combined imagery bands including the consequential FCC can be obviously delineated in Figure 3.8.

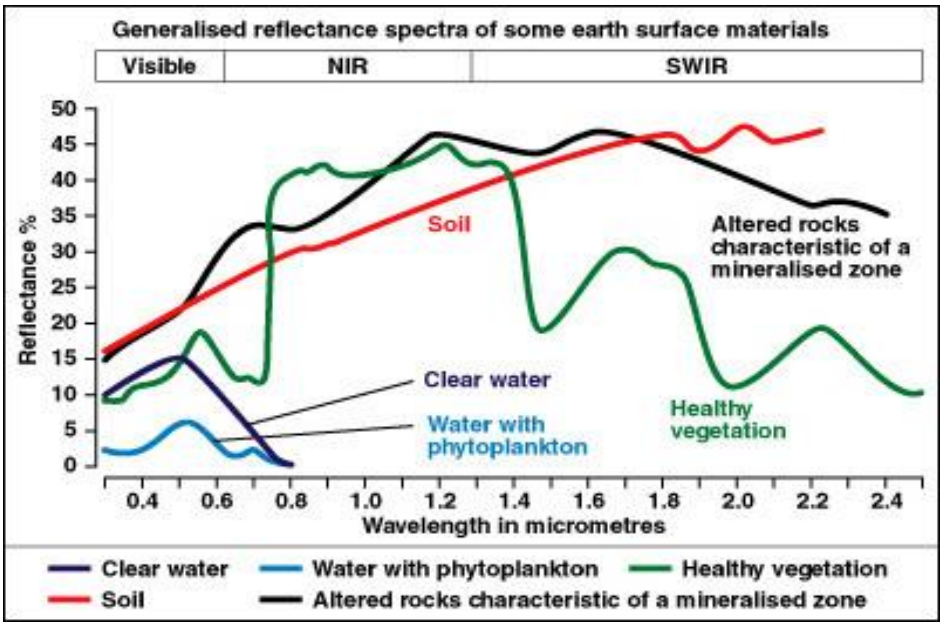

Figure 3.7 Spectral reflectance curves for vegetation, water, soil and altered rocks. (Source**:** RSAC – Remote Sensing Applications Consultants, 2013).

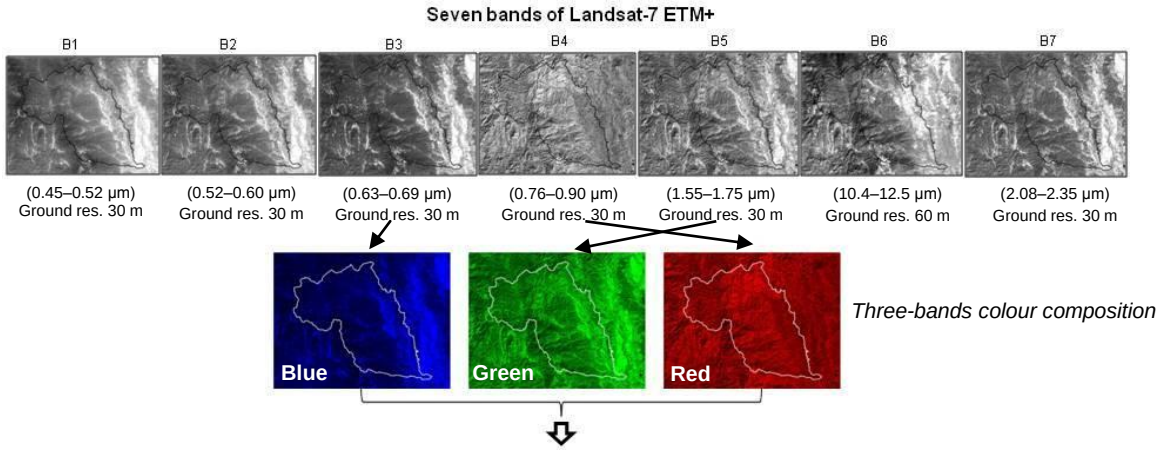

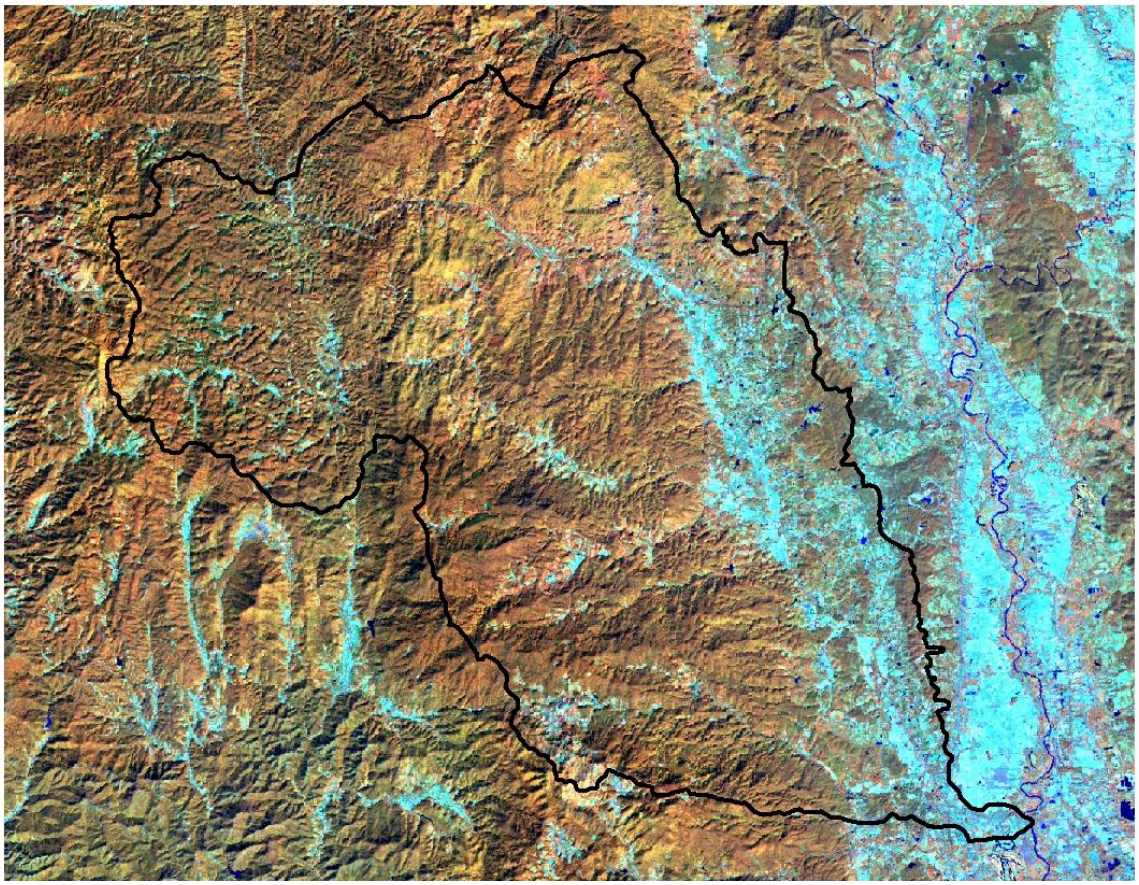

Figure 3.8 The false colour composite of Landsat-7 ETM+, band 354/BGR. (Source: Elaborated by the author based on data from the Geo-Informatics and Space Technology Development Agency (GISTDA), Thailand)

II. Training sites and samples – Training sites are areas of known land use/cover types determined based on available ground truth in the field or from inspection of aerial photographs (Hill *et al*., 2003). This thesis has generated training sites in order to define the spectral classes (signatures) and to check the reference data on ground truth, matching with the FCC (354/BGR) image for land use classification. All pixels in the image were compared to the spectral signatures of each cover and assigned to the cover classes considered based on classification scheme devised by Anderson *et al.* (1976). Consequently, the land use and land cover classification for 2009 has comprised five major classes (agriculture, bare/ fallow lands, forest, urban/ built-up areas and water body), including seven suborders as shown in Table 3.3.

Table 3.3 Classes used in land use/cover classification.

Major classes	**Minor classes**
A: Agriculture	A1: Annual field crop A2: Mixed orchards A3: Paddy fields
B: Bare/ Fallow lands	
F: Forest	F1: Evergreen forest F2: Deciduous forest
U: Urban/ Built up areas	U1: Urban area, city, town, commerce and services U2: Local villages/ communities
W: Water body	

For the training samples, this thesis used a stratified random sampling technique of known identity, spreading throughout a watershed within the training area. The strategy of sampling started to randomise the samples in the main classes first, and then considered random sampling in the minor classes (see Table 3.3). Moreover, the appropriate sample size in this fieldwork research was considered according to Lillesand and Kiefer (2002), who suggest that a minimum of 10*n* to 100*n* pixels be part of training areas (where *n* is the number of spectral bands). Also, Jones and Vaughan (2010) insist that 'the numbers of the order of 10*n* are preferable to allow good estimates of the variance and covariance properties of each class' (Jones and Vaughan, 2010, p. 189). Since Landsat TM/ETM+ imagery has seven bands, the requirement for sample size of the fieldwork data collection is therefore roughly 70 to 700 pixels per class. The number of polygons drawn for each information class is a minimum of 5–10 vector polygons (Gao, 2009).

III. Classification – At this stage, the maximum likelihood supervised classification technique was employed, using the training sites by means of estimating means and variances of the different classes, and hence to calculate the probability of any pixel falling in the given class (Perumal and Bhaskaran, 2010). The pixels were then assigned to the class with the highest probability or labelled as 'unclassified' if the probability values were all below a threshold set by the user (Ahmad and Quegan, 2012). Basically, the maximum likelihood classifier delineates ellipsoidal 'equiprobability contours' through a scattergram where the contour lines are associated with the probability of a pixel value being a member of one of the classes (Lillesand and Kiefer, 2002) (Figure 3.9).

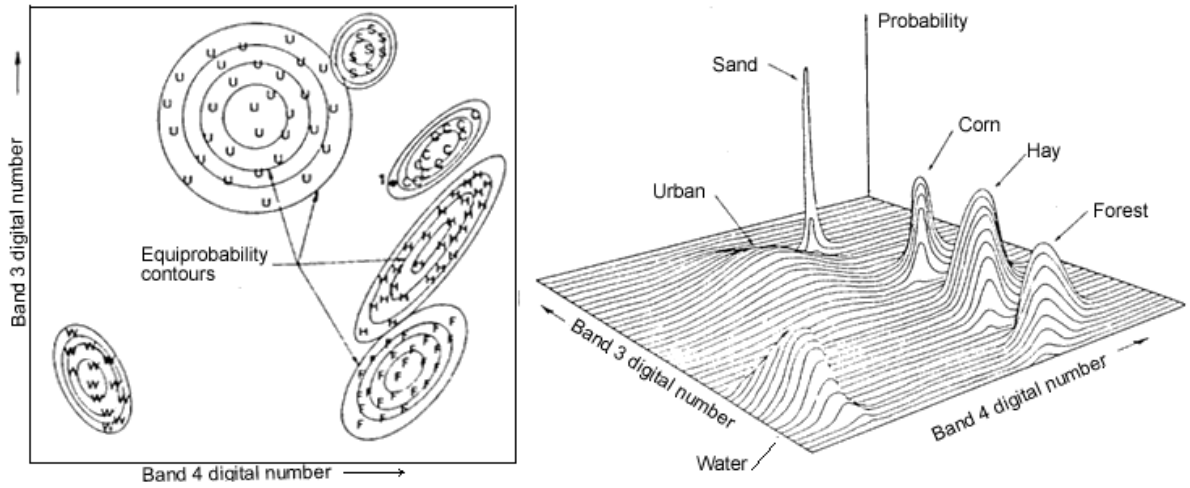

Figure 3.9 Equiprobability contours defined by a Maximum Likelihood Classifier. (Source: Adapted from Lillesand and Kiefer, 2002)

IV. Accuracy assessment – This final stage is essential to calculate the classification accuracy using an error matrix. The error matrix is the most common way to represent the classification accuracy of remotely sensed data. This method has been recommended by many researchers and should be adopted as the standard reporting convention (Congalton, 1991). A measure of overall behaviour of the maximum likelihood classification was determined by the overall accuracy, which is the total percentage of pixels correctly classified (Ahmad and Quegan, 2012). It can be computed as equation [3.1]. The second measure of classification accuracy, Kappa coefficient ($\hat{k}$), as expressed in equation [3.2], is the more discerning statistic parameter for comparing the accuracy of different classifiers, and offers better interclass discrimination than the overall accuracy measure (Gao, 2009).

$$\text{Overall accuracy (\%)} = \frac{\text{Sum of elements along the major diagonal}}{\text{Total number of reference pixels}} \text{ x } 100 \qquad [3.1]$$

$$\text{Kappa coefficient } (\hat{k}) = \frac{\Sigma_{i=0}^{n}(X_{ii} - \Sigma_{ci}\Sigma_{ri})}{N^2 - \Sigma_{i=1}^{r}(\Sigma_{ci}\Sigma_{ri})} \qquad [3.2]$$

Where *r* = number of rows and columns in the error matrix; X_{ii} = number of observations in row *i* and column *I*; $\sum_{ci} =$ marginal total of column *i*; $\sum_{ri} =$ marginal total of row *i* and *N* = total number of observations.

3.5.2 Data collection based on field reconnaissance survey

The 'vulnerable areas' connecting to soil erosion risk, such as gully erosion, bank erosion and unpaved roads, can be obtained from the field reconnaissance-based techniques. All of them were preliminarily surveyed and collected in the point-coordinates throughout the watershed using a portable GPS Magellan Triton 2000, which provided 3-metre accuracy (Magellan, 2013). In terms of gully, it was defined as 'the erosion process whereby runoff water accumulates and often recurs in narrow channels and, over short periods, removes the soil from this narrow area to considerable depth' (Poesen *et al*., 2003, p. 92). In addition, Tuckelboom *et al.* (2008) describe the gullies as recently developed drainage lines of ephemeral streams with steep-side channel banks. For implications for agricultural land, gullies are channels too deep to improve with normal tillage equipment, ranging from approximately 0.5 to 30 m depth (Poesen *et al*., 2003). Hence, this study has randomly collected the geo-position data (i.e., UTM coordinates) of gullies throughout the watershed as much as possible (Figure 3.10). Other linear landscape elements (channel depths >0.5 metres) possibly assumed to form gullies (e.g., ephemeral

streams, drill lines, dead fallows, and headlands) were also detected if applicable. In addition, the potentially vulnerable areas for gully erosion were additionally estimated at the locations using a simple GIS model. Regarding this case, it was assumed that every ephemeral stream at slope gradient exceeding 60% (very steep slope) can potentially develop to be an ephemeral gully (Turkelboom *et al.,* 2008). Consistent with Allen *et al.* (2008), approximately 50% of the sloping topography was highly correlated with all of gullies.

(a) Rill erosion at hill slope (slope angle: 22°)
UTM-X: 469718, UTM-Y: 2114160
Altitude: 857 m a.s.l.

(b) Gully erosion at hill slope (slope angle: 30°)
UTM-X: 482177, UTM-Y: 2088648
Altitude: 610 m a.s.l.

Figure 3.10 Rill and gully erosion in the Mae Rim watershed, NW Thailand. (Source: Field survey, taken on 26 July 2010).

In case of eroded riverbanks, the perennial river and its tributaries were specially observed when the streams had obviously exposed evidence of riverbank erosion (Figure 3.11). Furthermore, the potentially vulnerable areas for riverbank erosion had also been additionally estimated by applying a simple

GIS model. The potentially vulnerable area of river bank erosion was also estimated by buffering approximately 100 metres of distance from the two sides of the perennial stream line. A higher preference is given to rivers and tributaries that could have the potential for erosion and producing sediment fluxes downstream (Baird, 2007; Lorz *et al.,* 2010).

(a) Riverbank erosion at the Nam Mae Ram (A tributary of Mae Rim River) UTM-X: 492955, UTM-Y: 2093656 Altitude: 229 m a.s.l.

(b) Riverbank erosion at the Mae Rim River UTM-X: 488860, UTM-Y: 2099973 Altitude: 342 m a.s.l.

Figure 3.11 Riverbank erosion in the Mae Rim watershed, NW Thailand. (Source: Field survey, taken on 27 August 2010).

Regarding unpaved roads, they were mainly found in highland of the north-western of Thailand. Ketcheson *et al.* (1999) (cited in Fu *et al.*, 2010, p.2) stated that 'the surface of the unpaved road is generally the dominant source of sediment and much more common than mass wasting.' Additionally, Ziegler *et al.* (2000) found that unpaved roads in mountainous north-western Thailand produced as much as 80% runoff after rainfall was supplied at a very high rate of 105 mm hr^{-1} during 45-min simulations. Hence, the loose surface roads

delineated on the topographical map scale of 1:50,000 have been checked with the ground truth survey. Similar to the potential gully generation using the simple GIS model (Figure 3.12), the vulnerable unpaved roads were created by assuming that every unpaved road located on a very steep slope (slope gradient > 60%) can potentially cause soil erosion.

Topographical map scale 1: 50,000

(a) An unpaved road at altitude of 496 m a.s.l. (Location: UTM-X 481923, UTM-Y 2113469)

(b) An unpaved trail at altitude of 941 m a.s.l. (Location: UTM-X 479806, UTM-Y 2096183)

Figure 3.12 The unpaved road and trail in the Mae Rim watershed, NW Thailand. (Source: Field survey, taken on 8 August 2010).

3.6 Data analysis processes

This section is to explain in brief the processes of data analyses involved in implementing the three main result chapters of this thesis. Elaborate data analysis descriptions have then been supplemented in each results chapter.

The data analysis processes are divided into three parts: Part I (Chapter 4): data analysis process of estimating soil loss rates and generating a spatial distribution of soil erosion risk; Part II (Chapter 5): data analysis process of predicting suspended sediment yields using sediment rating curve technique and the RUSLE model in conjunction with two different concepts (i.e., the sediment transport capacity, STC; the spatially interpolation of sediment delivery ratio, SISDR); and Part III (Chapter 6): data analysis process of examining the potential effects of changes in land use and rainfall on soil erosion.

Part I: Data analysis process of estimating soil loss rates and generating a spatial distribution of soil erosion risk.

The RUSLE-GIS based model has been used as a tool for assessing mean annual soil loss rate at hill slope of a studied watershed and also generating a spatially distributed soil erosion risk. The six key controlling factors of RUSLE including rainfall-runoff erosivity, soil erodibility, slope length, slope steepness, cover management and supporting practice were used to calculate, depending on where the modelled area is located and what data was available. In this

thesis, the rainfall erosivity map (R) was generated by examining relations between the EI_{30} for Thailand (LDD, 2000) and the Modified Fournier Index (MFI) (Renard and Frimund, 1994) in addition to altitudes and geographical coordinates (latitude and longitude) of eleven rain-gauge stations located in and surrounding the study watershed area. All of the relationships were tested through multiple regression analysis in order to develop the 'best-fit' equation for predicting rainfall by forcing particular (independent) factors (i.e., altitudes, latitude and longitude). Once the best-fit equation was generated, the spatially-distributed rainfall erosivity map was therefore originated (see also Section 4.2.2). The soil erodibility map (K) was generated by assigning the soil erodibility values to the soil map of the watershed. The erodibility values used have been examined and estimated based on a mathematical approximation of soil erodibility nomograph by experts of the Land Development Department of Thailand (see also Section 4.2.3). The slope length and steepness map (LS) was generated based on equations proposed by Desmet and Govers (1996). This equation needs flow accumulation and slope angle in degrees for the calculation; both flow accumulation and slope degree can be derived from analyses of a digital elevation model (DEM) (see also Sections 4.2.4 and 4.2.5). The land use/cover map obtained from interpreting Landsat-7 ETM+ images was reassessed to generate the cover management map (C), while the support practice map (P) was used to set values ranging from 0 to 1, whereby the value 0 represents a very good man-made erosion resistance facility (e.g., built-up area and local villages) and the value 1 represents no man-made erosion resistance facility. For the P factor in Mae Rim, it has not been established for

all agriculture cover types except for paddy fields. Based on Ongsomwang and Thinley (2008), the P value for paddy field was set to 0.1 (see also Sections 4.2.6 and 4.2.7).

After accomplishing six thematic maps based on investigating six controlling factors, they were then overlaid to generate a map that indicates the rates of mean annual soil loss and spatially distributed areas vulnerable to soil erosion within the watershed (Figure 3.13).

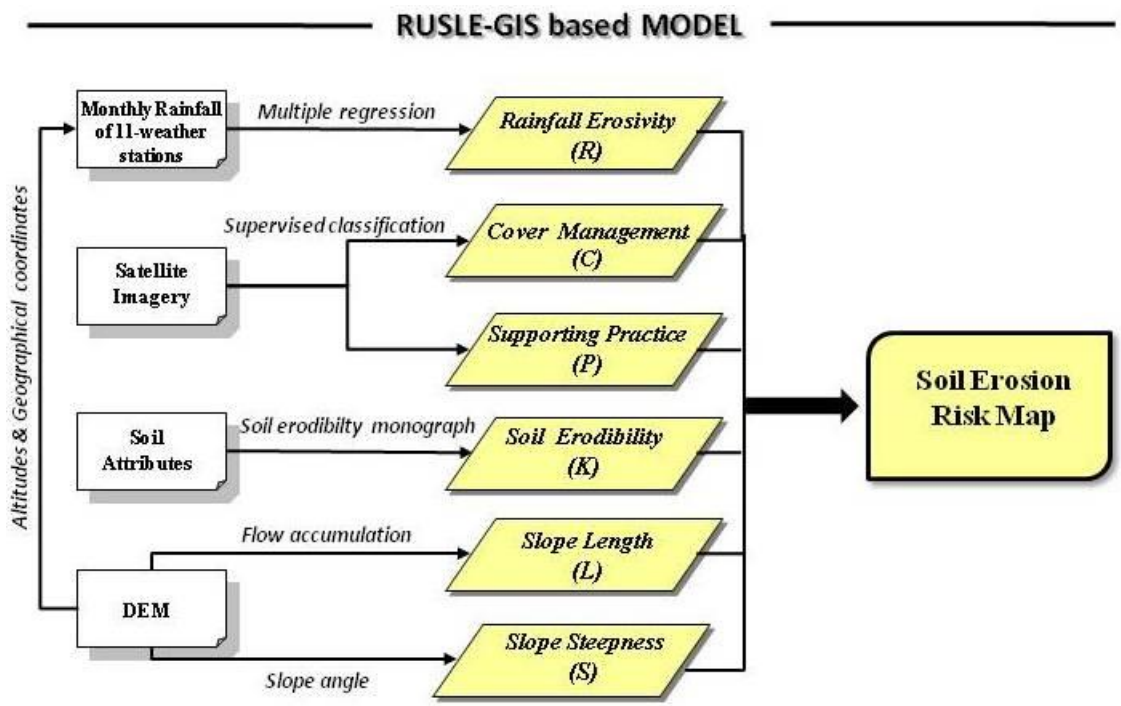

Figure 3.13 Conceptual frameworks of soil erosion rate estimation and soil erosion risk map generation based on six controlling factors of RUSLE model.

In addition, after generating the spatial variation of soil erosion risk map, the extremely severe soil erosion (erosive magnitude > 150 tonnes/ha/yr) predicted on the map was then been specifically investigated in order to prove the reliability of prediction of using model. Regarding this process, they were taken to compare and recheck with the ground truth data as well as vulnerable areas generated by applying the GIS technique.

Part II: Data analysis process of predicting suspended sediment yields using sediment rating curve technique and the RUSLE-GIS based model in conjunction with two different concepts (i.e., the sediment transport capacity and the spatially interpolation of sediment delivery ratio).

To study and predict suspended sediment yield (SSY) using the sediment rating curve, the suspended sediment concentration (SSC), suspended sediment load (SSL) and daily river discharge (Q) obtained from eight flow-gauge stations of watersheds in the Upper Ping River Basin were analysed and the relationships between SSC–Q and SSL–Q plotted. In addition,

In terms of predicting the SSY using the RUSLE model in conjunction with the STC concept, a map of soil loss rate estimated by the RUSLE-GIS-based model has been integrated pixel by pixel to the STC map. If the differentiation of the STC pixel value was smaller than the sediment flux reaching that pixel, the deposition was modelled. Nevertheless, if the differentiation of the STC pixel

value was more or equal to the sediment flux reaching that pixel, the sediment yield was modelled (see also Section 5.2.4).

For the SDR concept, the average slope gradient in % for each cell in the flow path generated from the DEM has been computed. Then, the SDR concept recommended by Onyando *et al.* (2005) and Hui *et al.* (2010) (see also Section 5.2.5) has been applied to develop a map, named 'spatial interpolation of SDR' or 'SISDR', by adopting the kriging interpolation technique in ArcGIS.

Moreover, the predicted sediment yields derived from the two different models, RUSLE–STC and RUSLE–SISDR, have also been taken to compare the efficiency and effectiveness between models. Nash and Sutcliffe's model efficiency (NSME) and the relative root mean square error (RRMSE) have been employed in this study for testing model validation.

Part III: Data analysis process of examining the potential effects of changes in land use and rainfall on soil erosion.

In terms of studying land use change affecting soil erosion, the land use maps between 1989 and 2009 classified from Landsat-5 TM and Landsat-7 ETM+ using the supervised maximum likelihood method, have been combined to generate a land use change map spanning the past 20 years for the Mae Rim watershed. In order to investigate the potential effects of land use change on

soil erosion, the generated land use change map has then been used to overlay again with the soil erosion risk map for 2009 (see also Section 6.2.1).

In terms of studying effects of changing rainfall erosivity on soil erosion, a map of rainfall erosivity change between 1989 and 2009 (derived from overlaying map operation in ArcGIS) has been used to combine with a soil erosion change map covering the same time frame. Moreover, in the final step of the rainfall erosivity analysis approach, the spatial relations of rainfall erosivity change and land use change have been taken to integrate with soil erosion change again by using GIS for assessing the spatial interconnection of both effects (rainfall and land use) on soil erosion in the study watershed area (see also Section 6.2.2).

The sensitivity analysis of soil erosion risk scenarios has been finally provided for examining relative effects of climate change and land use change. The two key controlling variables of the RUSLE model, rainfall erosivity (R) and cover management (C), were used to test various assumptions that are expected to occur in the future, while other variables of the RUSLE model (i.e., K, L, S and P) are unaltered. The sensitivity analysis approach has been additionally displayed in section 6.2.3 in more detail.

3.7 Chapter summary

This chapter has presented the research design of the thesis, which showed how the approaches for result chapters fit together. The study area context as well as site selection of the thesis together with the location, climate, hydrology and soil have been specifically characterised and discussed. The fieldwork data collected based on remote sensing method and field reconnaissance survey have been thoroughly elucidated, as well as the process of data analyses involved in implementing the three main result chapters (i.e., Chapters 4–6) of this thesis has been explained in brief. The next chapter estimates soil loss rate and generating a spatial distribution of soil erosion risk in the Mae Rim watershed, Northwest Thailand, to address the first research objective.

CHAPTER 4: SPATIAL VARIATIONS IN SOIL EROSION RISK IN MAE RIM WATERSHED USING RUSLE-GIS BASED MODEL

4.1 Introduction

Soil erosion is an environmental hazard that exposes negative effects and plays an important role as an obstacle to sustainable development. According to the Land Development Department (LDD) of Thailand, approximately 33% of the 51.3 million ha of the total geographical area is moderately to severely eroded. Suspended sediments from all watersheds in Thailand are estimated to be 27 million tonnes annually. About 12% of the total eroded land is under very severe erosion conditions and primarily under (upland) field crops with shifting cultivation (Babel *et al*., 2004).

The Mae Rim watershed is a tropical mountainous watershed situated in Northwest Thailand. This thesis has chosen the Mae Rim watershed as a case study under consideration for several reasons (see Section 3.2), which can be useful guidelines for decision makers or stakeholders for further planning and management practice.

However, the actual factors causing soil erosion in the Mae Rim watershed are poorly understood; in fact, there is still doubt about which key correlative factors (e.g., rainfall, soil composition, topography and land use) are significantly

associated with soil erosion production. Hence, this chapter aims to use the GIS-based RUSLE model to estimate soil erosion rate on a 25-m grid cell basis. The specific objectives of the study are to: (a) propose a multiple regression method for mapping the spatial distribution of rainfall-runoff erosivity factor of the RUSLE, based on available data for the area; (b) apply the Revised Universal Soil Loss Equation (RUSLE) with GIS in order to evaluate the potential soil loss for the Mae Rim watershed; and, (c) identify high erosion risk areas and examine the key controlling factors affecting an area of extremely severe soil erosion in the study area.

4.2 Methods and evaluations

4.2.1 Revised Universal Soil Loss Equation (RUSLE)

RUSLE is an empirically based model and is one of the most popular methods used for estimating soil erosion (Renard *et al.,* 2011). It is a very successful model due to its simplicity and the extensive database (Charlton, 2008). This model has provided a convenient tool for soil loss evaluation by taking the climate, geographical terrain, conservation support practice, soil and vegetation into consideration simultaneously (Zhou, 2008). The RUSLE can be expressed as equation [4.1]:

$$A = R \times K \times LS \times C \times P \qquad [4.1]$$

Where *A* is the computed spatial mean soil loss and temporal mean soil loss per unit area (tonnes ha^{-1} yr^{-1}); *R* is the rainfall-runoff erosivity factor (MJ mm ha^{-1} h^{-1} yr^{-1}); *K* is soil erodibility factor (tonnes h MJ^{-1} mm^{-1}); *LS* is slope length and steepness factors; *C* is cover management factor, and *P* is the conservation support practice factor.

Although the RUSLE has the same formula as its original version (i.e., USLE), it has several improvements in determining factors. These include, for instance, some new and revised isoerodent maps; a seasonal-varying approach adjusted for soil erodibility factor; a subfactor approach for evaluating the cover-management factor; a new equation, based on the ratio of rill to interrill erosion, and accommodating complex slopes, to reflect slope length and steepness; and new conservation-practice values (Renard *et al.*, 1997). However, because the 'RUSLE was originally developed for use in the USA and a majority of equations are specialised for use under American condition. Much work is now being done worldwide to adapt RUSLE to suit local conditions, resulting in new and slightly altered equations' (Dubber and Hedbom, 2008, p. 14).

4.2.2 Rainfall-runoff erosivity (R factor)

There are a lot of different ways to estimate the rainfall-runoff erosivity factor for the RUSLE. In this Chapter, two different methods are applied in order to find the best R values for the study area. From the previous studies, various methods are proposed in different areas particularly in northern Thailand (e.g., Merritt *et al.,* 1999; Bhattarai and Dutta, 2007; Tingting *et al.,* 2008; Hartcher

and Post, 2008; Krishna Bahadur, 2008; Ponsai *et al.,* 2010). For rainfall runoff erosivity factor (R), RUSLE assumes that when other factors are constant, soil losses from cultivated areas are directly proportional to rainstorm parameters. The rainfall runoff erosivity is calculated as a product of storm kinetic energy (E) and the maximum 30-minute storm depth (I_{30}) summed for storms in a year (Wischmeier and Smith, 1978). However, pluviograph and detailed rainstorm data are rarely available at standard meteorological stations (Arekhi *et al.,* 2012), and difficult to obtain in many developing countries, including Thailand. The relational equations are therefore commonly used to estimate R from the average annual rainfall (based on Wischmeier and Smith's concept), such as the following equation [4.2] which has been especially established as well as usually adopted for estimating R factor in Thailand (LDD, 2000; Kunta, 2009; Pongsai *et al*., 2010).

$$R_{THA} = 0.4699X - 12.1415 \qquad [4.2]$$

Where, RF is the rainfall runoff erosivity (MJ mm/ha/h/year) and X is an average annual rainfall (mm).

Another method applied for rainfall runoff erosivity factor estimation in this study is the Modified Fournier Index (MFI) (Arnoldus, 1980). The MFI can be expressed as:

$$MFI = \Sigma\, p^2 / P \qquad [4.3]$$

Where MFI is the Modified Fournier Index, p^2 is monthly rainfall (mm), and P is annual rainfall (mm).

Renard and Freimund (1994) proposed formulae to calculate the R factor by considering the MFI, which can be expressed as:

$$R_{MFI} = [0.07397 MFI^{1.847} / 1.72], \text{ when } MFI < 55 \text{ mm} \quad [4.4]$$

$$R_{MFI} = [95.77 - 6.081 MFI + 0.4770 MFI^2 / 17.2], \text{ when } MFI > 55 \text{ mm} \quad [4.5]$$

The Fournier Index gives indication of climatic aggressiveness, which has a high correlation with the amount of sediment washed into the stream by surface runoff (Maeda *et al*., 2010). It has also been widely applied in several studies (e.g., Irvem *et al.*, 2007; Beskow *et al.,* 2009; Rahman *et al.*, 2009).

As described earlier, two different approaches are introduced in this thesis in order to estimate the rainfall erosivity (R) factor for the RUSLE model. The first approach is the R factor applied especially for the entire area of Thailand, which is considered a regional approach, and the second is the R factor based on Modified Fournier Index (MFI), which is considered an international approach.

However, the regional approach as equation [4.2] provides the R values (R_{THA}) based on consideration of only average annual rainfall (mm), whereas the international approach as equation [4.5] includes more details, such as

seasonal periods (i.e., monthly rainfall and annual rainfall) for estimating the R values (R_{MFI}). According to Kunta (2009), seasonal changes affect MFI.

Thus, both approaches are adopted for estimating the R factor for the Mae Rim watershed in order to find the best R factor values by considering two variables (i.e., monthly rainfall and annual rainfall) in addition to the average annual rainfall variable.

From experiments, the R_{THA} and R_{MFI} based on two approaches are shown as columns 4 and 6 (Table 4.1). Both are tested by using simple linear regression. Results in Figure 4.1 show that the relationship of R factors between equation [4.2] and [4.5] are highly correlated (i.e., r = 0.99; r^2 = 0.98 and p-value < 0.001). In addition, a new equation for estimating the R factor (R_{MR}) for the Mae Rim watershed is developed as equation [4.6], with the new calculated values of the R factors (column 7 in Table 4.1).

Table 4.1 Rainfall erosivity values derived from 11 rain-gauge stations located within 30 km distance of the study area.

Rain-gauge stations	Period length recorded (year)	Mean total Annual RF (mm)	R_{THA} Eq. [4.2] (MJ mm/ha h yr)	MFI Eq. [4.3] (mm)	R_{MFI} Eq. [4.5] (MJ mm/ha h yr)	R_{MR} Eq. [4.6] (MJ mm/ha h yr)
1. Mae Rim	57	939.6	426.6	178.9	886.0	455.2
2. Mae Jo	32	1047.7	477.0	189.7	995.9	484.0
3. Mae Taeng	36	984.5	447.5	178.4	881.0	453.8
4. Samoeng	58	1152.4	525.9	201.3	1121.4	517.0
5. Gang Keud	28	1693.0	778.3	282.4	2205.6	802.0
6. MT Headwater	35	1273.3	582.4	207.7	1193.9	536.1
7. Huai Kok Ma	12	2130.5	982.6	326.1	2941.0	995.4
8. San Sai	57	1005.0	457.1	177.0	867.3	450.2
9. Phu Phing	33	1685.7	774.9	270.5	2023.3	754.1
10. Pai	51	960.6	436.4	183.8	935.5	468.2
11. Chiang Dao RI	33	1472.8	675.5	242.0	1620.6	648.3

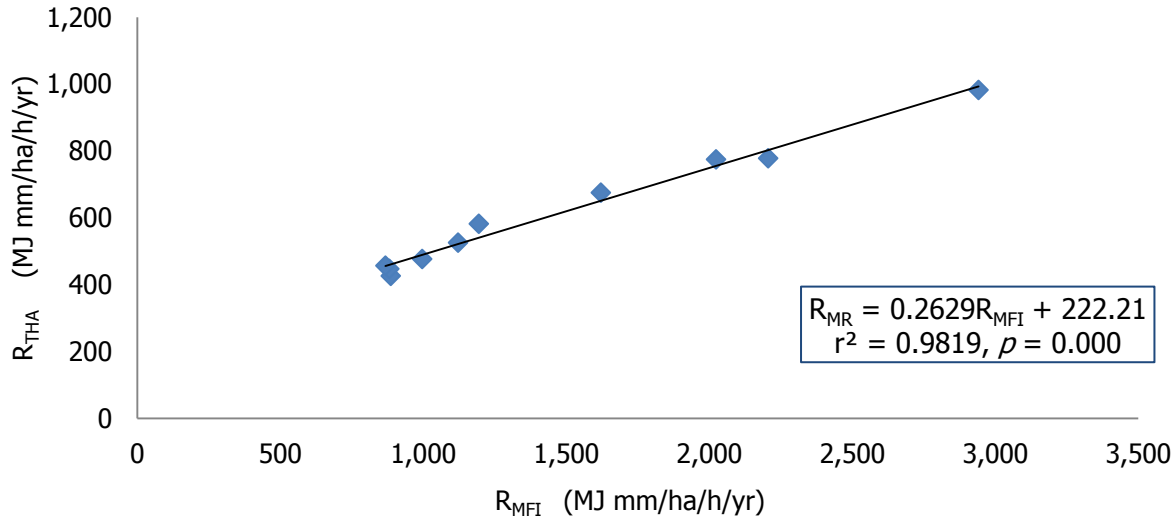

Figure 4.1 Relationships between predicted values of RF and predicted values of R_{MFI} from 11 rain gauging stations.

$$R_{MR} = 0.2629R_{MFI} + 222.21 \quad [4.6]$$

Where R_{MR} is the calibrated rainfall erosivity based on equation [4.2] and R_{MFI} is the modified Fournier index based on equation [4.5]

Given that R_{MFI} is an independent variable and RF varies based on R_{MFI}, the values of R_{MFI} from 11 rain-gauge stations were therefore taken to account again for calculating the new calibrated values of rainfall-runoff erosivity (R_{EI30}), using equation [4.6].

Evaluation of R factor

In this thesis, a rainfall erosivity map can be generated under the research assumption that the physiographical factors of landscape, such as altitude and geographical location (i.e., latitude and longitude), have significant influences on the spatial distribution of rainfall in the Mae Rim watershed. According to Marquínez *et al.* (2003), precipitation generally increases with altitude, but many authors have developed a relationship between precipitation and various topographical variables such as altitude, latitude, longitude, continentality, slope, orientation or exposure, using regression (Boer *et al*., 1993; Meusburger *et al.,* 2012; Mello *et al*., 2013).

Typically, the rainfall patterns in tropical climates include convectional, orographical, monsoonal and cyclonic rainfalls (Latrubesse *et al*., 2005). These

patterns are significantly related to altitude, latitude and longitude (Kutiel, 1988; Boer *et al*., 1993; Sepaskhah *et al*., 2007; Mello *et al*., 2013).

Altitude is an important factor controlling the distribution of rainfall as a result of orographical effect. Orographical rain is caused by moist air masses striking natural topographical barriers like mountains, which force them rising upwards, thereby cooling, condensing and falling as rain over the mountains (Thompson and Turk, 2007). This kind of rain occurs frequently for periods of over six months, from mid-May to mid-November. As a result, the windward slopes of mountain ranges in the Mae Rim watershed receive much more rain than the leeward slopes.

Latitude can also affect rainfall distribution. In particular, places located near the equator (low latitude), which are generally hot and humid, will receive more rain than places near the poles (high latitude) which lack humidity. This is because temperatures are higher near the equator, so there is more evaporation (Cunningham *et al.,* 2007). Roper (2011) points out that low latitude is related to high precipitation. According to his plots (Figure 4.2), it can be concluded that the precipitation rate (Figure 4.2a) tends to increase between latitudes of 30°S and 30°N, and reaches a peak at latitude of 10°N with a precipitation rate of 6.5 kg m^{-2} s^{-1}. However, there are minor peaks in the precipitation rate at latitudes about 50°S and 50°N. Moreover, precipitable water (Figure 4.2b) seeps off for latitudes towards the two poles. The largest amount of precipitable water is in the equatorial areas, at latitude of 5°N, where it reached a peak at 44 Kg m^{-2} in

2009. Hence, it is possible to infer that the southern areas at lower latitudes of the Mae Rim watershed at about 18°N are likely to get more rain than the northern areas at higher latitudes at about 19°N as an inverse correlation.

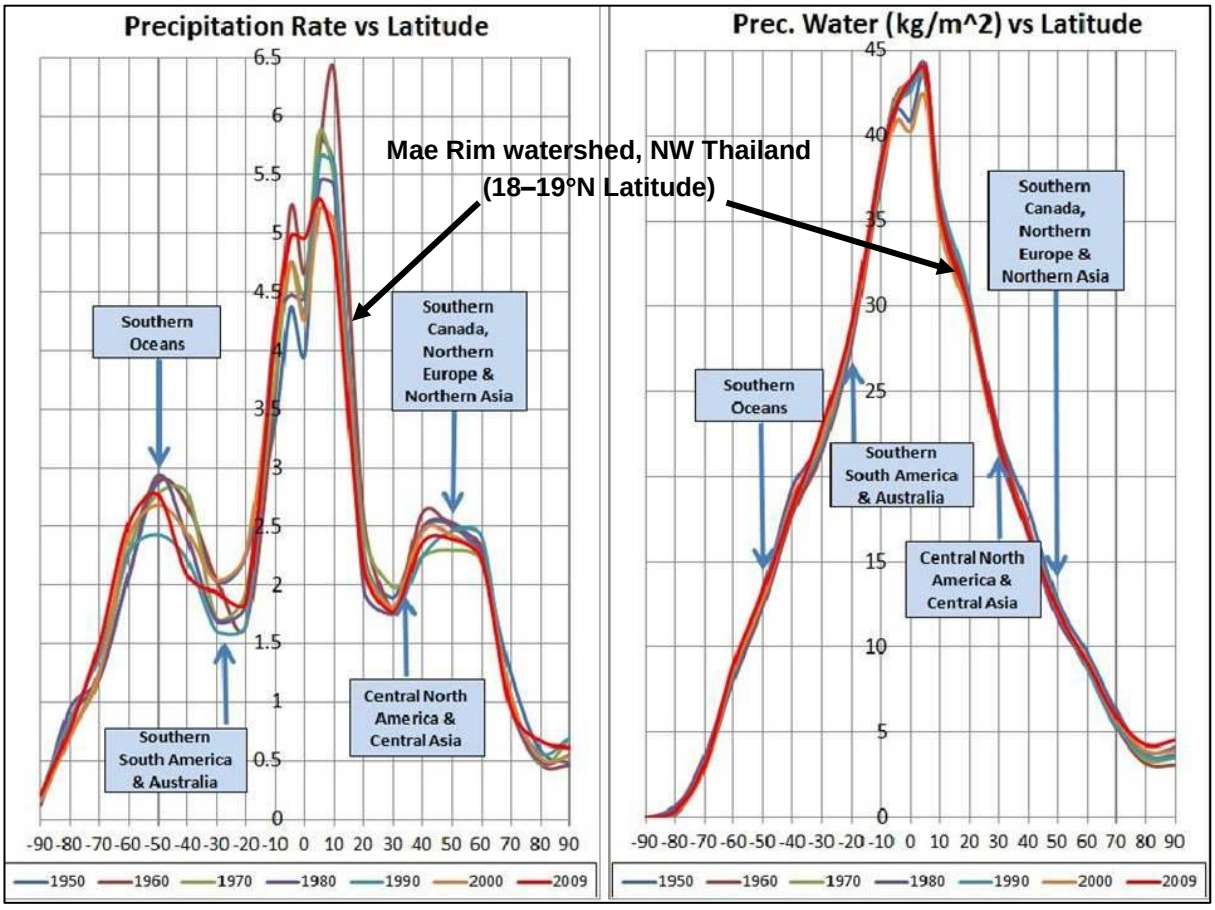

Figure 4.2 Global precipitation from 1950 to 2009 at different latitudes: (a) precipitation rate and (b) precipitable water against latitudes (Source: Roper, 2011)

Although longitude does not affect rainfall directly, the movement of air masses normally crossing over different longitudes (from West to East and from East to West) can potentially affect variations in rainfall. According to Kutiel (1988), the different longitudes of rainfall stations are represented as the distance of each station from the sea. The research of Boer *et al.* (1993) has revealed that

longitude tends to be highly correlated with summer rainfall variables. Similar to Mello *et al.* (2013), results obtained from Pearson's correlation coefficient test show that the rainfall erosivity values vary as a function of geographical coordinates, and also that the most important coefficient is associated with longitude. Therefore, in this research, it can be assumed that the rainfall measured at the various rain gauge stations situated in and around the Mae Rim watershed possibly decreases from westward to eastward due to the geographical distance (i.e., longitude) from the sea. The southwest monsoon and tropical cyclone generated from the Indian Ocean (Figure 4.3) are both major effects, causing rainfall to increase in the western areas close to the sea, rather than in the eastern areas of the watershed.

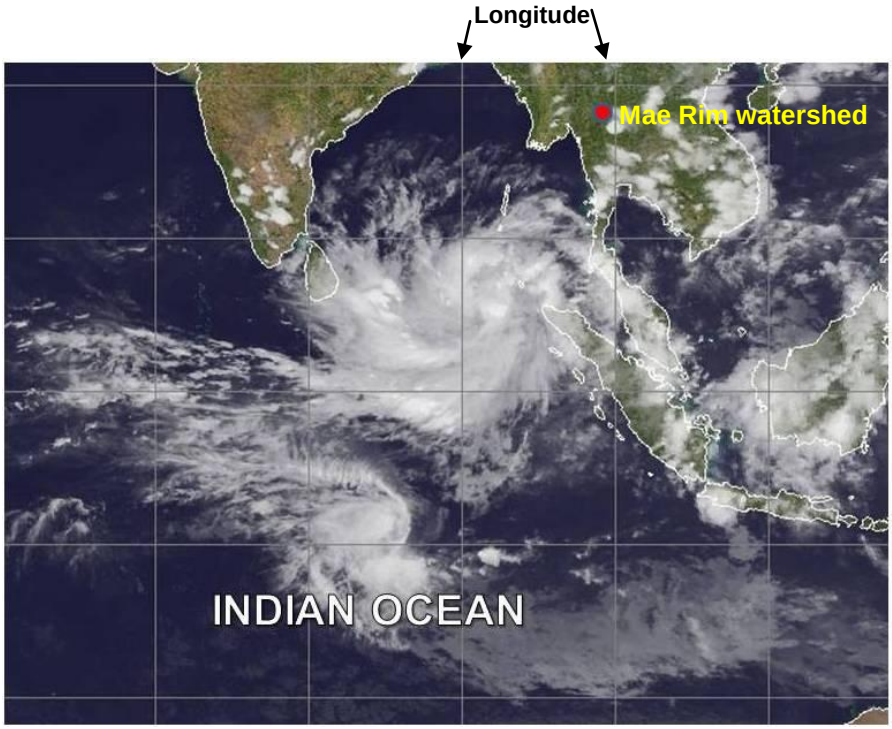

Figure 4.3 Double tropical cyclones that took place on May 10, 2013

Hence, the altitude, latitude and longitude of eleven rain gauge stations located in and surrounding the Mae Rim watershed were determined (Figure 4.4 and Table 4.2). Multiple regression analysis was then employed to test relations between independent variables (i.e., altitude, latitude and longitude) and rainfall erosivity in addition to originating new alternative equations for mapping the R factor.

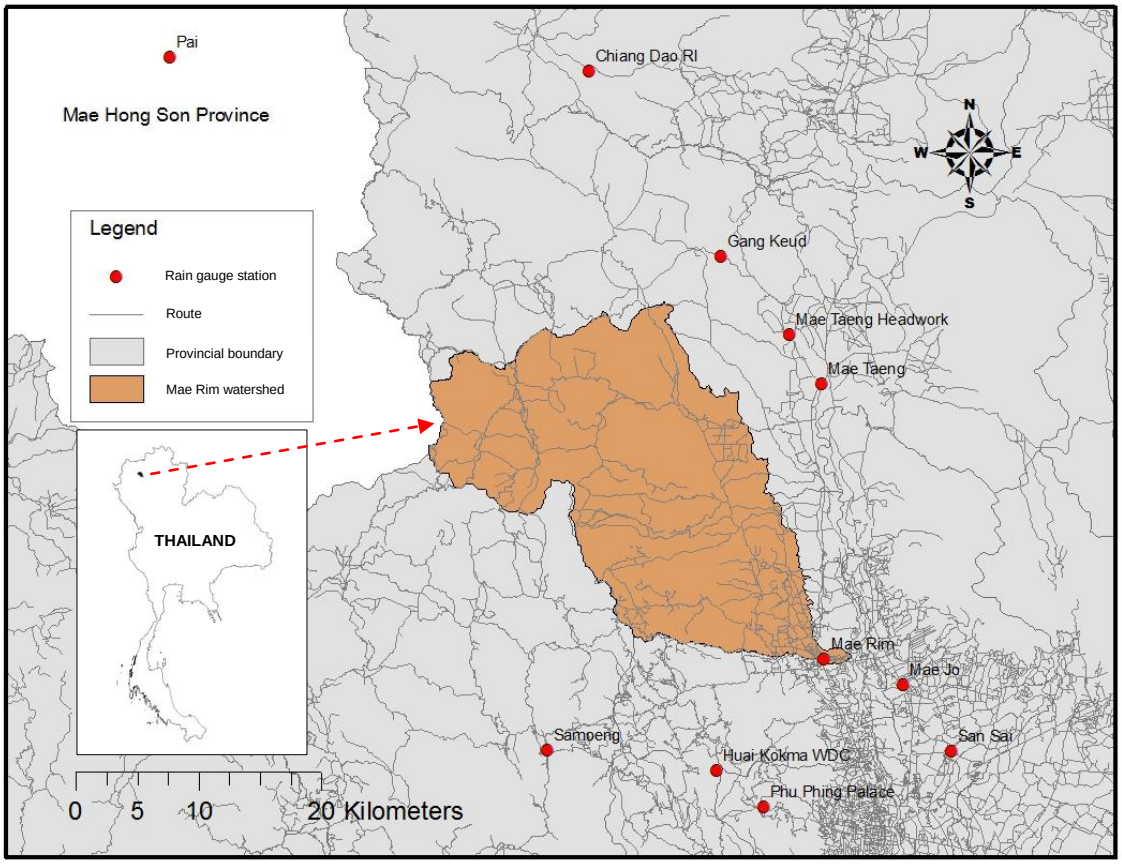

Figure 4.4 Locations of the 11 weather stations surrounding the Mae Rim watershed.

Table 4.2 Details of rain-gauge stations' locations (latitude/ longitude) and altitudes.

Rain-gauge stations	R factor (calibrated) (MJ mm/ha h yr)	Altitude (m a.s.l.)	Latitude (°N.)	Longitude (°E.)
1.Mae Rim	455.15	319.27	18.915	98.950
2.Mae Jo	484.03	317.18	18.897	99.011
3.Mae Taeng	453.82	340.00	19.118	98.948
4.Samoeng	517.01	532.26	18.848	98.736
5. Gang Keud	802.05	440.00	19.213	98.870
6. MT Headwork	536.09	360.00	19.514	98.923
7. Huai Kok Ma	995.41	1307.75	18.833	98.867
8. San Sai	450.23	305.26	18.848	99.058
9. Phu Phing	754.14	1410.60	18.807	98.903
10. Chiang Dao RI	648.26	1000.74	19.349	98.767
11. Pai	468.15	510.00	19.358	98.442

The dependent variable, RE_i, and independent (predictor) variables (i.e., altitude, latitude and longitude) in Table 4.2 are analysed in multiple regression. Ultimately, several equations generated from analyses are displayed as follows:

$RE_1 = 386.89 + 0.337Alt$ ($r = 0.77$; $r^2 = 59.5\%$; $p = 0.005$) [4.7]

$RE_2 = -147.97 + 0.342Alt + 27.92Lat$ ($r = 0.77$; $r^2 = 59.6\%$; $p = 0.027$) [4.8]

$RE_3 = -12221.72 + 0.35Alt + 127.48Long$ ($r = 0.78$; $r^2 = 60.8\%$; $p = 0.024$) [4.9]

$RE_4 = -20479.10 + 0.36Alt + 90.52Lat + 193.44Long$ ($r = 0.79$; $r^2 = 62\%$; $p = 0.066$) [4.10]

Where, RE_i is Rainfall erosivity (MJ mm/ ha h yr); Alt is Altitude (m a.s.l.); Lat is Latitude in degrees; Long is Longitude in degrees.

All equations derived from the multiple regression analysis (i.e., equations [4.7] – [4.10]) demonstrate that there are good relationships between dependent and independent variables as correlation coefficient values (r) ranged between

0.771 and 0.787. Consequently, this is consistent with the research assumption by the fact that the rainfall erosivity in the Mae Rim watershed is not only influenced by altitude, but that it also significantly depends on the geographical coordinates of the location (i.e., latitude and longitude).

For this chapter, equation [4.10] is selected to calculate rainfall erosivity values because it has a higher correlation coefficient r and r^2 than the others, i.e., r = 0.787 and r^2 = 62% (significant at 10% probability level). This corresponds to the argument of Boer *et al.* (1993, p. 612) that 'the predictor variables chosen were altitude, latitude and longitude; prior to analysis, these were centred to avoid potential numerical problems'. Similar to remarks of Meusburger *et al*. (2012), a regression model based on either only annual precipitation or altitude causes lower r^2 and heteroscedasticity of the residuals, corresponding to a non-normal distribution of them.

As a result, values of rainfall erosivity calculated based on equation [4.10] are assigned in every grid cell of the 25-m resolution DEM, and the spatially distributed rainfall erosivity map for 2009 is then generated as shown in Figure 4.5.

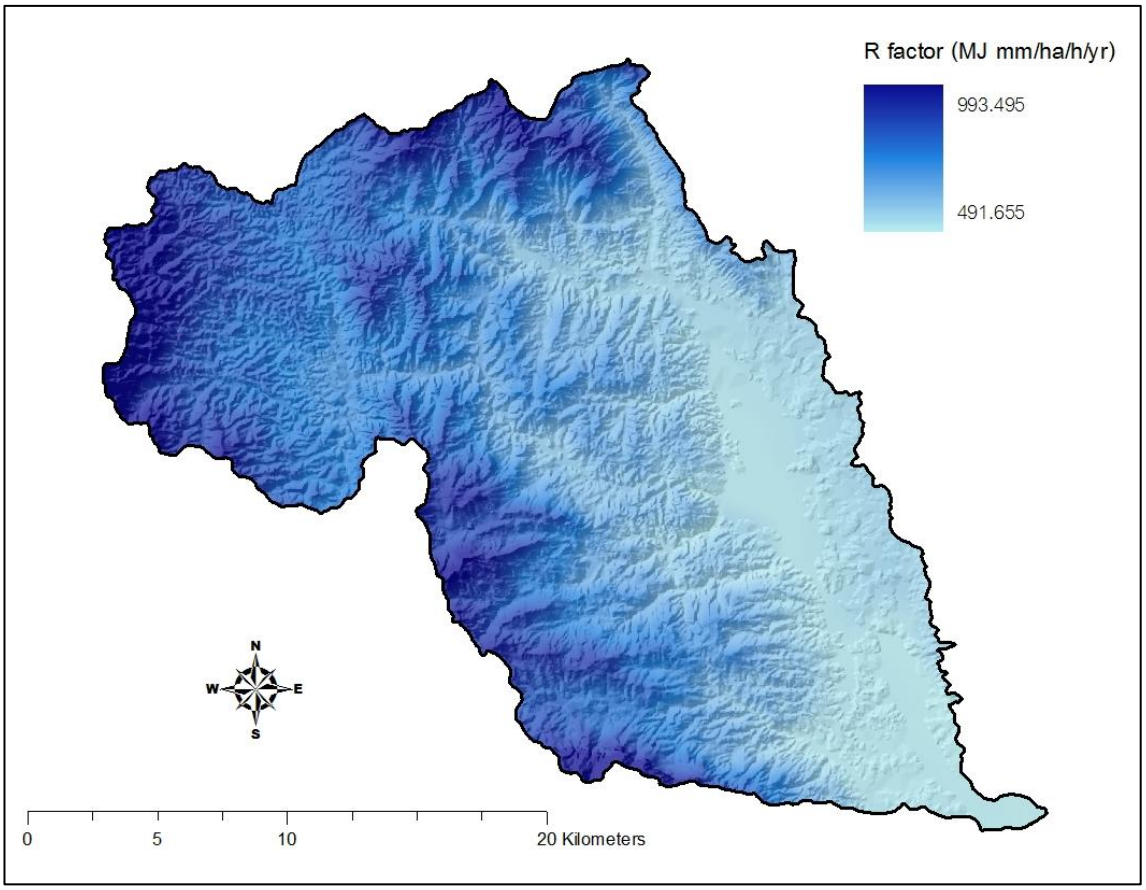

Figure 4.5 Spatial distribution of rainfall runoff erosivity on the Mae Rim watershed.

Figure 4.5 shows the spatial distribution of rainfall runoff erosivity on the Mae Rim watershed derived from the multiple regression method. The R value ranges between approximately 492 and 994 MJ mm/ha h yr, with the highest values in the western part (uplands) of the catchment and the lower values in the eastern part of the catchment (lowlands).

4.2.3 Soil erodibility (K factor)

Soil erodibility is generally recognised in hill-slope and fluvial geomorphology (Bryan, 2000). It is a main aspect of soil properties reflecting the susceptibility of soils to erosion (Wischmeier *et al.,* 1978; Song *et al.,* 2005), and is one of six

factors in the RUSLE, a most widely used model to predict long-term average annual soil loss (Wang *et al.,* 2001).

The soil erodibility (K factor) measures the inherent erodibility of soil under the standard RUSLE unit plot (22.12 m long on 9% slope with cultivation up and down the plot) (Wischmeier *et al*., 1978; Beskow *et al*., 2009). Under the unit plot circumstance, factors of slope length (L), steepness (S), cover management (C) and conservation support practice (P) equal one. It means that those factors have no influence on soil erosion on the unit plot, whereas soil erodibility (K) and rainfall-runoff erosivity (R) have units (Kinnell, 2008, 2010). As a consequence of this, the K factor will be equivalent to the ratio of the average annual soil loss to R factor, as shown equation [4.11].

$$K = A/EI_{30} \qquad [4.11]$$

Where K is the soil erodibility factor (tonnes h MJ^{-1} mm^{-1}); A is the average annual soil loss per unit area (tonnes ha^{-1} yr^{-1}); EI_{30} or R is the rainfall-runoff erosivity factor (MJ mm ha^{-1} h^{-1} yr^{-1}).

There are several methods to obtain the K values in the field site, for example:

(i) Soil erodibility nomograph method

The nomograph is developed to determine K values from soil properties (Wischmeier *et al*., 1978). The K factor can be determined by referencing a soil nomograph index where the silt fraction does not exceed 70% (Kinnell, 2010). Obtaining a value from this nomograph requires that five

characteristics of the soil are known. The relative percent of silt plus very silty sand, percent sand, percent organic matter, the soil structure and the soil permeability are looked up in a soil nomograph to estimate the K factor. The K factor is estimated through experimental equations such as equation [4.12] or the corresponding nomograph (Figure 4.6) (Wischmeier and Smith, 1978; Wang *et al.,* 2001; Lu *et al*., 2004; Schmitt, 2007).

$$K = (2.1 \times 10^{-4}) (12\text{-}OM) M^{1.14} + 3.25 (S\text{-}2) + 2.5 (P\text{-}3)/ 0.0759 \quad [4.12]$$

Where OM = % organic matter; M = particle size parameter [(%silt + %very fine sand) x 100-%clay]; S = soil structure class (1 = very fine granular, 2 = fine granular, 3 = medium or coarse granular, 4 = blocky, platy or massive); P = permeability class (1 = rapid, 2 = moderate to rapid, 3 = moderate, 4 = slow to moderate, 5 = slow, 6 = very slow).

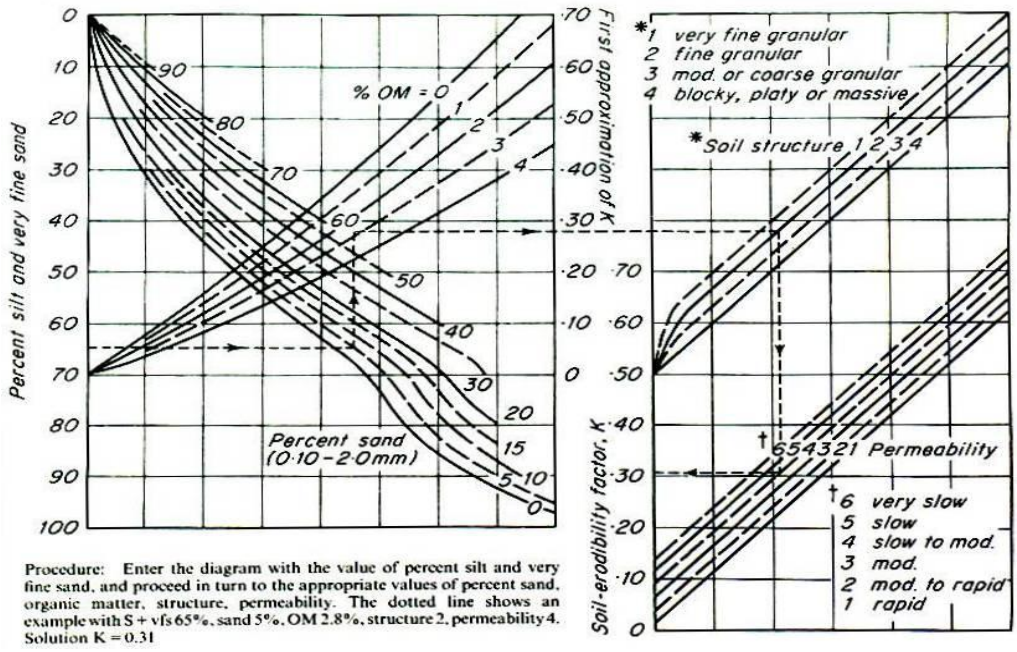

Figure 4.6 The soil erodibility nomograph (Source: Morgan and Nearing, 2011).

(ii) Williams et al.'s method

Williams *et al.* (1983) proposed a method to evaluate the K that is used in the EPIC model as expressed in equation [4.13] (Yang *et al.,* 2003). This formula was adopted in recent studies (e.g., Rahman *et al.*, 2009; Maeda *et al.*, 2010). This equation will commonly give a value ranging from 0.1 to 0.5 (Tangtham, 2002).

$$K = \frac{\{0.2 + 0.3 \exp [-0.0256Sd(1 - Si/100)]\} \times [Si/(Cl + Si)]^{0.3} \times \{1.0 - 0.25C/[C + \exp(3.72 - 2.95C)]\} \times [1.0 - 0.7(1 - Sd/100)]}{\{1 - Sd/100 + \exp [-5.51 + 22.9(1 - Sd/100)]\}} \quad [4.13]$$

Where Sd, Si, Cl and C represent sand (%), silt (%), clay (%) and carbon (%), respectively.

(iii) Shirazi and Boersma's method

Shirazi and Boersma (1984) (cited in Song *et al.,* 2005) proposed a method to calculate K value when lacking observation data, such as for soil structure and permeability (Shi *et al.,* 2004). This method can be expressed in the following equations [4.14] and [4.15] (Shi *et al.,* 2004; Märker *et al*., 2008; Xu *et al.*, 2008).

$$K = 7.594\left\{0.0034 + 0.0405\exp\left[-0.5\left((\log D_g + 1.659)/0.7101\right)^2\right]\right\} \quad [4.14]$$

$$D_g = \exp\left(0.01 \sum f_i \ln m_i\right) \quad [4.15]$$

Where D_g is geometric mean particle diameter; f_i is primary particle size fraction; m_i is arithmetic mean of the particle size limits of that size.

Evaluation of K factor

In this study, soil samples were not taken in the field because it was expensive and time consuming. Therefore, the K values used in this thesis were secondary data obtained from the Land Development Department (LDD) of Thailand. The LDD had directly observed and collected the soil samples throughout the country to examine the soil textures and properties in the laboratory and getting the calculated K values according to the mathematical approximation of soil erodibility nomograph method as shown in equation [4.12] and Figure 4.7. The K values were already provided and disseminated by the LDD for public and academic use (LDD, 2000). The LDD also provided the K values, dividing in accordance with different geographical features in each part of the country (Table 4.3). In particular, the K values of column 'N' (North) in both uplands and lowlands had been assigned by matching with the soil texture attributes contained in the existing digital (raster) soil map (scale 1: 50000) derived from the LDD.

Table 4.3 Soil erodibility in Thailand based on soil-texture classification.

Textures	K values									
	Uplands (altitude > 600 m a.s.l.)					Lowlands (altitude < 600 m a.s.l.)				
	NE	**N**	C/E	W	S	NE	**N**	C/E	W	S
Sand	-	**-**	-	0.05	0.04	-	**-**	-	0.05	0.04
Loamy sand	0.04	**0.05**	0.08	0.07	0.07	0.05	**0.06**	0.07	0.08	0.09
Sandy loam	0.29	**0.27**	0.30	0.19	0.20	0.26	**0.30**	0.26	0.34	0.30
Loam	0.29	**0.33**	0.33	0.30	0.33	0.35	**0.35**	0.43	0.33	0.34
Silt loam	0.37	**0.49**	0.56	0.21	0.40	0.34	**0.34**	0.47	0.44	0.39
Silt	-	**-**	-	-	-	-	**-**	-	-	0.57
Sandy clay loam	0.24	**0.21**	0.20	0.25	0.19	0.20	**0.22**	0.21	0.23	0.21
Clay loam	0.25	**0.24**	0.28	0.30	0.29	0.36	**0.27**	0.19	0.25	0.31
Silty clay loam	0.46	**0.35**	0.38	0.37	0.31	0.43	**0.42**	0.29	0.38	0.21
Sandy clay	-	**-**	0.15	-	-	-	**0.17**	0.17	0.18	0.18
Silty clay	0.23	**0.21**	0.26	0.19	0.22	0.27	**0.27**	0.23	0.29	0.29
Clay	0.13	**0.15**	0.14	0.12	0.11	0.15	**0.18**	0.18	0.14	0.14

(Source: Data from the Land Development Department (LDD) of Thailand)

Finally, the soil erodibility (K) map was generated by using ArcGIS 9.3 to show the spatial distribution of K factor. The soil erodibility of the Mae Rim watershed has values ranging between 0.21 and 0.35 tonnes h MJ^{-1} mm^{-1} (Figure 4.7). It should be noted that the highest value of K factor (0.35 tonnes h MJ^{-1} mm^{-1}) is a silty clay loam, which normally distributed on the upland areas (altitude > 600 m a.s.l.) and being descriped as easily eroding and moderately slow permeable soil (LDD, 2000).

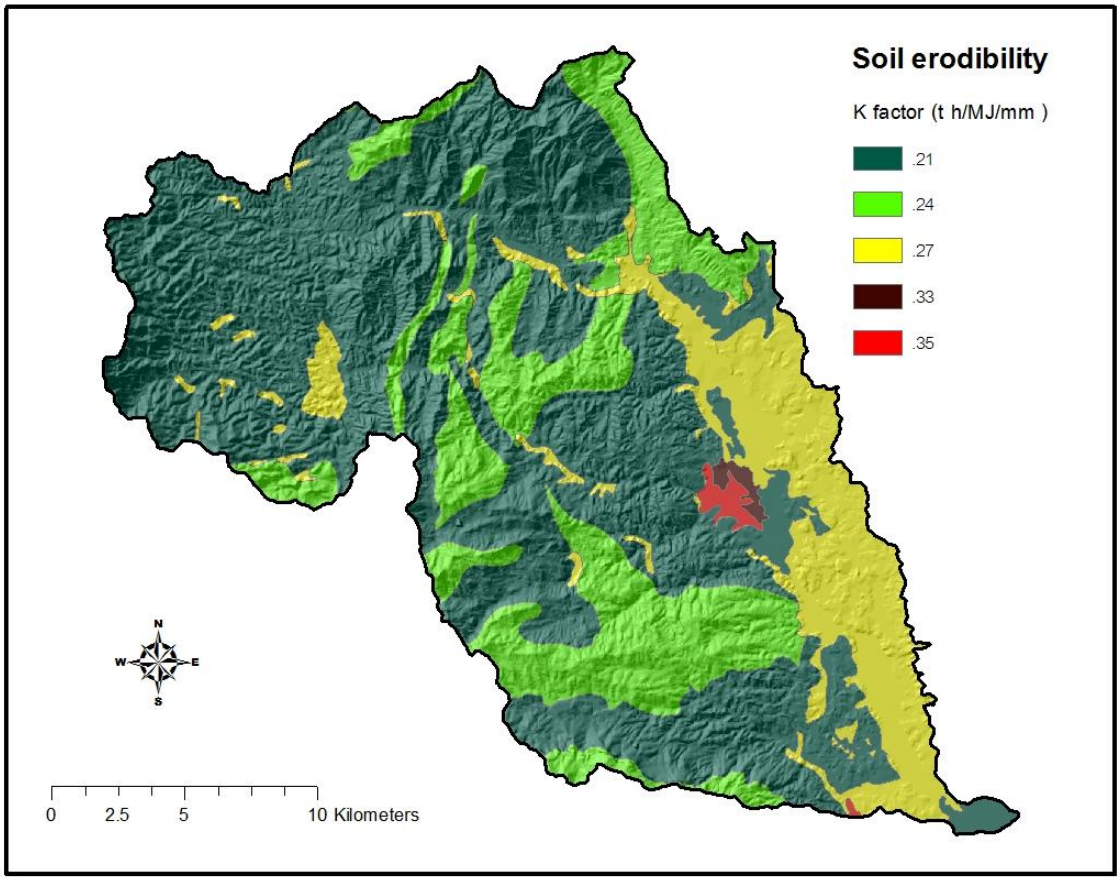

Figure 4.7 Spatial distribution of soil erodibility (K factor) on the Mae Rim watershed.

4.2.4 Slope length (L factor)

The L factor in the RUSLE is the distance from the point of origin of overland flow to the point where either the slope gradient decreases enough that deposition begins, or to where the flow connects to a river system (Wischmeier and Smith 1978; Merritt *et al*., 1999). The USLE was formulated from empirical data collected from uniform field plots with fixed parameters, referred to as the unit field plot length (22.13 m). The slope length factor is dimensionless because it is simply a ratio of the horizontal length of the actual field plot divided by the unit field plot length, raised to the exponent *m*. The L factor is defined as:

$$L = (\lambda / 22.13)^{m} \quad [4.16]$$

Where λ is the horizontal projection of slope length; exponent m is the variable slope length exponent that depends on slope steepness, being 0.5 for slopes greater than 5%, 0.4 for slopes between 3% and 5%, and 0.3 for slopes less than 3% (Wischmeier and Smith 1978; Debral *et al.*, 2008; Beskow *et al.,* 2009).

An example of hill-slope profile in Figure 4.8 shows an estimation of the slope length factor required for examining each particular hill-slope. In this case, the overland flow would begin if a large amount of water were poured onto the land surface. The slope length is measured from this point and would increase as overland flow moves further downhill. If at a certain area on the hill the slope steepness decreases considerably, it is assumed that both overland flow and sediment transport no longer occur and so sediment deposition begins. Deposition of sediment occurs when the flow can no longer maintain sufficient velocity to carry the sediment particles. The slope length measurement ends at this point. In situations where the land surface extends further downhill, the slope length calculations start again from that point of origin to where the slope profile decreases enough so that deposition occurs again (Khosrowpanah *et al.,* 2007).

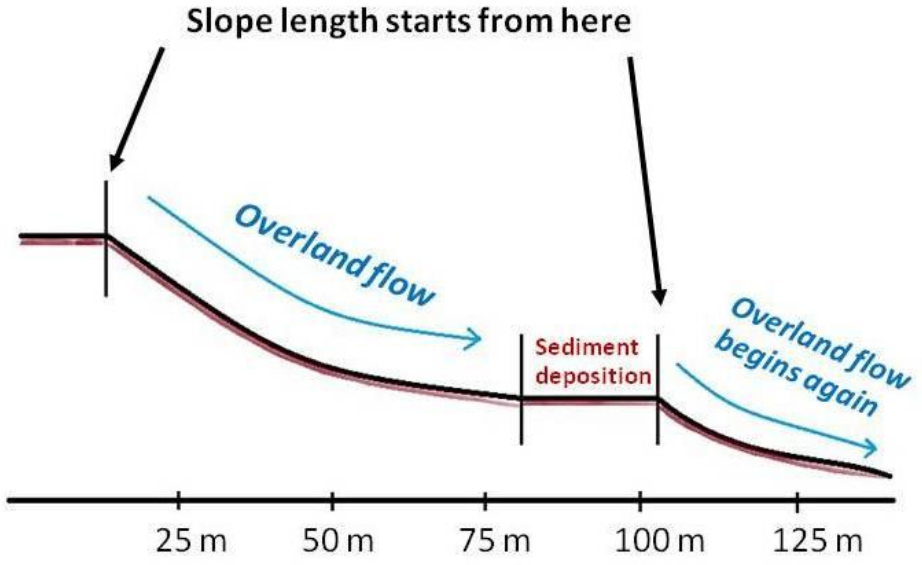

Figure 4.8 Estimation of the slope length on the example of the hill slope profile.

4.2.5 Slope steepness (S factor)

The S factor is fundamentally related to the L factor and is generally combined together in USLE calculations. When the LS factors are calculated, the corresponding equations normalize the values to the unit field plot parameters which are 22.13 m in length and have a 9 % slope, or about 5.14 degree slope angle. The original equation for expressing the slope steepness factor, S, was introduced by Wischmeier and Smith (1978) as:

$$S = 65.41 \sin^2\theta + 4.56 \sin\theta + 0.065 \qquad [4.17]$$

Where θ = slope angle in degrees.

Due to equation [4.17] over-predicting soil losses from high-gradient slopes, it has been replaced in RUSLE by McCool *et al.*'s formulae (cited in Renard *et al*., 2011, p. 144) as:

$$S = 10.8 \sin\theta + 0.03, \text{ gradient} < 9\% \qquad [4.18]$$

$$S = (\sin\theta / 0.0896)^{0.6}, \text{ gradient} \geq 9\% \qquad [4.19]$$

It should be noted that the slope is usually in degree format rather than percentage, when it is derived from DEM via GIS software (Fu *et al*., 2006).

To take advantage of DEM and GIS procedures, Desmet and Govers (1996) proposed the upslope contributing area, which is approximated simply using flow accumulation, to replace the slope's linear length (λ). Despite lots of relationships being available for estimation of LS factor, the following formula (equation [4.20]) has been widely used in several studies (e.g., Mutua *et al.,* 2006; Jain *et al.,* 2009; Terranova *et al.,* 2009; Jain and Das, 2010; Ranzi *et al*., 2011).

$$LS = (m+1)\left[\frac{A_{ij}}{a_0}\right]^m \left[\frac{\text{Sin}\,\theta_{ij}}{b_0}\right]^n \qquad [4.20]$$

Where A_{ij} (m) is upslope contributing area of a grid cell (i,j) or flow accumulation x cell size (Lim *et al.,* 2005; Fu *et al*., 2006); θ_{ij} is slope angle; a_0 is 22.1 m as a standard USLE plot length; b_0 = 9% = 5.14 degree is the slope of standard

USLE plot (Efe *et al.*, 2008); *m* and *n* are parameters obtained through calibration for a specific prevailing type of flow and soil conditions (Rodríguez and Suárez, 2010), normally ranging from 0.1 to 0.6 and from 1.0 to 1.4, respectively (Terranova *et al.,* 2009).

Although there are a variety of exponent values chosen for the *LS* equation (Table 4.4), *m* and *n* used in this study have been set up as 0.4 and 1.3, respectively, as a result of that this study area has a high variability of land cover and soil properties under which both flow types (i.e., laminar and turbulent flows) occur (Oliveira *et al*., 2013). Furthermore, for situations where the rill and gully erosion dominates (e.g., bare land and disturbed land), these parameter are usually set as *m* = 0.6 and *n* = 1.3; where the laminar erosion prevails (e.g., forested lands), the values of exponent *m* and *n* are low (i.e., *m* = 0.1 and *n* = 1) (Mitasova *et al*., 2000).

Table 4.4 The exponent values of *m* and *n* set, for LS factor equation, in different sites.

Researchers	**Parameters**		**Research area**
	m	***n***	
Mitasova *et al.* (1996)	0.6	1.3	Central Illinois and the Yakima Ridge, USA
Lim *et al*. (2005)	0.4	1.3	Sudong watershed, Korea
Mutua *et al*. (2006)	0.6	1.3	Masinga catchment, Kenya
Jain *et al*. (2009)	0.4	1.3	Himalayan watershed, India
Abu Hammad (2011)	0.4	1.3	Palestinian highland, Palestine
Krishna Bahadur (2009)	0.4	1.3	Nam Wa watershed, Thailand
Jain and Das (2010)	0.6	1.3	Haharo sub-catchment, India

Evaluation of LS factor

In this study, the *LS* factor was calculated based on the digital elevation model (DEM) at 25-m resolution. The DEM was generated from a 1:50,000 topographical map of Thailand with 20-m contour interval (Figure 4.9).

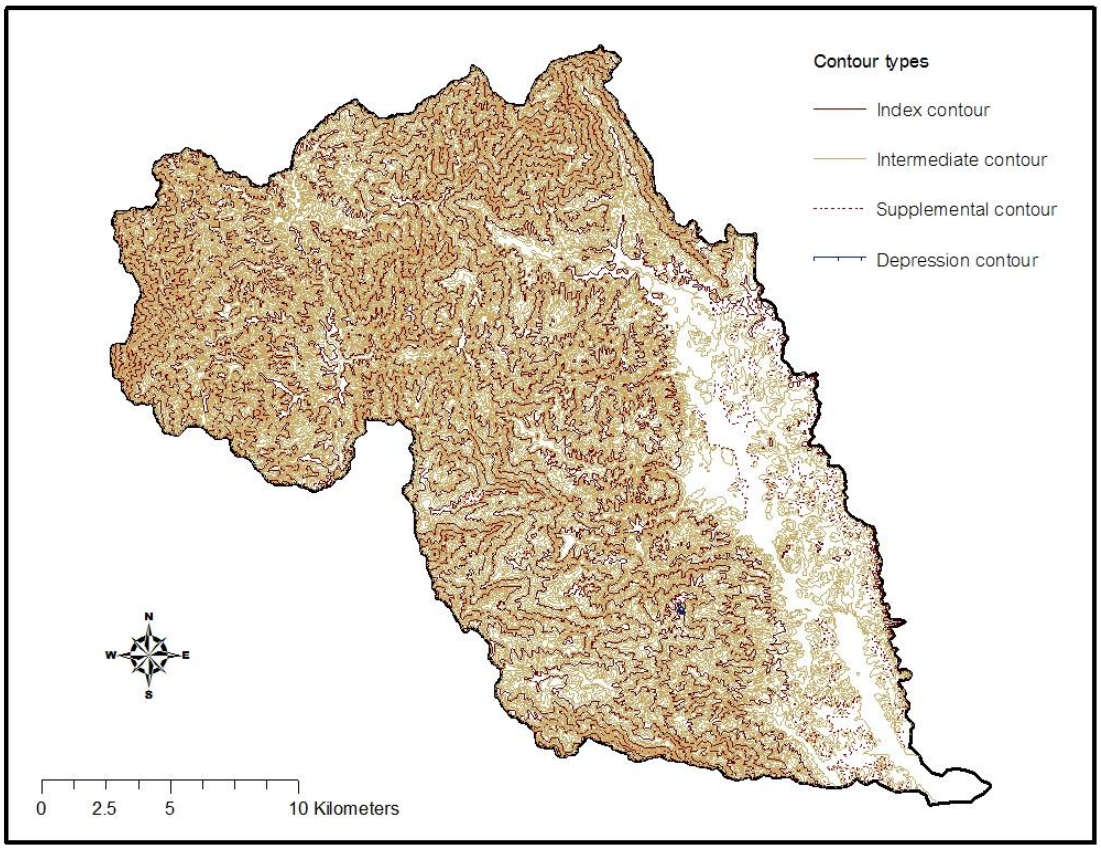

Figure 4.9 The 1:50000 scale topographical map of the Mae Rim watershed with 20-m contour interval. (Source: Data from the Royal Thai Survey Department).

The vector elevation map was initially calculated to the TIN (Triangulated irregular network). TIN is a representation of the 3D vector point file. In the next step, the TIN file was converted to a raster file with a grid cell size of 25 x 25 m, using the 3D analyst tools of the ArcGIS software, and then to a DEM (Figure

4.10). The DEM represents the surface terrain of the catchment and permits the retrieval of geographical information.

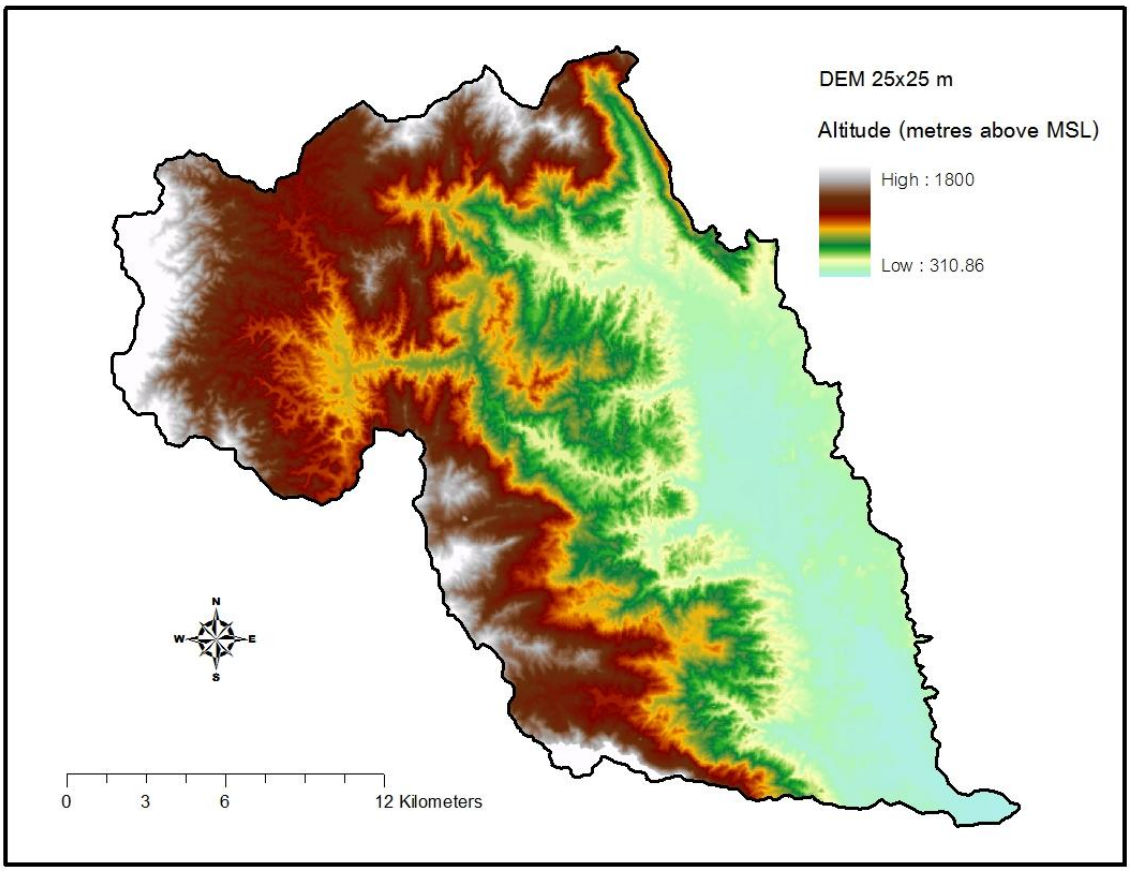

Figure 4.10 DEM; resolution 25 m.

(i) Slope length mapping

Slope length (*L*) is likely the most complex factor to estimate (Cohen *et al.,* 2005) as the slope length raster map needs to be sequentially calculated starting with DEM, flow direction and through flow accumulation. As the first step, before performing any hydrological analysis the elevation value was modified by filling the sinks in the original DEM. This was done to avoid problems such as local barriers that trap water flow for drainage network

extraction (Bou Kheir *et al.*, 2008). Also, this was done using the Fill tool under Hydrology toolbox in the Spatial Analyst of ArcGIS.

(a) Flow direction – it was generated from the Fill grid or Depressionless DEM. The flow direction tool takes a terrain surface and identifies the down-slope direction for each cell. This grid shows the on surface water flow direction from one cell to one of the eight neighbouring cells (Figure 4.11). Running the flow direction function in ArcGIS assigns a numerical value to each grid cell according to the direction of steepest descent (i.e., N, S, E, W, NE, NW, SE, SW). The raster map of flow direction of the Mae Rim watershed is illustrated in Figure 4.12.

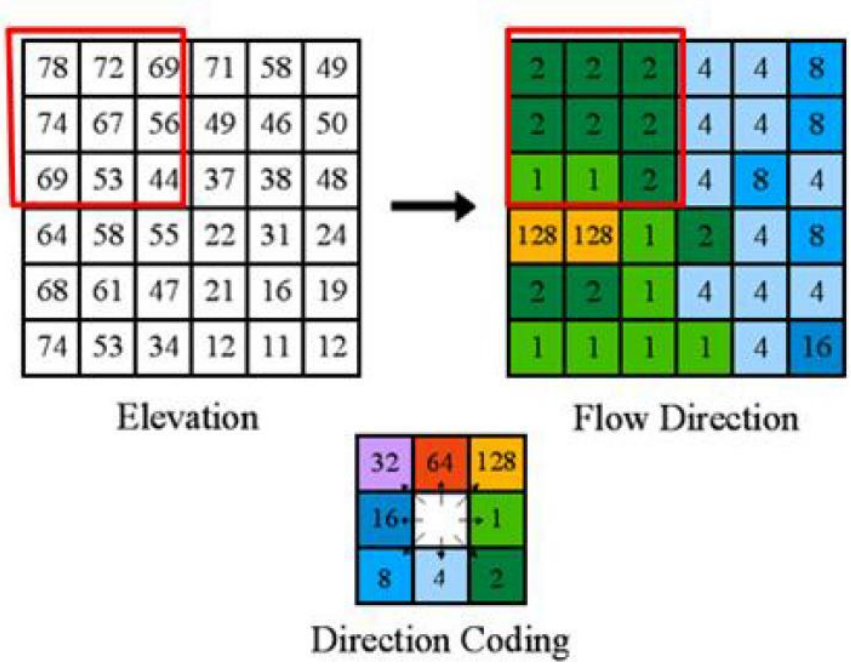

Figure 4.11 Illustration of Flow directions in ArcGIS. (Source: ESRI, 2012).

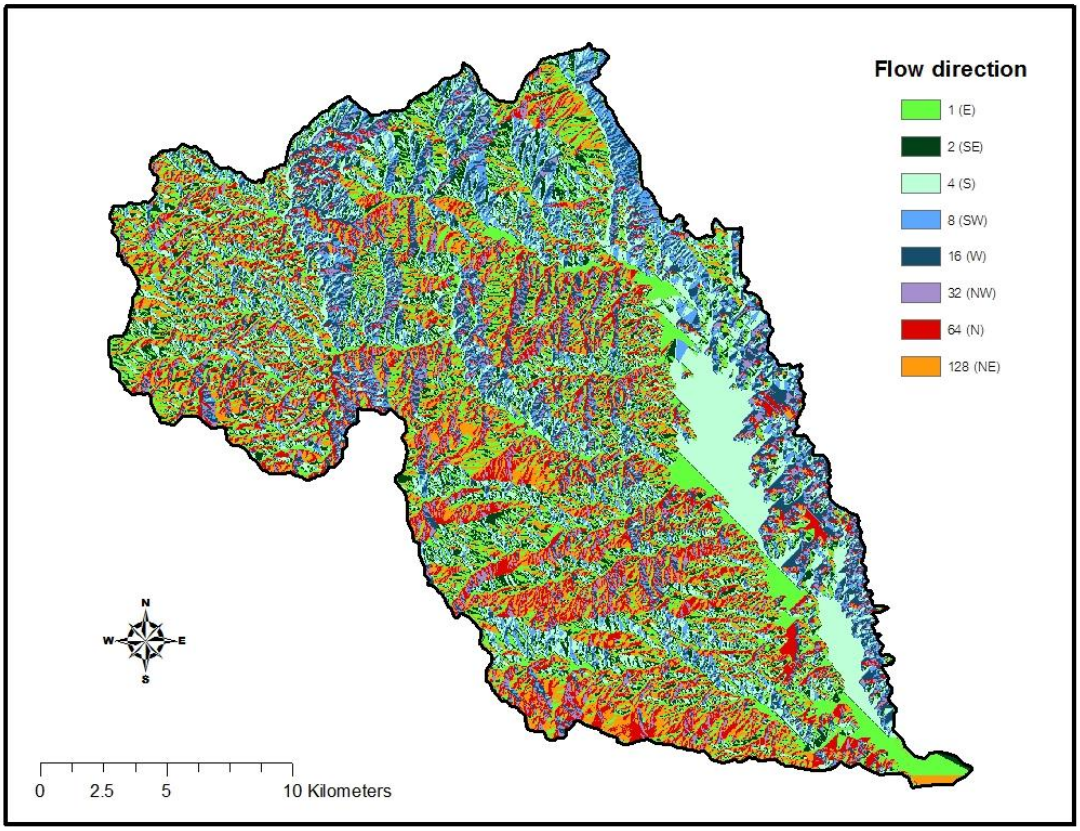

Figure 4.12 The raster map of flow directions of the Mae Rim watershed

(b) Flow accumulation – calculated based on the flow direction. The flow accumulation identifies 'the number of upgradient grid cells, or those cells that drain through a particular grid cell, and therefore the likelihood of a river existing at that cell' (Graham *et al.,* 1999, p. 583). This was done using the flow accumulation tool under the Hydrology toolbox in the Spatial Analyst Tool of ArcGIS (Figure 4.13). The raster map of flow accumulation of the Mae Rim watershed is illustrated in Figure 4.14.

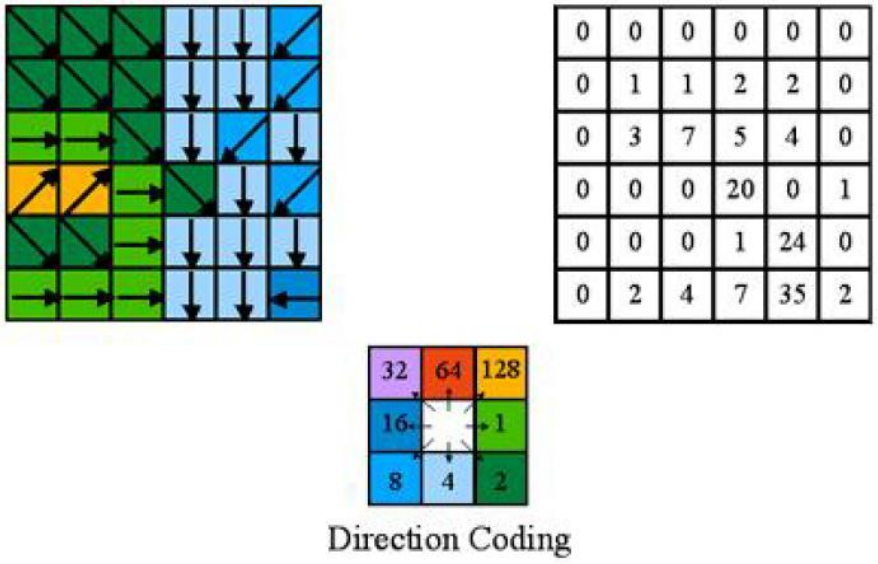

Figure 4.13 Illustration of flow accumulation in ArcGIS. (Source: ESRI, 2012)

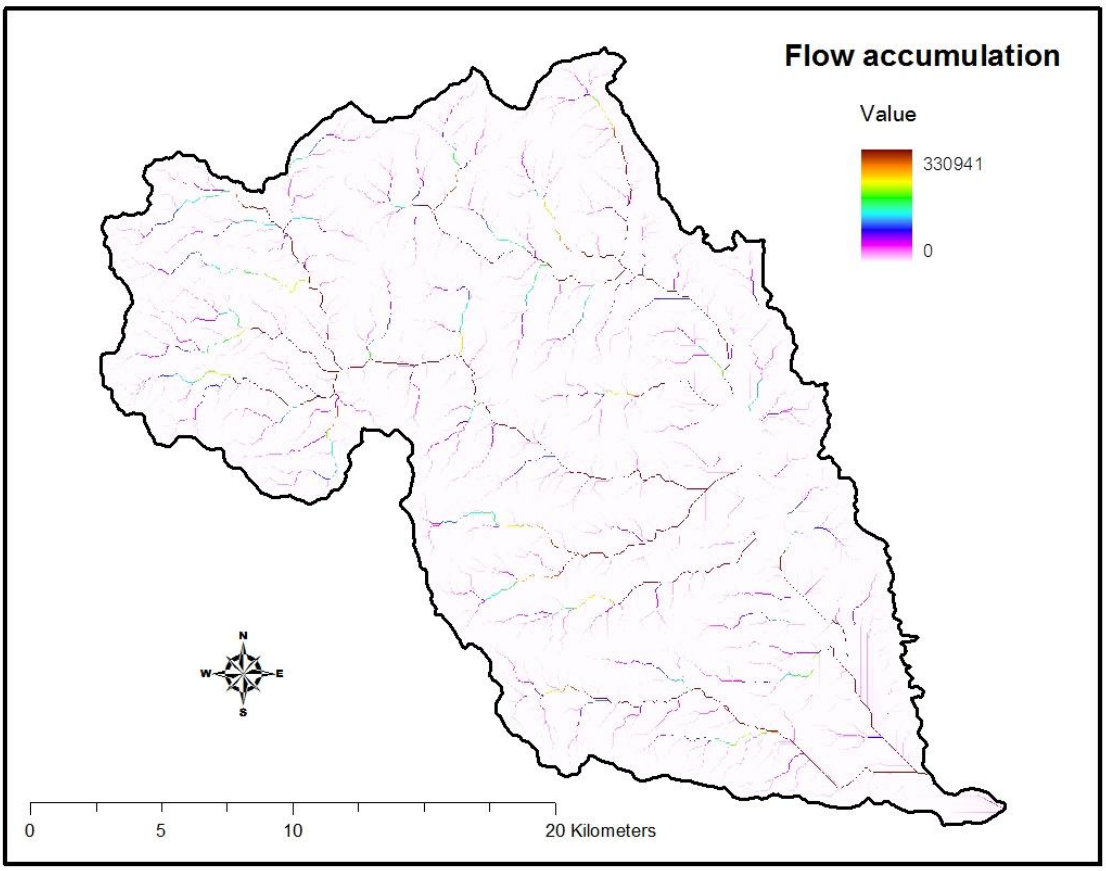

Figure 4.14 The raster map of flow accumulation of Mae Rim watershed

(ii) Slope angle mapping

The slope angle in degrees can be derived from the DEM. ArcGIS uses a specific numerical method called the 'Deterministic-8' or 'D-8' method to calculate the slope angle for each grid cell. The DEM matrix is analysed in a moving 3 x 3 window shown below (Figure 4.15). The four grid cells closest to the centre cell are weighted twice as much as the four grid cells located diagonally to the centre cell.

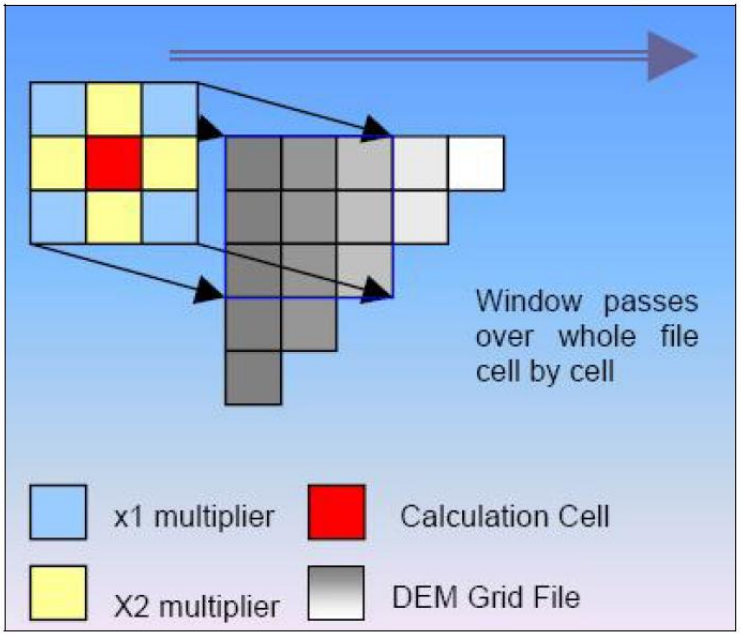

Figure 4.15 Illustration of moving 3 x 3 window (Source: Khosrowpanah *et al*., 2007).

The following algorithm is applied to each grid cell with respect to the centre cell, labelled **e** in the illustration below (Figure 4.16).

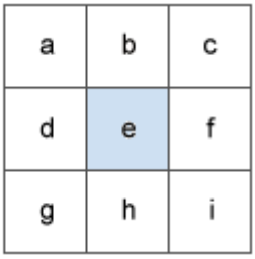

Figure 4.16 Example of 3 x 3 matrix, each grid has an elevation value

The elevation values of neighbouring cells (Figure 4.14) were used to calculate the slope of raster cells according to equations [4.21] – [4.23] (Burrough and McDonell, 1998):

$$dZ/dX = (c + 2f + i) - (a + 2d + g) / (8 * \text{cell size } X) \quad [4.21]$$

$$dZ/dY = (g + 2h + i) - (a + 2b + c) / (8 * \text{cell size } Y) \quad [4.22]$$

$$\Theta_e = \arctan \sqrt{(dZ/dX)^2 + (dZ/dY)^2} \quad [4.23]$$

Where Θ_e is slope steepness for cell e (degrees); *a, b, c, …, i* are elevation values of DEM cells around the active cell (m); *cell size X,Y* is the width of cells in direction X or Y (m).

Finally, the slope angle map in degrees of the Mae Rim watershed is illustrated in Figure 4.17.

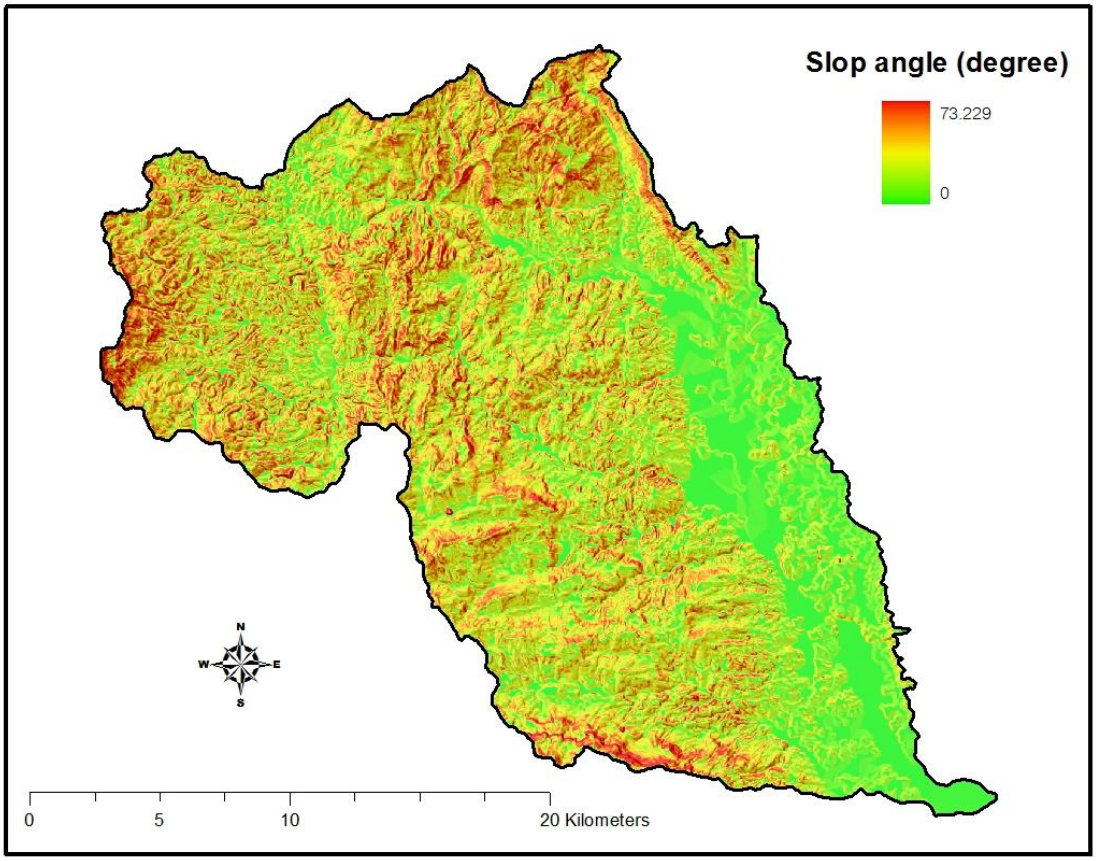

Figure 4.17 The raster map of slope angle in degrees of Mae Rim watershed.

(iii) LS factor mapping

After the maps of flow accumulation and slope angle in degree were produced, the final step is to run the formula provided by Desmet and Govers (1996) as equation [4.20], using the Raster Calculator function in ArcGIS. A procedural diagram of the workflow regarding the *LS* factor estimation can be summarised in Figure 4.18 and the final output of the slope length factor map of the Mae Rim watershed is also illustrated in Figure 4.19.

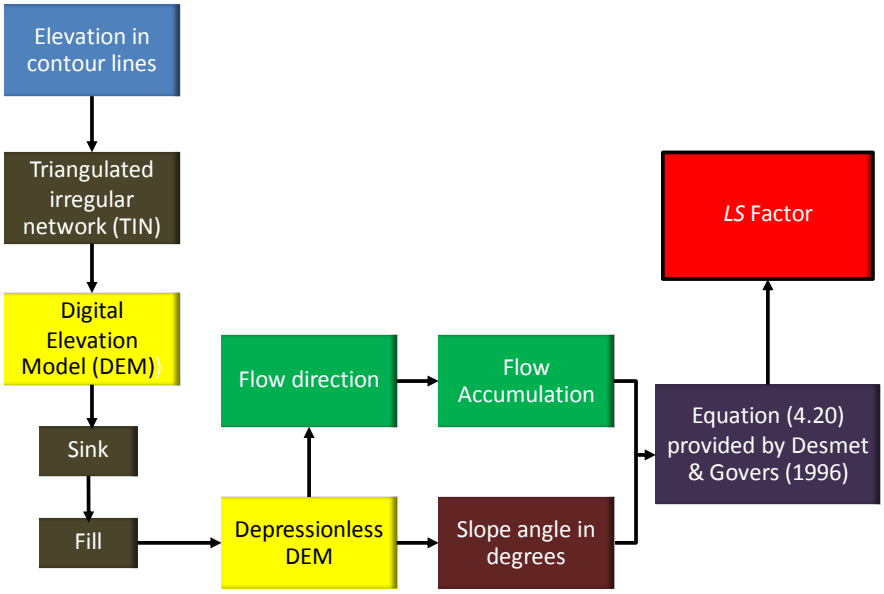

Figure 4.18 Diagram of implementing the LS factor with ArcGIS software.

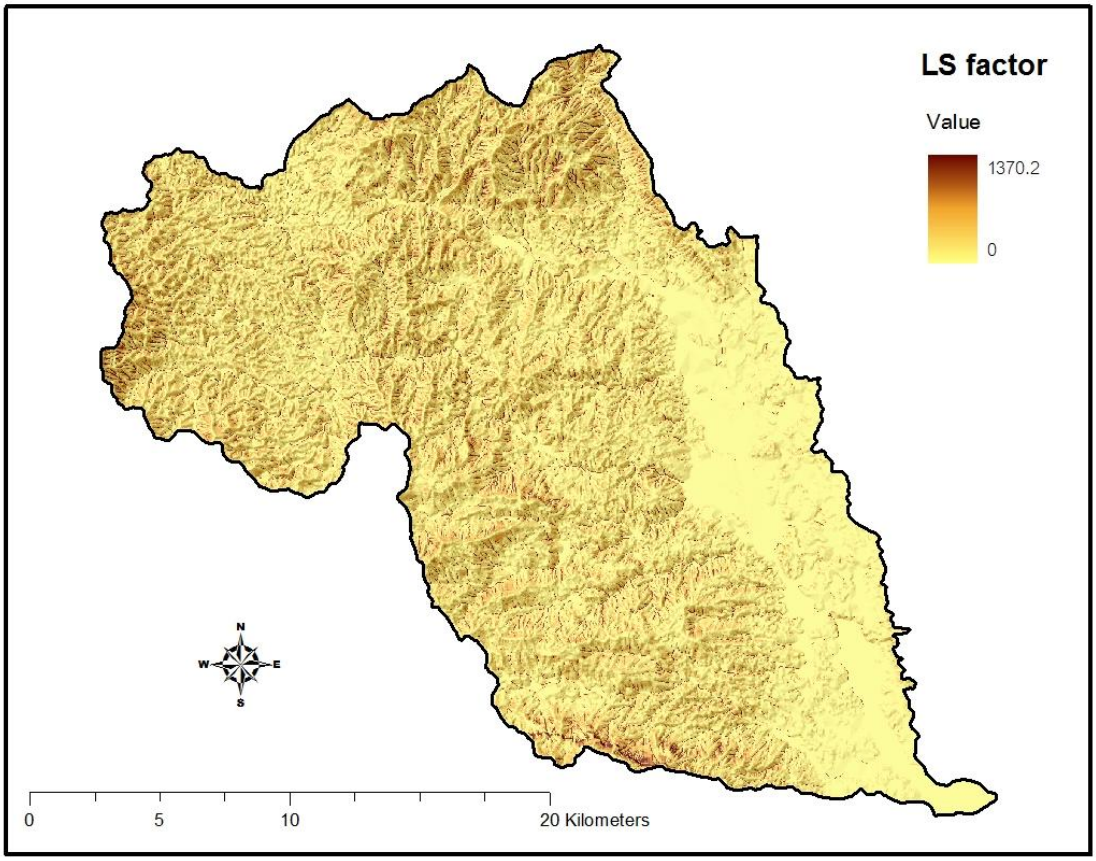

Figure 4.19 The spatial distribution of *LS* factor on the Mae Rim watershed.

In addition, the statistical values of the LS factor estimated by ArcGIS allow us to conclude that the mean value of LS factor is 9.99 with a standard deviation of 20.42. The minimum value is 0 and the maximum value is 1370.2.

4.2.6 Cover management or land cover (C factor)

The C factor is defined as the ratio of soil loss from land cropped under specific conditions to the corresponding soil loss from a continuously tilled fallow area (Wischmeier and Smith, 1978; Kefi *et al.,* 2012), and is used to reflect the effect of cropping and management practices on soil erosion rates in agricultural land and ground cover on reducing the soil erosion in forested regions (Renard *et al*., 2011). In addition, the C factor represents the protective coverage of canopy and organic material in direct contact with the ground. As the vegetation cover increases, the soil loss decreases (Arekhi *et al*., 2012). In RUSLE, the C factor can be computed from soil loss ratios (SLR), according to equation [4.24] (Renard *et al*., 2011):

$$SLR = PLU \times CC \times SC \times SR \times SM \qquad [4.24]$$

Where*: SLR* = Soil loss ratio for given conditions (dimensionless);

PLU = Prior land use sub factor (dimensionless);

CC = the canopy cover sub factor (dimensionless);

SC = Surface cover sub factor (dimensionless);

SR = Surface roughness sub factor (dimensionless);

SM = Soil moisture sub factor (dimensionless)

The final C value shown in equation [4.25] is obtained by using the SLR values for different time periods and weighting them with the EI_{30} values of the same periods. This causes vegetation cover during rainy seasons to have greater impact on the C-factor than vegetation during dry seasons when little erosion occurs (Dubber and Hedbom, 2008).

$$C = \frac{\sum_{t=1}^{n} SLR_t \times EI_{30,t}}{EI_{30,tot}} \qquad [4.25]$$

Where t = time periods with individual EI_{30}-values; n = number of different time periods.

However, the dependence of such factors in equations: [4.24] and [4.25] are difficult to evaluate because it always depends upon environmental variations and other factors in the year (e.g. land uses, agricultural activities and plant phenology) (Bosco *et al.,* 2009). Moreover, there is usually a lack of detailed information in developing countries. To locally evaluate and then extrapolate to system of interest is expensive and may be tough in operating relative factors on a large scale (Trabucchi *et al.,* 2012).

As a result of different patterns of land cover with respect to spatiotemporal changes, remote sensing satellite imageries are currently widely used for estimating the C factor (Prasannakumar *et al*., 2011). The C factor can be considered from both supervised and unsupervised classification using satellite

images, and then C factor value was assigned for each class from the literature (Cohen *et al*., 2005; Beskow *et al.,* 2009; Hui *et al*., 2010). Some studies employed the regression model to make correlation analysis between C factor values measured in field or obtained from guide tables and the Normalized Difference Vegetation Index (NDVI) (e.g., De Jong *et al*., 1999; Lin *et al*., 2002; De Asis and Omasa, 2007; Karaburun, 2010; Arekhi *et al.,* 2012).

However, this research employed the supervised classification method of Maximum Likelihood to classify land use/cover for developing a land use/cover map of the study area, and the C factor values based on RUSLE guide tables were then assigned to each pixel in the land use/cover class (Hill *et al.,* 2003; Shalaby and Tateishi, 2007). The Landsat TM satellite images (path/row: 131/47), acquired in July 2009 (rainy season), have been used for determining land use/cover, and preparing the C factor layer for the Mae Rim watershed.

Because considerably more sediment is transported during the rainy season, selection of satellite images for a study of either soil erosion or of sediment yields caused by land use variability during the rainy season is important, especially in terms of assessing soil losses as well as appropriate planning of land use and land management practices throughout the watershed.

Dry season satellite images may not be appropriate, nor do they relate to the purposes of this research, which mainly focuses on estimation of soil losses and identification of spatial distribution of erosion risk areas in the Mae Rim watershed. In addition, using a land use map interpreted from the dry season

satellite images in order to assign the C factor values through application of the RUSLE may lead to a discrepancy in results that cannot be actually used in management practice. Because of the small amount of rainfall and the scarcity of surface water during the dry period, land use and land cover at this time of year cannot be employed as potential sources to predict severe soil erosion areas when compared with the rainy season. A land use map interpreted from rainy season satellite images is preferable. In particular, information regarding rainy season land use can be helpful for the people who are directly impacted by soil erosion in preparing suitable management measures in order to prevent or minimise severe erosion before the rainy season begins.

Based on equations [3.1] and [3.2] (see Section 3.4.1 for accuracy assessment), the maximum likelihood classification yields an overall interpretation accuracy of land use/cover classification of 87% and the Kappa coefficient ($\hat{k}$) 0.76, indicating relatively high agreement with the ground truth (Table 4.5). Thus, the accurate land use/cover map for 2009 interpreted from satellite image is shown in Figure 4.20.

Table 4.5 Error matrix for supervised classification approach.

Ground Classes	Satellite image classes									
	Evergreen forest	Deciduous forest	Water body	Paddy fields	Mixed orchards	Field crops	Villages	Urban area	Bare land	Row Total
Evergreen forest	**260**	66	19	1	0	0	15	2	0	363
Deciduous forest	0	**53879**	634	0	0	0	28	0	0	54541
Water body	0	2764	**7526**	0	309	3	380	70	85	11137
Paddy fields	3	0	20	**5435**	92	7	63	262	4	5886
Mixed orchards	0	84	57	97	**671**	0	467	438	8	1822
Field crops	0	48	104	165	18	**145**	32	7	43	562
Villages	1	161	154	25	710	0	**1070**	514	22	2657
Urban area	0	0	18	313	330	0	251	**458**	15	1385
Bare land	0	28	418	102	309	9	270	131	**277**	1544
Column Total	264	57030	8950	6138	2439	164	2576	1882	454	**79897**

Overall classification accuracy = 87.26%; Kappa coefficient ($\hat{k}$) = 0.7593.

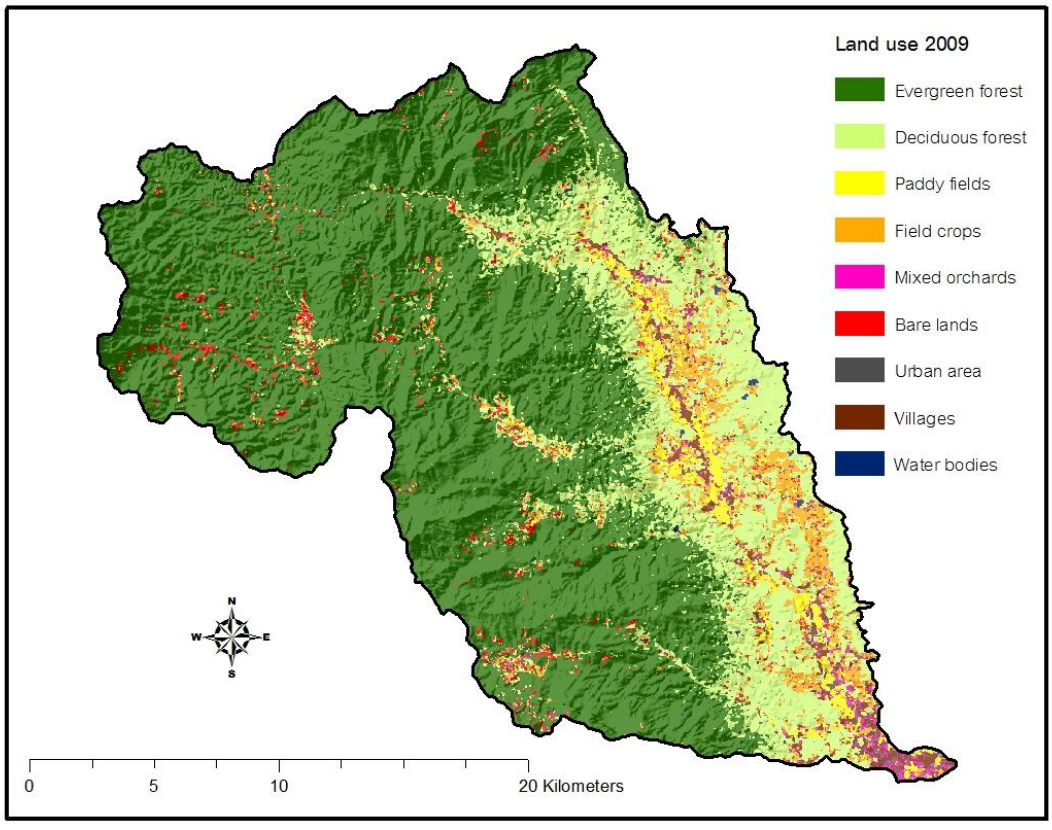

Figure 4.20 Land use/cover map of the Mae Rim watershed in 2009.

4.2.7 Conservation support practice (P factor)

P factor is the soil loss ratio with a specific support practice to the corresponding soil loss with up and down slope tillage (Beskow *et al*., 2009; Arekhi *et al*., 2012). The P factor value will reduce when there are more effective supporting mechanical practices such as contouring, strip cropping, terracing and retention ditches. When there are no conservation support practices in the area of interest, maximum values of 1 will be assigned, meaning no land use influence. For the P factor in Thailand, it has not been established for all agricultural cover types except for paddy field (P factor = 0.1) (Ongsomwang and Thinley, 2008).

Evaluation of C and P factors

Based on the RUSLE guide tables (Wischmeier and Smith, 1978; Morgan, 2005), the values of the C and P factors were already set by the Land Development Department (LDD), Thailand for the whole country (Table 4.6). In this research, the information on northern Thailand was used to calculate C and P factors for running the model RUSLE due to the study area being located in the north and northwest of the country.

Table 4.6 C and P factors developed by LDD were evaluated based on land use and vegetation covers, separate into five regional parts of the country.

Land use classes	*North East*		*North*		*Central/East*		*West*		*South*	
	C	**P**	**C**	**P**	**C**	**P**	**C**	**P**	**C**	**P**
Paddy field	0.28	0.1	**0.28**	**0.1**	0.28	0.1	0.28	0.1	0.28	0.1
Field crop	0.525	1	**0.474**	**1**	0.485	1	0.485	1	0.322	1
Fruit tree	0.15	1	**0.15**	**1**	0.15	1	0.15	1	0.15	1
Horticulture	0.3	1	**0.3**	**1**	0.3	1	0.3	1	0.3	1
Orchard	0.6	1	**0.6**	**1**	0.6	1	0.6	1	0.6	1
Swidden cultivation	0.25	1	**0.25**	**1**	0.25	1	0.25	1	0.25	1
Grassland	0.1	1	**0.1**	**1**	0.1	1	0.1	1	0.1	1
Mixed agriculture	0.225	1	**0.225**	**1**	0.225	1	0.225	1	0.225	1
Evergreen forest	0.003	1	**0.003**	**1**	0.003	1	0.003	1	0.003	1
Deciduous dipterocarp forest	0.048	1	**0.048**	**1**	0.048	1	0.048	1	0.048	1
Mixed deciduous dipterocarp forest	0.02	1	**0.02**	**1**	0.02	1	0.02	1	0.02	1
Forest plantation	0.088	1	**0.088**	**1**	0.088	1	0.088	1	0.088	1
Bare land	0.25	1	**0.25**	**1**	0.25	1	0.25	1	0.25	1
Bare land for agriculture	0.25	1	**0.25**	**1**	0.25	1	0.25	1	0.25	1
Urban area	0	0	**0**	**0**	0	0	0	0	0	0
Village	0	0	**0**	**0**	0	0	0	0	0	0
Water body	0	0	**0**	**0**	0	0	0	0	0	0

Source: LDD (2000).

Finally, the cover management (C) and conservation support practice (P) maps were combined and generated using ArcGIS 9.3, providing the spatially distributed CP factors, as shown in Figure 4.21.

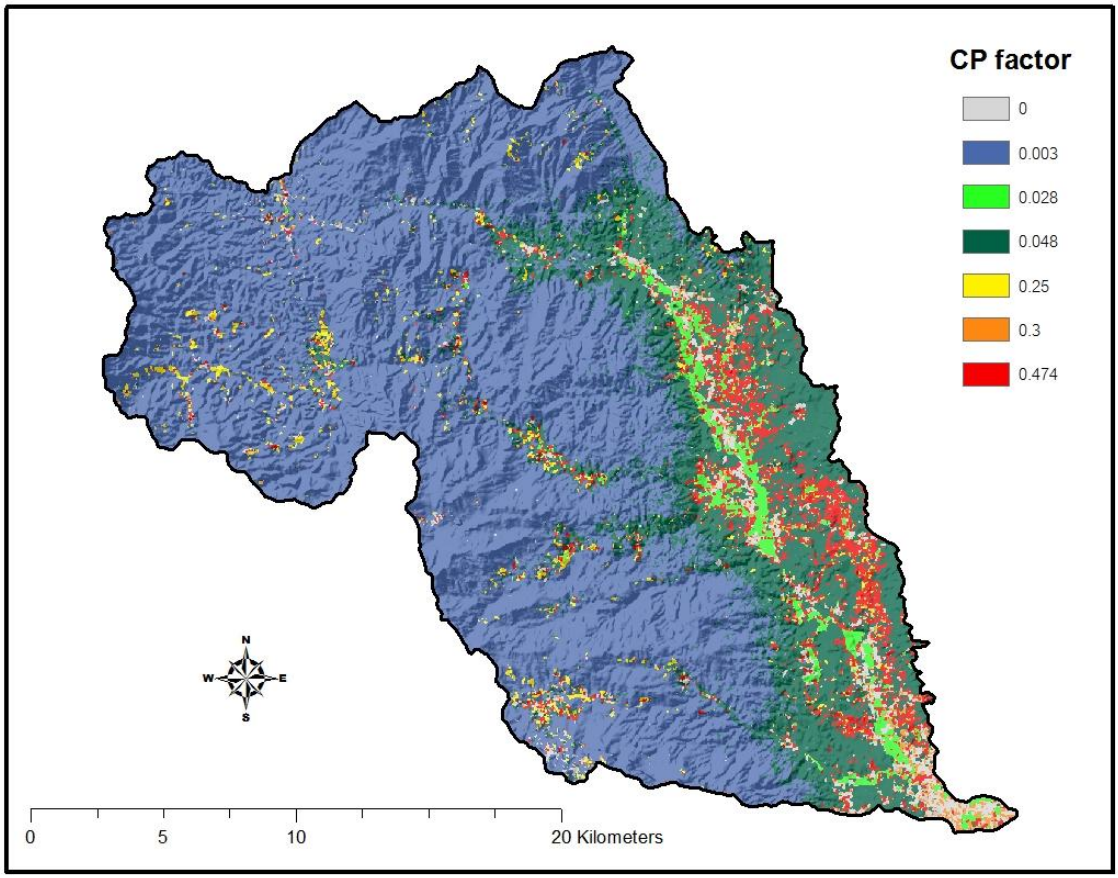

Figure 4.21 Spatial distribution of CP factor in Mae Rim watershed.

4.3 Results

4.3.1 Spatial variation of annual soil loss in watershed area

The average annual soil loss in the Mae Rim watershed was computed by multiplying the six major factors according to the RUSLE formula equation [4.1]. As presented in Figure 4.22, the annual soil loss in most of the area ranges between 0 and 48,049 tonnes $ha^{-1}\,yr^{-1}$; the mean value is 31.11 tonnes $ha^{-1}\,yr^{-1}$ with a standard deviation of 264.18 tonnes $ha^{-1}\,yr^{-1}$. The predicted soil loss rate indicates that this watershed area is a huge sediment source. It is believed that this watershed contains many steep slopes and bare lands spreading around in

addition to intensive farming in the uplands. Our results therefore support the predicted soil loss as very high in particular areas.

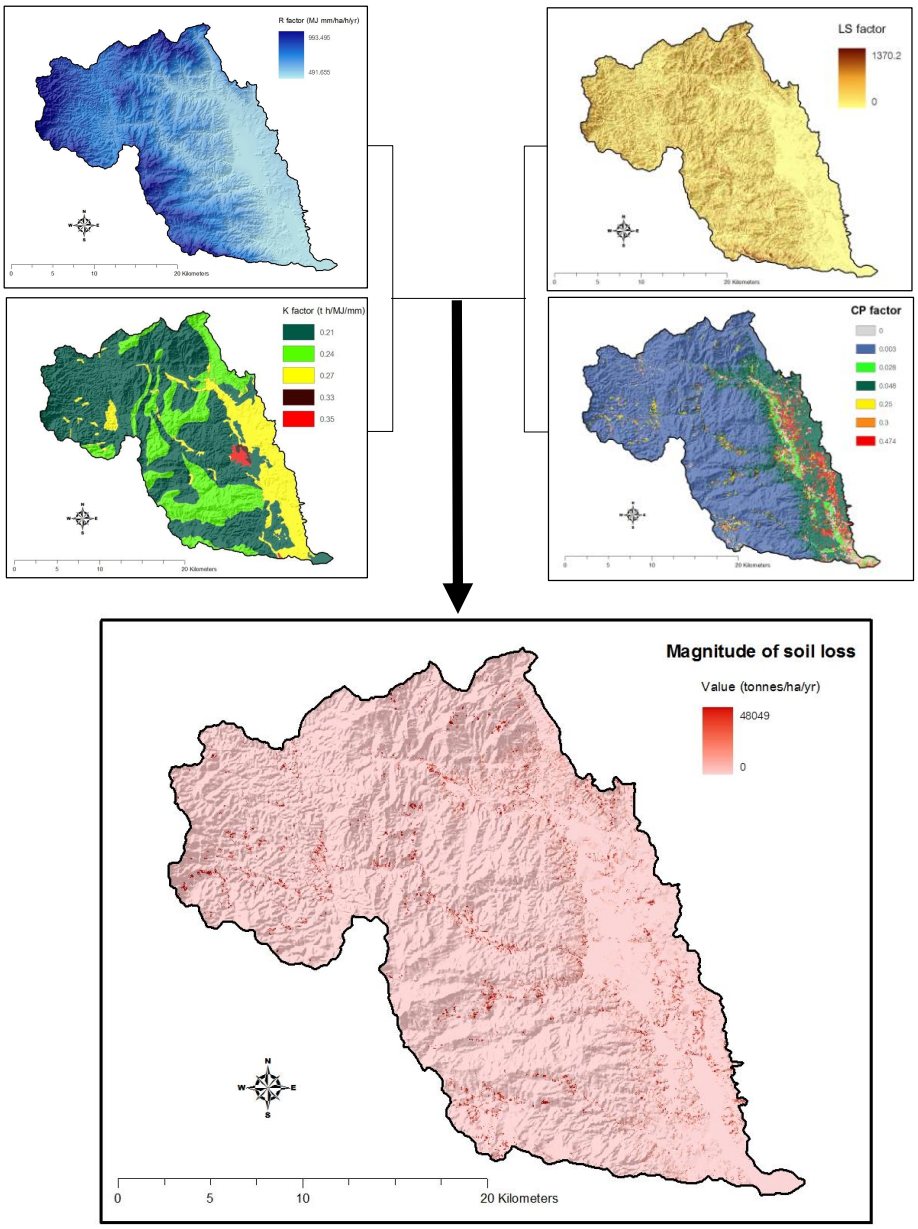

Figure 4.22 Spatial variation of annual soil loss map in Mae Rim Watershed, NW Thailand, derived from calculation of RUSLE equation [4.1], i.e., A = RKLSCP.

4.3.2 Spatial variation of soil erosion intensity

In terms of an intensity classification of soil erosion risk, the criteria for grouping in each class are alterable, and not standardised. In this study, the degree of severity of soil loss was categorised into four classes, based on criteria of soil erosion risk classification by degree suggested by FAO (2006). As a result, the spatial variation of soil erosion risk in the Mae Rim watershed and details of soil erosion intensity classes and ranges of soil loss rates are shown in Figure 4.23 and Table 4.7, respectively.

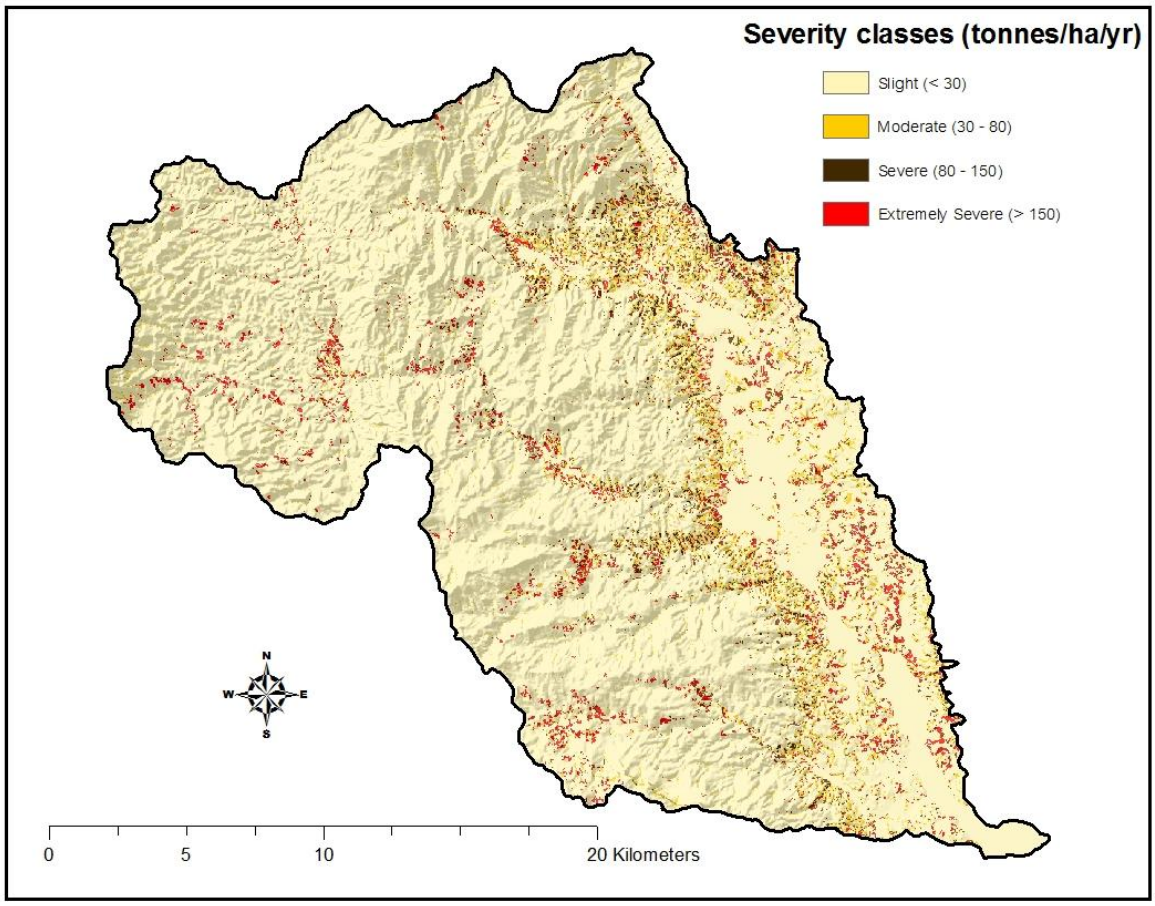

Figure 4.23 Spatial variation of soil erosion risk in Mae Rim watershed

Table 4.7 Soil erosion severity classes and ranges of soil loss rate.

Watershed area	Soil loss rate (tonnes ha^{-1} yr^{-1}) / severity classes				Total
	< 30 Slight	30 – 80 Moderate	80 – 150 Severe	> 150 Extremely Severe	
Size (km^2)	454.10	29.98	12.49	18.43	515
% of total area	88.17	5.82	2.43	3.58	100

Figure 4.23 illustrates that 6% or 31 km^2 of watershed area (i.e., severe + extremely severe) are areas of concern for soil erosion; 5.8% of watershed area is moderate, while 88% of the watershed area is mostly slight. However, despite only 4% being an extremely severe area, it should be realised and immediately prioritised to manage soil conservation in particular, since such an extremely severe source can generate soil erosion that averages more than 150 tonnes/ha in every year.

In addition, the result of spatial variation of soil erosion risk map has been compared with the terrain map (Figure 4.24). According to Gale (2000), the terrain can be classified based on slope gradient (in degrees); it is divided into four levels: flat (<10°), sloping (10°–25°), steep (25°–40°) and very steep (>40°). Results from Table 4.8 illustrate that for almost half of the watershed area (49.5%), soil erosion has largely occurred on the sloping terrain, while for the rest of the soil erosion, about 35% and 15% of the total area has taken place on the flat terrain and precipitous areas (i.e., steep and very steep slopes), respectively.

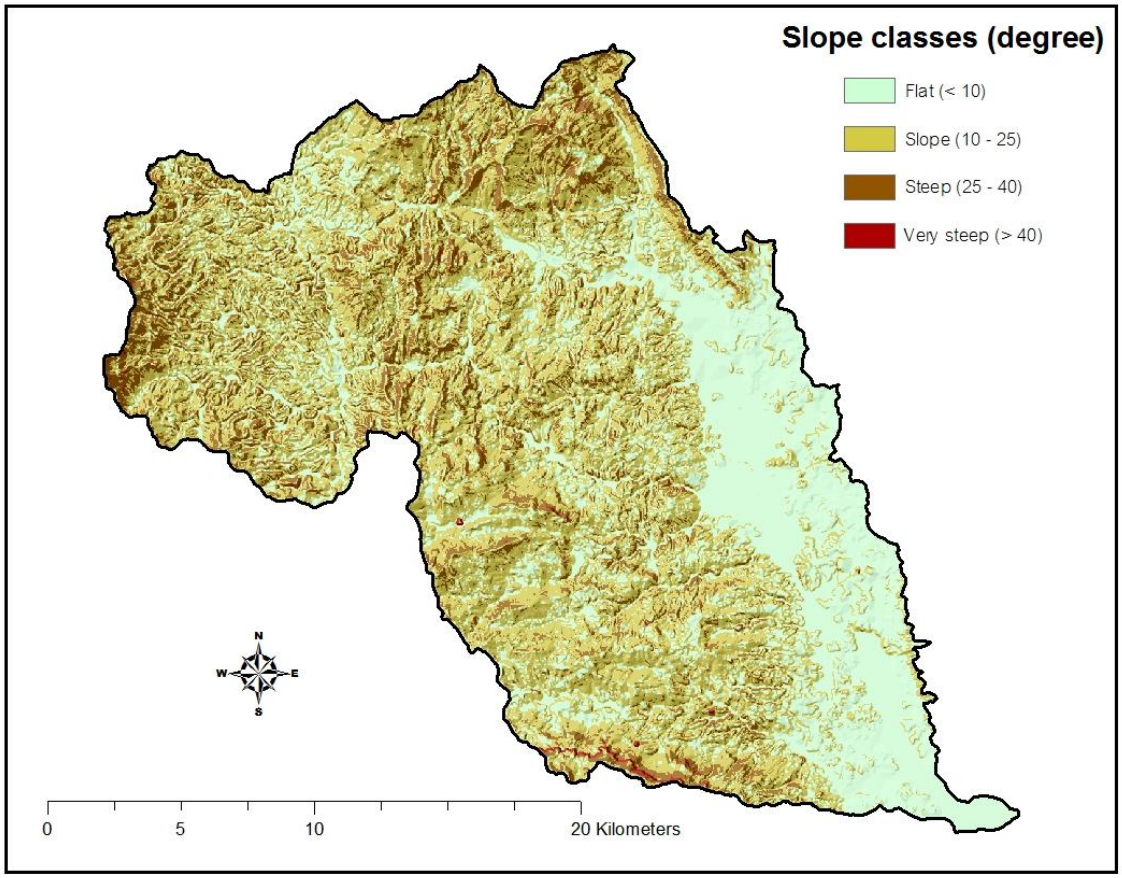

Figure 4.24 Terrain map based on the ground slope in degree.

Table 4.8 Comparing areas of soil erosion risk and slope classes/terrains of Mae Rim watershed, NW Thailand.

Slope class in degree	Watershed area ratio in each severity class								Total area	
	Soil loss rate (tonnes ha^{-1} yr^{-1}) - severity classes									
	<30 Slight		30–80 Moderate		80–150 Severe		>150 Extremely Severe		Km^2	%
	Sq. Km	(%)	Sq. Km	(%)	Sq. Km	(%)	Sq. Km	(%)		
< 10° (Flat)	165.30	32.10	7.98	1.55	3.83	0.74	5.42	1.05	182.5	35.4
10° – 25° (sloping)	218.20	42.37	20.25	3.93	5.87	1.14	10.47	2.03	254.8	49.5
25° – 40° (Steep)	69.21	13.44	1.58	0.31	2.77	0.54	2.46	0.48	76.0	14.8
> 40° (Very steep)	1.40	0.27	0.18	0.03	0.02	0.00	0.08	0.02	1.7	0.3
	454.11	88.18	29.99	5.82	12.49	2.42	18.43	3.58	515.0	100.0

The reason why the sloping terrain is the major areas of soil erosion risk is due to the fact that such areas are used for intensive field crop farming, which may result in soil degradation. Some land has been left uncultivated or unused for too long in accordance with the technique of traditional shifting cultivation. This land is therefore easy to be washed and eroded by runoff and rainstorms. In the mountainous areas, despite the steep slope, these areas are plentifully covered by the canopy of forest trees and vegetation. It can reduce the impact of soil erosion from rain as well as soil properties contained in the hill evergreen forest of the Mae Rim watershed that are mostly fertile, very deep and well drained; particularly in the areas at an altitude of 1,000 metres above sea level known as 'head watershed', when the rain falls to the ground, it can easily infiltrate and percolate through the pore spaces of the soil. As a result, soil erosion risk in mountainous area is less than sloping or rolling lands.

4.3.3 Examining the spatial soil erosion risk map with data collected on the ground

After generating the spatial variation of soil erosion risk map in the Mae Rim watershed as displayed in Figure 4.23, the locations on the map for extremely severe soil erosion (erosive magnitude >150 tonnes ha^{-1} yr^{-1}) have been extraordinary focused in order to prove the reliability of prediction of using this model; they were taken to compare and recheck with the 69 ground-point samplings collected from the ground truth survey (Figure 4.25).

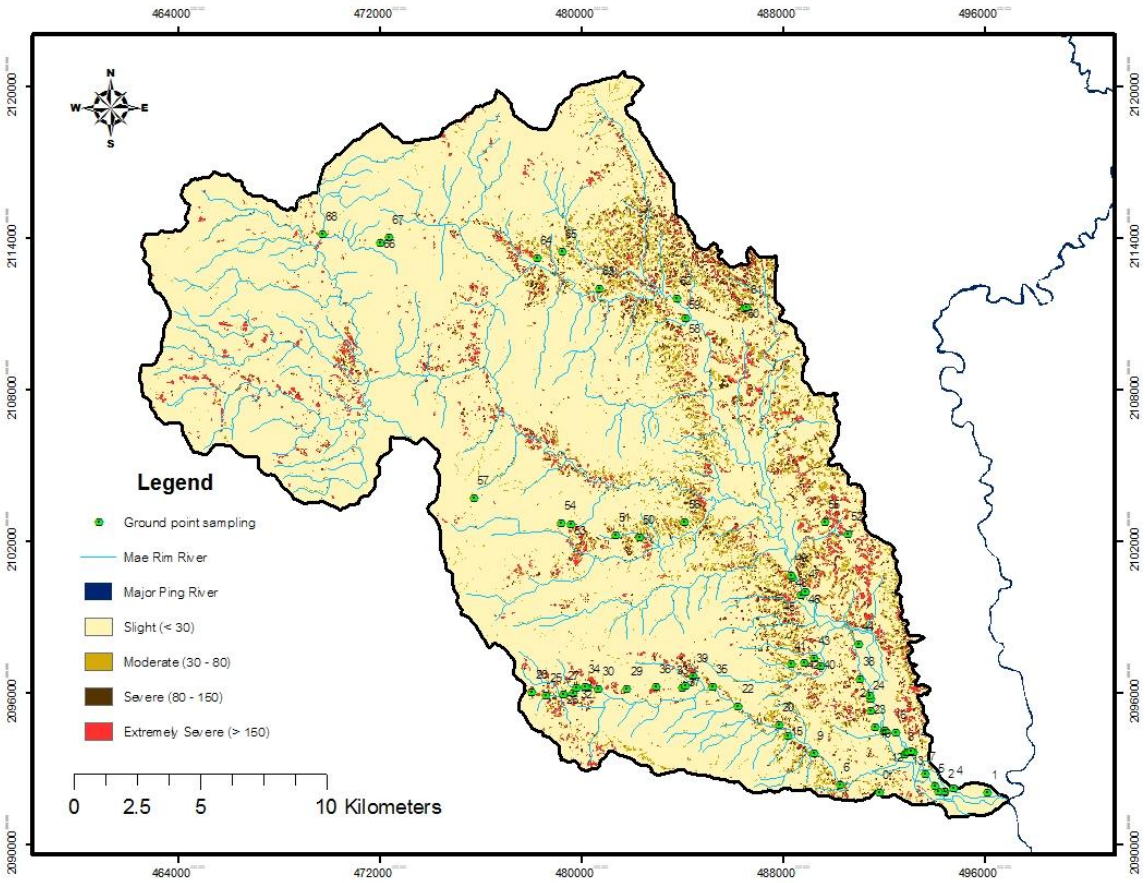

Figure 4.25 The 69 ground-point samplings obtained from actual field visit between 8 July and 31 August 2010, Mae Rim watershed.

As a result, there are some 'vulnerable areas' (e.g., gully, bare soil and riverbank erosion) collected from the ground truth survey that indicates corresponding points on the extremely severe soil erosion on the map (Figure 4.26).

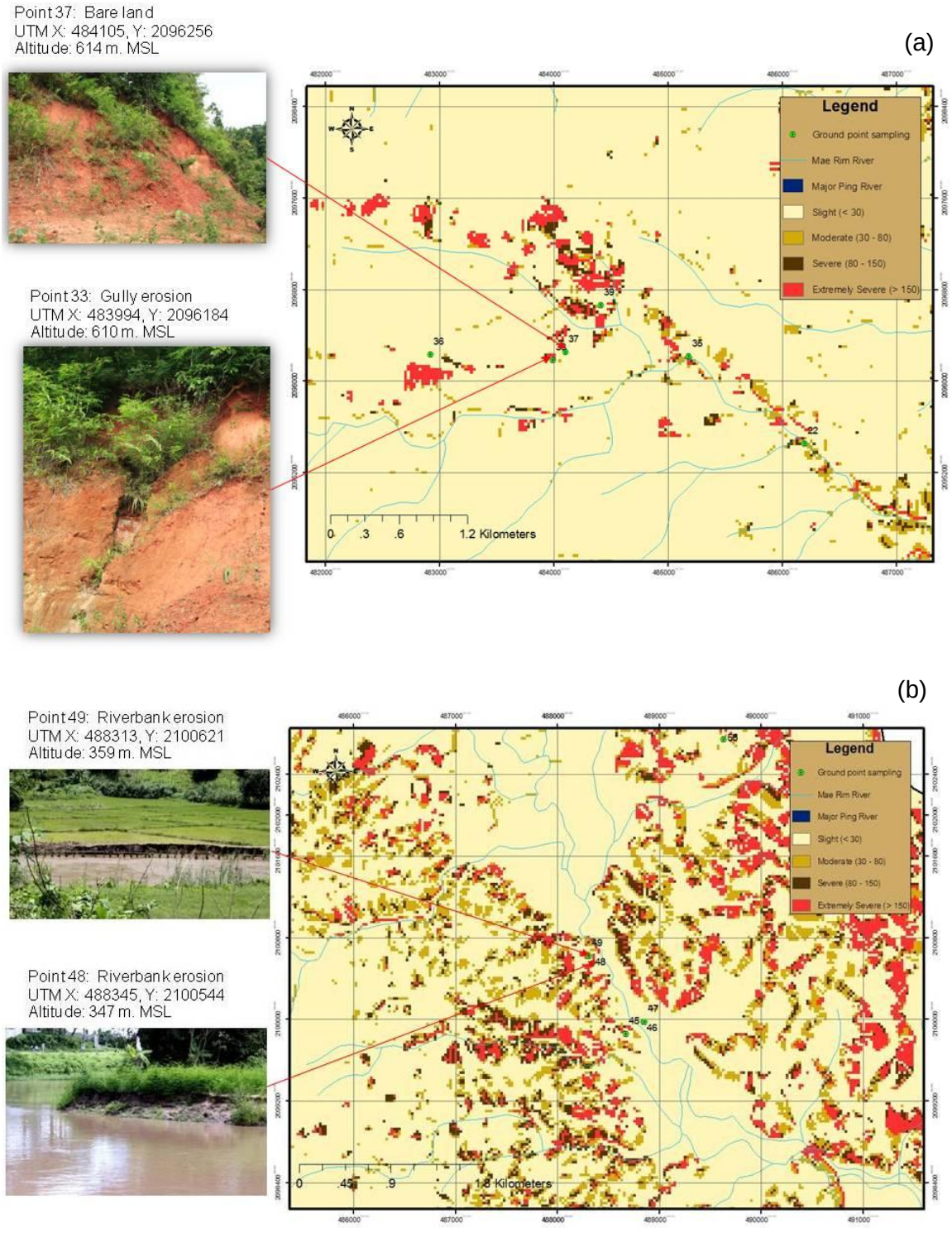

Figure 4.26 Typically examining the predicted extremely severe areas of soil erosion (red colour) with vulnerable points collected from actual field visit in the Mae Rim watershed. (a) Bare soil and gully erosion, and (b) riverbank erosion.

Alternatively, the extremely severe soil erosion predicted on the map (Figure 4.23) can be examined with the potential gullies, unpaved roads and riverbank erosion, which are additionally developed by applying the GIS technique. As a result, the outputs processed from the GIS applications to predict the potentially vulnerable areas of gully, unpaved road and riverbank erosion, based on methodological criteria of this thesis (see Section 3.5.2), are shown in Figure 4.27, 4.28 and 4.29, respectively.

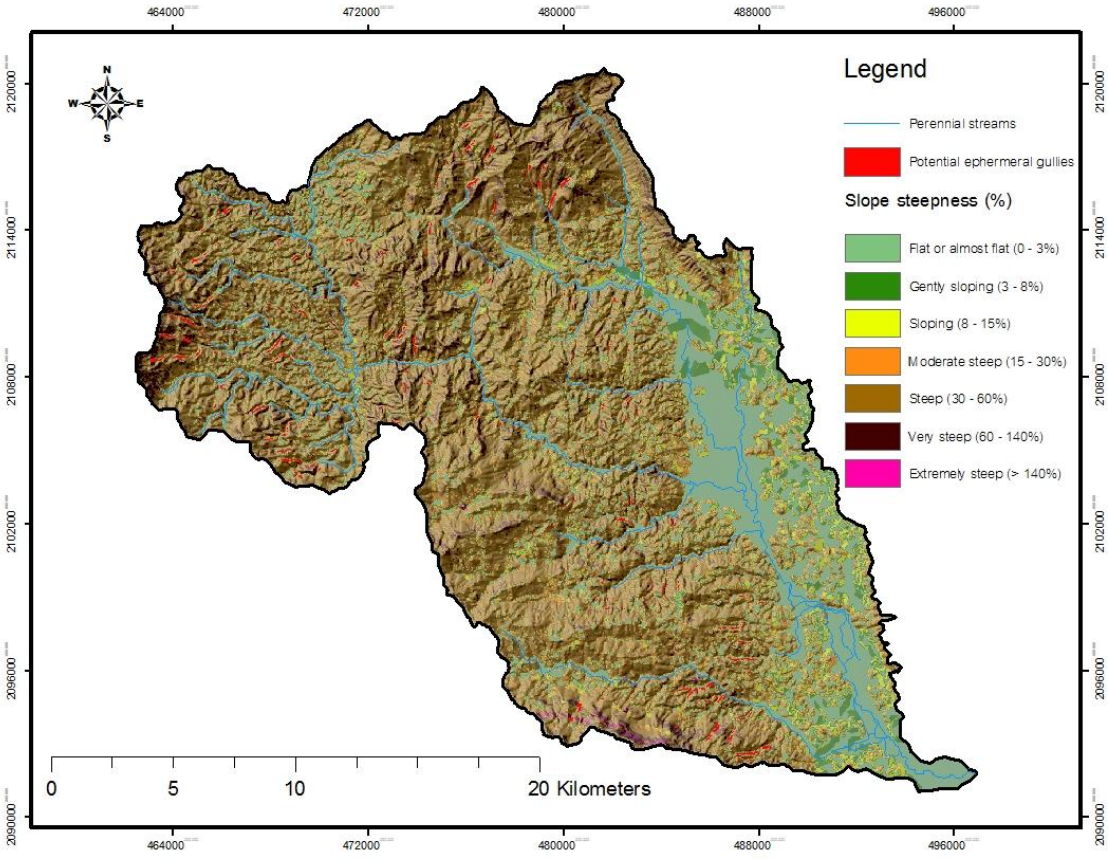

Figure 4.27 The spatial distribution of potentially vulnerable areas for gully erosion.

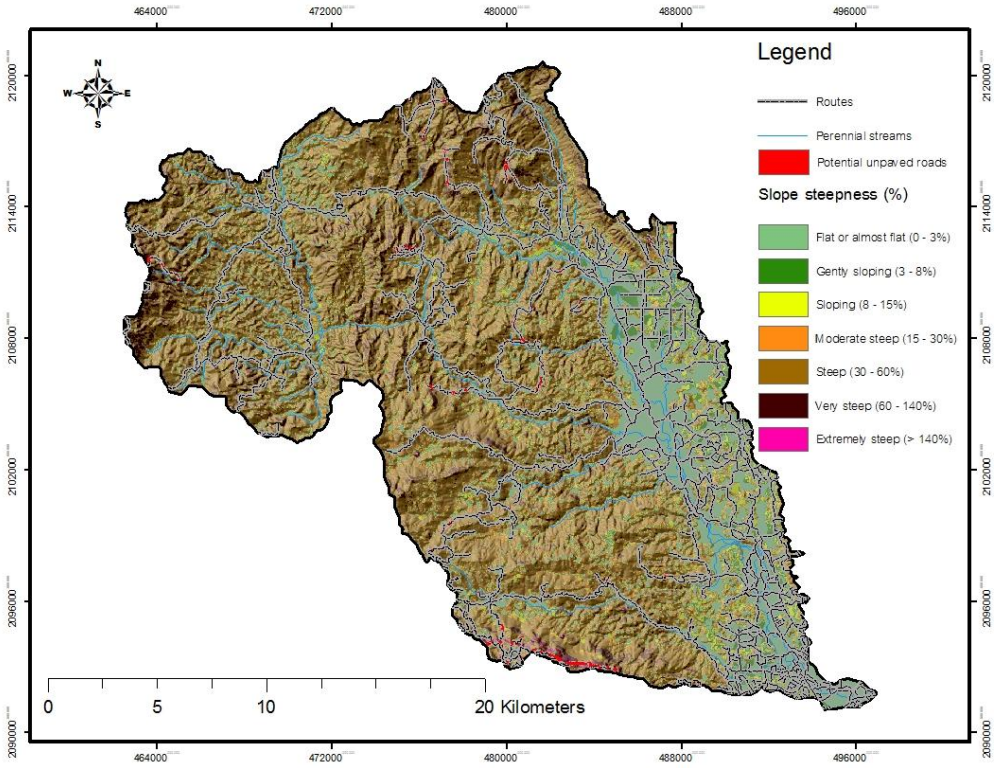

Figure 4.28 The spatial distribution of potentially vulnerable areas for unpaved roads.

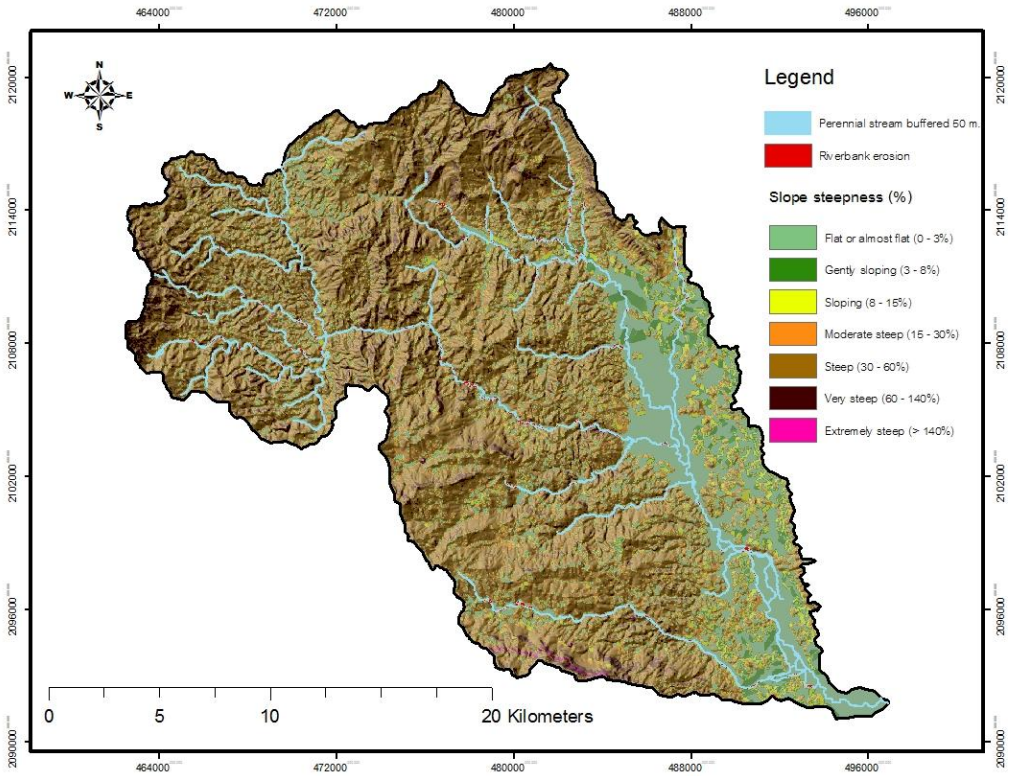

Figure 4.29 The spatial distribution of potential riverbank erosion.

From Figures 4.27–4.29, it can be summarised that there are small proportions of potentially vulnerable areas of gully, unpaved road and riverbank erosion, i.e., 0.6 % (303 ha), 0.2% (119 ha) and 5% (2,459 ha) of the watershed area, respectively (Table 4.9).

Table 4.9 Cross-tabulation of the potentially vulnerable areas of soil erosion per watershed size (in ha) and severity classes.

Severity classes	Potentially vulnerable areas of soil erosion per watershed size (ha)						Total	
	Ephemeral gully	%	Unpaved road	%	River bank	%	Area (ha)	%
Slight	276.79	0.54	101.58	0.20	2,146.29	4.17	2,524.66	4.90
Moderate	10.61	0.02	7.49	0.01	138.39	0.27	156.49	0.30
Severe	5.24	0.01	2.56	0.00	59.96	0.12	67.76	0.13
Extremely severe	10.67	0.02	7.49	0.01	114.43	0.22	132.59	0.26
Total	**303.31**	**0.59**	**119.11**	**0.23**	**2,459.08**	**4.78**		

When taking these vulnerable points to compare with the spatial soil erosion risk map produced by RUSLE-GIS-based modelling, it was found that most vulnerable points tend to relate to the slightly severe soil erosion risk (4.9% of the watershed area), whereas less than 1% of the area or about 200 ha is of concern for soil conservation and management plans in the vulnerable areas (a combination of severe and extremely severe areas). Moreover, when considering each type of the potentially vulnerable areas, riverbank erosion was highly associated with extremely severe soil erosion areas, followed by gully and unpaved roads, with their size as 114 ha, 11 ha and 7 ha, respectively.

4.3.4 Examining key controlling factors in RULSE relating to severity classes of soil erosion

The key controlling factors in the RUSLE used to test soil erosion severity classes in the Mae Rim watershed comprise of rainfall erosivity (R), topography (LS), land use/ cover types (CP) and soil types (K). Table 4.10 shows the subsequent results yielded from data comparison, using a cross-tabulation between the four key controlling factors and soil erosion classes.

Table 4.10 Cross-tabulation between key controlling factors and soil erosion classes.

Variables		Watershed area ratio in each severity class								Total area		Specifically examining in **'extreme severity'**	
		Soil loss rate (tonnes $ha^{-1} yr^{-1}$) - Severity classes											
		< 30 Slight		30 - 80 Moderate		80 - 150 Severe		> 150 Extremely severe				% of soil loss area in each variable	Rank
		(Km^2)	(%)	(Km^2)	(%)	(Km^2)	(%)	(Km^2)	(%)	(Km^2)	%		
Rainfall erosivity (R factor)	**< 550**	158.98	30.82	22.01	4.26	8.44	1.64	10.96	2.13	200.39	38.91	**5.47**	**1**
	550 - 650	134.11	25.99	3.79	0.74	2.07	0.40	4.16	0.81	144.14	27.99	2.89	2
	650 - 750	125.02	24.24	1.53	0.30	0.57	0.11	2.44	0.47	129.55	25.16	1.88	3
	> 750	39.55	7.67	0.56	0.11	0.08	0.01	0.74	0.14	40.93	7.95	1.80	4
		457.66	**88.71**	**27.89**	**5.41**	**11.15**	**2.16**	**18.30**	**3.54**	**515.00**	**100.00**		
Topography (LS factor)	0 - 20	400.72	77.67	23.80	4.61	8.95	1.74	12.57	2.44	446.04	86.61	2.82	4
	20 - 40	46.44	9.00	1.00	0.19	1.75	0.34	3.51	0.68	52.70	10.23	6.67	3
	40 - 60	7.12	1.38	0.61	0.12	0.17	0.03	0.95	0.19	8.84	1.72	10.72	2
	> 60	3.39	0.66	2.49	0.48	0.28	0.05	1.26	0.25	7.42	1.44	**16.96**	**1**
		457.67	**88.71**	**27.89**	**5.40**	**11.15**	**2.16**	**18.29**	**3.55**	**515.00**	**100.00**		
Land use/cover types (CP factor)	Evergreen forest	335.40	65.02	4.11	0.80	0.75	0.14	0.99	0.19	341.25	66.26	0.29	9
	Deciduous forest	73.04	14.17	20.52	3.98	7.34	1.43	4.82	0.94	105.73	20.53	4.56	4
	Field crops	15.77	3.05	1.80	0.35	1.87	0.36	7.28	1.42	26.71	5.19	27.24	2
	Paddy field	10.35	2.01	0.61	0.12	0.13	0.03	0.19	0.04	11.28	2.19	1.68	7
	Mixed orchards	4.07	0.79	0.36	0.07	0.31	0.06	0.76	0.15	5.50	1.07	13.79	3
	Bare lands	4.04	0.78	0.47	0.09	0.69	0.13	4.11	0.80	9.31	1.81	**44.16**	**1**
	Urban area	1.94	0.38	0.03	0.00	0.02	0.00	0.06	0.01	2.05	0.40	2.93	5
	Villages	11.64	2.26	0.18	0.03	0.12	0.02	0.27	0.05	12.21	2.37	2.21	6
	Water bodies	0.93	0.18	0.02	0.00	0.00	0.00	0.01	0.00	0.96	0.19	1.04	8
		457.19	**88.63**	**28.10**	**5.44**	**11.22**	**2.17**	**18.49**	**3.59**	**515.00**	**100.00**		
Soil types (K factor)	Sandy clay loam	280.01	54.28	15.91	3.08	5.91	1.15	8.82	1.71	310.66	60.32	2.84	4
	Clay loam	104.38	20.23	6.06	1.18	3.09	0.60	3.76	0.73	117.30	22.78	3.21	2
	Sandy loam	65.42	12.68	7.82	1.52	3.40	0.66	5.69	1.10	82.33	15.99	**6.91**	**1**
	Loam	1.64	0.32	0.09	0.02	0.04	0.01	0.05	0.01	1.82	0.35	2.75	5
	Silty clay loam	2.66	0.51	0.11	0.02	0.05	0.01	0.09	0.02	2.90	0.56	3.09	3
		454.10	**88.02**	**29.99**	**5.82**	**12.50**	**2.43**	**18.42**	**3.56**	**515.00**	**100.00**		

From Table 4.10 it can be summarised that most controlling factors in approximately 94% of the watershed area related to areas of slight–moderate severe soil erosion (0–80 tonnes ha^{-1} yr^{-1}), while only 6% of the watershed area related to areas of severe–extremely severe soil erosion (over 80 tonnes ha^{-1} yr^{-1}). However, to achieve awareness of the most concerning areas that should be urgently managed for soil conservation practice in this study area, each variable of the key controlling factors has therefore been investigated by specifically focusing on the source of extremely severe soil erosion (erosive magnitude > 150 tonnes ha^{-1} yr^{-1}). Thus, it can be concluded that:

(1) The highest level of rainfall erosivity (erosive magnitude > 750 MJ mm ha/h per year) in this study area has the lowest relation to the extremely severe class of soil erosion (i.e., 1.8% of eroded area in each variable sub-class). In contrast, the lowest level of rainfall erosivity (erosive magnitude < 550 MJ mm ha/h per year) mostly relates to an extremely severe soil erosion source (i.e., 5% eroded area in each variable sub-class).

(2) Topography or slope length and steepness (LS factor) has a direct correlation with very severe soil loss in the Mae Rim watershed. It means that the extremely severe soil erosion that took place on this area is very sensitive to an increased value of LS factor. From Table 4.10, it can be seen that the slope length and steepness > 60 (dimensionless) mostly affects soil erosion at extremely severe level (i.e., 17% eroded area in each variable sub-class).

(3) In terms of land use/cover types, the bare land (44%) is the most sensitive to generating soil erosion at extremely severe levels, followed by agricultural land such as field crops (27%) and mixed orchards (14%).

(4) Regarding soil types covered in the study area, it was found that the sandy loam (K value = 0.27) is the soil type most sensitive to extremely severe soil erosion on this watershed (i.e., 7% eroded area in each variable sub-class).

The results from Table 4.10, however, merely reveal what variables of each controlling factor are closely related to generating extremely severe soil erosion in the Mae Rim watershed. It is not able to identify the magnitude of the relationship between the key controlling factors and soil erosion loss rates. For this reason, Pearson's correlation coefficient has been used to determine the magnitude of the relationship at a significance level of 0.01.

Table 4.11 Pearson's correlation test.

		SE_Rate	R_Factor	LS_Factor	K_Factor	CP_Factor
SE_Rate	Pearson Correlation	1	-0.046**	0.263**	0.022**	0.300**
	Sig. (2-tailed)		0.000	0.000	0.000	0.000
	N	130457	130457	130457	130457	130457
R_Factor	Pearson Correlation	-0.046**	1	0.090**	-0.320**	-0.318**
	Sig. (2-tailed)	0.000		0.000	0.000	0.000
	N	130457	130457	130457	130457	130457
LS_Factor	Pearson Correlation	0.263**	0.090**	1	-0.153**	-0.199**
	Sig. (2-tailed)	0.000	0.000		0.000	0.000
	N	130457	130457	130457	130457	130457
K_Factor	Pearson Correlation	0.022**	-0.320**	-0.153**	1	0.231**
	Sig. (2-tailed)	0.000	0.000	0.000		0.000
	N	130457	130457	130457	130457	130457
CP_Factor	Pearson Correlation	0.300**	-0.318**	-0.199**	0.231**	1
	Sig. (2-tailed)	0.000	0.000	0.000	0.000	
	N	130457	130457	130457	130457	130457

** Correlation is significant at the 0.01 level (2-tailed).

The results shown in Table 4.11 can be summarised that all of the four-key controlling factors are correlated with soil loss generation at statistically significant level ($p < 0.001$). Particularly, land use/land cover (CP factor) and

slope length/steepness (LS factor) are linearly correlated with the soil loss rate in the watershed. Their correlation coefficients (*r*) of 0.3 and 0.263 can be interpreted based on Hopkin (1997)'s criteria (cited in Kotrlik and Williams, 2003, p. 5) (see Table 4.12), indicating that there are moderate and small (almost moderate) correlations between the CP and LS factors, respectively, and the soil loss rate in the Mae Rim watershed. Meanwhile, the relationships between the soil erosion losses and rainfall erosivity (R-factor) as well as the relationship between the soil erosion losses and erodibility (K-factor) are insubstantial correlation (–0.046 and 0.022, respectively). Additionally, the four key controlling factors have been plotted as independent variables on the X-axis against the rate of soil erosion losses on Y-axis as the dependent variable to illustrate the data dispersion of their correlations (Figure 4.30).

Table 4.12 Indicator for interpreting magnitude of the effect in correlation coefficients

Source	Statistic	Value	Interpretation
Hopkin (1997)	Correlation Coefficients (*r*)	0.90–1.00	Nearly, practically, or almost: perfect, distinct, infinite
		0.70–0.90	Very large, very high, huge
		0.50–0.70	Large, high, major
		0.30–0.50	Moderate, medium
		0.10–0.30	Small, low, minor
		0.00–0.10	Trivial, very small, insubstantial, tiny, practically zero

(Source: Adapted from Kotrlik and Williams, 2003, p.5).

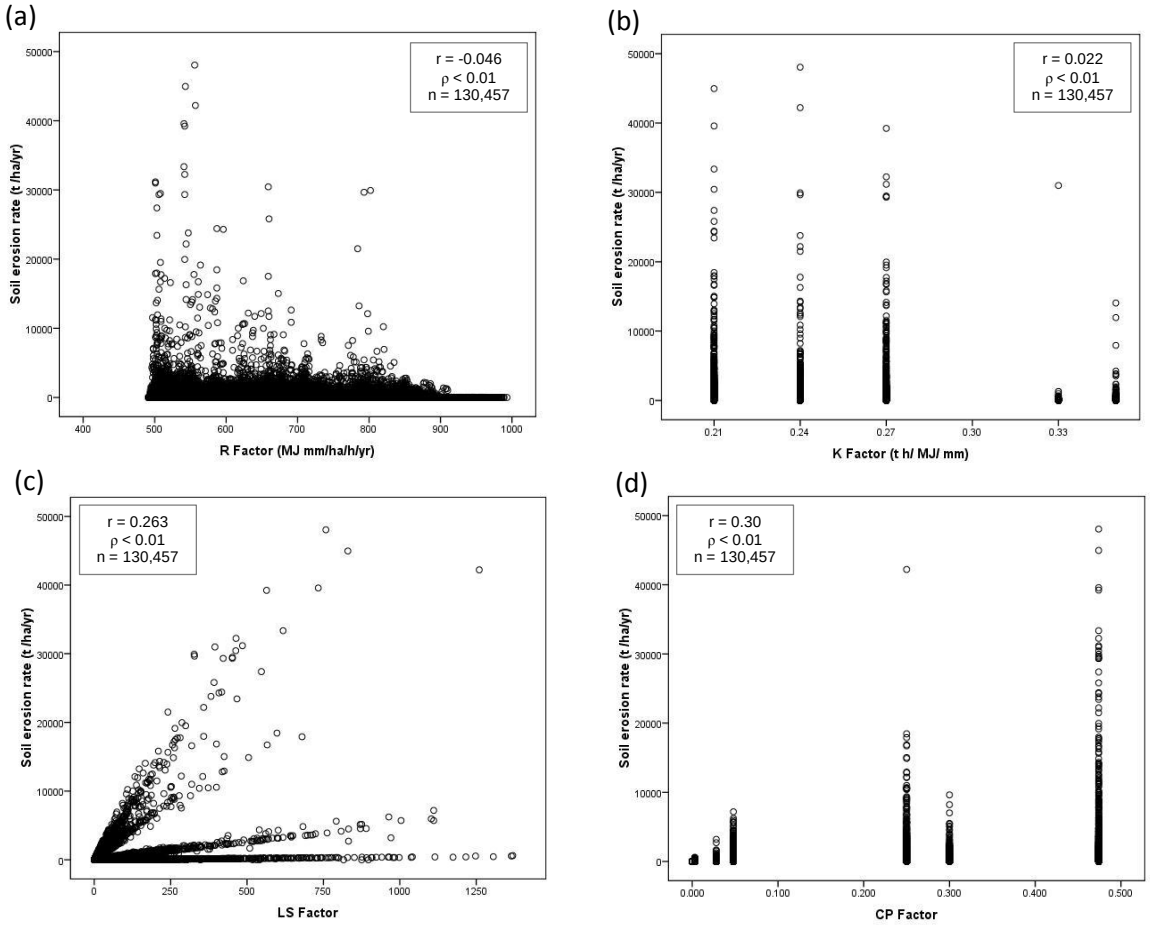

Figure 4.30 The correlation between soil erosion rates and the key controlling factors in RUSLE: (a) R factor – SE rate relationship; (b) K factor – SE rate relationship; (c) LS factor – SE rate relationship; (d) CP factor – SE rate relationship.

4.4 Discussion

The computed output of soil erosion prediction in the Mae Rim watershed was found to be between 0 and 48,089 tonnes ha^{-1} yr^{-1}; the mean annual soil loss rate was predicted of 31.11 tonnes ha^{-1} yr^{-1}. The result seems to be a very high rate in terms of the maximum soil loss prediction. However, this maximum value of 48,049 tonnes ha^{-1} yr^{-1} is only in one pixel, covering about 625 m^2 (0.0625

ha). It is probably because of the extreme value in the LS factor, which is a result of the problems in DEM extrapolation. Nonetheless, the extreme value can only be verified with field-checking (Ramli *et al.,* 2004). When comparing the predicted value of maximum soil loss that was also predicted by applying the same RUSLE model with other tropical watersheds especially in similar environments such as Tropical Asia, it was found that the predicted value of maximum soil loss in the Mae Rim watershed is less than that in the Cameron Highlands of Malaysia by three times (135,000 tonnes ha^{-1} yr^{-1}) by Ramli *et al*. (2004) and by two times (83,240 tonnes ha^{-1} yr^{-1}) in the Upper Min River Basin of SW China was estimated by Zhou (2008).

Regarding mean annual soil loss prediction using the RUSLE-GIS based model, there have been found in four watersheds from literatures reviews that their predictions were even closer to the predicted rate of the Mae Rim watershed (31.11 tonnes ha^{-1} yr^{-1}), despite differentiations in watershed sizes. For instance, Arekhi *et al*. (2012) applied the RUSLE and GIS for estimating soil erosion and sediment yield in a 480 km^2 are of the Cham Gardalan watershed in west Iran. Their predicted result shows the mean annual soil loss rate 39 tonnes ha^{-1} yr^{-1}. In another watershed in Thailand, Ongsomwang and Thinley (2008) quantified the mean annual soil loss rate using the RUSLE at about 31 tonnes ha^{-1} yr^{-1} in area of 782 km^2 of the Lam Phra Phloeng watershed in northeast Thailand. In Sri Lanka, Wijesekera and Samarakoon (2001) found the mean annual soil loss rate to be 30 tonnes ha^{-1} yr^{-1}, which is a result of a calculation using the original USLE model for the watershed area of 23,000 km^2

in Kegalle District. Lastly, Yue-Qing *et al.* (2008) also used the RUSLE model to predict mean annual soil loss in the Maotiao River watershed (3,109 km^2); 29 tonnes ha^{-1} yr^{-1} is the mean annual soil loss result revealed from their publication. Other research relating to studying soil erosion assessment by applying the (R)USLE model at watershed level is assembled and compared in Table 4.13

Table 4.13 Comparison of the estimated soil erosion rates using USLE/RUSLE.

Region	Study area		Soil erosion rate (tonnes ha^{-1} yr^{-1})			Source
	Name	Size (km^2)	Min	Max	Mean	
1. Malaysia	Langkawi Island	478	0	135,000	n/a	Ramli *et al.* (2004)
2. SW China	Upper Min River Watershed	23,040	325	83,240	n/a	Zhou (2008)
3. NW Thailand	Mae Rim Watershed	515	0	48,049	31.11	Semmahasak (2013) (this thesis)
4. NW Thailand	Mae Pan Sub-Catchment	45	0	16,549	n/a	Merritt *et al*. (1999)
5. Indonesia	Sampean Watershed	700	0	11,579	n/a	Faisol and Indarto (2010)
6. W Iran	Cham Gardalan Watershed	480	0	6,369	38.81	Arekhi *et al*. (2012)
7. NW Laos	Vieng Phoukha District	1,949	0	2,500	81	Dubber and Hedbom (2008)
8. Nepal	Khachi Khola Watershed	3719	0	2,042	315	Jha and Paudel (2010)
9. NE Thailand	Lam Phra Phloeng	782	0	923	31	Ongsomwang and Thinley (2008)
10. Sri Lanka	Kegalle District	23,000	0	887	29.7	Wijesekera and Samarakoon (2001)
11. N Thailand	Upper Nam Wa Watershed	646	0	800	21	Krishna Barhadur (2009)
12. SW China	Maotiao River Watershed	3,109	0	200	29	Yue-Qing *et al.* (2008)
13. Turkey	Seyhan River Basin	21,000	0	200	16	Irvem *et al*. (2007)
14. NE India	Dikrong River Basin	1,556	21	173	57	Pandey *et al.* (2009)
15. NW Turkey	Buyukcekmece Lake	630	0	109	2	Demirci and Karaburun (2012)

In terms of examining the key controlling factor affecting soil erosion production, land use/cover and topographical factors (CP and LS factors) are more dominant effects than rainfall erosivity and soil types (R and K factors) in the Mae Rim watershed. From the results obtained from comparison of data between the four controlling factors and the spatially distributed soil erosion risk map (by specifically focusing on extremely severe soil erosion areas), as well as testing the correlation coefficients using Pearson's method, it can be obviously indicated that two key controlling factors (i.e., CP and LS factors of RUSLE) are significant influences and moderate correlations on soil erosion in the Mae Rim watershed. It was similar to the study by Hui *et al.* (2010) who used USLE to predict soil erosion risk in the Liao Watershed, China. They found that LS and C factors were highly correlated with soil erosion. Likewise, Zhou (2008), Arekhi *et al*. (2010) and Abu Hammad (2011) have all clearly indicated that soil erosion is very sensitive to the LS factor, while Fu *et al.* (2006) applied RUSLE to estimate impacts of no-till practice on soil erosion in the Pataha Creek Watershed, SE Washington, USA. They concluded that agricultural land and the mines are the areas that experience the highest erosion.

4.4.1 Potential management practices on soil erosion in Mae Rim watershed

Research results revealed that topographical factors (LS), especially the slope length and slope steepness > 60 (dimensionless), greatly affect soil erosion at an extremely severe level (i.e., erosive magnitude > 150 tonnes ha^{-1} yr^{-1}). Additionally, ground cover factors (CP), especially bare land (without vegetation

cover) and field crop land, are also associated with the same level of extremely eroded soil. Moreover, the major determinants, including rainfall erosivity, soil erodibility, slope terrain, and ground cover directly affecting detachment of soil material (Lal, 2001; Dlamini *et al.,* 2011) are examined by using Pearson's correlation coefficient test. The results reveal that there are moderate correlations between the CP and LS factors and soil loss production (i.e., 0.3 and 0.263, respectively, with statistical significance $p < 0.01$), while other factors, such as rainfall erosivity (R) and soil erodibility (K), seem to be insubstantially correlated to soil erosion (i.e., –0.046 and 0.022, respectively, with statistical significance $p < 0.01$).

Even though the risk areas of severely eroded soil are significantly correlated with the extreme length and steepness of slopes in the Mae Rim watershed, the results obtained from the RUSLE-GIS-based model (see Figure 4.24; Table 4.8) reveal that the areas in the zones from severe to extremely severe erosion risk (i.e., soil loss rates ranging between 80–150 tonnes ha^{-1} yr^{-1} and over 150 tonnes ha^{-1} yr^{-1}) on the very steep slopes (slope gradient of more than 40°) appear as fractional patches totalling about 10 ha, compared to those on the sloping lands (slope gradient ranging from 10° to 25°) of about 1,630 ha in the total watershed area. The reason for this difference is that the virgin forests in the steep lands at an altitude above 1,000 m a.s.l. have been retained for preservation purposes in accordance with Thai government policy (Suraswadi *et al*., 2005), whilst farming is allowed on most sloping areas and they are used intensively for increased production of commercial field crops (e.g., maize,

soybeans, cabbage, potatoes and onions) in addition to traditional paddy rice (e.g., glutinous rice). Consequently, most sloping lands (moderate steep slopes) of the Mae Rim watershed have become areas of high erosion risk and degraded land.

It is essential that effective measures of soil conservation and management be adopted in order to prevent or minimise negative impacts from erosion risk. Consequently, this research has proposed general soil erosion risk management strategies in the Mae Rim watershed (Table 4.14), by focusing on areas of land which are vulnerable to severe soil erosion (i.e., the erosion vulnerable areas of bare land and field crop land dispersed along the various terrain slopes, ranging between 10°–25° and >25°). However, bare lands and field crop lands distributed on the flat terrains (slope < 10°) are not considered here because 'the flat terrain is usually stable in the sense that there is no or little soil loss hazard due to sheet erosion or mass movement; if terrain is gently sloping, susceptibility remains low' (Shrestha *et al.,* 2004, p. 150).

Table 4.14 General soil erosion risk management strategies—Mae Rim Watershed, NW Thailand.

Land cover related to high erosion risk (soil loss >80 t/ha/yr)	Terrain slope class (Inclination)	Area (ha)	General management strategies
Bare land	Sloping land (10°–25°)	474	- Rehabilitation and improvement of soil fertility through cover crop approach
	Steep to very steep land (25°–73°)	119	- Restoration of forest through approaches of afforestation and reforestation
Field crop land	Sloping land (10°–25°)	522	- Mulching with weeds and crop residues - Alley cropping (Hedgerow intercropping)
	Steep to very steep land (25°–73°)	57	- Planting stiff grass hedge across hillslope - Construction of terrace

I. Management practices on bare lands

As proposed management strategies, on all bare lands (without vegetation cover) on the steep to very steep areas of the Mae Rim watershed with topographical slope gradients of more than 25° (>44% slope), priority must be given to forest protection by restoration of forests (replanting trees) through afforestation and reforestation. Afforestation is commonly meant to imply planting trees in areas that were not previously covered by forest, whilst reforestation is the restocking of existing forests which have been depleted and which have suffered from deforestation (Forsyth, 2005). Both approaches can help produce a natural barrier that helps to prevent soil from being washed away by runoff during the rainy season. In addition to reducing the force of raindrops hitting the soil, these approaches can maintain a surface litter layer that can absorb water and minimise the overland flow generation (Forsyth and Walker, 2008). To suit the local climatic conditions and soil properties in the Mae Rim watershed, indigenous forest tree species, such as figs (*Ficus Spp*), legumes (*Leguminosae*), and oaks and chestnuts (*Fagaceae*), are recommended for replantation (Fróis *et al.*, 2008). According to Fróis *et al.* (2008), there are at least 47 indigenous fig species, 61 native legumes trees, and 40 species in the *Fagaceae* family growing in northern Thailand. Moreover, all can grow well in degraded sites, especially at high altitudes with low nutrient levels and are able to create dense canopies to prevent soil erosion. In a similar study based on field performance, Elliot *et al*. (2003) found a high survival and growth rate of the fig tree, one of the nine species ranked as excellent framework species. It is also suitable for forest restoration in tropical hill

evergreen forests, which are normally located at high altitudes (>1,000 m a.s.l.) of tropical mountainous regions in north and northwest Thailand.

On sloping landscapes (inclinations ranging from 10° to 25°), bare lands occur because natural vegetation has been cleared and the land is utilised intensively for agricultural production without efficient treatment, resulting in soil nutrient depletion and subsequent abandonment (Sakurai *et al*., 1996). Thus, the appropriate management strategy in cases like this should be to rehabilitate and improve the patches of sloping bare lands in order to restore soil fertility. The proposed strategy of planting crops/shrubs/trees species that can biologically fix nitrogen in the soil according to the cover crop approach could possibly be applied on barren areas or degraded lands (Recha *et al.,* 2014). According to the research of Tudsri and Kaewkunya (2002), Sidle *et al*. (2006), and Ogunlana *et al.* (2010), grass species (e.g., *Dwarf Napier* and *Ruzi* grasses) and the perennial legume species (e.g., *Leucaena leucocephala*) have been widely used in Southeast Asia. Their benefits include not only providing increased nitrogen in the soil, but also conserving the soil on bare lands as a deterrent to direct raindrop impact on bare soil surfaces. Thus, nitrogen-fixing plants species like grasses and perennial legume trees are suitable for planting on the slopes of bare lands of the Mae Rim watershed.

II. Management practice in field crop lands

Thai law prohibits cultivating on slopes steeper than 20° (>35% slope). Nevertheless, many ethnic minorities (hill tribes) occupying the highlands of

north and northwest Thailand for centuries have encroached and cultivated intensively on steep slopes for subsistence (Sang-Arun *et al*., 2006). Thus, encouraging highland farmers to plant tree crops, rather than existing traditional field crops, may be quite difficult to implement, not to mention requiring more time and expense. Therefore, planting stiff grass hedges (e.g., vetiver) across the hill slopes would be a preferable and economical choice for highland farmers to minimise soil loss on their steep agricultural lands. Donjadee *et al.* (2010) found, in experimental plots with land slopes (30, 40 and 50 percent) under three simulated rainfall intensities (60, 85 and 110 mm h^{-1}) that the vetiver grasses tested on several experimental plots can decrease runoff volume and soil loss in steep slope areas by 39–69% and 56-88%, respectively. Therefore, establishment of vetiver grass hedge barriers can reduce the effect of slope length and steepness by changing the overland flow direction, reducing the velocity of water flow, providing surface protection against raindrop impact, and forming barriers to trap soil before it moves downslope (Abu Hammad, 2011). Furthermore, vetiver grasses can be used to prevent gully incision. According to Poesen *et al*. (2003), plantation of stiff grass hedge barriers across concentrated flow zones can retard and disperse surface runoff as well as control gully erosion.

Alternatively, terraces could be constructed on steeply sloped terrain as a means of reducing erosion. Terraces can make cultivating on steep slopes easier, especially when accompanied by diversion ditches which can help control excess water runoff (Recha *et al.,* 2014). In addition, Sherstha *et al.*

(2004) view the terrace technique as a possible way of cultivation on steep slopes that can conserve more soil. However, establishing terraces to prevent soil loss from water runoff is costly. Many highland farmers may not be able to afford the high cost of terrace constructions. Moreover, substandard terraces cannot control soil erosion effectively, especially when wet (Sidle *et al.*, 2006). Hence, farmers should carefully consider whether to construct terraces for reducing erosion on steeply sloped areas, and should also be aware of environmental impacts caused by construction.

Regarding management of field crop lands in areas of moderately sloped terrain, surface mulching and alley cropping are suggested as ways for local farmers to reduce surface erosion. Mulching is the process of covering the soil surface with organic matter to create conditions that are more favorable for plant growth, improving the decomposition and mineralisation of organic material in the soil and protecting the soil from erosion (Recha *et al.,* 2014). Mulching with weeds and crop residues can cause a major reduction in runoff by protecting soil surfaces that are prone to crusting from raindrop action (Panomtarinichigul, 2006). Alley cropping (hedgerow intercropping) is a system of growing annual crops between rows of trees, shrubs or perennial legumes to form hedgerows (Recha *et al.,* 2014). Planting perennial plants as hedgerows along the contours and growing agricultural crops in the alleyways can act as biological barriers to trap sediments flowing from the upland, and also minimise soil erosion by reducing surface runoff velocity, leading to higher deposition of soil sediment (Paningbatan *et al.,* 1995). As described above, it is reasonable to

recommend that both mulching and alley cropping can be adopted as effective techniques for intensive farming on sloping lands of the Mae Rim watershed. In conclusion, because of simple implementation and low-cost erosion control techniques, the methods of surface mulching and alley cropping are preferable.

4.5 Conclusion

Soil erosion is considered a serious problem in developing countries, including Thailand, which has limited technical and financial resources to study erosion. The Mae Rim watershed is a sub-watershed of the Upper Ping River Basin of Northern Thailand that has encountered a serious problem, because of steep slopes, high rainfall and increased shifting cultivations by hill tribes. It is thought by some that the activities of these tribes can exacerbate soil erosion and increase the flux of sediment into rivers, floodplains and reservoirs. This chapter aimed to use RUSLE-GIS-based modelling to estimate the soil erosion rate on a 25-m grid cell basis for the Mae Rim watershed, northwest Thailand. In order to achieve the research aim, it was therefore designed with three specific objectives: firstly, to propose a multiple regression method for mapping the spatial variation of rainfall runoff erosivity factor of the RUSLE, based on available data in the area; secondly, to apply the Revised Universal Soil Loss Equation (RUSLE) with GIS in order to evaluate the potential soil loss for the Mae Rim watershed, Northern Thailand; and thirdly, to identify the high erosion risk areas and examine the key controlling factors affecting an area of extremely severe soil erosion in the study area.

GIS techniques were successfully applied to assess soil erosion factors. The raster map of spatial variation of rainfall runoff erosivity (R) was derived from the multiple regression equation by forcing altitude, latitude and longitude of the study area. As well as other factors such as soil erodibility (K), slope length and steepness (LS), cover management and conservative support practice (CP) factors were assigned the values for generating the thematic raster maps based on 25-m grid cells. These 25-m resolutions of raster maps were multiplied as detailed in equation [4.1] by using the raster calculator in the spatial analyst of ArcGIS 9.3. In general, it is clear from the results of this study that RUSLE in conjunction with GIS functionality is a powerful model to spatially make qualitative and quantitative assessments of soil erosion risk for conservation management purposes.

The RUSLE's factors were calculated using local data that was collected specifically for Mae Rim watershed. The R value ranged between approximately 492 and 994 MJ mm ha^{-1} h^{-1} yr^{-1}; the maximum rainfall erosivity value mostly occurred in the west part of the catchment (uplands), while the minimum rainfall erosivity value mostly appeared in the east part of the catchment (lowlands). The LS factor in the watershed varied from 0 to 1370.2, the mean LS factor is 9.99 with a standard deviation of 20.42. For K, C and P values were between 0.13 and 0.37, 0 and 0.474, and 0 and 1, respectively.

The results illustrate that the mean annual soil loss rate which was derived from an application of the RUSLE-GIS-based model is fairly high. The maximum

value of annual soil loss is 48,049 tonnes ha^{-1} yr^{-1}, while the mean annual soil loss is about 31 tonnes ha^{-1} yr^{-1} with standard deviation of 264 tonnes ha^{-1} yr^{-1}. The results from spatial relation between controlling factors and soil erosion classes in the Mae Rim watershed showed that the area of extremely severe soil erosion is significantly correlated with the high slope length and steepness (LS) in addition to bare lands and field crop lands on the catchment.

Furthermore, the results from Pearson's correlation coefficient indicated that the land use/land cover (CP factor) and slope-length (LS factor) were moderately correlated with the rate of soil erosion generation in the Mae Rim watershed. At a significance level of 0.01, their correlation coefficients are 0.3 and 0.26, respectively, whereas the erosivity (R-factor) and erodibility (K-factor) seem to be insubstantial correlations with soil erosion generation. These imply that if there were any changes taking place in land use/cover, slope length or slope gradient, they could possibly affect soil erosion changes in the Mae Rim watershed more so than changes in rainfall erosivity and soil types.

4.6 Chapter summary

In this chapter, the RUSLE-GIS-based modelling was used to compute the mean annual soil loss, and to map the spatially-distributed soil erosion risk in the Mae Rim watershed. Moreover, the key controlling factors which interact to generate the extremely high soil erosion rates in the Mae Rim watershed have been indicated, and found that bare land, field crop land and high steep slope are significantly associated with extremely soil erosion in the Mae Rim

watershed, respectively. In terms of soil loss prediction, because of the unavailability of the actual measured soil erosion values in the Mae Rim watershed and the fact that none of the previous case studies had carried out an estimation of the soil erosion in the whole area, the mean annual soil loss predicted based on RUSLE-GIS modelling has not been validated numerically. However, model validation can generally be conducted by comparison between predicted and measured mean annual sediment yields at the basin outlet or gauging stations (e.g., Ranzi *et al*., 2012; Shi *et al.,* 2012), which will be described in detail and evaluated in the Chapter 5.

CHAPTER 5: ESTIMATING SUSPENDED SEDIMENT YIELDS USING A SEDIMENT RATING CURVE AND EROSION MODELS

5.1 Introduction

In order to address the second research objective, this chapter focusses on the assessment of mean annual sediment yields in Northwest Thailand watersheds by using the sediment rating curve method and the soil erosion model, RUSLE. The specific objectives of this chapter are: (i) to estimate the suspended sediment fluxes and yields in catchments selected as representatives in the Upper Ping River Basin using the sediment rating curve method, and (ii) to estimate and verify the sediment yield rates as a result of applying the coupling of the RUSLE-GIS-based model with different concepts between sediment delivery ratio (SDR) and sediment transport capacity (STC), by considering the actual measured rates that extrapolate from the best-fitted equation of the sediment rating curve method.

The sediment rating curve method can be used to extrapolate the suspended sediment fluxes and yields in both natural streams and artificial channels. Most scholars (e.g., Walling, 1977; Asselman, 2000; Kao and Liu, 2001; Picouet *et al.,* 2001) have usually chosen this method for their studies in cases of either reduction of intense sediment sampling, lack of continuous monitoring or failure to collect the suspended sediment concentration for all flow events (Walling and

Webb, 1981; Horowitz, 2003; Francke *et al.,* 2008; Gao, 2008; Smith, 2008). On the other hand, the sediment rating curve method still has some limitations. Gao (2008) briefly notes that suspended sediment fluxes do not actually only depend on discharge but also upstream supply that is associated with geological and geomorphological conditions, soil types and land use / land cover. As a result, the relationships between suspended sediment fluxes and discharge display significant scatter (Walling, 1977; Walling and Webb, 1981). In addition, the annual sediment load or sediment yield can be overestimated and the error estimates can substantially vary from the actual ones between −80% and 900% (e.g., Walling, 1977; Dickinson, 1981; Asselman, 2000; Smith, 2008). Mano *et al*. (2009) state that two types of errors (i.e. under- or over-estimating suspended sediment fluxes), can occur during flux measurements. The possible factors include: (a) an inappropriate sampling frequency; (b) the logarithmic transformation of the original data; (c) not subtracting non-denudational components of the river's load (e.g., atmospheric chloride and geothermal compounds, organic matter, and dry fallout); (d) ignoring of bedload; and (e) the spatial and temporal variability of the suspended sediment concentration in rivers can induce large errors or statistical bias in flux estimations (Walling and Webb, 1981; Lawler, 1991; Gao, 2008).

Because of some contained limits in the sediment rating curve method as mentioned above, as well as an inability to elucidate the dynamics of suspended sediment transport within the watershed (Gao, 2008), various types of sediment modelling are thus introduced instead of the sediment rating curve.

Even though many types of sediment modelling can be beneficially used for describing or simulating the physical processes of sediment availability, removal and transport, in addition to estimating sediment fluxes on larger scales (e.g., watersheds or basins), the modelling with regard to sediment yield estimation still needs validation against observed data.

Bhattarai and Dutta (2007) broadly group erosion modelling for sediment yield estimation into two categories: (1) physically based modelling, and (2) empirical modelling. Meanwhile, Merritt *et al.* (2003) argue that there is generally no single type of modelling that is best for all applications, but the most suitable one will depend on the intended use and characteristics of the catchment or watershed being considered. Although physically based modelling has obviously been more reliable and accurate than empirical modelling in terms of relying on mathematical equations to explain various hydrological and sediment processes on hill slopes and channels (Gao, 2008), empirical modelling, e.g. RUSLE, is still widely applied all over the world for the estimation of surface erosion and sediment yield from watershed areas (e.g., see Section 1.3).

Although the RUSLE cannot estimate sediment yield directly, the sediment delivery ratio (SDR) concept has been adopted in conjunction with RUSLE to estimate sediment yield in various spatial scales (Lin *et al.,* 2002; Amor *et al.,* 2004; Lim *et al.,* 2005; Mutua *et al.,* 2006; Ricker *et al.,* 2008). The SDR is the ratio of the suspended sediment yield at the downstream point of interest (watershed outlet), or a specific channel cross-section, to gross erosion rates in

the whole watershed, as expressed in equation [5.11]. There is, however, still debate about the concept (Kinnell, 2008; Ding and Richards, 2009) due to the fact that gross erosion is not only at least as difficult to predict as sediment yield, but their ratio is also even more uncertain (Lane *et al*., 1997; De Vente *et al.,* 2007). In addition, Ding and Richards (2009) ascribe that the SDR deals with watershed as lumped, and it does not consider the spatial variation in sediment delivery processes within the watershed (Van Rompaey *et al.,* 2001; Alatorre *et al.,* 2010).

With existing limits in the SDR concept as mentioned above, an alternative concept, like sediment transport capacity (STC), seems to be a better way than the SDR with its ability to demonstrate the movement of soil material down a slope to downstream. In addition, the STC concept is used to represent the potential sediment flux and as a basis for scaling actual erosion rates (Prosser and Rustomji, 2000), and its formulae are expressed as equations [5.7] and [5.8].

However, both SDR and STC concepts have still been widely used in conjunction with RUSLE for assessing soil loss and sediment yield (e.g. Lin *et al.,* 2002; Amor *et al.,* 2004; Lim *et al.,* 2005; Mutua *et al.,* 2006; Bhattarai and Dutta, 2007; Ricker *et al.,* 2008; Jain *et al*., 2009; Hui *et al*., 2010; Jain and Das, 2010; Saidi *et al.,* 2010). In Thailand, only few publications can be found in regards to the study of sediment yield estimation using RUSLE in conjunction with either of the SDR or STC concepts (e.g., Bhattarai and Dutta, 2007; Saidi

et al., 2010). Yet, the efficacy between SDR and STC concepts connecting the model, and the accuracy of estimated sediment yield rates are still in doubt in terms of application for Thailand's watershed studies. Consequently, these uncertainties have significantly challenged and persuaded the author to study both the application of the rating curve method and erosion modelling for estimation of sediment fluxes and yields in Northwest Thailand watersheds, and also include these in the modelling validations.

5.2 Methods

5.2.1 Data availability

The suspended sediment concentration (SSC) and runoff data have been recorded during the past decade by the Royal Irrigation Department of Thailand (RID). Thirteen flow-gauging stations are located throughout the Upper Ping River Basin (Figure 5.1). Of these, three stations have recorded the SSC for at least fifteen years; five stations have five or more years of data and another five stations have less than five years of data.

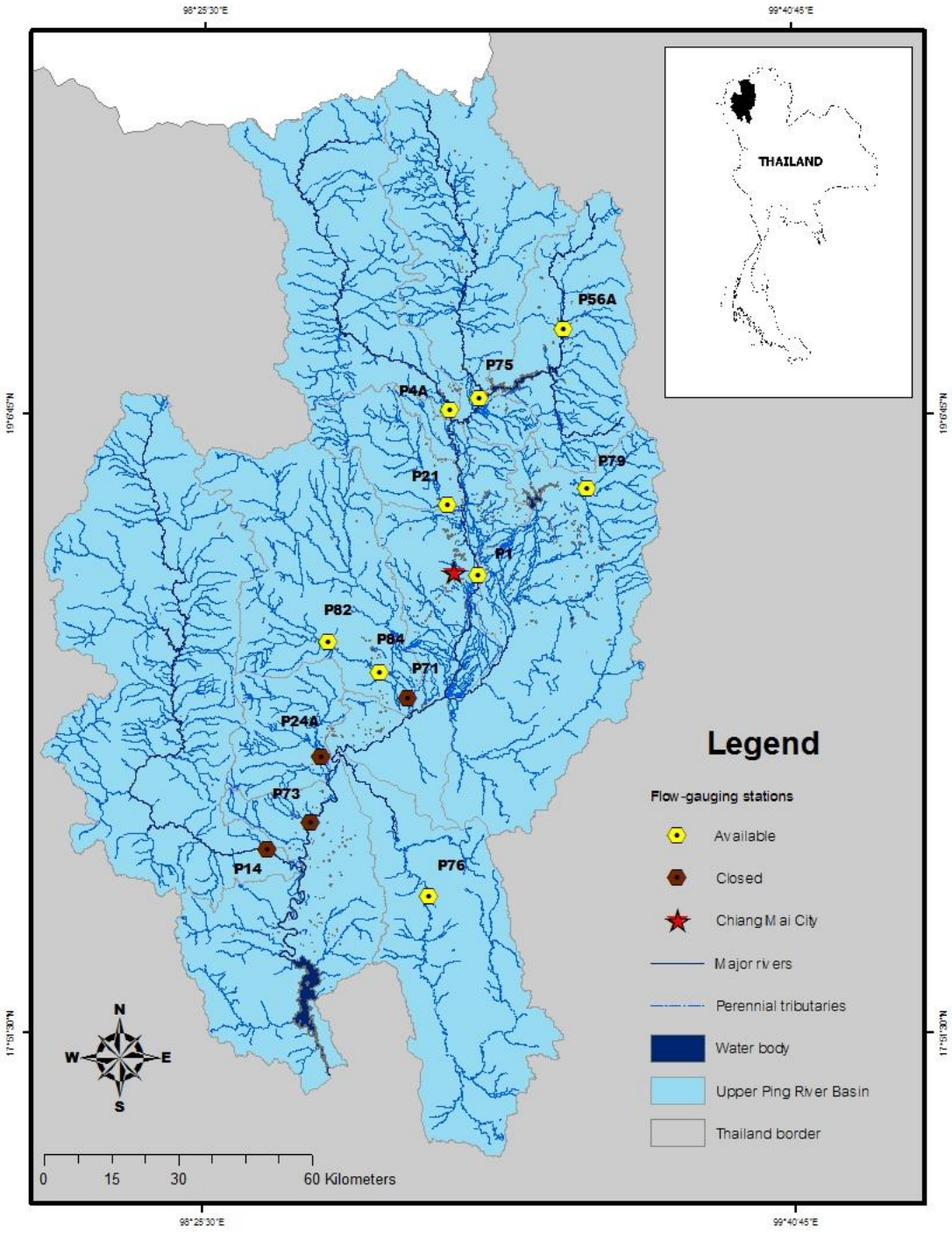

Figure 5.1 Upper Ping River Basin

However, it is not possible to study all catchments of the Upper Ping River Basin because of unavailable, incomplete and unobtainable data in some catchments during fieldwork data collection. As a result, in terms of studying the

sediment yield estimation using the sediment rating curve method, eight catchments provide measured data – river discharge, suspended sediment concentrations and loads for their individual catchment areas – have been selected as the case study areas for this thesis. Those catchments include: (1) Upper Mae Ping, (2) Middle Mae Ping, (3) Mae Taeng, (4) Mae Rim, (5) Mae Ngad, (6) Upper Mae Wang, (7) Lower Mae Wang, and (8) Li (Table 5.1).

Table 5.1 Details of watershed data in the Upper Ping River Basin

	Watershed name	*DBA (km^2)	Station code	Station name	Location		Data period		Conditions of data	Site selected
					Lat. (N)	Long. (E)	Start	End		
UPPER PING RIVER BASIN	1. Upper Mae Ping	3,090	P75	Ban Cholae	19°08′58″	99°00′43″	2001	-	Available	✓
	2. Middle Mae Ping	6,355	P1	Nawarat Bridge	18°47′10″	99°00′27″	1993	-	Available	✓
	3. Lower Mae Ping	16,815	P73	Ban Sop Soi	18°17′25″	98°39′01″	2001	2007	Unavailable	✗
	4. Mae Taeng	1,929	P4A	Ban Mae Taeng	19°09′49″	98°55′03″	1992	-	Available	✓
	5. Mae Chaem	3,927	P14	Ta Kham Bridge	18°13′50″	98°33′38″	1968	2005	Unavailable	✗
	6. Mae Rim	515	P21	Ban Rim Tai	18°55′45″	98°40′51″	2001	-	Available	✓
	7. Mae Klang	611	P24A	Pracha Uthit Bridge	18°23′15″	98°40′51″	1997	2001	Unavailable	✗
	8. Mae Ngad	539	P56A	Ban Rom Klao	19°16′49″	99°11′23″	2000	-	Available	✓
	9. Mae Khan	1,299	P71	Ban Klang	18°32′13″	98°51′45″	2001	2002	Unavailable	✗
	10. Upper Mae Wang	389	P82	Ban Sob Win	18°39′46″	98°21′54″	2006	-	Available	✓
	11. Lower Mae Wang	493	P84	Ban Pan Ton	18°35′19″	98°47′58″	2006	-	Available	✓
	12. Mae Kuang	1,703	P79	Ban Mae Wan	18°57′43″	99°14′26″	2007	2009	Incomplete	✗
	13. Li	1,541	P76	Ban Mae E-Hai	18°08′07″	98°54′12″	2001	-	Available	✓

Note: *All data used in this research are available till the end of water year 2009; *DBA is Drainage Basin Area (km^2)*

With regard to the SSC sampling, it has been undertaken by the depth-integrated method using, e.g. US DH-48, US DH-49 and US DH-59 samplers (Royal Irrigation Department, 2011). The sampled sediment concentrations are determined in the RID laboratory, mostly by filtration technique on pre-weighted fibreglass filters (the pour size = 0.45 μm), then dried and weighted (Achite and Ouillon, 2007). The SSC is expressed as parts per million (ppm), but typically measured in units of milligrams per litre (mg/l), by dry weight of the sample. Suspended sediment samples in Thailand are usually collected at least twice a month (i.e., more than 20 times a year), and are used to develop sediment rating curves for each stream gauging station site, where values of suspended sediment loads (tonnes/day) are plotted against the river discharge at the time of sampling**.**

Figure 5.2 shows the river discharges (Q) plotted against the number of suspended sediment concentration samplings taken, ranging between 32 and 40 times a year, at eight river gauging stations in the typical water year 2009, during April 1st, 2009 – March 31st, 2010. The maximum SSC sampling (i.e., 40 samples) was obtained from station P1 in Middle Mae Ping watershed (Figure 5.2b), whereas P4A and P82 of Mae Taeng and Upper Mae Wang watersheds, respectively, are the stations obtaining the minimum SSC samplings – at 32 samples (Figures 5.2d and 5.2g).

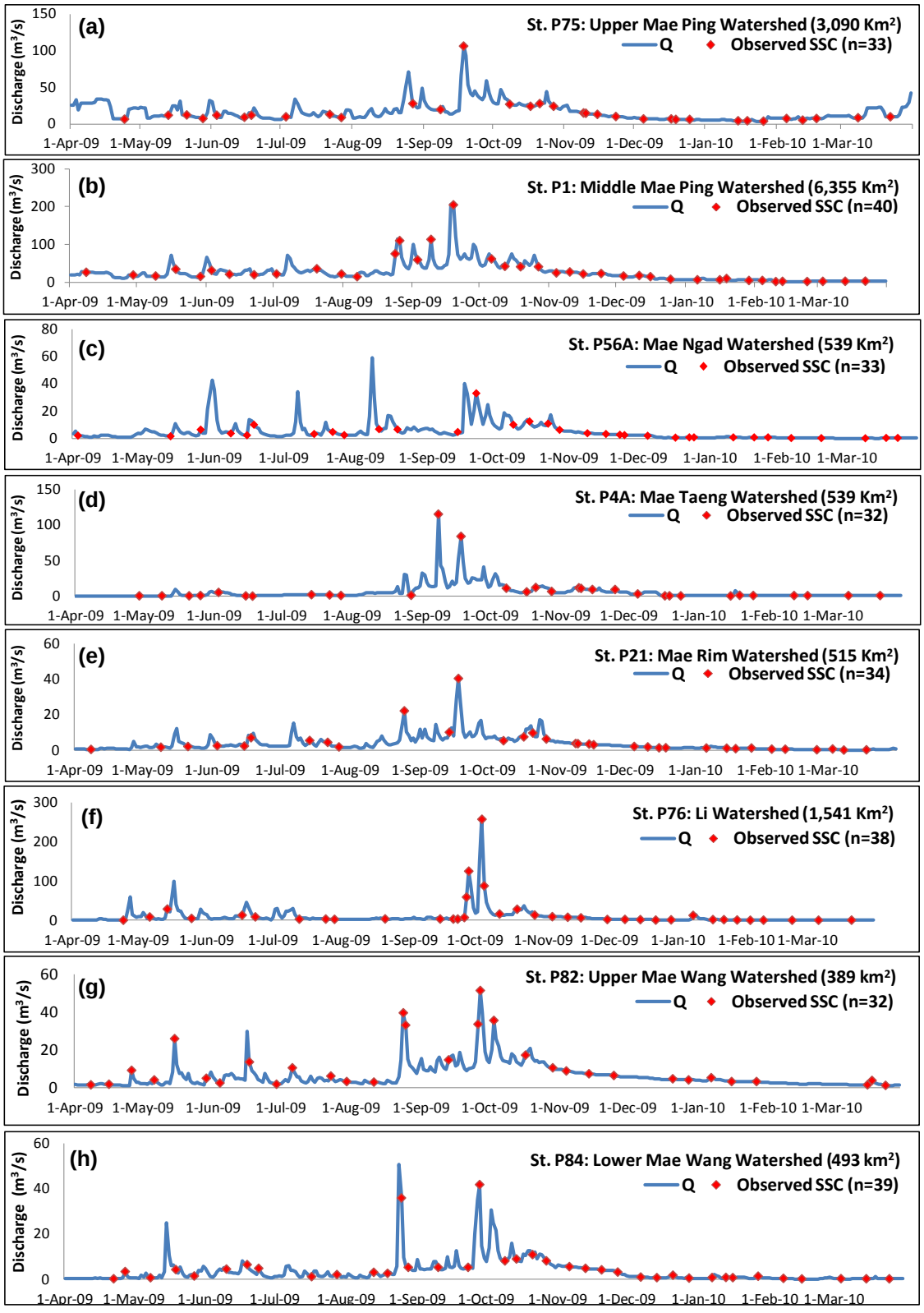

Figure 5.2 Sampling numbers of observed suspended sediment concentration (n) which were taken at eight river gauging stations during April 1st, 2009 – March 31st, 2010 (i.e., water year 2009).

There are several procedures to estimate preliminary daily sediment loads by multiplying suspended sediment concentration and river discharge at the time of sampling (e.g., Dickinson, 1981; Walling and Webb, 1981). However, the estimated sediment loads obtained from using these different approaches can also provide variations in precision and accuracy of estimated values (Lawler, 1991).

The following formula is used for calculating the preliminary suspended sediment loads (Guyot *et al*., 1996; Lidén, 1999; Kao and Liu, 2001; Horowitz, 2003) and will also be used in this study.

$$\mathrm{SSL} = \mathrm{Q} \times \mathrm{SSC} \times 0.0864 \qquad [5.1]$$

Where SSL is estimated suspended sediment loads (tonnes/day); Q is river discharge at time of sampling (m^3/s); SSC is suspended sediment concentration at time of sampling (mg/l), and 0.0864 is a coefficient value based on the unit of measurement of water discharge. Due to the fact that water discharge data in the metric system are typically reported in 'm^3/s' and suspended sediment load data in 'tonnes/day'. If water data are in cubic metres per second, the weight of 1 cubic metre of water is 1 metric ton (tonne), and the time interval is 24 hours (Porterfield, 1972); therefore $\left(\frac{86{,}400 \text{ seconds per day x 1 tonne per cubic metre}}{1{,}000{,}000}\right)$ is a derivation of the coefficient value, or conversion factor, used for equation [5.1]. In addition, daily loads were estimated as the product of the instantaneous daily

measurement of discharge and suspended sediment concentration, integrated over the entire day, and were summed to give total storm sediment loads (Luk *et al.,* 1997; Horowitz, 2003; Ward, 2008).

5.2.2 Estimation of sediment yield by using the sediment rating curve

The rating curve was developed by relating suspended sediment concentrations, or loads, to discharges over a range of discharge events (Achite and Ouillon, 2007; Gao, 2008). In the absence of manpower or automatic equipment for frequent sampling, many workers have used the sediment rating curve technique to estimate the suspended sediment concentrations or loads for subsequent flux calculations (Horowitz, 2003; Kisi *et al.,* 2006).

The sediment rating curve commonly represents a functional relationship of the form (Picouet *et al*., 2001; Horowitz, 2003; Kisi *et al.,* 2006; Smith, 2008) below:

$$SSC_{RC} = \alpha Q^{\beta} \qquad [5.2]$$

or

$$SSL_{RC} = \alpha Q^{\beta} \qquad [5.3]$$

Where Q is river discharge (m^3/s); SSC_{RC} and SSL_{SC} are suspended sediment concentration (mg/l) and suspended sediment load (tonnes/day) for the rating curve, respectively. Variables α and β are dimensionless regression coefficients (Asselman, 2000), and are estimated by the ordinary least squares regression of the log transformed variables SSC or SSL and Q (Horowitz, 2003). Although

equations for SSC–Q and SSL–Q relationships have been successively adopted recently, they still have differences in their performance. Achite and Ouillon (2007, p.195) conclude that 'the use of the SSC–Q relationship and the multiplication of SSC by Q thus appear to introduce less error than using the law SSL–Q, even though the SSL–Q relationship presents a higher correlation'.

5.2.3 Estimation of sediment yield by using RUSLE-GIS-based model

As a result of RUSLE not providing an ability to account for deposition in a prediction of sediment yield at the watershed outlet or downstream point of interest (De Vente *et al.,* 2005), the concepts of 'sediment transport capacity' (STC) and 'sediment delivery ratio' (SDR) are usually employed to simulate the spatial process of sediment erosion, deposition and outflow (Jain and Das, 2003; Jain *et al.*, 2009) in addition to calculating the amount of sediment yield within the drainage basin area in conjunction with the RUSLE.

(1) Sediment Transport Capacity (STC)

As has already been implied in Chapter 1 (see Section 1.4), the concept of STC is the transport limiting delivery and is used for representing the potential sediment flux and also as a basis for scaling actual erosion rates (Prosser and Rustomji, 2000). It was developed based on Meyer and Wischmeier's (1969) conceptualisation of 'erosion as a two-phase process comprising the detachment and transport of soil particles by rainfall and runoff' (cited in Morgan and Nearing, 2011, p.12) (see Figure 1.4).

To predict sediment yield by using the coupled RUSLE-STC, Van Rompaey *et al.* (2005) suggest the following equation for computing the annual sediment transport capacity. The formula here is widely used in several recent works (e.g. Feng *et al*., 2010; Shi *et al*., 2012)

$$STC = K_{TC} R K (LS - 5.3 S^{0.8}) \quad [5.4]$$

Another formula proposed by Verstraeten *et al.* (2007) is:

$$STC = K_{TC} R K A^{1.4} S^{1.4} \quad [5.5]$$

Where: STC = sediment transport capacity (tonnes ha^{-1} yr^{-1}); K_{TC} = transport capacity coefficient (−); R = rainfall erosivity factor of RUSLE (MJ mm/ha h yr); K = soil erodibility factor of RUSLE (tonnes h/ MJ mm); LS = slope length and steepness factor; A = upslope area (m^2); and S = local slope gradient (m m^{-1}).

K_{TC} reflects the effects of vegetation cover on overland flow sediment transport (De Vente *et al.,* 2008, 2009), and is used for calibration by applying the model with a wide range of K_{TC}, which generally ranges from 0 to 0.5 (Jordan *et al*., 2005). Also, Jordan *et al.* (2005) found that the calibrated K_{TC} values that suit well and poorly vegetated areas are 0.11 and 0.25, respectively.

Since K_{TC} strongly depended on land use and land cover types, it is in order to co-relate it with the vegetative index value of the area to get the spatial

distribution of transport capacity coefficient (Jain and Das, 2010). In addition, Jain and Das (2010) suggest the transport capacity coefficient is empirically linked to the Normalised Difference Vegetation Index (NDVI) derived from satellite imagery. The NDVI can be expressed as:

$$\mathrm{NDVI} = \frac{\mathrm{Band4} - \mathrm{Band3}}{\mathrm{Band4} + \mathrm{Band3}} \qquad [5.6]$$

Where Band3 (λ = 0.63 – 0.69 μm) is visible red (VR);

Band4 (λ = 0.75 – 0.90 μm) is a near infrared (NIR)

The possible range of NDVI values is between −1 and 1. Typically, a higher positive value for a pixel in NDVI indicates more dense vegetation, whereas a lower negative value for a pixel in NDVI indicates bare soil (Jones and Vaughan, 2010). Also, Jain and Das (2010) propose a new relation of K_{TC} for cell size area, which is hypothesised as an exponential function of NDVI, as in the formula shown below:

$$\mathrm{K_{TCi}} = \beta \exp\left[\frac{-\mathrm{NDVI_i}}{1 - \mathrm{NDVI_i}}\right] \qquad [5.7]$$

Where $\mathrm{NDVI_i}$ is the NDVI value for cell i; β is a scaling factor, which can be examined through calibration and also provides a wide range of situations

(Figure 5.3). In addition, Jain and Das (2010) suggest that β = 1 (i.e., no scaling) is most sensitive to sediment yield at their site (i.e., Simra gauging site, India),

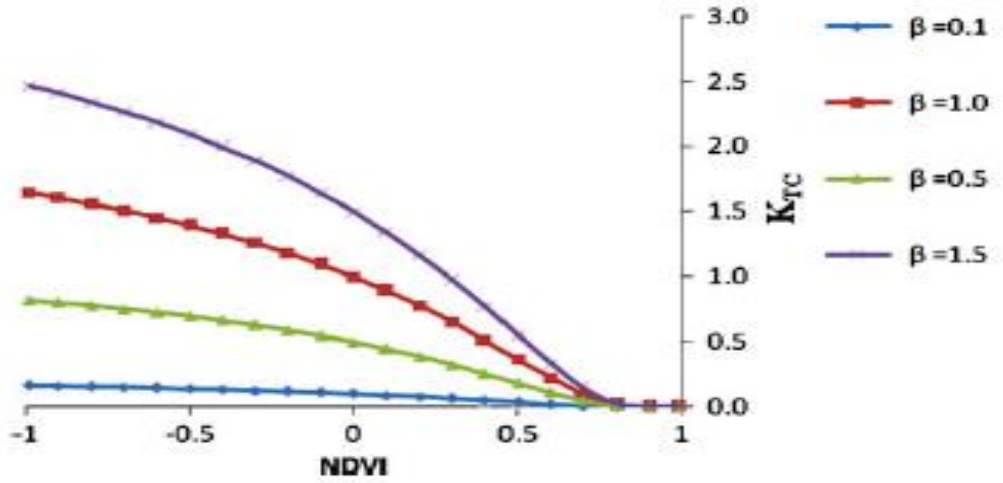

Figure 5.3 Effect of scaling coefficient β on computed K_{TC} value

(Source: Jain and Das, 2010)

However, this thesis provides the β tests in a range of between 0.07 and 1 through calibration of transport capacity coefficient (K_{TC}), in order to minimise error and inprove a predicted specific sediment yield (SSY) at river gauging station P21 of the Mae Rim watershed, in particular.

In the model application, soil erosion and sediment transport capacity are known as pixels, sediment is routed through the basin towards the river along a runoff pattern that is calculated with a multiple-flow algorithm (Desmet and Gover, 1996; De Vente *et al.*, 2008). Consequently, if the differentiation of the STC pixel is smaller than the sediment flux reaching that pixel, the deposition is

modelled. On the other hand, if the differentiation of STC pixel is greater than or equal to the sediment flux reaching that pixel, the sediment yield is modelled.

(2) Sediment delivery ratio (SDR)

Sediment yield is usually not available as a direct measurement but it can be estimated through the sediment delivery ratio concept. Ouyang and Bartholic (1997) stated that the sediment delivery ratio is perhaps referred to as a 'transmission coefficient'. In addition, it is often used for correcting the reduction effect (Lu *et al.,* 2006) and most commonly defined as the fraction of the sediment delivered at the watershed outlet or sediment yield to gross erosion within the basin (Walling, 1983; Lim *et al.,* 2005). The SDR is dimensionless and expressed as follows:

$$\mathrm{SDR} = \mathrm{SY} / \mathrm{E} \qquad [5.8]$$

Where SDR is sediment delivery ratio (in a fraction); SY is average annual sediment yield per unit area (tonnes km^{-2} yr^{-1}); E is gross erosion per unit area over the measuring point (tonnes km^{-2} yr^{-1})

SDR normally has a value range between 0 and 1 due to the sediment deposition occurring before reaching the watershed outlet. Also, the various values of SDRs have been adopted popularly in conjunction with USLE/RUSLE to estimate sediment yields in several countries as listed in Table 5.2 below.

Table 5.2 The typical varieties of SDR values used for estimating the specific suspended sediment yields in several countries

Country	Watershed		SDR value	Authors
	Name	Size (km^2)		
Thailand	Mun	69,000	0.83 – 1.0	Bhattarai and Dutta (2007)
Kenya	Masinga	6,262	0.29	Mutua *et al.* (2006)
China	Liao	3,530	0.206	Hui *et al.* (2010)
Indonesia	Sumani	583	0.105	Aflizar *et al.* (2010)
Iran	Cham Gardalan	480	0.23 – 0.49	Arekhi *et al.* (2012)
Malaysia	Kelang	380	0.27	Balamurugan (1991)
Greece (1993)	Lagadas	246	0.55	Bakker *et al.* (2008)
Portugal (1990)	Amedoria	44	0.14	
Belgium (2001)	Hangeland	13	0.65	
France (2001)	Lautaret	13	0.30	
South Korea	Sudong	11	0.24 – 0.45	Lim *et al*. (2005)

There is no explicit procedure regarding SDR estimation, although USDA has published a handbook in which the SDR is related to drainage area (Ouyang and Bartholic, 1997; Mutua *et al.,* 2006). One of the most popular methods used to estimate SDR for a large catchment scale is through the empirical SDR-area power function (Lu *et al.,* 2006):

$$\mathrm{SDR} = \alpha \mathrm{A}^{\beta} \qquad [5.9]$$

Where A is drainage area (km^2); α and β *are* empirical parameters. The inverse relationship between SDR and drainage area (or the exponent β being a negative) can be explained in terms of the decreasing slope and channel gradients related to the increasing basin size (Walling, 1983). During transport

through a watershed, more sediment is trapped in footslopes, concavities, alluvial plains and other sinks, meanwhile, erosion does not increase or even decrease because of decreasing hill-slope gradients downstream (De Vente *et al.,* 2007).

Other attempts to develop equations suitable for estimating SDR in conjunction with RUSLE-GIS-based modelling include that of Williams and Berndt (1972) (cited in Hui *et al.,* 2010, p.945) who specify a main channel slope is more significant effect than other parameters (e.g., length of watershed, drainage network, watershed area, runoff-rainfall erosivity, land use/land cover and sediment particle size effects) in regard to predicting SDR. The equation can be expressed as follows:

$$\mathrm{SDR} = \quad 0.627\mathrm{SLP}^{0.403} \qquad [5.10]$$

Where, SLP (%) is the slope of the main stream channel. This equation is recommended by Onyando *et al*. (2005) and Hui *et al.* (2010), with regard to providing a reasonable prediction, and in a case where data is inadequate.

Tim *et al*. (1992) (cited in Fistikoglu and Harmancioglu, 2002, p.455) have proposed an equation that the SDR can be calculated from the relief and slope of the watershed, water body and land use data maps according to the expression:

$$SDR = \exp(-k\,S\,L) \quad [5.11]$$

Where, k is a coefficient varying with land cover; S is the slope function; L is the length of the flow path between each cell and the watershed outlet.

Moreover, Ferro and Minacapilli (1995) hypothesise that SDR in grid cells is a strong function of the travel time of overland flow within the cell, and the SDR can be estimated as the following equation:

$$SDR = \exp(-\gamma t_i) \quad [5.12]$$

Where, γ is a coefficient considered as constant for a given catchment, generally varying from 0.5 to 2.0 (Fu *et al.*, 2006); t_i is the travel time (hr) for cell i to the nearest channel cell. It is assumed that the sediment that reaches the stream network takes the same travel time as the runoff (Fu *et al*., 2006; Mutua *et al.,* 2006; Bhattarai and Dutta, 2007).

Although many authors (e.g., Van Rompaey *et al.*, 2001; Kinnell, 2008; Jain *et al.*, 2009) have indicated that the concept of STC is somewhat stronger than SDR in terms of dealing with the deposition process, the estimated sediment yield values seem to be ambiguous regarding the efficacy of estimation when compared with an application of SDR. Meanwhile, many authors have also shown the estimated sediment yield rates computed from the coupled RUSLE-SDR, in which their outputs are proved to be at an acceptable level (e.g., Lim *et*

al., 2005; Fu *et al.,* 2006; Bhattarai and Dutta, 2007; Ricker *et al.,* 2008; Mutua *et al.,* 2009; Hui *et al.,* 2010).

Regarding SDR concept, due to the fact that the SDR is affected by the topographical features of the watershed, in particular by the channel slopes contained in the watershed (Muklislin and Sukoco, 2011). As such, a watershed with short and steep slopes will deliver more sediment to a main stream channel than a watershed with flat and wide valleys (Ouyang and Bartholic, 1997). Consequently, this research has derived the SDR from surface interpolation. The unique point of this new approach is an application of the spatial surface interpolation method in ArcGIS spatial analyst, e.g., Kriging, to model the spatially distributed SDR along slope gradients of main streams across a watershed. This idea develops from Williams and Berndt's concept as equation [5.10], and is named Spatial Interpolation of SDR (SISDR). This approach has not been seen in any literature so far.

In short, both concepts of the innovative version of the sediment delivery ratio suggested by this research (i.e. SISDR and the STC concept) are applied in conjunction with RUSLE-GIS-based modelling for estimating the sediment yield in the selected watershed as well as verifying the efficiency of both models (Figure 5.4).

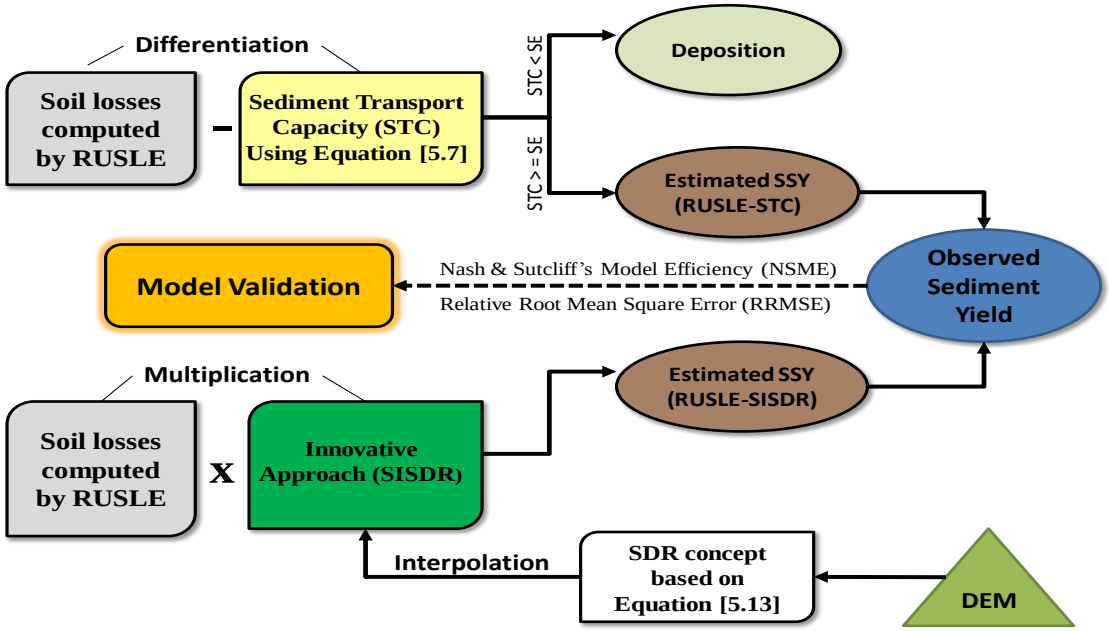

Figure 5.4 Conceptual framework of applying the RUSLE-STC and RUSLE-SISDR modelling to estimate specific sediment yields (SSY) in the study area, and model validations

5.3 Sediment Yield Results

This section is divided into three subsections which include: 5.3.1 Sediment yield rates estimated from sediment rating curves, 5.3.2 Sediment yield rates estimated from the coupled RUSLE-STC and RUSLE-SISDR, and 5.3.3 Model validation.

5.3.1 Sediment yield rates estimated from sediment rating curves

Results of data collection of river discharge and suspended sediment concentrations throughout the Upper Ping River Basin from RID, collected

during a fieldwork trip in Thailand in 2010, found that the hydrological data that can be used to study sediment yield estimations in this research are available for eight watersheds (i.e., 61.5% of the total watersheds), which include the watersheds of: (1) Upper Mae Ping, (2) Middle Mae Ping, (3) Mae Ngad, (4) Mae Taeng, (5) Mae Rim, (6) Upper Mae Wang, (7) Lower Mae Wang and (8) Li.

Each watershed has different periods of sediment samplings. Apparently, the Middle Mae Ping watershed (station P1) has the longest period of sediment sampling that began in 1993, while the Mae Taeng watershed (station P4A) has the shortest sampling period, from 2007 to present. Figure 5.5 illustrates the temporal variation of flow and suspended sediment concentration in each station. The top three ranks of highest suspended sediment concentration (SSC) have taken place in the Lower Mae Wang, the Upper Mae Wang and the Mae Taeng watersheds with SSCs of 4,800, 3,300 and 2,500 mg l^{-1}, respectively. These coincidentally occurred at the same period of the water year during August to September in 2007, and corresponded to the rainy season in Thailand. In the same way, the highest river discharge is found at station P1 (Figure 5.5b) located in the Middle Mae Ping watershed, this station measured the annual peak discharge as approx. 820 m^3/s in August 2005, 480 m^3/s in August 2001 and 410 m^3/s in September 2003.

The relationships of discharge and SSC as depicted in Figure 5.5 (a–h) reveal the gaps in sediment sampling. Not only a lack of SSC data throughout the year

at some stations, such as station P76 of the Li watershed in 2006 (Figure 5.5f), but also the very infrequent collections of the suspended sediment concentration in some water years (e.g., SSCs collected as occasional 3 times/year in 2005 and 2006 in the Li and Middle Ping watersheds, respectively, and 5 times/year in 2006 in the Upper Mae Ping, Mae Ngad and Mae Rim watersheds) can miss the significant events of suspended sediment concentration data, resulting in the subsequent estimations of sediment load and yield to be inaccurate.

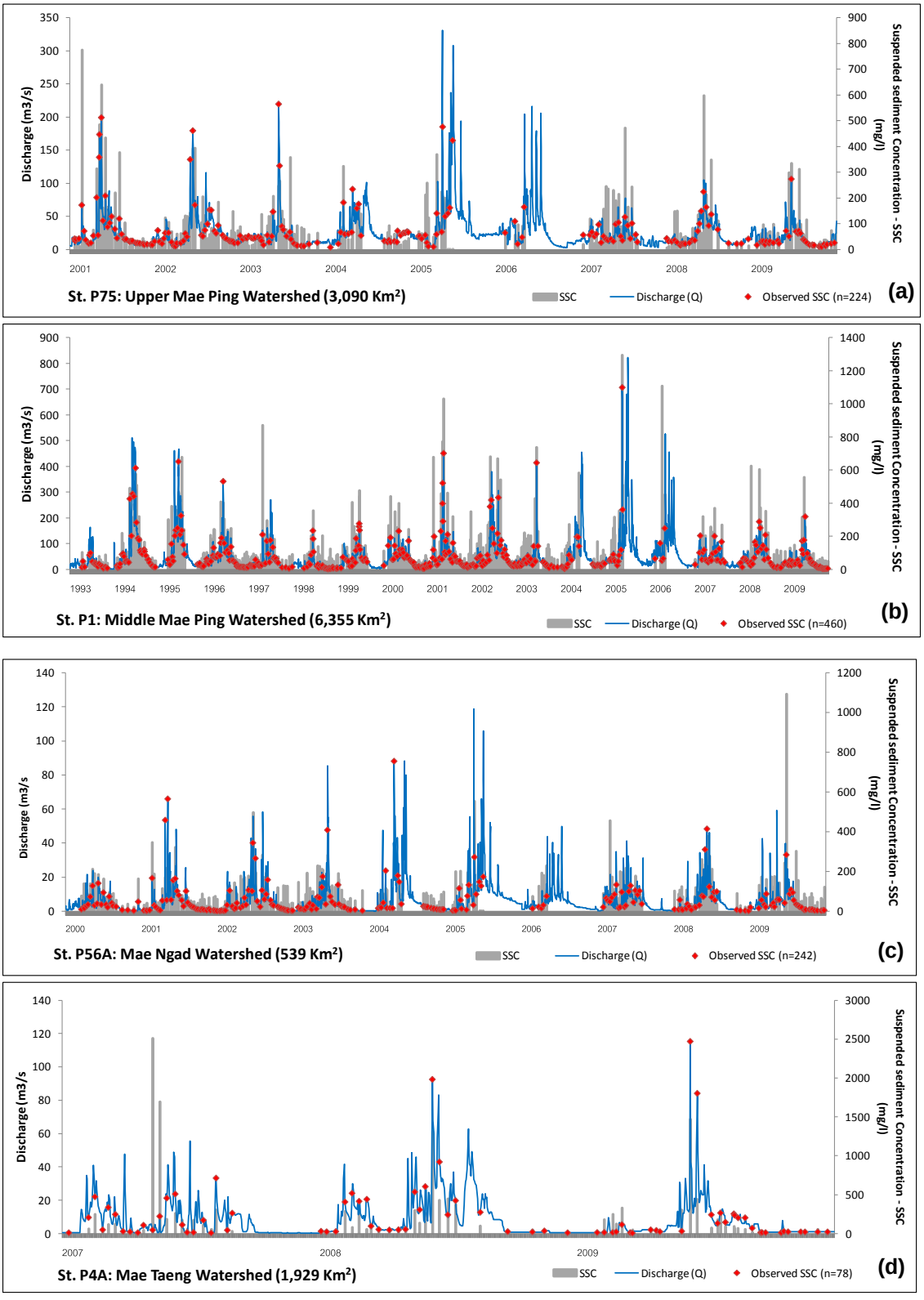

Figure 5.5 Various time series of discharges and suspended sediment concentrations at eight flow-gauging stations, located on their eight watershed outlets in the Upper Ping River Basin, Northwest Thailand.

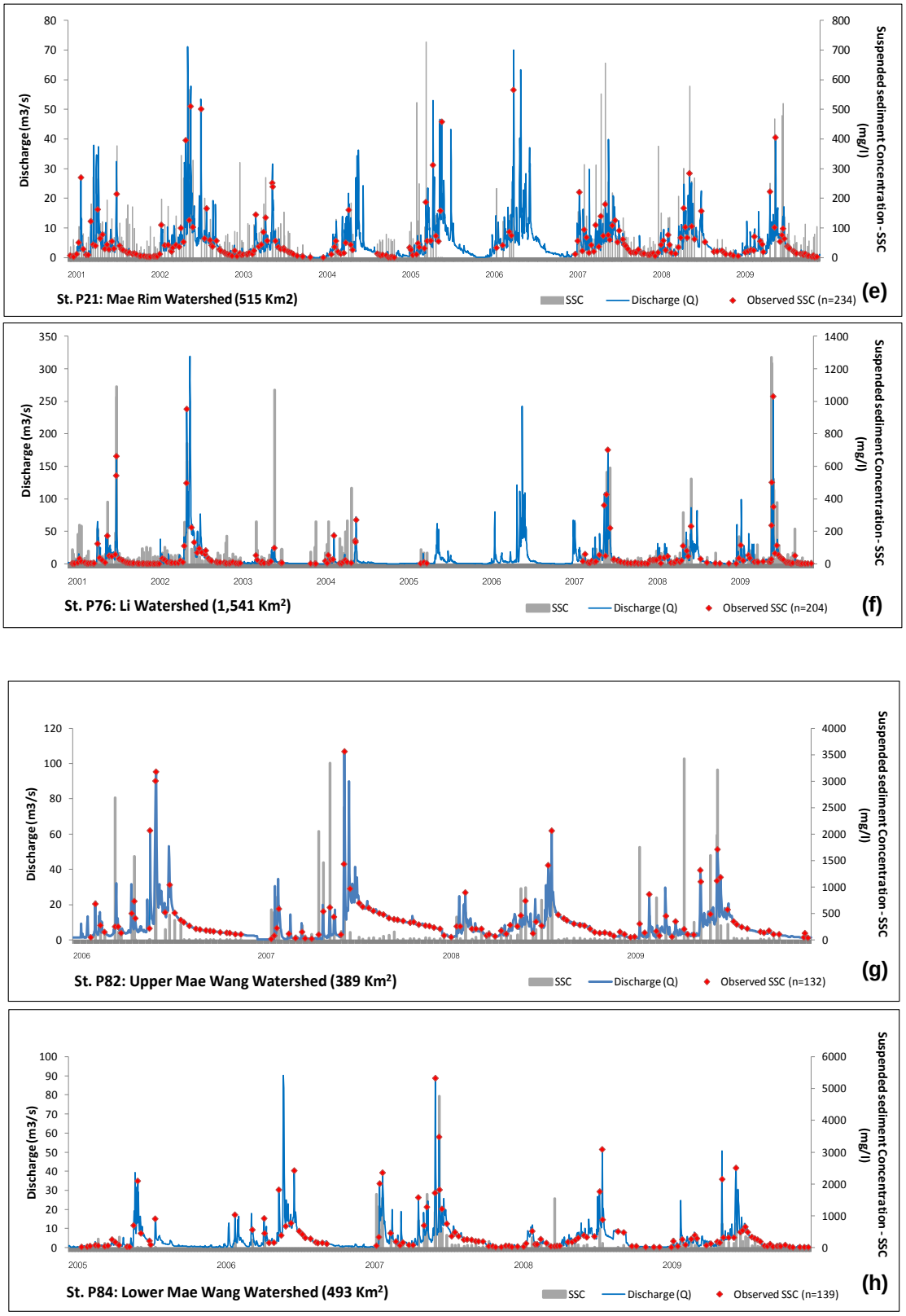

Figure 5.5 (cont.): Various time series of discharges and suspended sediment concentrations at eight flow-gauging stations, located on their eight watershed outlets in the Upper Ping River Basin, Northwest Thailand.

Regarding the annual suspended sediment yield estimation, this study employs the sediment rating curve method to derive the power equation, basing on equation [5.2], for estimating the suspended sediment concentration of eight watersheds. Consequently, it can be concluded that the best-fit regression relationships provide the coefficient of determination (r^2) of SSC_{RC}–Q at all eight watersheds range from 0.23 to 0.58; correlation coefficient (*r*) range from 0.5 to 0.8; *p*-value < 0.001 (Figure 5.6 a–h).

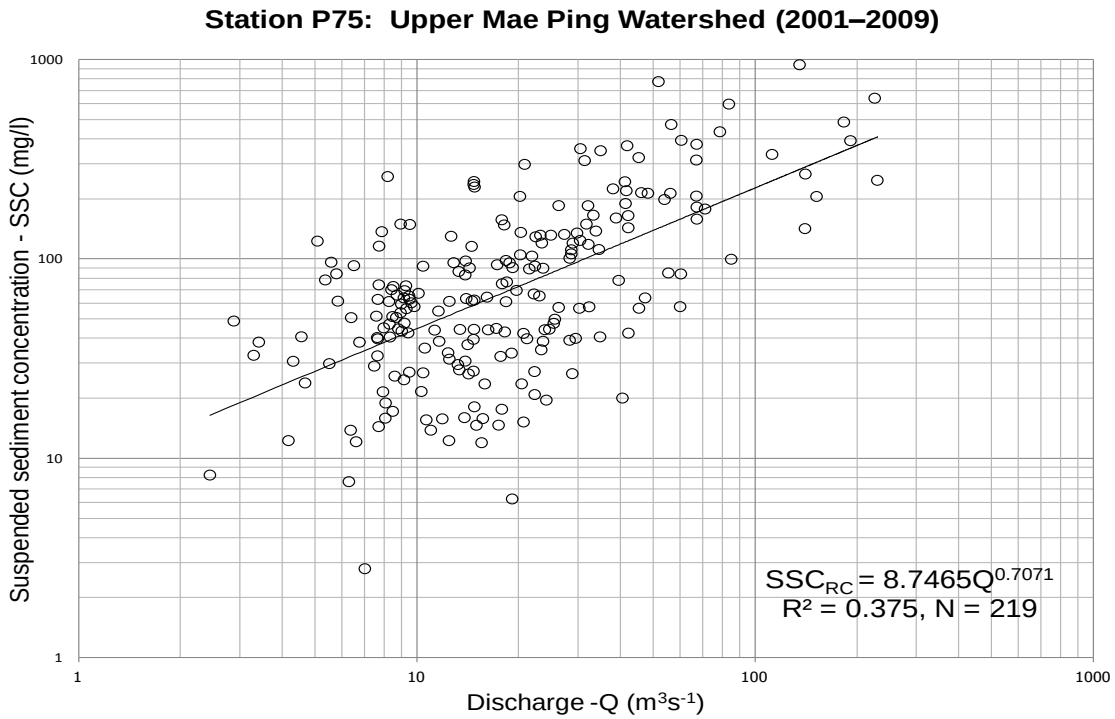

Figure 5.6a Correlation between SSC_{RC} and Q values of the sediment rating curves fitted using power-law relationships at station P75, Upper Mae Ping watershed (data observed between water year 2001 and 2009).

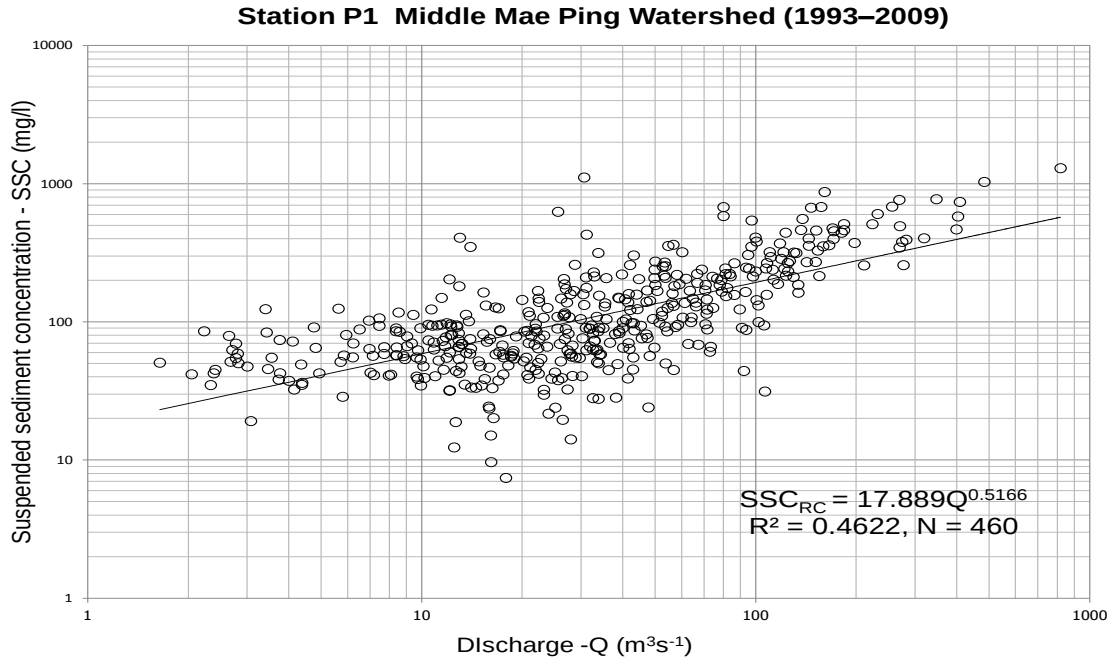

Figure 5.6b Correlation between SSC_{RC} and Q values of the sediment rating curves fitted using power-law relationships at station P1, Middle Mae Ping watershed (data observed between water year 1993 and 2009).

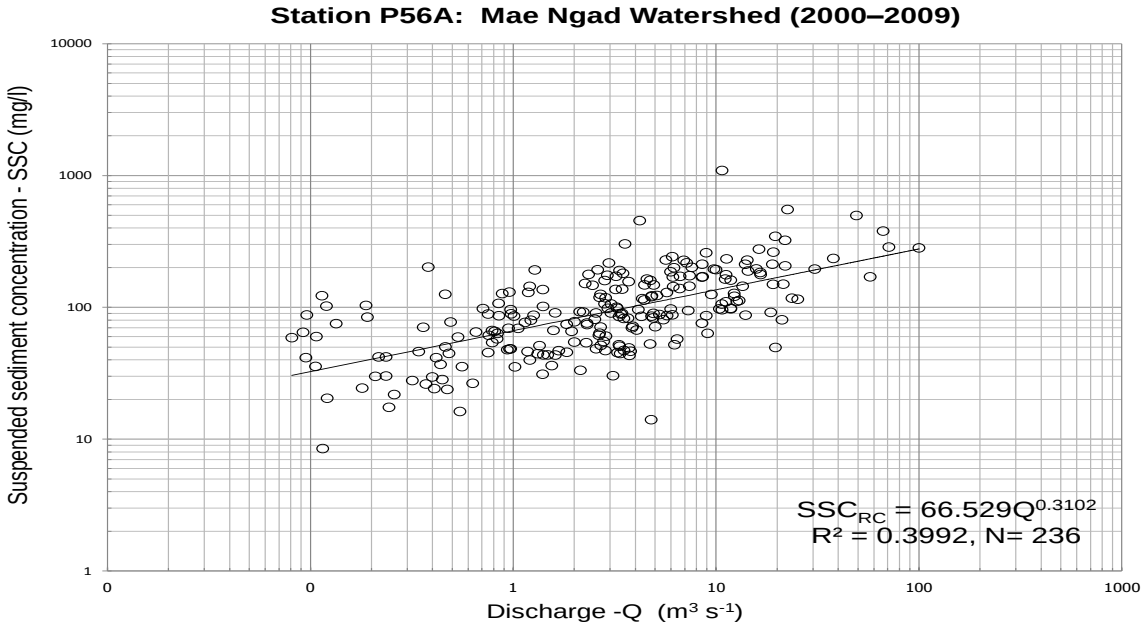

Figure 5.6c Correlation between SSC_{RC} and Q values of the sediment rating curves fitted using power-law relationships at station P56A, Mae Ngad watershed (data observed between water year 2000 and 2009).

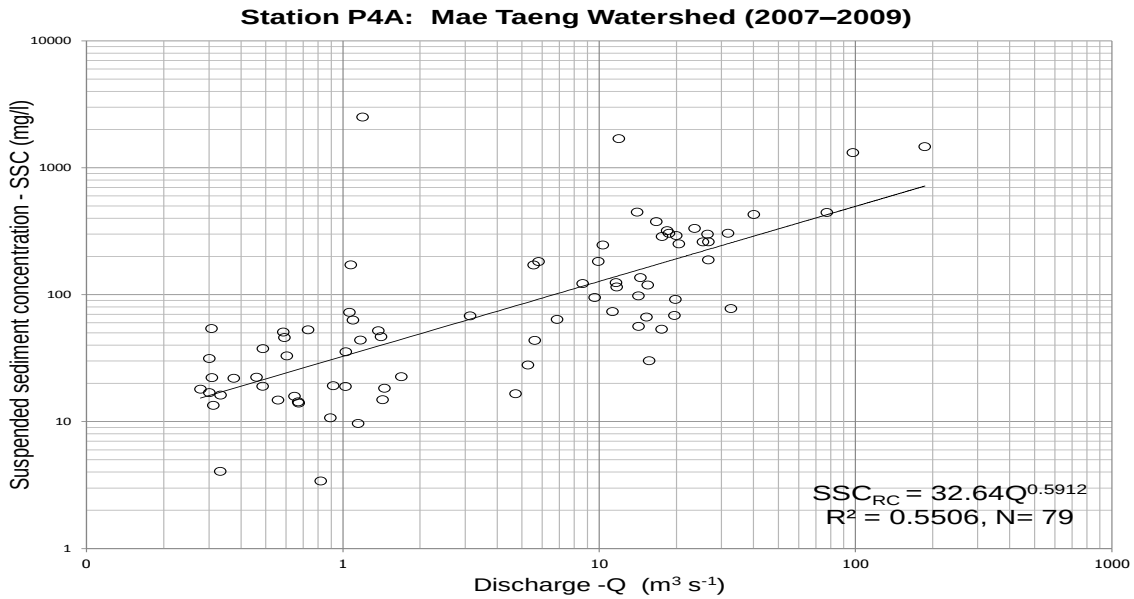

Figure 5.6d Correlation between SSC_{RC} and Q values of the sediment rating curves fitted using power-law relationships at station P4A, Mae Taeng watershed (data observed between water year 2007 and 2009).

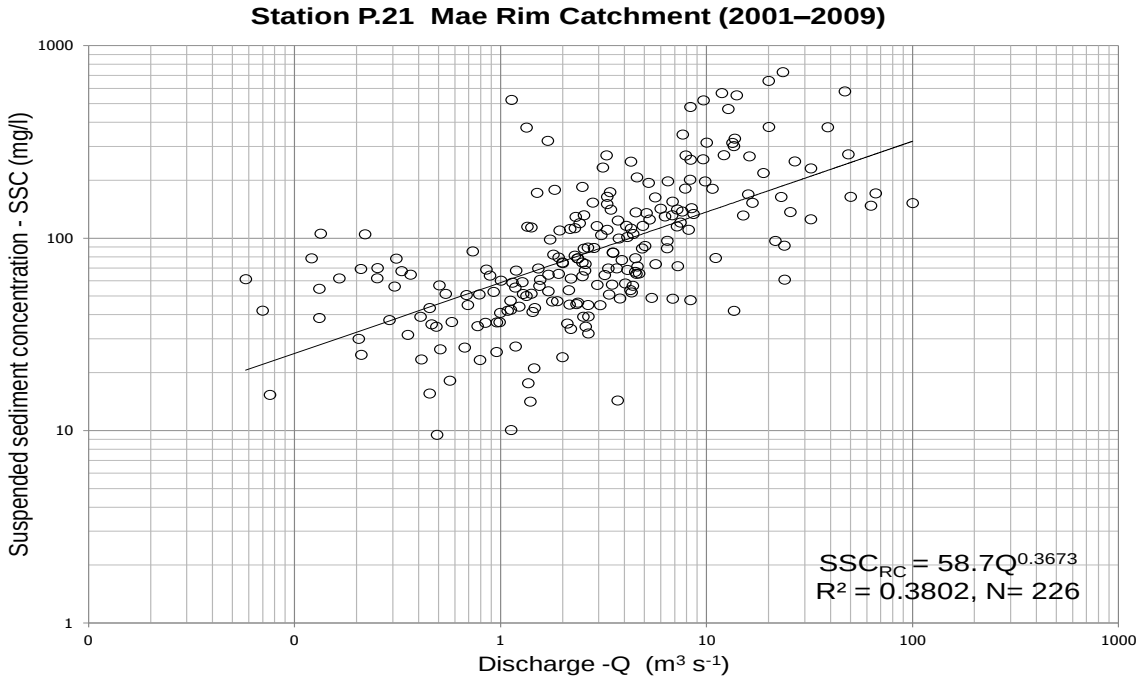

Figure 5.6e Correlation between SSC_{RC} and Q values of the sediment rating curves fitted using power-law relationships at station P21, Mae Rim watershed (data observed between water year 2001 and 2009).

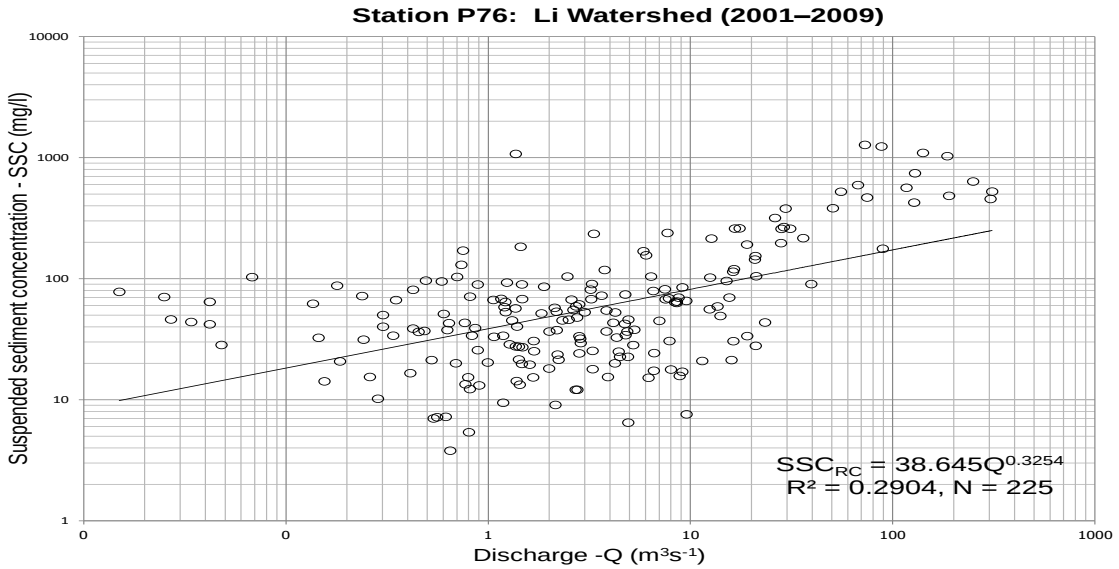

Figure 5.6f Correlation between SSC_{RC} and Q values of the sediment rating curves fitted using power-law relationships at station P76, Li watershed (data observed between water year 2001 and 2009).

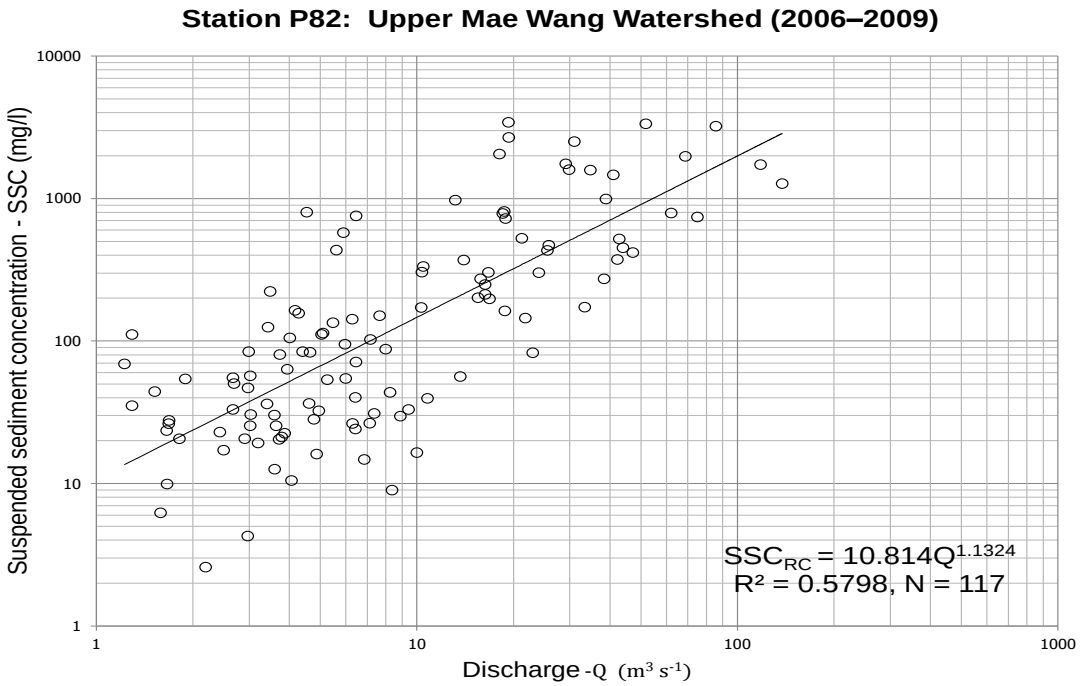

Figure 5.6g Correlation between SSC_{RC} and Q values of the sediment rating curves fitted using power-law relationships at station P82, Upper Mae Wang watershed (data observed between water year 2006 and 2009).

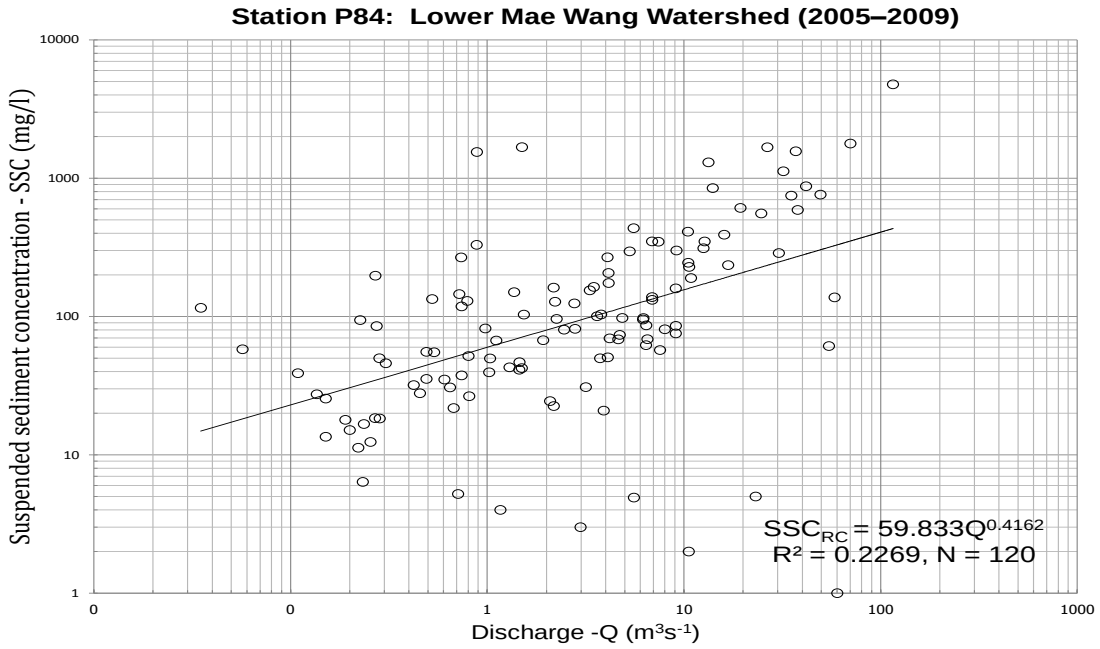

Figure 5.6h Correlation between SSC_{RC} and Q values of the sediment rating curves fitted using power-law relationships at station P84, Lower Mae Wang watershed (data observed between water year 2005 and 2009).

Table 5.3 Watershed rating curve estimations of total study period SSC and SSL for estimating SY in water year 2009.

Watershed	*DBA (km^2)*	*Gauge Station*	*Alt. (m)*	*Period*	*No. of Sampling*	*Mean Q (m^3/s)*	*Mean SSC (mg/l)*	*Mean SSL ($t\ day^{-1}$)*	*Log-log functions*	*Rating equations (Total period)*	r^2	*r*	*p value*	*Tot. SSL_{2009} (100 tonnes)*	*SSY_{2009} ($t\ km^{-2}\ yr^{-1}$)*
1. Upper Mae Ping	3,090	P75	345	2001-2009	219	28.3	107	495	Linear	$SSC_{RC} = 8.7465Q^{0.7071}$	0.375	0.612	< 0.001	37384	1209.84
2. Middle Mae Ping	6,355	P1	305	1993-2009	460	55.9	149	1,486	Linear	$SSC_{RC} = 17.889Q^{0.5166}$	0.462	0.680	< 0.001	52799	830.83
3. Mae Ngad	539	P56A	416	2000-2009	236	7.1	113	108	Linear	$SSC_{RC} = 66.529Q^{0.3102}$	0.399	0.632	< 0.001	5285	980.52
4. Mae Taeng	1,929	P4A	340	2007-2009	79	13	195	653	Linear	$SSC_{RC} = 32.64Q^{0.5912}$	0.551	0.742	< 0.001	6946	360.08
5. Mae Rim	515	P21	320	2001-2009	226	6.5	119	114	Linear	$SSC_{RC} = 58.7Q^{0.3673}$	0.380	0.616	< 0.001	3754	728.93
6. Upper Mae Wang	389	P82	450	2006-2009	117	15.6	362	1,194	Linear	$SSC_{RC} = 10.814Q^{1.1324}$	0.580	0.762	< 0.001	19510	5015.42
7. Lower Mae Wang	493	P84	330	2005-2009	120	8.6	227	669	Linear	$SSC_{RC} = 59.833Q^{0.4162}$	0.227	0.476	< 0.001	3497	709.33
8. Li	1,541	P76	365	2001-2009	225	16.4	119	672	Linear	$SSC_{RC} = 38.645Q^{0.3254}$	0.290	0.539	< 0.001	8267	536.47

Note: DBA = Drainage basin area, Alt. = Altitude, No. = Number, Q = River discharge, SSC = Suspended sediment concentration, SSL = Suspended sediment load, r^2 = correlation of determination, *r* = correlation coefficient, *p* value = probability of obtaining set-statistic at least as extreme as the one was actually observed, Tot. = Total, SSY = Specific sediment yield (i.e. Total SSL/DBA).

Table 5.3 has clearly summarised the results of the rating curve estimation of the total study period load in all eight watersheds of the Upper Ping River Basin, Northwest Thailand. The instantaneous sediment loads and discharges in the water year of 2009 (from 1 April 2009 to 31 March 2010) are used to estimate the watershed suspended sediment yields. In addition, the total suspended sediment loads calculated over a continuous period of the water year 2009 are divided by the drainage area to obtain the specific sediment yield (SSY) rates for the given watersheds. The SSY rates for eight watersheds in 2009 as shown in Table 5.3 (Column 16) provides an overview of the sediment eroded from the upland hillslope area of watershed and shows that some fractions of sediment can reach the downstream outlets of watersheds in the Upper Ping River Basin. The rates of specific sediment yield range between 350 and 5,050 tonnes km^{-2} yr^{-1}. Of these, the Upper Mae Wang watershed generates the highest amount of the SSY in the Upper Ping Basin of approximately 5,015 tonnes km^{-2} yr^{-1}, with the Upper Mae Ping and Mae Ngad watersheds generating 1,210 and 981 tonnes km^{-2} yr^{-1}, respectively, while the amount of SSY in the Mae Taeng watershed is the smallest at 360 tonnes km^{-2} yr^{-1} because of the watershed size effect (1,929 km^2). On the other hand, considering annual sediment load (tonnes/year) the Middle Mae Ping is ranked top and could create total suspended sediment loads of 5,279,900 tonnes yr^{-1} in 2009. The Upper Mae Ping and Upper Mae Wang watersheds follow in second and third places with 3,738,400 and 1,951,000 tonnes yr^{-1}, respectively, while the amount of the total SSL in the Lower Mae Wang watershed is the smallest at only 349,400 tonnes yr^{-1} (Figure 5.7).

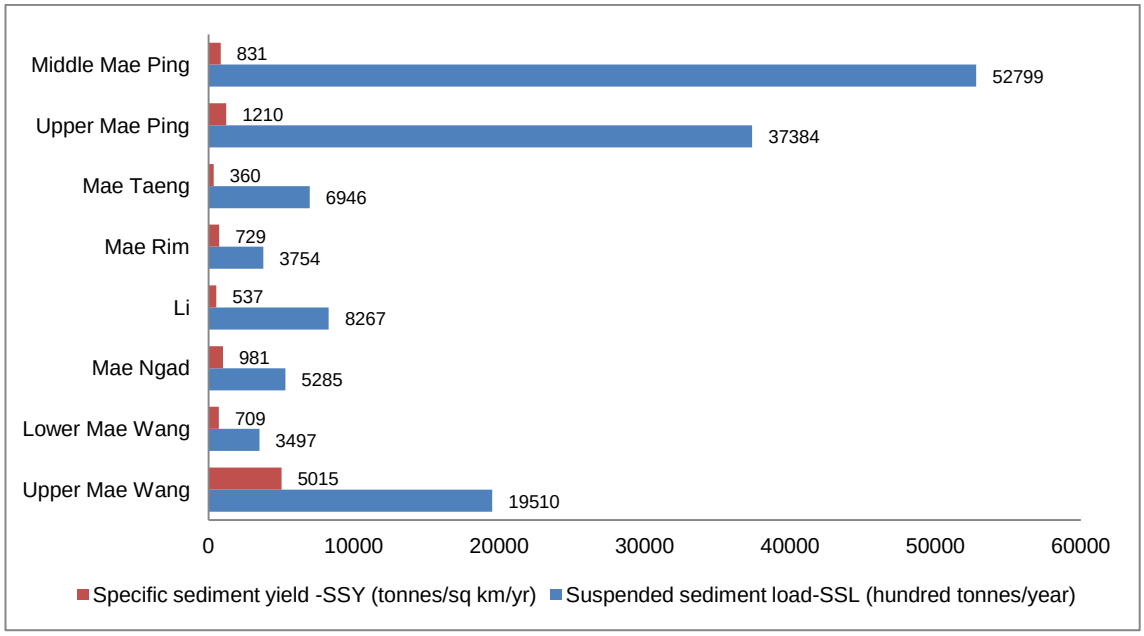

Figure 5.7 Annual sediment loads in hundred tonnes/year and specific sediment yields in tonnes/km^2/year in eight watersheds of the Upper Ping River Basin.

Moreover, when determining the relationships between SSY and drainage area, it was found that the eight watersheds of the Upper Ping River Basin are negative or have an inverse relation (Figure 5.8).

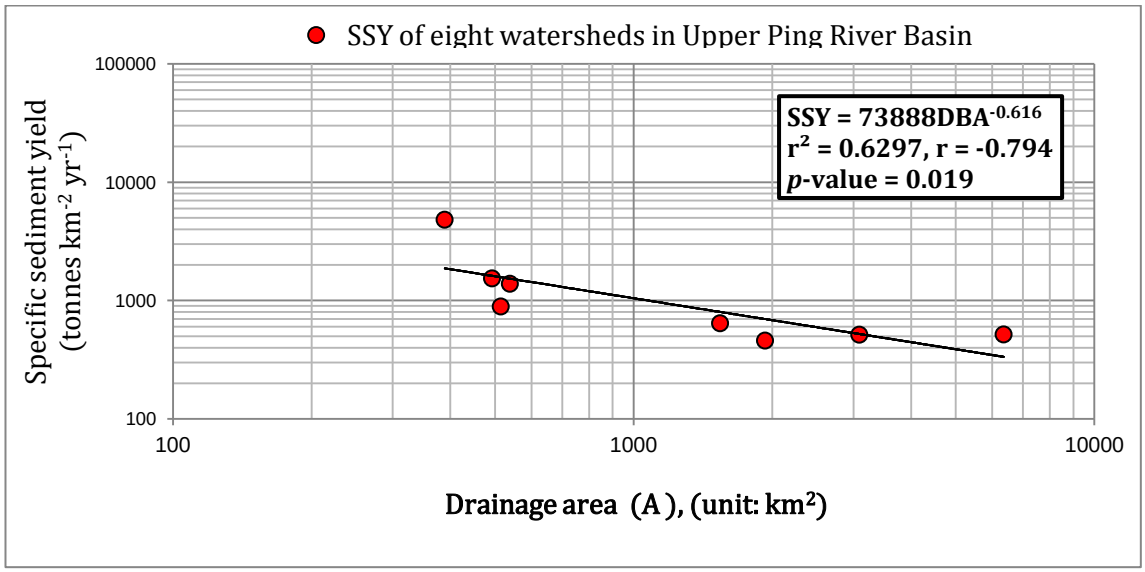

Figure 5.8 The negative relation between SSY and drainage basin area (DBA) for the Upper Ping River Basin, Northwest Thailand.

Based on these data there appears to be a strong negative relation on the rating curve at significant levels 0.05 with $r = -0.794$, $r^2 = 0.63$ and p value = 0.019. The equations of SSY-A relationships for catchments in the Upper Ping River Basin can be established as:

$$SSY = 73888\ DBA^{-0.616} \quad [5.13]$$

Where, SSY is specific sediment yield (tonnes km^{-2} yr^{-1}); DBA is drainage area (km^2)

Thus, the scatter plot in Figure 5.8 demonstrates that within the Upper Ping River Basin the smaller watersheds have a higher SSY than the larger watersheds. Effects from local conditions, e.g. geomorphology, topography and vegetation cover, are dominant decreasing SSY with increasing watershed drainage area (De Vente and Poesen, 2005).

5.3.2 Sediment yield rates estimated from the coupled RUSLE-STC and RUSLE-SISDR

(1) Sediment yield rate estimated by RUSLE-STC Modelling

As with the previous explanation in the methodology (see Section 5.2.3), to estimate the sediment yield by using only RUSLE is not possible because this model does not estimate the amount of sediment reaching the downstream area as well as ignoring sediment deposition. Consequently, the concept of sediment transport capacity (STC) is therefore widely used to associate with RUSLE, not

only to estimate sediment erosion and sediment yield, but also to quantify sediment deposition.

The Mae Rim watershed was chosen for testing the model, and the result of the soil erosion value by using RUSLE-GIS-based modelling has already been assessed and illustrated in Chapter 4 (see Section 4.3.1). The model has calculated the mean annual soil loss rate for the Mae Rim watershed in 2009 as 31.11 tonnes ha^{-1} yr^{-1}, or, as a conversion, 3,111 tonnes km^{-2} yr^{-1} (i.e., 1 ha = 0.01 km^2).

Before estimating sediment yield, it is essential to calculate the sediment transport capacity (STC). Consequently, equation [5.4] is adopted for this study to establish the spatial distribution of sediment transport capacity in the Mae Rim watershed. As a result of using various scaling factors (β) ranging from 0.07 to 1.5, the various spatially distributed K_{TC} have been generated by computation based on equation [5.7] (Figure 5.9).

Figure 5.9 represents the minimum K_{TC} values, which are related to well vegetated areas in watershed, ranging from 0.01 (at β = 0.07) to 0.32 (at β = 1.5), meanwhile the maximum K_{TC} values, which play as poorly vegetated areas, vary from 0.36 (at β = 0.07) to 7.70 (at β = 1.5). Next, the STC maps varying on the scaling factors are then created based on equation [5.4], and also providing values of the sediment transport capacity ranging between –18.67 (at β = 0.07) and 145,958 tonnes (at β = 1.5) (Figure 5.10).

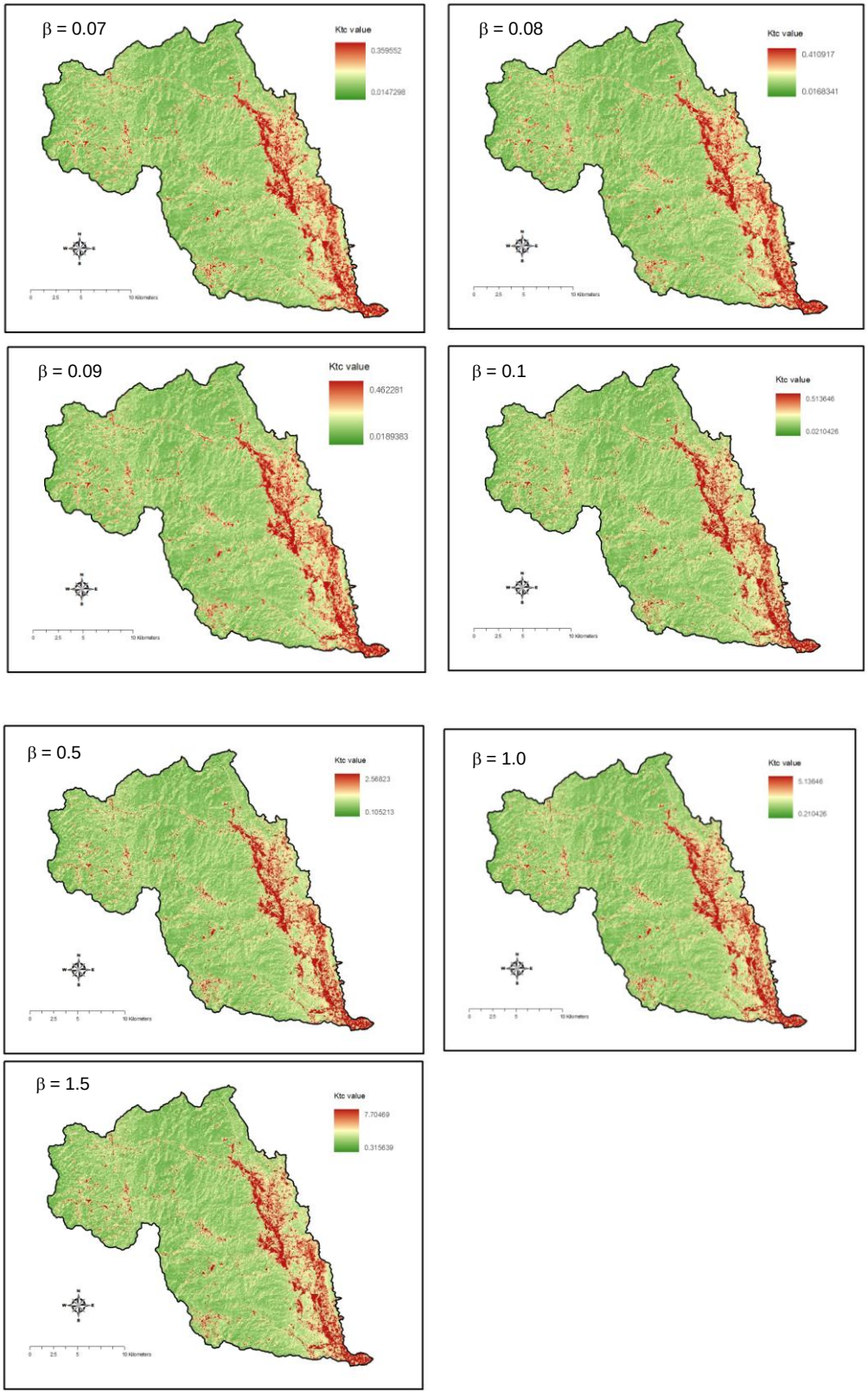

Figure 5.9 Spatial pattern sensitivity of Ktc values, derived from calculation based on an equation [5.7]

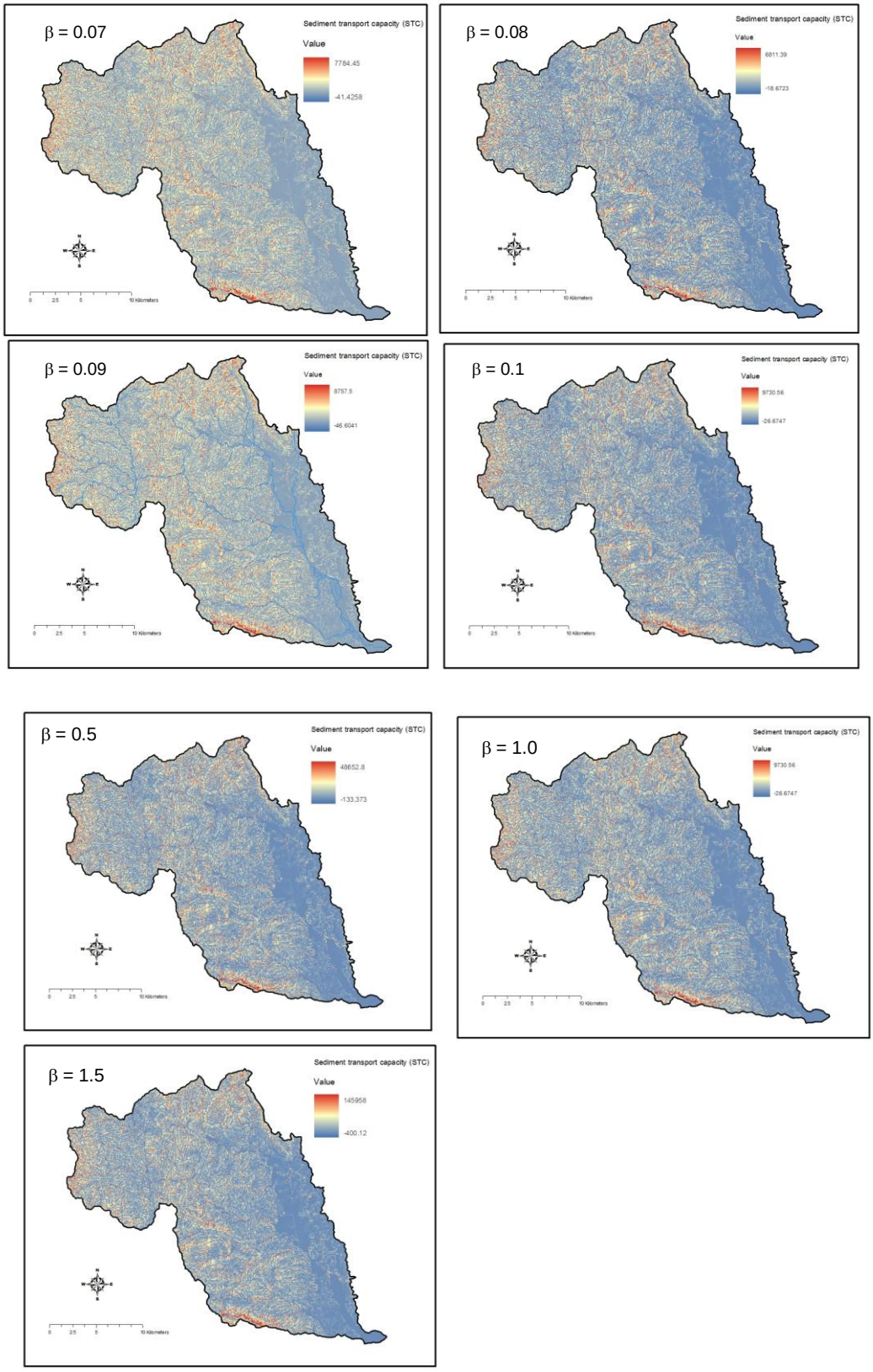

Figure 5.10 Spatial pattern sensitivity of STC values, derived from calculation based on Equation [5.4]

Due to the fact that soil erosion and sediment transport capacity are known as pixels, sediment is routed through the basin towards the river along a runoff pattern (Desmet and Gover, 1996). As discussed in the section 5.2.3, the deposition is modelled if the differentiation of the STC pixel is smaller than the sediment flux reaching that pixel. On the other hand, the sediment yield is modelled if the differentiation of the STC pixel is greater than or equal to the sediment flux reaching that pixel (De Vente *et al.*, 2008). Under these circumstances, the results of spatially distributed sediment deposition (+) and erosion (–) are thus produced (Figure 5.11).

Figure 5.11 demonstrates that amounts of deposition and erosion are depended on difference of scaling factors. The lower values of β affect an increment of sedimentation and decrement of erosion, and vice versa; for example, using β = 0.1 in calculation provides maximum amounts of sedimentation (43,812 tonnes) larger than that using β = 0.5, 1.0 and 1.5, which provide amounts of sedimentation of 26,863, 9,596 and 1,316 tonnes, respectively. Conversly, using β = 0.1 provides the maximum rate of erosion, being almost 6, 12 and 18 times smaller than that using β = 0.5, 1.0 and 1.5, respectively.

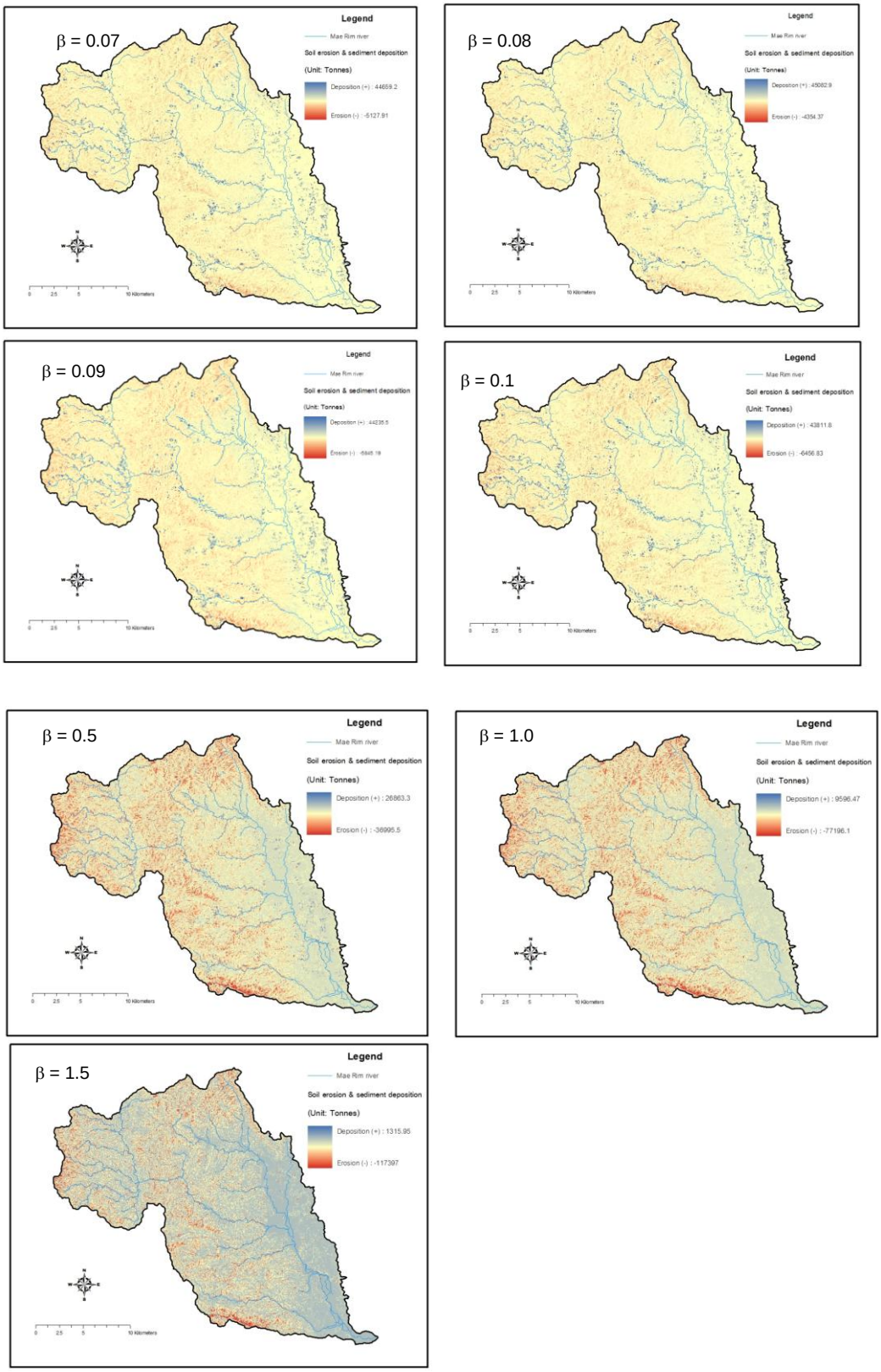

Figure 5.11 The spatial distribution sensitivities of soil erosion and sediment deposition maps for the year 2009 in the Mae Rim watershed.

The computed values of soil erosion and sediment deposition, as illustrated in Figure 5.11, are originated from subtraction between an existed spatial variation of the soil erosion map (see Figure 4.22) and a spatial distribution map of the sediment transport capacity (Figure 5.10). Verstraeten *et al.* (2007) stated that the total gross erosion rate of a watershed is the sum of the values of soil erosion rate in every grid cell within its boundary. To calculate the true net erosion, it is necessary to subtract the total amount of sediment deposition. Hence, an amount of sediment yield is the net erosion minus the net sedimentation. Such a concept mentioned above can be depicted in Figure 5.12.

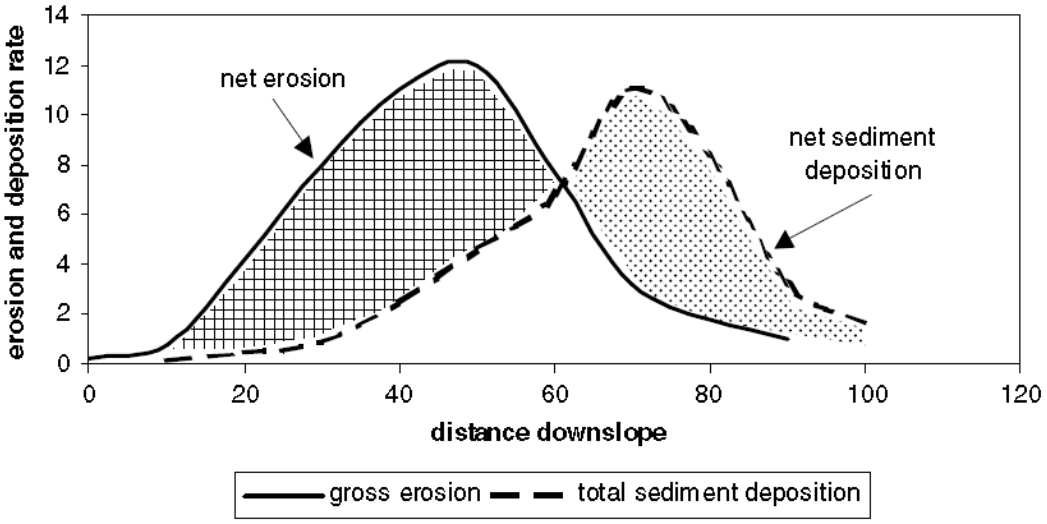

Figure 5.12 Depiction of soil erosion, sediment deposition and sediment delivery concepts for a hypothetical slope (Source: Verstraeten *et al*., 2007)

Based on the concept according to Vastraeten *et al.* (2007), the sediment yield can be computed by subtraction between the mean net erosion and mean net deposition, and also eventually provide the mean value of specific suspended

sediment yield rate (SSY) in year 2009 as summarised in Table 5.4, including maps depicted as Figures 5.13 and 5.14, respectively.

Table 5.4 Various values of K_{TC}, STC, mean net erosion and sedimentation, predicted SSY_{2009} and percentage variation of prediction obtained from testing scaling factor (β)

Scaling factor (β)	Ktc (Eq. 5.7)		STC (Eq. 5.4)			Mean net erosion (tonnes/ha/yr)	Mean net sedimentation (tonnes/ha/yr)	Predicted SSY_{2009} (tonnes/ha/yr)	Percentage (%) difference from observed SSY_{2009} (7.29 t/ha/yr)
	Min	Max	Min	Max	Mean				
0.07	0.01	0.36	–18.67	6811.4	28.93	42.66	44.62	–1.96	–126.89
0.08	0.02	0.41	–41.43	7784.5	33	49.74	43.28	6.46	–11.38
0.09	0.02	0.46	–46.6	8757.5	37.13	56.86	42.19	14.67	101.23
0.1	0.02	0.51	–26.67	9732.6	41.32	64.03	41.36	22.67	210.97
0.5	0.11	2.57	–133.37	48652.8	206.61	308.46	33.87	274.59	3667
1.0	0.21	5.14	–266.75	97305.6	413.23	625.16	29.50	595.66	8071
1.5	0.32	7.70	–400.12	145958.0	619.84	930.45	37.77	892.68	12145

Table 5.4 illustrates the different values of mean net erosion and net sedimentation based on variation of scaling factors used for model predicition. However, the predicted results of SSY in 2009 (predicted SSY_{2009}) provided by the model is varying. In particular, when compared with the observed SSY, the scaling factor β equal to 0.08 provides a better predicted result of SSY that matches with the value of observed SSY_{2009} (i.e., 7.29 tonnes ha^{-1} yr^{-1}); a percentage variation from the observed SSY_{2009} is –11% (i.e., closer than the other percentage variations from the observed SSY_{2009}) at river gauging station P21. Thus, I took β = 0.08 as a main for calculating the STC and SSY based on the RUSLE-STC concept in this study.

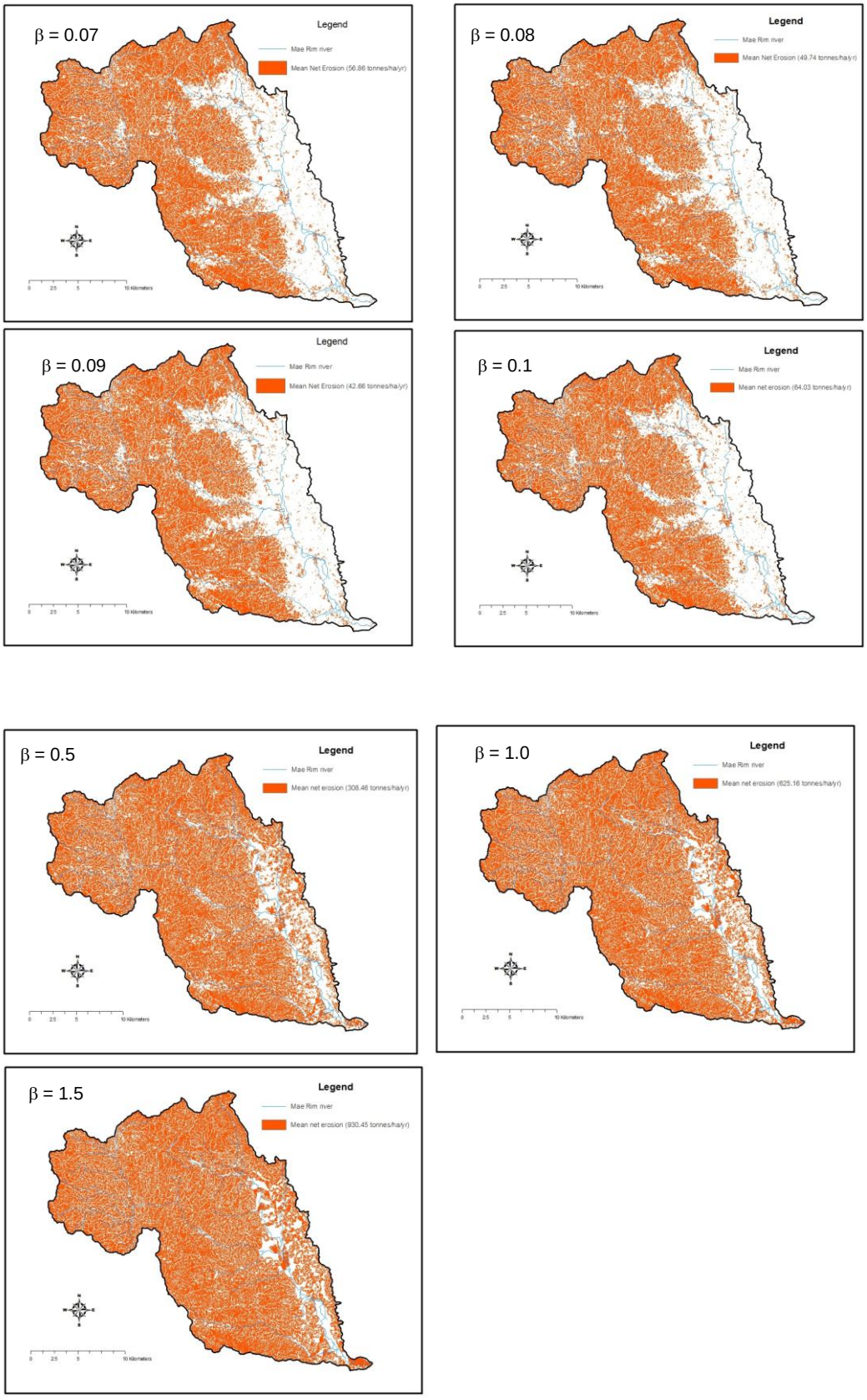

Figure 5.13 Depictions of net erosion in the Mae Rim watershed

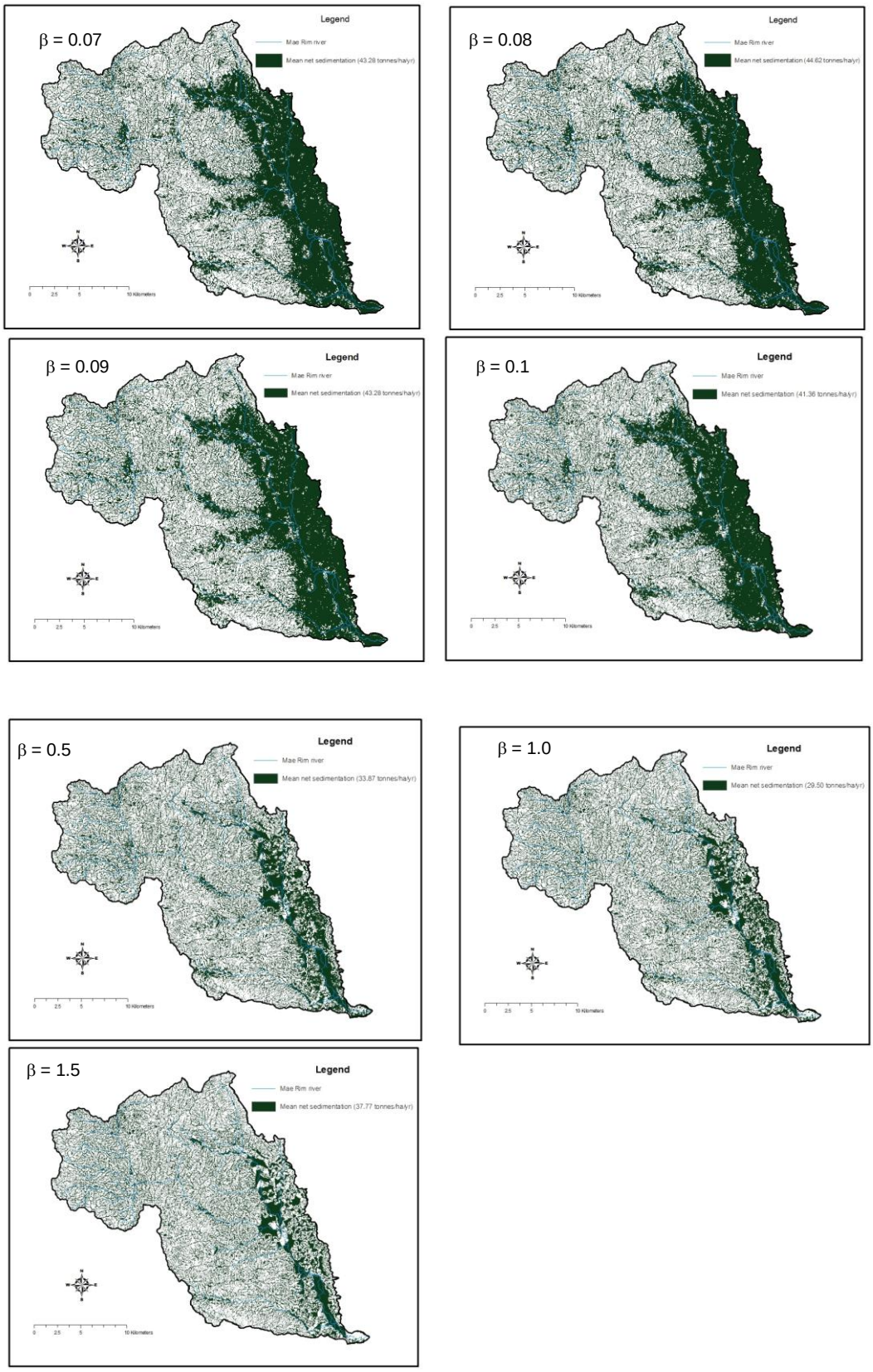

Figure 5.14 Depiction of net sedimentation in the Mae Rim watershed.

Finally, the spatially distributed sediment yields estimated on the Mae Rim watershed are categorised into four vulnerable classes as shown in Figure 5.15.

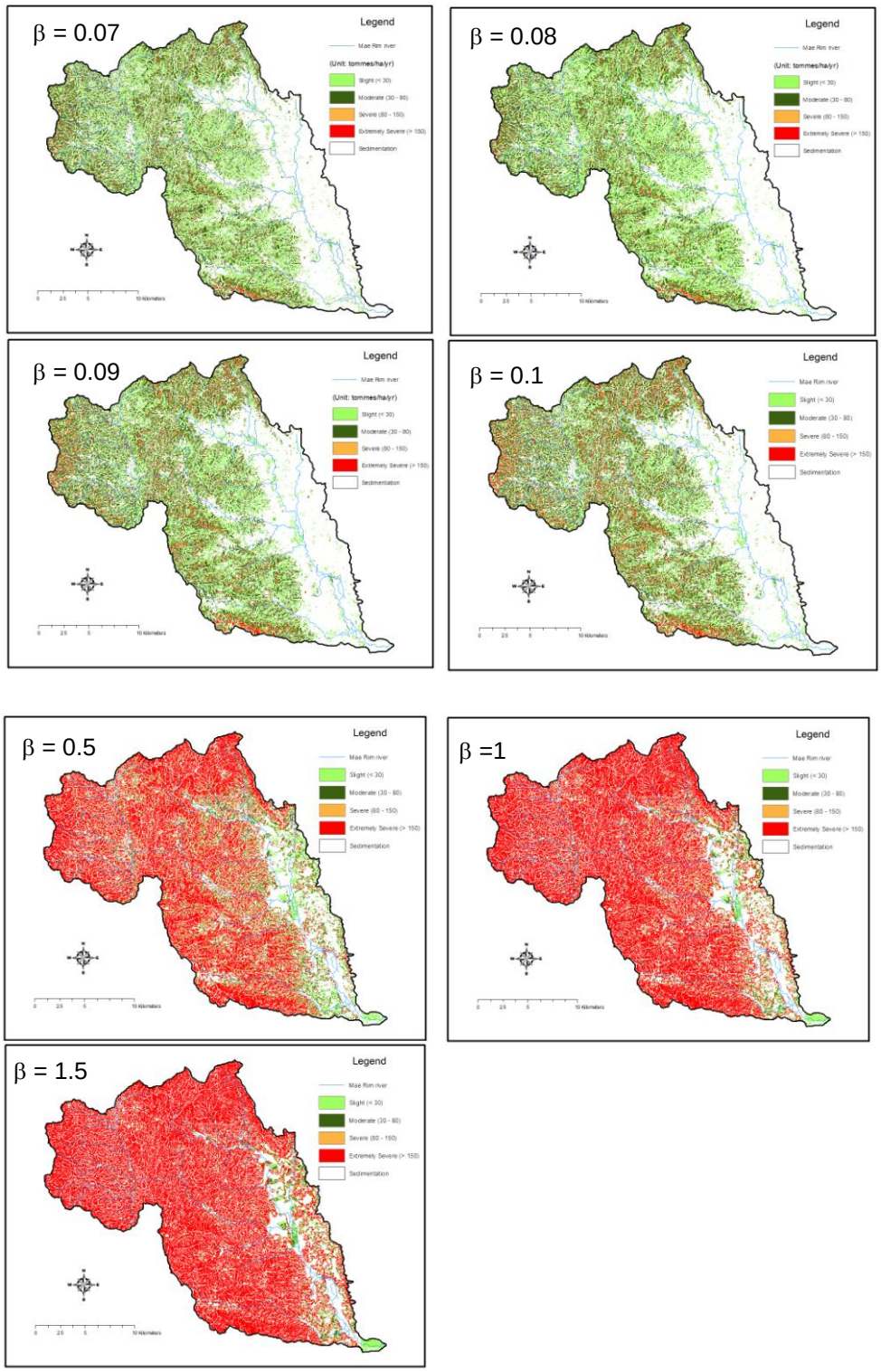

Figure 5.15 The intensity classes of sediment yield in the Mae Rim watershed.

Maps from Figure 5.15 obviously reveal that there are extreme overpredictions (exaggerations) of sediment yield amounts as a result of using high values of β (i.e., $\beta \geq 0.5$) in prediction. Consequently, more than 60% of areas in the Mae Rim watershed are very serious sources of huge sediments that produce sediment yields > 150 tonnes/ha/yr, unlike to other maps using lower values of β (i.e., $\beta \leq 0.1$). For more detailed data are exhibited in the Table 5.5.

Table 5.5 Sensitivity analysis of scaling factor affecting the spatial distribution of sediment yield risk across the Mae Rim watershed

	Suspended sediemnt yield (tonnes/ha/yr)							
Scaling factor (β)	< 30 Slight		30-80 Moderlate		80 - 150 Severe		> 150 Extremely severe	
	Area in ha	(%)	Area in ha	(%)	Area in ha	(%)	Area in ha	(%)
0.07	26,691	51.83	19,834	38.51	3,487	6.77	1,488	2.89
0.08	22,355	43.41	22,438	43.57	4,723	9.17	1,984	3.85
0.09	18,870	36.64	23,904	46.42	6,166	11.97	2,561	4.97
0.1	16,080	31.22	24,591	47.75	7,612	14.58	3,217	6.25
0.5	3,973	7.71	5,867	11.39	8,751	16.99	32,909	63.90
1.0	2,282	4.43	2,768	5.37	3,921	7.61	42,528	82.58
1.5	1,997	3.88	2,096	4.07	2,578	5.01	44,828	87.04

Especially focusing on β=0.08 (a significant variable selected for this thesis in regard to predicting suspended sediment yields based on RUSLE-STC approach), it can be concluded that around 43% of the watershed area has a sediment yield of 'slight' (i.e., sediment yield < 30 tonnes ha^{-1} yr^{-1}), while 4% of the watershed area is 'extremely severe' in sediment yield (i.e., sediment yield > 150 tonnes ha^{-1} yr^{-1}) which dominantly appears as a red colour at southern edge of the Mae Rim watershed.

(2) Sediment yield rate estimated by RUSLE-SDR Modelling

Sediment delivery ratio (SDR) is one of the approaches to use in conjunction with RUSLE for estimating the sediment yield of the watershed. As previously mentioned, this research has proposed an innovative method developed from the concept of Williams and Berndt, as expressed in equation [5.10]. This equation is computed by using ArcGIS and illustrated in Figure 5.16.

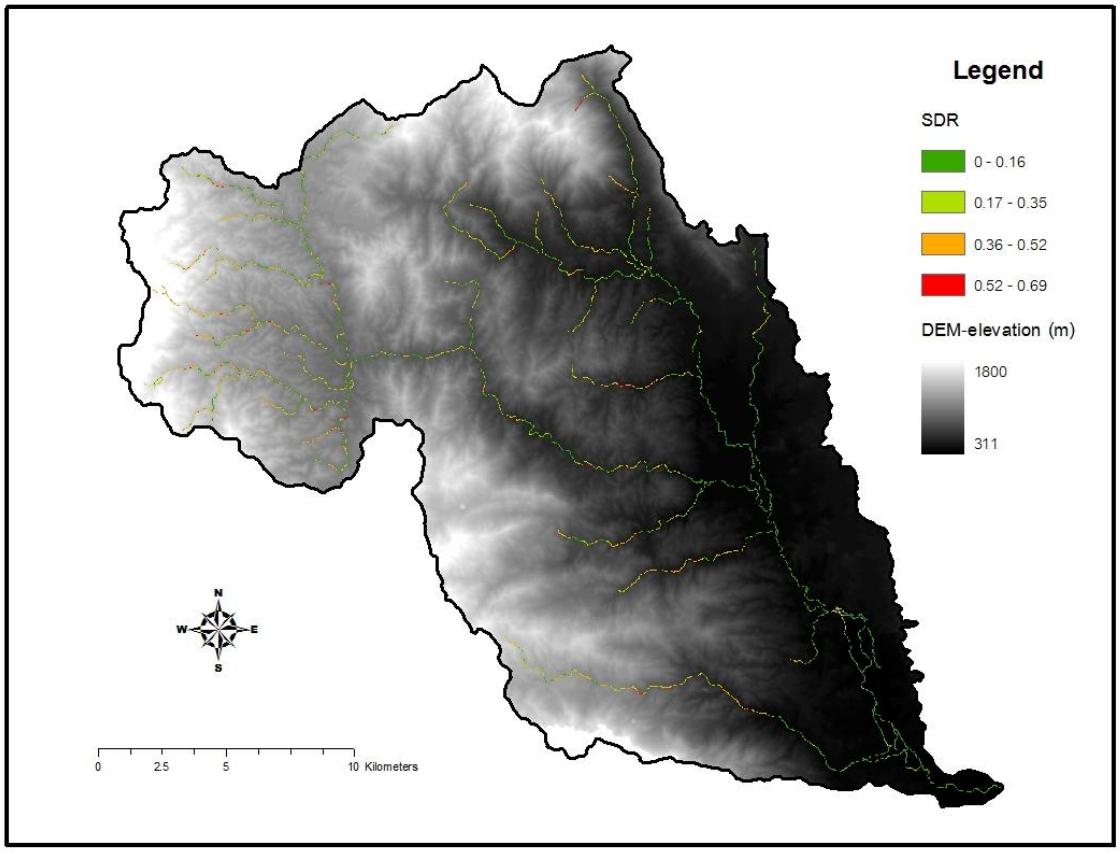

Figure 5.16 The SDR values varying on main streams or channel slopes within the watershed.

Figure 5.16 shows the values of SDR ranging between 0 and 0.69 (mean SDR value is 0.26) on the different slope gradients of the main stream. It is clear to depict the higher SDR relating to increasing elevation, while the lower SDR that

is represented as a dark green colour appears clearly in the eastern part of watershed.

Not only that, this research has additionally developed with the adoption of the Kriging interpolation for an innovation that creates the spatial distribution of SDR (SISDR) on the slope channel within the watershed. The concept of Kriging interpolation assumes that the distance and direction between sample points reflects a spatial correlation that can be used to describe the surface variation (Childs, 2004). The output of the innovative SISDR is depicted in Figure 5.17.

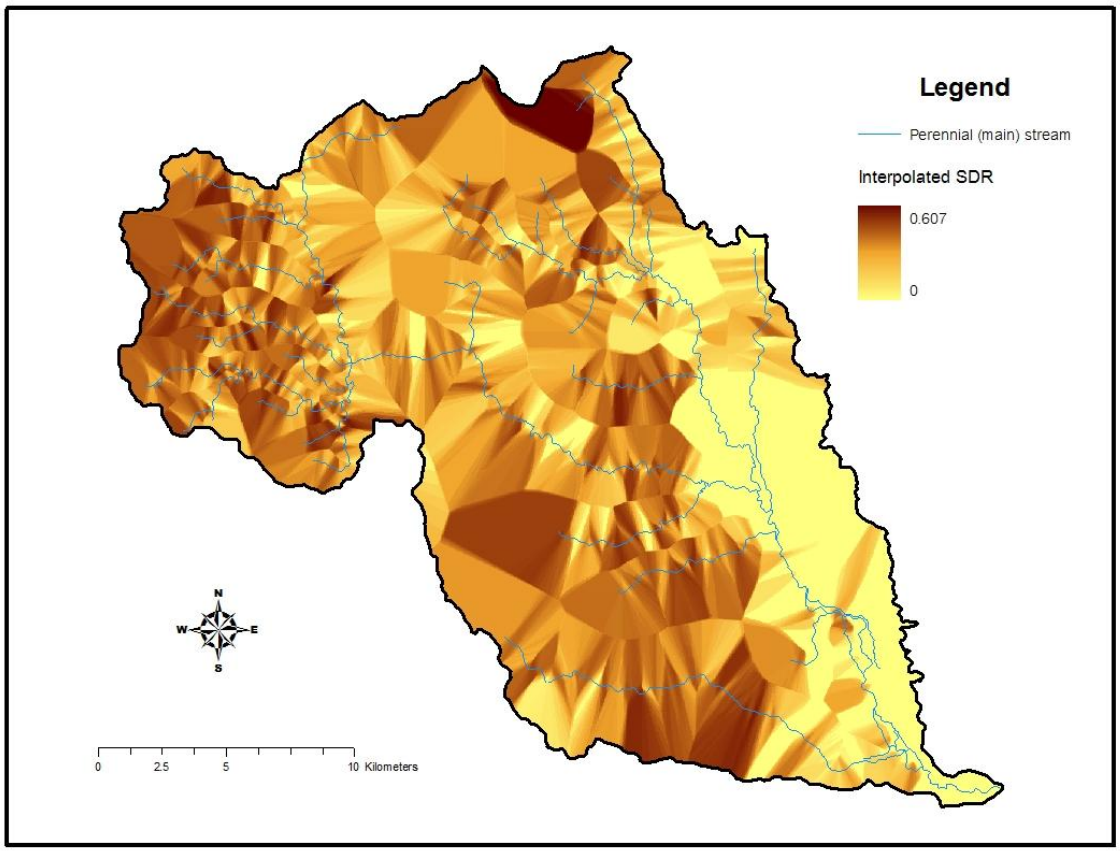

Figure 5.17 The innovative method for creating the spatial distribution of sediment delivery ratio (SISDR) within the Mae Rim watershed.

This idea of SISDR is to produce the spatial SDR throughout the watershed by interpolating points estimated from equation [5.10]. As a result, every grid cell has the SDR values which vary on the slope gradient of the main stream within the watershed.

The RUSLE-SISDR modelling uses the soil loss equation of RUSLE multiplied by SISDR to calculate sediment yield as the following equation:

$$\mathrm{SSY} = [\mathrm{RKLSCP}] \times [\mathrm{SISDR}] \qquad [5.14]$$

Where, SSY is the estimated mean specific sediment yield per unit area (tonnes ha^{-1} yr^{-1}); R is the rainfall-runoff erosivity factor (MJ mm ha^{-1} h^{-1} yr^{-1}); K is the soil erodibility factor (tonnes h MJ^{-1} mm^{-1}); LS represents the slope length and slope steepness factors; C is the cover management factor, P is the conservation support practice factor; SISDR is the spatial distribution of the SDR value.

The output of spatially-distributed sediment yield is depicted in Figure 5.18, and the computed mean specific sediment yield in the year 2009 from RUSLE-SISDR is equal to 7.42 tonnes ha^{-1} yr^{-1} (742 tonnes km^{-2} yr^{-1}), while the minimum and maximum vary from 0 – 17,080 tonnes ha^{-1} yr^{-1}.

Finally, the annual sediment yield in 2009 estimated in the Mae Rim watershed is categorised into four vulnerable classes as shown in Figure 5.19. From the map, it can be concluded that 96.5% of the watershed area has a 'slight' sediment yield (i.e., sediment yield < 30 tonnes ha^{-1} yr^{-1}), while approximately 1% of the watershed area is 'extremely severe' in sediment yield (i.e., sediment yield > 150 tonnes ha^{-1} yr^{-1}).

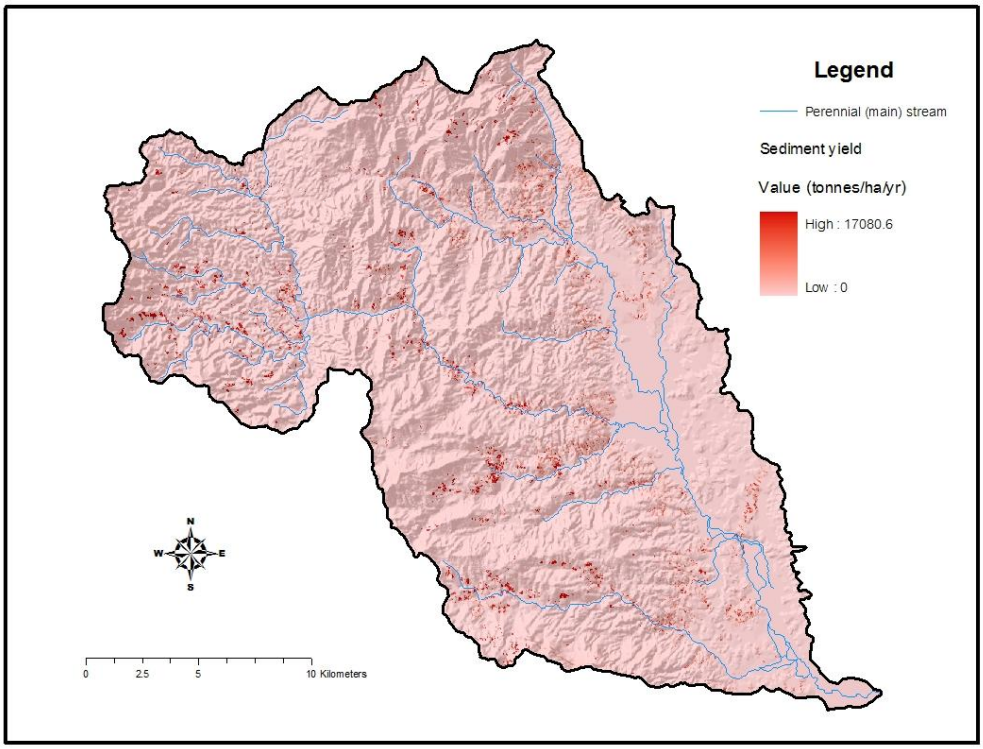

Figure 5.18 The spatial sediment yield magnitudes in the Mae Rim watershed

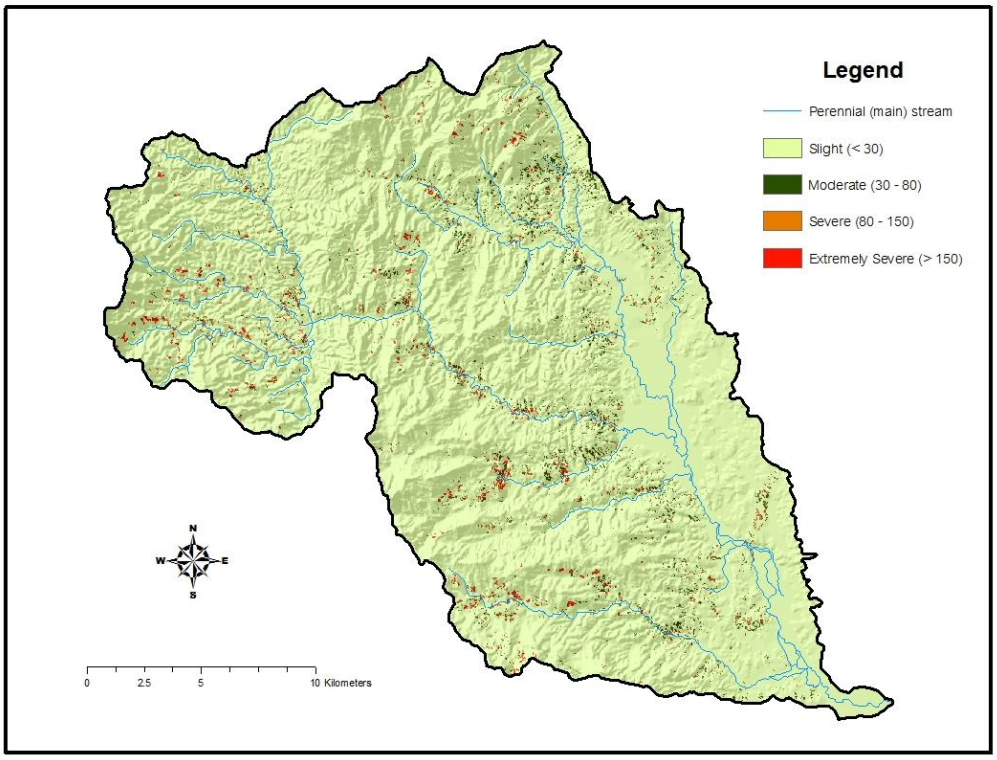

Figure 5.19 The intensity classes of sediment yield in the Mae Rim watershed.

5.3.3 Model Validation

The specific suspended sediment yield (SSY) value from the sediment rating curve is the actual sediment fluxes measured at gauging stations, while the estimated SSY from modelling used is lumped. However, the main purpose of this research is to test the efficacy of the model particularly in prediction of the SSY in the selected watershed, with the Mae Rim watershed chosen as the case study (Table 5.5).

Table 5.5 The estimated total SSL (unit: 100 tonnes yr^{-1}) of the Mae Rim watershed from 2001 – 2009

Water year	Apr	May	Jun	Jul	Aug	Sep	Oct	Nov	Dec	Jan	Feb	Mar	Annaul SSL 100 t yr^{-1}	Annail SSY t km^{-2} yr^{-1}
2001	149	522	209	558	443	339	500	322	297	238	153	150	3,880	753
2002	293	675	603	738	1,218	1,053	974	829	862	609	324	446	8,624	1,675
2003	154	158	254	246	289	264	233	185	130	120	56	12	2,101	408
2004	67	290	253	471	369	526	341	274	215	227	47	180	3,260	633
2005	246	413	466	879	723	931	749	503	483	360	120	143	6,016	1,168
2006	443	832	798	1,110	1,142	1,018	847	651	536	473	284	378	8,512	1,653
2007	290	516	584	578	649	689	611	529	411	393	277	324	5,851	1,136
2008	290	419	246	615	654	591	763	456	406	403	202	338	5,383	1,045
2009	232	309	310	324	492	485	504	309	257	234	107	191	3,754	729
Max	443	832	798	1,110	1,218	1,053	974	829	862	609	324	446	8,624	1,675
Mean	240	459	414	613	664	655	614	451	400	340	174	240	5,265	1,022
Min	67	158	209	246	289	264	233	185	130	120	47	12	2,101	408

SSY = Mean total $SSL_{2001\text{-}2009}$ / Drainage area (515 km^2); unit: 100 tonnes km^{-2} yr^{-1}

= (5,265/ 515) x 100 tonnes km^{-2} yr^{-1}

= 1,022 tonnes km^{-2} yr^{-1}

The percentage differences between the predicted specific sediment yields from modelling tested (i.e., RUSLE-STC Modelling and RUSLE-SISDR Modelling) and the actual measured specific sediment yield in water year 2009 (i.e., 729 tonnes km^{-2} yr^{-1}) have been firstly assessed using the following equation (Horowitz, 2003):

$$\% \text{ Difference} = \frac{(\text{Predicted value} - \text{Measured value})}{\text{Measured value}} \text{ x } 100 \qquad [5.18]$$

The calculated value from equation [5.18], a negative percentage implies 'underestimation' and a positive percentage implies 'overestimation'.

Hence, the % difference between the predicted SSY_{2009} and the measured SSY_{2009} in this study found that the coupled RUSLE-STC Modelling (i.e., 646 tonnes km^{-2} yr^{-1}) provided an underestimate of the mean annual suspended sediment yield (i.e., –11%), while the coupled RUSLE-SISDR Modelling (i.e., 742 tonnes km^{-2} yr^{-1}) provided an only slightly overestimate of the mean annual suspended sediment yield (i.e., 2%).

In addition, validation of efficiency in modelling based on different concepts (i.e., STC and SISDR) in this study uses the estimated SDR values of each modelling instead of estimated sediment yield rates, compared with the actual measured SDR of the Mae Rim watershed. Nash and Sutcliffe's Model efficiency (NSME) is adopted for the verification of the modelling (e.g., Verstraeten *et al*., 2003; De Vente *et al*., 2005, 2008; Haregeweyn *et al.,* 2008).

$$\mathrm{NSME} = 1 - \frac{\sum (O_i - P_i)^2}{\sum (O_i - O_{mean})^2} \qquad [5.19]$$

Where, NSME = Nash and Sutcliffe's model efficiency; O_{mean} = the mean observed value; O_i = the observed value; P_i = the predicted valued. The model efficiency can range from - α to 1 and represents the proportion of the initial variance accounted for by the model. The closer the NSME value approaches 1, the more efficient the model. Negative values of NSME indicate that the model

produces more variation than could be observed, i.e. the model is insufficient (Verstraeten *et al*., 2003; Haregeweyn *et al.,* 2008).

An estimator of associated error that is independent of the specific units, in which the values are expressed, is the Relative Root Mean Square Error (RRMSE):

$$\text{RRMSE} = \frac{\sqrt{\frac{1}{n}\sum_{i=1}^{n}(O_i - P_i)^2}}{\frac{1}{n}\sum_{i=1}^{n} O_i} \qquad [5.20]$$

Where RRMSE is Relative Root Mean Square Error; n is number of observation; O_i is the observed value; P_i is the predicted valued. Values for RMSE range from 0 to α, and the closer the RRMSE approximates to zero (perfect model), the better the model performances (Haregeweyn *et al.,* 2008).

Table 5.6 Comparison of NSME and RRMSE using measured and predicted SDR values.

Soil erosion	Measured value (2009)		Mean-measured value (2001-2009)		RUSLE-STC		RUSLE-SISDR		NSME		RRMSE	
(tonnes/km^2/yr)	SSY	SDR	SSY	SDR	SSY	SDR	SSY	SDR	RUSLE-STC	RUSLE-SISDR	RUSLE-STC	RUSLE-SISDR
3111	729	0.23	1022	0.33	646	0.13	742	0.26	0.00	0.91	0.43	0.13

From Table 5.6, it can be concluded that the SDRs of: actual measured value in water year 2009, mean actual measured value from 2001–2009, RUSLE-STC, and RUSLE-SISDR are 0.23, 0.33, 0.13 and 0.26, respectively. When taking the

mean SDR values of RUSLE-STC and RUSLE-SISDR to validate with Nash and Sutcliffe's model efficiency and Relative Root Mean Square Error, the results show as below:

$$NSME_{RUSLE\text{-}STC}\ (0.00) < NSME_{RUSLE\text{-}SISDR}\ (0.91)$$

$$RRMSE_{RUSLE\text{-}STC}\ (0.43) > RRMSE_{RUSLE\text{-}SISDR}\ (0.13)$$

In conclusion, the concept of innovative SISDR is better than the STC concept in terms of both model efficiency (i.e., NSME = 0.95 which is closer to '1') and performance (i.e., RRMSE = 0.13 which is closer to '0').

When replacing the measured and predicted SDR values with the measured and predicted SSY values to test the NSME, i.e., Equation [5.19], and RRMSE, i.e., Equation [5.20], there are apparently different results from the previous test (Table 5.6).

Table 5.7 Comparison of NSME and RRMSE using measured and predicted SSY values.

Soil erosion	Measured value (2009)		Mean-measured value (2001-2009)		RUSLE-STC		RUSLE-SISDR		NSME		RRMSE	
(tonnes/km^2/yr)	SSY	SDR	SSY	SDR	SSY	SDR	SSY	SDR	RUSLE-STC	RUSLE-SISDR	RUSLE-STC	RUSLE-SISDR
3111	729	0.23	1022	0.33	646	0.13	742	0.26	0.92	0.99	0.11	0.02

From Table 5.7, Nash and Sutcliffe's model efficiency and Relative Root Mean Square Error provide similar results as Table 5.5, when taking SSY values

instead of SDR values to validate modelling. The result can be concluded as below:

$$NSME_{RUSLE\text{-}STC}\ (0.92) < NSME_{RUSLE\text{-}SISDR}\ (0.99)$$

$$RRMSE_{RUSLE\text{-}STC}\ (0.11) > RRMSE_{RUSLE\text{-}SISDR}\ (0.02)$$

When the SSY values are taken into account for modelling validation, the coupled innovative RUSLE-SISDR and RUSLE-SRC provide very good efficient modelling for SSY predictions (i.e., NSME = 0.99 and 0.92, respectively, which are closer to '1'); the coupled RUSLE-SISDR provides a model efficiency for SSY prediction slightly better than the RUSLE-SISDR. Consistent with the RSME results, the coupled innovative RUSLE-SISDR provides a better model performance in SSY prediction (RRMSE = 0.02) than the coupled RUSLE-STC (RRMSE = 0.11) due to its value being closer to zero.

5.4 Discussion

In an overall comparison of model efficiency between the coupled RUSLE-STC and RUSLE-SISDR, it can be concluded that the RUSLE-SISDR modelling could be applied quite well to estimate SSY values in the watersheds of Northwest Thailand, or even other sites. The overview of validated values deriving from NSME and RRMSE are good in terms of validating the model efficiency and performance with the predicted SSY.

Even though the innovative SISDR is able to predict well in SSY at watershed scale, Van Rompaey *et al.* (2001), in contrast, argue that the concepts of SDRs are unable to estimate the sediment deposition within the watershed. Nevertheless, each erosion model should be used depending on the purposes. This is in agreement with Merritt *et al.* (2003, p.769), who remark that 'choice of a suitable model structure relies heavily on the function that the model needs to serve', in other words, emphasis on the process purpose or emphasis on the output purpose. In addition, Gao (2008) also notices that the simple lumped concept of SDR may perform equally well as the distributed model of STC due to the uncertainty and additional errors deriving from more parameter inputs in the distributed model often outweighing the potential improvement in prediction. For example, the transport capacity coefficient (K_{TC}) in the STC equation [5.4] needs to be a calibrated value, which provides a better STC, before estimating soil loss, sediment deposition and sediment export (see Table 5.2).

Regarding comparison of specific sediment yield to other watersheds, the relationships between specific sediment yields and drainage basins in eight watersheds of the Upper Ping River Basin illustrate the negative relation based on the rating curve plotted in this study, as shown in Figure 5.8. Such a result shows a decreasing SSY with increasing drainage area as a general condition (Walling, 1983), and this is due to the fact that in a larger basin there is possibly more opportunity for sediment deposition to be on the way (De Vente and Poesen, 2005). Based on this research finding, the watersheds in the Upper Ping River Basin provide the negative equation as $SSY = 73888A^{-0.616}$ with the

explained variance (r^2) = 0.63, r = −0.794 and p value = 0.019. The computed value of exponent β in this research (i.e., β = −0.616) is closer to the worldwide estimated β value (i.e., β = −0.5) which is suggested by Syvitski *et al*. (2005) who have estimated the absolute sediment yield (tonnes yr^{-1}) in worldwide rivers based on an assumed global relation between sediment yield and drainage area, in combination with a relief ratio and estimated mean surface temperature (De Vente *et al.,* 2007). Furthermore, the slope of negative relation between SSY and drainage area (A) in the Upper Ping River Basin seems a rather uniform variation, as De Vente *et al*. (2007) reveal that the uniform slope of the relation β values generally vary between −0.06 and −0.85.

Nonetheless, an inverse relationship of SSY-A for the Upper Ping River Basin established in this research has differed from Lorsirirat and Maita (2006), who indicate that the exponent β value of the equation relating SSY and basin area has a positive value for the Ping River Basin (i.e., $SSY=12.96\ A^{0.219}$ with the explained variance (r^2) = 0.943 and total stations (n) = 61). It is possible to think that the output of Lorsirirat and Maita (2006) has altogether combined the Upper and Lower Ping River Basin, where there is an overview of sediment sources, e.g. agricultural activities, particularly more field crop cultivation in the lowland near the main rivers than the upper part of the basin, resulting in increased sediment production at the basin outlet, and, of course, influencing the SSY-A relationship into becoming positive.

Among the eight sub-watersheds of the Upper Ping River Basin, the Upper Mae Wang watershed is the only site of Northwest Thailand that produces a mean annual specific suspended sediment yield over 5,000 tonnes km^{-2} yr^{-1}. Besides, its mean annual SSY is almost 42 times and 21 times greater than the global and Asian mean values, respectively, cited by Tamrazyan (1989) (Table 5.8). However, in comparison to the other watersheds recorded across the world, the given SSY value of the Upper Mae Wang watershed is still 11 times smaller than the world's highest rate of mean annual SSY at China's Huangfushuan watershed (Walling and Webb, 1996), which recorded, in 1980, a mean annual SSY exceeding 50,000 tonnes km^{-2} yr^{-1}. Additionally, the mean specific suspended sediment yield rates for other watersheds in the world are also presented in Table 5.9.

Table 5.8 Mean annual discharge and SSY in different regions of the world.

Region	Mean annual river discharge (km^3 yr^{-1})	Mean annual sediment yield (tonnes km^{-2} yr^{-1})	Reference
Globe	42,720	120	Tamrazyan (1989)
Eastern hemisphere	23,035	133	„
Western hemisphere	19,685	91	„
Asia	13,564	242	„
South America	11,800	138	„
North America	7,885	56	„
Africa	3,940	32	„
Europe	3,140	53	„
Oceania	2,090	148	„
Australia	301	17	„

Table 5.9 Reported values of mean annual specific suspended sediment yield for global watersheds.

Watershed	Country	DBA (km^2)	Mean annual sediment yield ($t\ km^{-2}\ yr^{-1}$)	Reference
Huangfushuan (1980)	China	3,199	53,500	Walling and Webb (1996)
Erjenhsi (1980)	Taiwan	350	28,911	Walling and Webb (1996)
Tsengwen (1983)	Taiwan	1,000	28,000	Walling and Webb (1996)
Dali (1980)	China	187	21,700	Walling and Webb (1996)
Waiapu (1982)	New Zealand	1,378	19,970	Griffiths (1982)
Perkerra (1974)	Kenya	1,310	19,520	Dunne (1974)
Waingaromia (1982)	New Zealand	175	17,340	Griffiths (1982)
Hokittka (1982)	New Zealand	352	17,070	Griffiths (1982)
Upper Solo (1988)	Indonesia	176	16,116	Loebis and Taryana (1988)
Jökulsá á Sólheimasandi (1973-88)	Iceland	78	14,482	Lawler (1991)
Cilutung (1981)	Indonesia	600	12,000	Hardjowitjitro (1981)
Cikeruh (1981)	Indonesia	250	11,200	Hardjowitjitro (1981)
Aure (1981)	New Guinea	4,360	11,126	Walling and Webb (1996)
Shenchong (1989)	China	0.73	9,430	Luk *et al.* (1997)
Masinga (2004)	Kenya	6,262	8,740	Mutua *et al.* (2006)
Tirtomoyo (1988)	Indonesia	152	8,159	Loebis and Taryana (1988)
Keduwang (1988)	Indonesia	392	7,272	Loebis and Taryana (1988)
Mangatu (1982)	New Zealand	155	7,045	Griffiths (1982)
Tahakenui (1982)	New Zealand	21	6,969	Griffiths (1982)
Waipaoa (1982)	New Zealand	1,582	5,836	Griffiths (1982)
Upper Mae Wang (2009)	Thailand	389	5,015	Semmahasak (2013)
Gräelva (1992)	Norway	48	3,789	Bogen (1996)

5.5 Conclusion

The high amount of suspended sediment yield in the main streams is currently a concern for worldwide basin management because the excessive suspended sediment can lead to the problem of water pollution. The tropical mountainous watershed in the Upper Ping River Basin are selected as a case study of this research because it has apparently experienced land degradation and soil erosion, particularly on upland slopes, causing the lowland to be flooded regularly in the rainy season.

Estimates of suspended sediment yield can be conducted in several ways. The popular methods are extrapolation from a sediment rating curve and application of erosion modelling. The results estimated based on the sediment rating curve method as equation [5.3] illustrate that the rate of specific suspended sediment yields range between 350 and 5,050 tonnes km^{-2} yr^{-1}. The Upper Mae Wang watershed generates the highest amount of the specific suspended sediment yield (SSY), in the Upper Ping River Basin, of approximately 5,015 tonnes km^{-2} yr^{-1}. The Upper Mae Ping and Mae Ngad watersheds followed in second and third positions with amounts of 1,210 and 981 tonnes km^{-2} yr^{-1}, respectively, while the amount of SSY in the Mae Taeng watershed is the smallest at 360 tonnes km^{-2} yr^{-1}, because of the watershed size effect (1,929 km^2). Considering, in particular, annual sediment load (tonnes/year), however, the Middle Mae Ping watershed is in the top rank, and it created total suspended sediment loads of 5,279,900 tonnes yr^{-1} in 2009. The Upper Mae Ping and Upper Mae Wang watersheds followed in second and third positions with amounts of 3,738,400 and 1,951,000 tonnes yr^{-1}, respectively. The amount of annual suspended sediment load in the Lower Mae Wang watershed was the smallest at only 349,700 tonnes yr^{-1}.

With regard to applying erosion modelling to estimate suspended sediment yield, empirically based modelling, e.g. RUSLE, is selected for this research. However, such modelling is only able to estimate the amount of sediment eroded from the surface, and is unable to estimate suspended sediment yield. Consequently, the concepts of sediment transport capacity (STC) and sediment

delivery ratio (SDR) are employed and combined with RUSLE for computing the amounts of mean annual specific sediment yield (SSY) within the Mae Rim watershed, which is chosen as an experimental watershed for the modelling performance and efficiency test.

Particularly in STC concept, the transport capacity coefficient (K_{TC}), which reflects the effects of vegetation cover on overland flow sediment transport, is used for calibration by applying the model with a wide range of K_{TC} (generally ranges between 0 between 0.5). Since K_{TC} strongly depends on land use and land cover types, Jain and Das (2010) suggest the K_{TC} is empirically linked to the Normalised Difference Vegetation Index (NDVI) derived from satellite imagery, and can be calculated based on Equation [5.7]. To obtain the K_{TC} value suitable for prediction of mean annual SSY in 2009, the given values of scaling factor β, including of 0.07, 0.08, 0.09, 0.1, 0.5, 1.0 and 1.5, are tested through calibration in order to minimising error between observed and predicted SSY. As a result, it is found that $\beta = 0.08$ is sensitive to the mean annual SSY in 2009 at river gauging station P21 of the Mae Rim watershed, and also provides the K_{TC} values, ranging between 0.02 and 0.41 (see also Table 5.2). Thus, a calibrated $\beta = 0.08$ is adopted as a key of scaling factor for computing the STC in this study.

The predicted mean annual SSY value, for the water year 2009, derived from the coupled RUSLE-STC, is 646 tonnes km^{-2} yr^{-1}, whereas the coupled RUSLE-SISDR predicts the mean annual SSY value as 742 tonnes km^{-2} yr^{-1}. These

predicted values are underestimate and slightly overestimate, i.e. −11% and 2%, respectively, when assessing the percentage difference from the actual measured value based on the equation suggested by Horowitz (2003).

Moreover, to compare the model efficiency and performance between the two different approaches, RUSLE-STC and RUSLE-SISDR, Nash and Sutcliffe's model efficiency (NSME) and relative root mean square error (RRMSE) are adopted for these tests.

Apparently, when testing with NSME and RRMSE by using the predicted mean SDR values with the measured value, the RUSLE- SISDR provides much more better modelling in terms of efficiency and performance than the RUSLE-STC, i.e., $NSME_{RUSLE\text{-}SISDR}$ = 0.91 is closer to '1' than $NSME_{RUSLE\text{-}STC}$ = 0.00, and $RRMSE_{RUSLE\text{-}SISDR}$ = 0.13 is closer to '0' than $RRMSE_{RUSLE\text{-}STC}$ = 0.43.

Also, when the predicted mean annual SDRs are replaced by the predicted mean annual SSY, the results show the RUSLE-SISDR to be slightly accurate than the RUSLE-STC because both the NSME and RRMSE provide slightly better values of model efficiency and performance than the RUSLE-STC, i.e., $NSME_{RUSLE\text{-}SISDR}$ = 0.99 is closer to '1' than $NSME_{RUSLE\text{-}STC}$ = 0.92, and $RRMSE_{RUSLE\text{-}SISDR}$ = 0.02 is closer to '0' than $RRMSE_{RUSLE\text{-}STC}$ = 0.11.

All in all, the findings in this research can help to answer the questions surrounding the difference in concept between STC and SDR when combined

with RUSLE, and the RUSLE-SISDR model can provide a better result in the mean annual SSY prediction.

Besides, this thesis introduces an innovative technique regarding interpolation of sediment delivery ratio (SDR), based on the concept of William and Berndt (1972) (cited in Hui *et al*., 2010, p.945) that the slope gradient of the main river is more significant than other parameters in terms of sediment production. It also provides spatially-extrapolated values of every cell within the watershed.

A watershed with short and steep slopes will deliver more sediment to a main stream channel than one with flat and wide valleys (Ouyang and Bartholic, 1997). Therefore, in order to visualise the spatial distribution of SDR across the hillslope, the Krigging method (Childs, 2004) is introduced for interpolation of the SDR values, which are computed based on the main stream gradients as equation [5.10]. This spatially distributed SDR map contains the interpolated values in each cell. Thus, each cell value of SDR multiplied by the computed soil erosion amounts, which are obtained from the RUSLE model, represent the spatial distribution of suspended sediment yield (SSY). Advantages of the innovative technique introduced in this research are not limited to use for the identification of sediment source areas across the Mae Rim watershed. It can also assist in predicting sediment yield at the point of interest. As noted by Hui *et al.* (2010), the spatially distributed SDR map reflects the ultimate nature of sediment delivery from erosion in steeper locations, where it will have a greater chance of being transported into the channels than it would have downslope.

Consequently, the innovative RUSLE-SISDR modelling could be utilised by other researchers who are interested in sediment yield prediction. The strength of this model not only provides a better SSY prediction result, as well as being easy to conduct between the data input and the model, but also depicts the spatial distribution of the SDR (see Figure 5.17). However, the limitation of the RUSLE-SISDR is that it is unable to predict the sediment deposition. Depending on the purpose, if the researchers need to pay more attention to the processes of soil erosion, the RUSLE-STC should be recommended.

5.6 Chapter summary

This chapter has assessed suspended sediment yield by using a sediment rating curve and RUSLE-GIS-based model. Regarding use of the sediment rating curve in prediction, the SSL-Q relationship proposed as Equation [5.3] was employed herein to extrapolate suspended sediment fluxes and yields. In terms of sediment yield prediction by applying RUSLE-GIS-based model, two different concepts including sediment transport capacity (STC) and innovative approach 'spatial interpolation of sediment delivery ratio (SISDR)' have been adopted in conjunction with RUSLE to model and evaluate sediment yield. Results from comparative studies of model efficiency between the coupled RUSLE-STC and RUSLE-SISDR concluded that the innovative RUSLE-SISDR has given more reasonable validation in estimation of mean annual specific sediment yield (SSY) in the Mae Rim watershed (i.e., Nash and Sutcliffe's model efficiency (NSME) = 0.99 and Relative Root Mean Square Error (RRMSE) = 0.02, which were closer to '1' and '0', respectively), compared to the

coupled RUSLE-STC (i.e., NSME = 0.92 and RRMSE = 0.11). In the next chapter, soil erosion under changes in land use and rainfall erosivity will be investigated, and also sensitivity analysis will be undertaken to explore the relative influence of these two factors on soil erosion.

CHAPTER 6: THE EFFECTS OF LAND USE AND RAINFALL CHANGES ON SOIL EROSION IN MAE RIM WATERSHED, NW THAILAND

6.1 Introduction

Understanding the relative importance of changes in land use and rainfall is essential for modelling an erosion processes hazard assessment, and for future scenarios of change (Yang *et al*., 2003; Diodato, 2006; Mango *et al*., 2011; Montenegro and Ragab, 2012). According to Allison and Thomas (1993), there is much to be learned from evidence of past changes on the environment as a result of human activities. In some cases, evidence from the past provides input for modelling and predicting future changes (e.g., Jordan *et al.,* 2005; Diodato, 2006; Ward *et al.,* 2009). Several studies have demonstrated that climate and land use changes can have significant impacts on soil erosion by water (e.g., Asselman *et al.,* 2003; Zhang and Nearing, 2005; Bakker *et al*., 2008; Bosco *et al.,* 2009; Fu *et al.,* 2009; Wei *et al.,* 2009; Zhang *et al*., 2009; Feng *et al*., 2010; Ma *et al.,* 2012). Moreover, Chang (1993) stated that the high rainfall erosivity and rapid deforestation in tropical Asia, especially in Thailand and Philippines, have been the major contributing causes to the soil erosion problem.

The uplands of northwestern (NW) Thailand have become a concern with regard to soil erosion susceptibility because of their undulating topography, steep slopes and heavy rainfall. Additionally, natural land degradation and soil

fertility depletion have accelerated over the past two decades; as a result of the increasing encroachment of agricultural activities on steeply sloping lands, without effective land management practices (George *et al.,* 2009). Many scholars believe that the conversion of forest to agricultural land especially for 'intensive swidden cultivation' on the sloping upland areas can cause greater effects on the watershed and soil degradation (e.g., Ziegler *et al*., 2004; Thanapakpawin *et al*., 2006; Verburg *et al.,* 2006; Fukushima *et al*., 2008). 'Intensive swidden cultivation' refers to slash-and-burn agriculture that is characterised by cutting and burning vegetation, before leaving the cleared patches to fallow for short term periods (1 or 2 years), or even not to fallow at all (Fox *et al*., 1994; Palm *et al*., 2005; Fukushima *et al*., 2008; Ziegler *et al.,* 2009). However, land without trees or forest canopies exposes soil to greater splash action from rainfall, and further enhances erosion by overland flow. In Figure 6.1, the intensive swidden cultivation in various sloping areas, which are generally found in the upland of the Mae Rim watershed (above 600 m a.s.l.), clearly indicate that change of land use from forest to agriculture may affect or relate to soil erosion events in the area.

Figure 6.1 Steep slope agriculture in the Mae Rim watershed, NW Thailand, taken from the field observation in July 2011: (a) Many hill-slope areas of the Mae Rim watershed were transformed by hill-tribe farmers for cultivation; (b) Patches from hillside to hilltop were left fallow with sparse vegetation or without it altogether; (c) The remaining tree strums and exposed soil on steeply sloping land can be generally found in the upland area of Mae Rim watershed.

Many scholars have rated the effects of climate change as having a lesser impact on soil erosion than the effects of changing land use in the tropical region (e.g., Chang, 1993; Dale, 1997; Verburg *et al.,* 2006). However, heavy rainfall intensity in the mountainous tropical regions, especially during the wet season, can cause severe soil loss if inappropriate land management practices

are applied (Schiettecatte *et al.,* 2008). Maeda *et al.* (2010) have ascribed that changes in precipitation amounts and intensity caused by climatic change, may increase the erosive energy available in rainfall for detaching and carrying sediments. Therefore, achieving an understanding of rainfall variation over space and time is important for future soil conservation planning and land use management; it is the initial and essential driving force for natural runoff generation and soil variation (Wei *et al.,* 2009).

In conclusion, as a result of rainfall that tends to occur in the one monsoon season's high-magnitude storms (Forsyth and Walker, 2008), as well as rapid changes of land use over the past two decades, especially in the conversion of forest to agriculture in the Mae Rim watershed, it is extremely challenging to obtain answers as to the real causes of soil erosion, which are related to both or either of factors (i.e. land use and rainfall changes). Moreover, research on soil erosion impacted by the rainfall and land use changes in NW Thailand is very rare. This is because the knowledge and understanding of the processes involved with the rainfall and land use changes are fragmented, and mostly restricted to a specific area (Romeo, 2001). As a consequence, studying the variation of soil erosion by water, with reference to both climate and land use changes, will help to achieve a better knowledge and understanding of the erosion phenomena. Furthermore, alternative scenarios including rainfall erosivity, land use and soil erosion changes, can be used as additional tools for informing the planning and management of the watershed.

Hence, this chapter is established, based on the aims of applying a RUSLE-GIS-based model, in order to undertake a sensitivity analysis of the potential effects of changes in rainfall and land uses on soil erosion rates. This analysis will center on the selected Mae Rim watershed, and intends to improve knowledge and understanding in the changing factors and processes that determine soil surface losses. To achieve this aim, the following specific objectives of this chapter are to:

(a) Simulate the spatial changes of land use and rainfall erosivity using GIS.

(b) Delineate the effects of land use change and rainfall erosivity change on soil erosion between 1989 and 2009.

(c) Test a sensitivity analysis of the effects of controlling variables in each soil erosion risk scenario, under various assumed conditions.

6.2 Methods

This research is conducted based on the availability of data obtained from direct fieldwork observation and government agencies. This data has been taken into account when analysing and assessing the effects of land use and rainfall erosivity changes on the Mae Rim watershed from 1989 to 2009, including a sensitivity analysis of modelling, by using the methods described below.

6.2.1 Land use change analysis approach

To analyse land use changes in different time periods over the past two decades in the Mae Rim watershed, two different period sets of multi-spectral Landsat-5 TM and Landsat-7 ETM+ imageries, with spatial resolution 30 m (acquisition date in August 1989 and July 2009, respectively), were used; this was because it was an inexpensive technology with a high monitoring frequency (rendering an image of the same area every 16 days), that covered a large area suitable for developing soil conservation planning for a large catchment (De Asis and Omasa, 2007). Besides, a selection of images captured at different periods over 20 years was sufficient to detect changes in land use (Verburg *et al.,* 2006; Hartter *et al.,* 2008). Both satellite image datasets were geo-referenced and the data was projected to WGS84, UTM zone 47N, with a root mean square error of less than 0.5 pixels.

In land use classification, the land use map from 2009 was already classified by using a supervised classification with a maximum likelihood method. For the land use classification from 1989, it was conducted through a visual interpretation based on the general knowledge of spectral reflectance of the earth surface feature. The ground-truth information, topographical maps, and an existing land use map from 1989, from the Land development Department of Thailand (LDD), were used to verify and adjust the accuracy of the Landsat imagery classification. Accordingly, based on the USGS land use and land cover system for use of Remote Sensing Data at the primary and secondary levels (Gao, 2009), the land use classification of the Mae Rim watershed

includes: (1) urban area, (2) evergreen forest, (3) deciduous forest, (4) field crops, (5) water body, (6) mixed orchards, (7) bare fallow land, (8) paddy fields and (9) villages. Finally, the output of the land use classification of the Mae Rim watershed in 1989 is shown as Figure 6.2. In addition, an overall interpretation accuracy of the 1989 land use classification, using test samples of accuracy assessment, is 89%, with a Kappa coefficient (*k*) of 0.887 (Table 6.1).

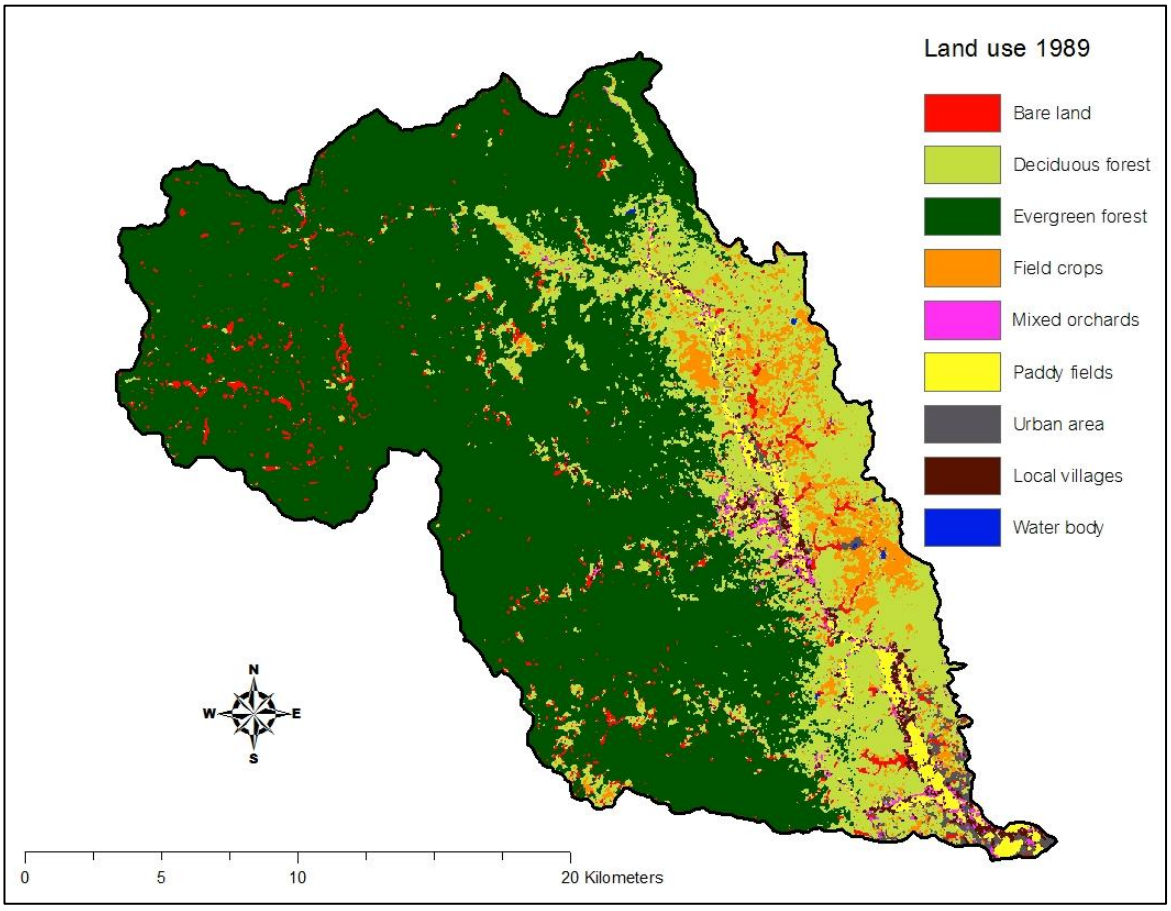

Figure 6.2 Land use map of Mae Rim watershed in 1989

Table 6.1 Error matrix for land use supervised classification in 1989

	Reference Data									
Ground Classes	Satellite image classes									
	Evergreen forest	Deciduous forest	Water body	Paddy fields	Mixed orchards	Field crops	Villages	Urban area	Bare fallow	Row Total
Evergreen forest	**49404**	627	0	60	1	0	4	0	2	50098
Deciduous forest	1818	**6009**	1	84	69	41	22	24	4	8072
Water body	2	6	**179**	5	13	0	0	3	0	208
Paddy fields	30	60	1	**8769**	114	0	108	193	0	9275
Mixed orchards	135	110	1	146	**1041**	0	139	124	0	1696
Field crops	53	782	0	2	9	**337**	1	19	3	1206
Villages	198	217	0	500	531	1	**357**	272	0	2076
Urban area	8	92	0	244	251	1	111	**415**	0	1122
Bare fallow	557	80	0	3	13	0	0	5	**239**	897
Column Total	52205	7983	182	9813	2042	380	742	1055	248	**74650**

Overall classification accuracy = 89.41%

Kappa coefficient (k) = $\frac{Observed\ accuracy - chance\ agreement}{1 - chance\ agreement} = 0.887$

Land use maps from 1989 to 2009 were firstly combined to generate land use change scenarios between 1989 and 2009. Then, this land use change scenario (1989–2009) was taken to overlay with the soil erosion risk map for 2009 (present soil erosion risk scenario), which was derived from the RUSLE-GIS-based model, to examine and assess effects of land use changes on soil erosion in the Mae Rim watershed. For the concise processes of analysing the impacts of land use change on the soil erosion of the Mae the Rim watershed, the following diagram is illustrative (Figure 6.3):

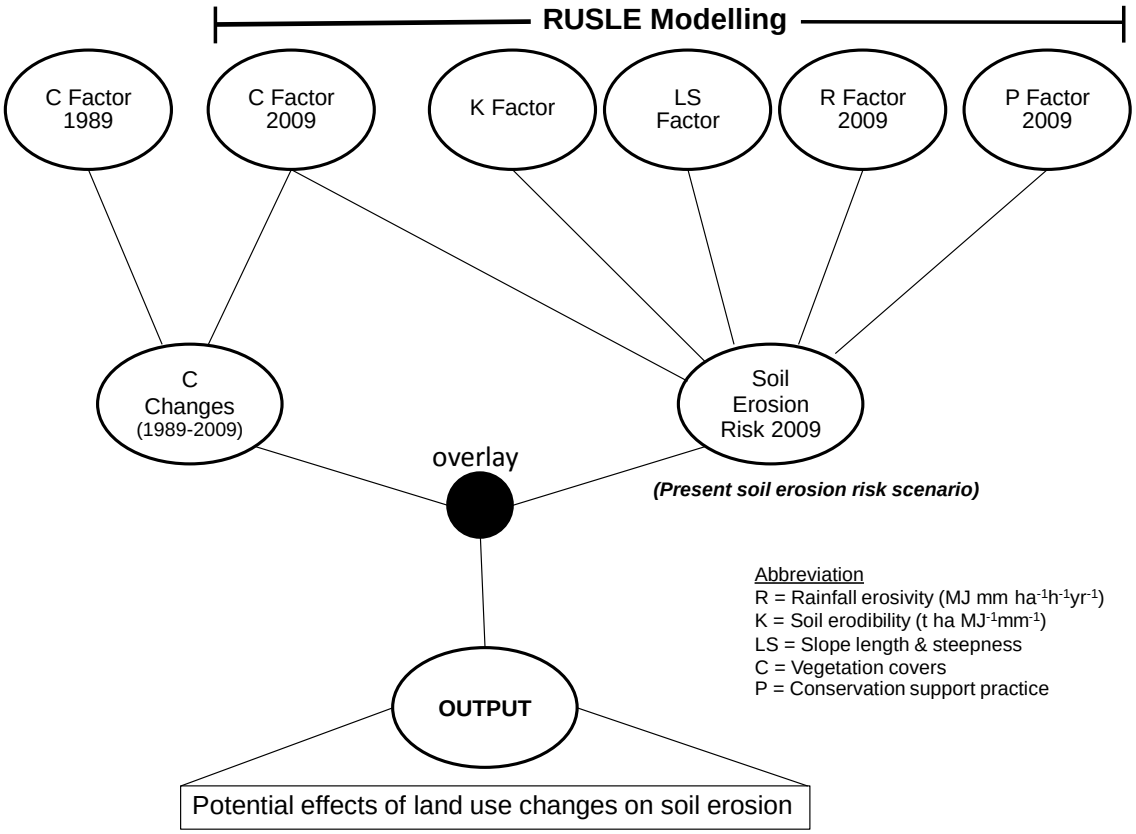

Figure 6.3 Procedure to assess effects of land use changes on soil erosion

6.2.2 Rainfall erosivity change analysis approach

Thailand can be described as a humid tropical region where the mean temperature of the coldest month is above 18°C and the duration of the wet season exceeds 4.5 months (Chang, 1993). The convection, convergence, orographic, and cyclonic are the major mechanisms of rain generation that cause more than 100 mm of rainfall in a wet month. In the rainy season, raindrop impact is significant in initiating energy that erodes existing soil and generates runoff to convey soil particles through a downstream channel. The soil surface will be extremely eroded, provided that the heavy rainfall of

thunderstorms or tropical monsoons take place in areas where there is insufficient vegetative coverage to protect the soil.

(1) Establishing rainfall erosivity map for 1989

In terms of evaluating rainfall-runoff erosivity, this can generally be calculated from an annual summation of rainfall data using rainfall energy over 30-min duration (Wischmeier and Smith, 1978). The Land Development Department of Thailand (LDD, 2000) developed various equations (based on Wischameier and Smith's concept) and then proposed an equation that fitted all rainfall amounts in Thailand, as expressed in equation [4.2] (see Section 4.2.2). In addition, the Modified Fourier Index (MFI), proposed by Renard and Frimund (1994), is another approach which has been used to calculate rainfall-runoff erosivity in this research, using equations [4.3] to [4.5]. This method is developed based on an empirical relationship between rainfall erosivity and the Fournier Index (Founier, 1960 cited from Maeda *et al*. 2010, p.282). To get the best equation for evaluating rainfall-runoff erosivity for a specific area, such as the Mae Rim watershed, this research has therefore developed a new equation by calibrating two different approaches between equations [4.2] and [4.5] (see Section 4.2.2).

Because this chapter has focused on studying rainfall erosivity change between 1989 and 2009 in the Mae Rim watershed, maps of rainfall erosivity need to be produced separately to compare and assess the differentiation of rainfall erosivity between those two different years (see Chapter 4). The monthly and yearly rainfall data for 1989 from 11 weather stations was estimated based on a

new calibrated equation as discussed above. Figure 6.4 shows the regression plot between two different approaches of rainfall-runoff erosivity estimations in 1989.

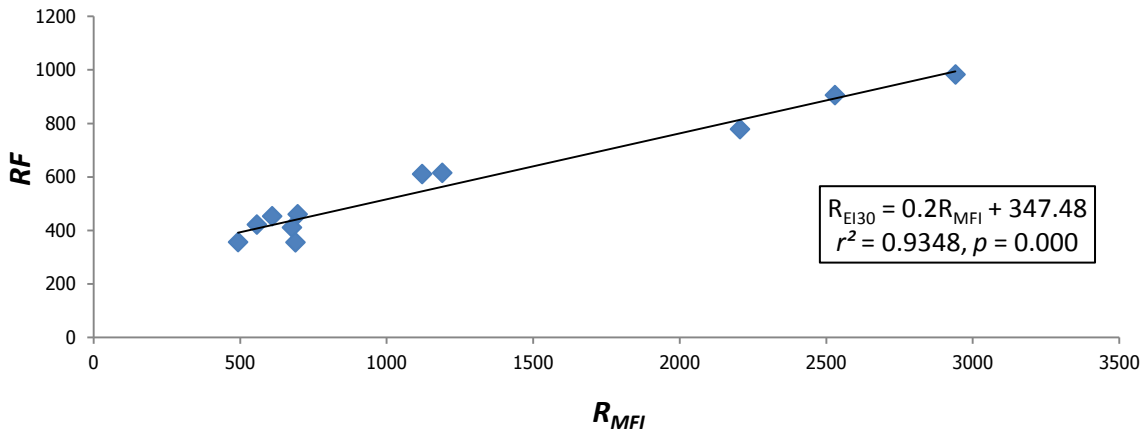

Figure 6.4 Relationship between R factor (RF) and Modified Fournier Index (R_{MFI}), based on rainfall data in 1989

The statistical values obtained from linear regression analysis in Figure 6.4 illustrate a high correlation of calibration (i.e., r = 0.97; r^2 = 0.93, p-value < 0.001), including a new calibrated equation provided for estimating rainfall-runoff erosivity as shown below.

$$RF = 0.2R_{MFI} + 347.48 \quad [6.1]$$

Where RF is the calibrated rainfall erosivity index based on equation [4.2]; R_{MFI} is modified Fournier Index of rainfall based on equation [4.5].

Given that R_{MFI} is an independent variable and RF varies based on R_{MFI}, the values of R_{MFI} from 11 rain gauge stations in 1989 were thus taken to account

again for calculating the new calibrated values of rainfall-runoff erosivity, or R_{EI30} (calibrated), using equation [6.1]. Hence, the following results of recalculated values are shown in Table 6.2.

Table 6.2 Rainfall-runoff erosivity values that are derived based on several equations

Rain gauge stations	RF Eq. [4.2] (MJ mm/ha h yr)	MFI Eq. [4.3] (mm)	R_{MFI} Eq. [4.5] (MJ mm/ha h yr)	R_{EI30} (calibrated) Eq. [6.1] (MJ mm/ha h yr)
1. Mae Rim	356.24	139.08	492.84	446.05
2. Mae Jo	460.22	164.31	696.17	486.71
3. Mae Taeng	452.98	154.04	609.16	469.31
4. Samoeng	410.87	162.07	676.75	482.83
5. Gang Keud	778.30	282.37	2205.55	788.59
6. MT Headwater	610.56	207.02	1120.89	571.66
7. Huai Kok Ma	982.57	326.06	2941.03	935.69
8. San Sai	421.75	147.52	556.93	458.87
9. Phu Phing	905.46	308.12	2529.56	853.39
10. Chiang Dao RI	615.05	213.10	1189.64	585.41
11. Pai	355.36	163.45	688.72	485.22

Actually, rainfalls occurring in NW Thailand are influenced by convectional, monsoonal, orographical, and cyclonic effects. Thus, this study has proposed a new method for evaluating the spatially-distributed rainfall erosivity values by forcing altitude, latitude and longitude into each grid cell of the watershed. In this case the multiple regression technique was adopted to test relationships between several independent variables (i.e., altitude, latitude and longitude) and a dependent variable (i.e., rainfall-runoff erosivity) (Table 6.3), and also to

generate new alternative equations suitable for mapping the rainfall erosivity factor.

Table 6.3 Details of rain gauge stations' locations (latitude–longitude) and altitudes

Rain gauge stations	R_{EI30} (MJ mm/ha h yr)	Altitude (m. asl)	Latitude (degrees)	Longitude (degrees)
1.Mae Rim	446.05	319.27	18.915	98.950
2.Mae Jo	486.71	317.18	18.897	99.011
3.Mae Taeng	469.31	340.00	19.118	98.948
4.Samoeng	482.83	532.26	18.848	98.736
5. Gang Keud	788.59	440.00	19.213	98.870
6. MT Headwork	571.66	360.00	19.514	98.923
7. Huai Kok Ma	935.69	1307.75	18.833	98.867
8. San Sai	458.87	305.26	18.848	99.058
9. Phu Phing	853.39	1410.60	18.807	98.903
10. Chiang Dao RI	585.41	1000.74	19.349	98.767
11. Pai	485.22	510.00	19.358	98.442

The dependent variable, R_{EI30}, and independent (predictor) variables (i.e., altitude, latitude and longitude) in Table 6.2 were analysed in multiple regression. Outputs deriving from analyses subsequently displayed several equations for the rainfall-runoff erosivity estimation with statistical values as follows:

$RE_1 = 385.89 + 0.34Alt$ ($r = 0.794$; $r^2 = 63.0\%$; $p = 0.004$) [6.2]

$RE_2 = -57.77 + 0.34Alt + 23.16Lat$ ($r = 0.795$; $r^2 = 63.1\%$; $p = 0.018$) [6.3]

$RE_3 = -16454.23 + 0.35Alt + 170.27Long$ ($r = 0.810$; $r^2 = 65.6\%$; $p = 0.014$) [6.4]

$RE_4 = -25796.08 + 0.37Alt + 102.4Lat + 244.89Long$ ($r = 0.819$; $r^2 = 67.1\%$; $p = 0.041$) [6.5]

Where RE_i is Rainfall erosivity (MJ mm/ ha h yr); Alt is Altitude (m. above sea level); Lat is Latitude in degrees; Long is Longitude in degrees.

All equations derived from the multiple regression analysis (e.g., equations 6.2–6.5) demonstrate that there are good relationships between dependent and independent variables as correlation coefficient values (*r*) ranging between 0.7994 and 0.819. It implies that the rainfall erosivity in the Mae Rim watershed is not only influenced by altitude, but also depends on the geographical coordinates of location (i.e., latitude and longitude). For this chapter, the equation [6.5] has been selected to calculate rainfall erosivity values because of having higher correlation coefficient *r* and r^2 than others (i.e. r = 0.819; r^2 = 67.1%) and *p* value < 0.05. As a result, values of rainfall erosivity calculated based on equation [6.5] had been assigned in every grid cell of the 25 m. resolution DEM, and the spatially-distributed rainfall erosivity map for 1989 was then generated as shown in the following Figure 6.5.

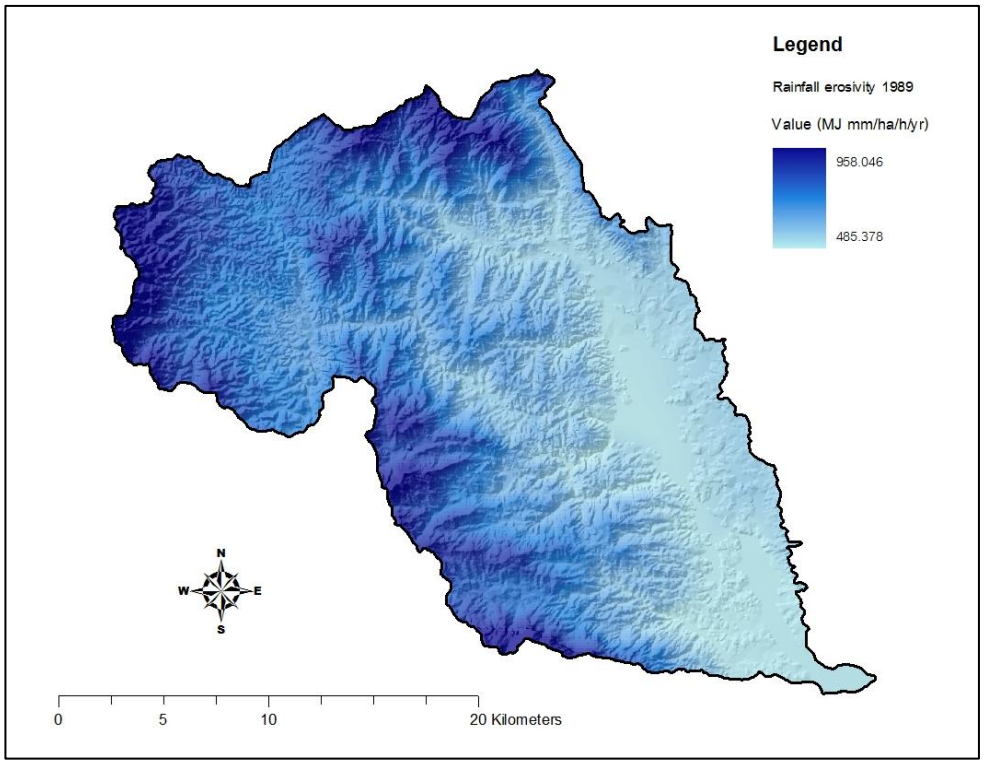

Figure 6.5 The spatially distributed rainfall erosivity map in 1989, Mae Rim watershed.

(2) Analysing and assessing rainfall erosivity affecting soil erosion.

To analyse the potential effects of rainfall erosivity change on soil erosion in the Mae Rim watershed, the GIS approach was used for combining rainfall erosivity maps for 1989 and 2009. Also, the rainfall erosivity change scenario was generated by the subtraction of pixel-by-pixel values between the data from two different time periods, using the raster calculator function in the spatial analyst tool of ArcGIS. In the process of subtracting pixel values of the temporal changing rainfalls, the spatially distributed rainfall erosivity map for year 2009 is set as a reference map and subtracted by the rainfall erosivity map for year 1989. Hence, the positive values for a pixel in the subtracted map indicate an increasing rainfall, and vice versa.

With regard to investigating the potential effects of changing rainfall erosivity on soil erosion, as depicted in the diagram below (Figure 6.6), the scenario of changing rainfall erosivity was overlaid with the changing soil erosion scenario. Likewise in order to generate a rainfall erosivity change scenario, the soil erosion maps for 1989 and 2009 were combined and then established the changing soil erosion scenario from the subtraction operation. In the process before the combination and subtraction of the maps, the soil erosion map for 1989 had been regenerated as a similar method of generating a soil erosion map for 2009 (except R and CP factors were reassigned for 1989), as described previously in Chapter 4 (see Section 4.2.2). Hence, the output derived from a map overlay operation could identify the spatially-correlated effects of rainfall erosivity change during 1989–2009 on the changing soil erosion of the Mae Rim watershed.

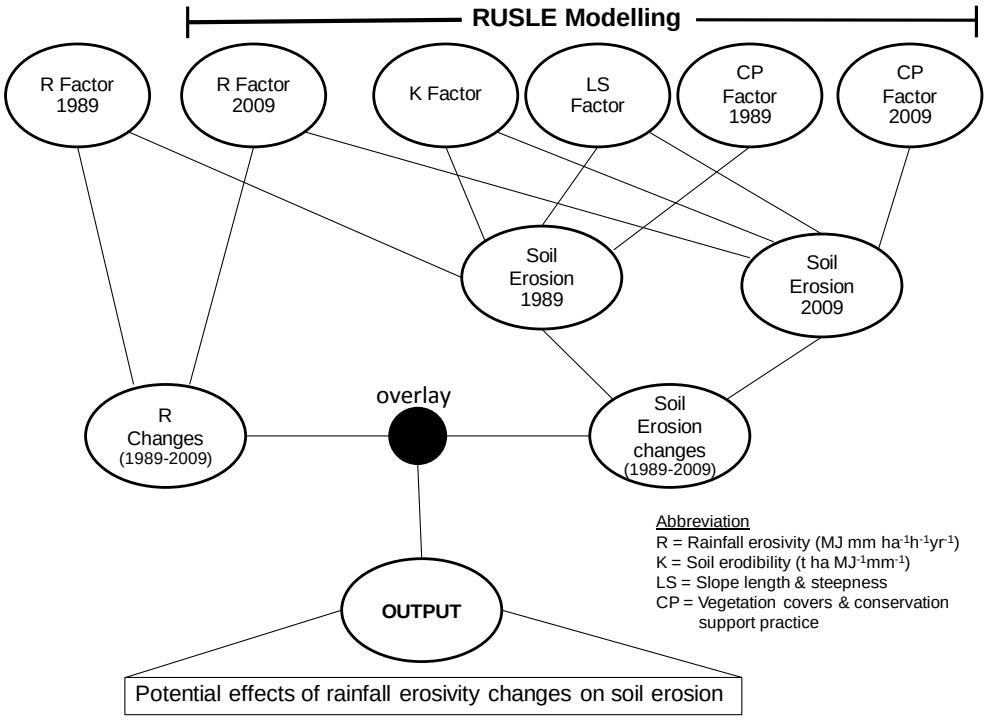

Figure 6.6 Procedure to assess effects of changing rainfall erosivity on soil erosion.

(3) Investigating rainfall erosivity affecting soil erosion based on land use change scenario.

Both land use and rain erosivity changes significantly affected soil erosion change (Diodato, 2006). In addition, an understanding of integrating both effects is an essential step and able to effectively lead to natural resource conservations (Maeda *et al*., 2010). As such, in the final step of the rainfall erosivity analysis approach, the spatial relation of a rainfall erosivity-soil erosion map and the land use change scenario between 1989 and 2009 have been taken to integrate again by using the GIS technique for investigating the spatial interconnection of both effects on soil erosion in the Mae Rim watershed.

6.2.3 Sensitivity analysis of soil erosion risk scenarios

For the purposes of this research, to examine the relative effects of climate and land use change on soil erosion in the Mae Rim watershed, the sensitivity analysis method is used to test the key controlling variables of RUSLE modelling, such as rainfall erosivity (R) and vegetation covers (C), under various assumptions that are expected to occur in the future. The sensitivity analysis of the modelling is carried out by increasing and decreasing the given input variables and parameters to investigate how model output variables react to the input changes (De Roo and Offermans, 1995; Mulligan and Wainwright, 2004; Candela *et al*., 2012). Whilst R and C variables are controlled model inputs, residual variables consisting of soil erodibility (K), slope length and steepness (LS) and conservation support practice (P) are unaltered.

For this thesis, rainfall erosivity (R) variable is varied ±20%, in order to inspect magnitudes of sensitivity of soil erosion to a given change in the input factors. Such values set for the R variable follow the hypothetical decrement and increment of current rainfall conditions by -20% and +20%, which is a result of consideration on climate change projection over Thailand. According to research on future climate change (from 2011 to 2059) of Reda *et al.* (2013), in terms of rainfall amount in the Ping River Basin of northern Thailand, it tends to increase by 20%, whilst the length of rainy season would remain the same but with higher rainfall intensity. Regarding variable C, based on the concept of Thanapakpawin *et al.* (2006), bare fallow and field crop lands on the upland (above 600 m a.s.l.) and lowland (below 600 m a.s.l.) were assumed to expand around existing patches as 75 m or a triple of 25 m pixel size of area. The following future scenarios under variability of expected assumptions for sensitivity analysis experiments are detailed in Table 6.4.

Table 6.4 Rainfall erosivity and land use change scenarios for sensitivity analysis.

Variables	Scenario	Instructions for achieving future scenarios
R	S1	➢ Change in rainfall erosivity only by increasing (i.e. +20%)
	S2	➢ Change in rainfall erosivity only by decreasing (i.e. -20%)
C	SA	➢ Reversal of bare land/fallow and field crops to evergreen forest (>1000 m asl) and deciduous forest (< 1000 m asl)
	SB	➢ All bare land/ fallow and field crops expand to a triple pixel size of area, i.e. 75 metres, around all existing bare land and field crop patches (pixel resolution: 25x25 m.)
	SC	➢ Upland field crops have expanded (75 m around existing patches), while bare land/ fallow and lowland field crops convert to forests.
	SD	➢ Lowland field crops have expanded (75 m around existing patches), while bare land/ fallow and upland field crops convert to forests.
	SE	➢ Bare land/ fallow has expanded, while all field crop areas remain the same as year 2009
	SF	➢ Upland field crops have expanded (75 m around existing patches), while bare land/ fallow and lowland field crops remain the same as year 2009
	SG	➢ Lowland field crops have expanded (75 m around existing patches), while bare land/ fallow and upland field crops remain the same as year 2009
+R & C	S1A	➢ Increasing Rainfall erosivity (+20%) with conversion of bare land/fallow and field crops to evergreen forest (>1000 m asl) and deciduous forest (< 1000 m asl)
	S1B	➢ Increasing Rainfall erosivity (+20%) with expansions of bare land/ fallow and field crops (i.e. 75 m around all existing bare land and field crop patches)
	S1C	➢ Increasing Rainfall erosivity (+20%) with expansion of upland field crops (75 m around existing patches), while bare land/ fallow and lowland field crops all convert to forests.
	S1D	➢ Increasing Rainfall erosivity (+20%) with expansion of lowland field crops (75 m around existing patches), while bare land/ fallow and upland field crops all convert to forests.
	S1E	➢ Increasing Rainfall erosivity (+20%) with expansion of bare land/ fallow, while all field crop areas remain the same as year 2009
	S1F	➢ Increasing Rainfall erosivity (+20%) with expansion of upland field crops (75 m around existing patches), while bare fallow and lowland field crops remain the same as year 2009
	S1G	➢ Increasing Rainfall erosivity (+20%) with expansion of lowland field crops (75 m around existing patches), while bare fallow and upland field crops remain the same as year 2009
–R & C	S2A	➢ Decreasing Rainfall erosivity (-20%) with conversion of bare land/fallow and field crops to evergreen forest (>1000 m asl) and deciduous forest (< 1000 m asl)
	S2B	➢ Decreasing Rainfall erosivity (-20%) with expansions of bare land/ fallow and field crops (i.e. 75 m around all existing bare land and field crop patches)
	S2C	➢ Decreasing Rainfall erosivity (-20%) with expansion of upland field crops (75 m around existing patches), while bare land/ fallow and lowland field crops all convert to forests.
	S2D	➢ Decreasing Rainfall erosivity (-20%) with expansion of lowland field crops (75 m around existing patches), while bare land/ fallow and upland field crops all convert to forests.
	S2E	➢ Decreasing Rainfall erosivity (-20%) with expansion of bare land/ fallow, while all field crop areas remain the same as year 2009
	S2F	➢ Decreasing Rainfall erosivity (-20%) with expansion of upland field crops (75 m around existing patches), while bare fallow and lowland field crops remain the same as year 2009
	S2G	➢ Decreasing Rainfall erosivity (-20%) with expansion of lowland field crops (75 m around existing patches), while bare fallow and upland field crops remain the same as year 2009

6.3 Results

6.3.1 Effects of land use change on soil erosion change during 1989 - 2009

The land use change detection map of the Mae Rim watershed from 1989 to 2009 was generated based on the map overlaying operation in GIS as shown in Figure 6.7. Accordingly, sixty-six classes of land use changes and one class of unchanged land use were detected and extracted through the cross-tabulation GIS module. In addition, details of land use change from 1989 to 2009 can be exhibited as the following Table 6.5.

Table 6.5 Cross-tabulation of land use classes from 1989 to 2009 (area in ha)

	2009									
1989	Bare land	Deciduous forest	Evergreen forest	Field crops	Mixed orchards	Paddy fields	Urban area	Local villages	Water body	Total (ha)
Bare land	244	258	432	243	30	86	8	60	7	1367
Deciduous forest	237	6496	1338	1293	177	194	54	426	37	10251
Evergreen forest	398	2340	32093	211	30	13	9	188	24	35304
Field crop areas	59	1086	81	536	45	41	18	68	5	1940
Mixed orchards	9	116	17	81	43	65	17	57	2	408
Paddy fields	14	51	0	136	79	579	46	66	3	976
Urban area	8	87	9	102	92	72	38	154	4	568
Local villages	11	138	12	98	77	73	18	233	1	660
Water body	0	4	0	1	0	2	1	0	17	26
Total (ha)	981	10577	33983	2700	572	1125	209	1252	100	51500

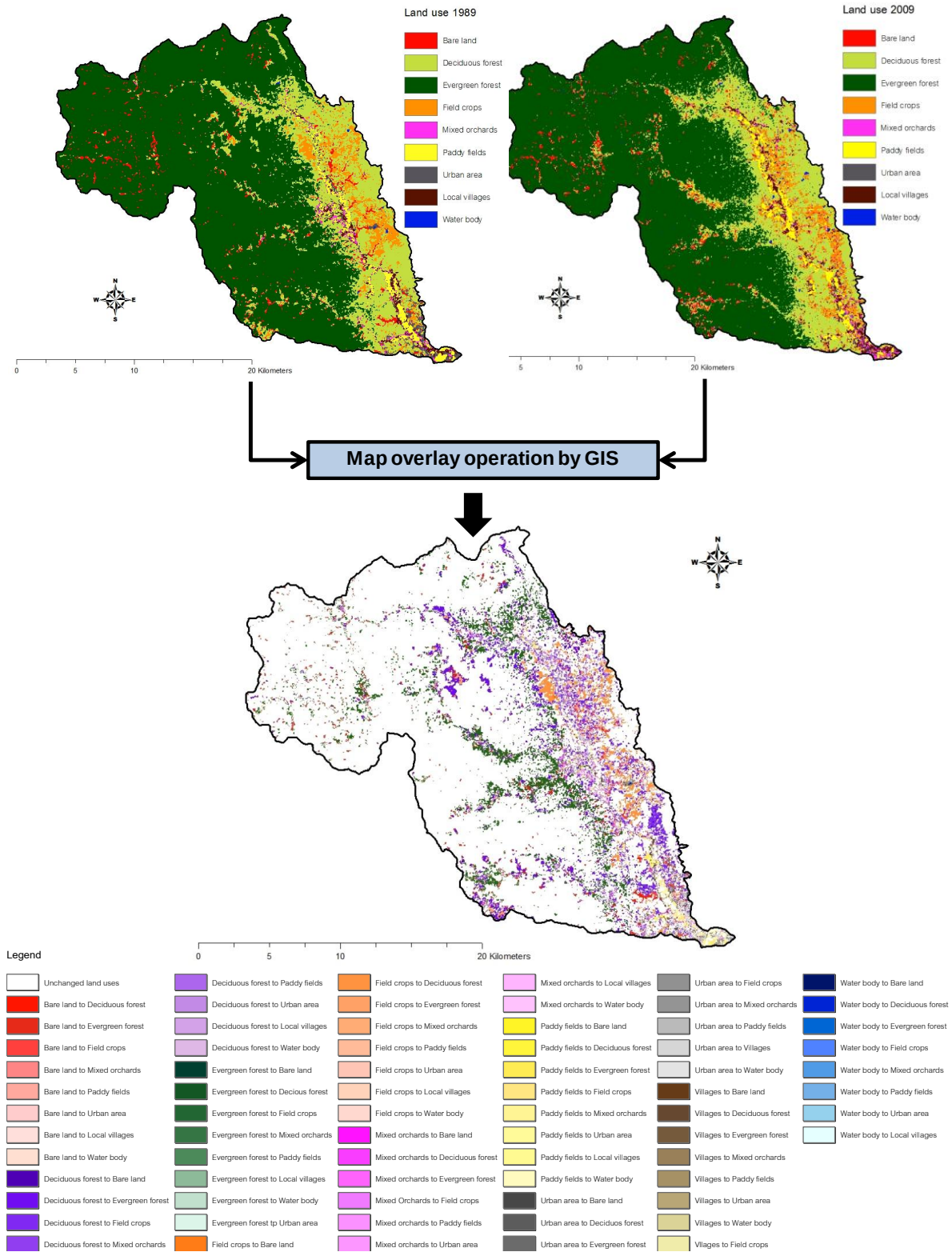

Figure 6.7 The spatially-distributed land use change scenario from 1989 to 2009

From Table 6.5, it can be concluded that a 78.25% of total area (i.e. 40,279 ha) in the Mae Rim watershed remained as unchanged land use, which included evergreen forest (63.32%), deciduous forest (12.61%), paddy fields (1.12%), field crop areas (1.04%), bare land (0.47%), local villages (0.45%), mixed orchards (0.08%), urban area (0.07%) and water bodies (0.03%), respectively, while a 21.75% of total land use areas (i.e., 11,221 ha) did change (Figure 6.7).

Regarding transitions of forested area in the Mae Rim watershed; the indications were that slight changes occurred over the study period, for example, the evergreen forest had decreased at the rate of –4%, while the deciduous forest had increased at the rate of 3%. The causes of the evergreen forest declining were due to it becoming deciduous forest (6.6%) and bare land (1.1%) since 1989, while deciduous forest increased in 2009 because it had been transformed from evergreen forest (22.1%) and field crop areas (10.3%), respectively, since 1989. Moreover, between 1989 and 2009, there was a significant increase in field crop areas at the rate of 28%. Most of them were converted from deciduous forest (47.9%) and bare land (9%), respectively. In addition, there was an explicit decrease in bare land at the rate of –40% in 2009 as a result of it returning to forestlands, i.e., the bare land had reverted to evergreen forest (31.6%) and deciduous forest (18.9%) since 1989. With regard to assessing impacts of land use change on soil erosion, results derived from overlaying maps between land use change during 1989–2009 and soil erosion risk in 2009, by using GIS, can be depicted as below (Figure 6.8).

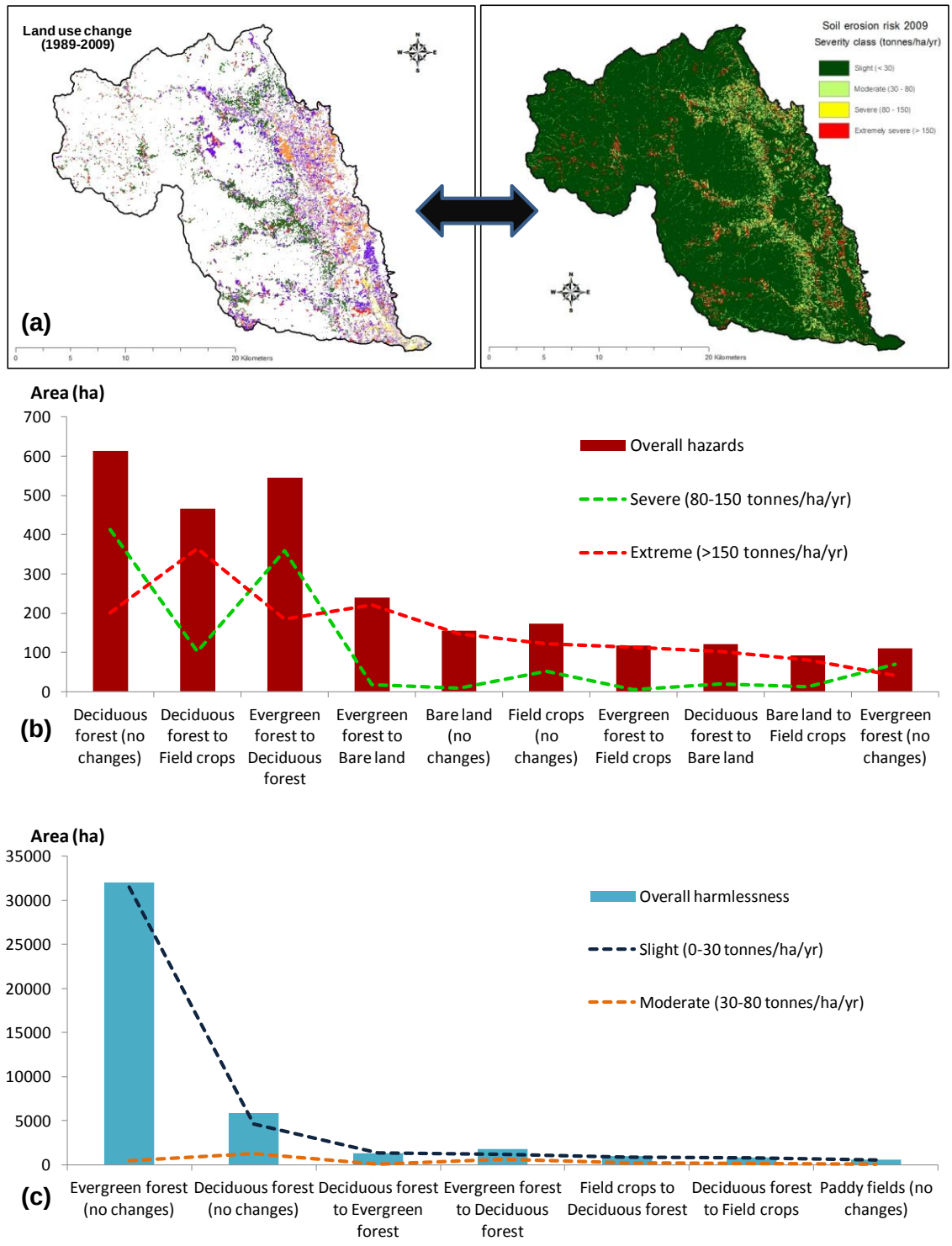

Figure 6.8 Combination of maps between land use change during 1989–2009 and soil erosion risk in 2009 (a) to examine types of land use change that show an extreme impact on soil erosion risk (b) and types of land use change that slightly impact on soil erosion risk (c).

Figure 6.8 illustrates clearly how changing land uses affect soil erosion with varying degrees of severity. For the present soil loss scenario (soil erosion risk map in 2009), the varying degrees of soil loss were classified into four categories, based on the criteria of soil erosion risk classification by degree recommended by FAO (2006). Hence, the "severity" classes of soil erosion adjusted for the Mae Rim watershed were detailed in following Table 6.6.

Table 6.6 Classification of soil erosion, by degree (FAO, 2006)

Soil erosion (tonnes/ha/yr)	Severity classes	Description
0-30	Slight	Some evidence of damage to surface horizons. Original biotic functions largely intact.
30-80	Moderate	Clear evidence of removal of surface horizons. Original biotic functions partly destroyed.
80-150	Severe	Surface horizons completely removed and subsurface horizons exposed. Original biotic functions largely destroyed.
>150	Extreme	Substantial removal of deeper subsurface horizons (badlands). Original biotic functions fully destroyed.

In terms of erosion hazard (Figure 6.8b), an extreme soil erosion, over 150 tonnes/ha/yr, mostly occurred in areas of conversion from deciduous forest to field crops (364 ha), followed by areas of conversion from evergreen forest to bare land (220 ha) and unchanged deciduous forest (200 ha), while the severe soil loss, between 80 and 150 tonnes ha^{-1} yr^{-1}, took place mostly in unchanged deciduous forest (413 ha) and areas of conversion from evergreen forest to deciduous forest (360 ha). However, when considering an overall hazard of soil erosion resulting from integration of two severity classes (i.e. extreme and severe soil losses), it indicated that the deciduous forest was the most vulnerable area for soil erosion in the Mae Rim watershed (613 ha), followed by

the area of conversion from evergreen forest to deciduous forest (545 ha) and the area of conversion from deciduous forest to field crops (467 ha), respectively.

Regarding virgin or unchanged evergreen forest; in general there was a slight degree of soil erosion (0 – 30 tonnes ha^{-1} yr^{-1}) occurring on such an area of 31,522 ha. Also, when integrating the slight and moderate severities of soil loss for assessing an overall harmlessness of soil erosion risk, the unchanged evergreen forest remains the most dominant area (31,981 ha), while there is relatively less of a problem with soil erosion in the Mae Rim watershed.

6.3.2 Effects of rainfall change on soil erosion change during 1989 – 2009

(1) Rainfall erosivity change scenario

The spatial distribution of rainfall erosivity maps in the Mae Rim watershed illustrated the minimum and maximum values ranging from 485.38 – 958.05 MJ mm/ha h yr for 1989 and 491.66 – 993.50 MJ mm/ha h yr for 2009. As a result of combining two different time period maps of rainfall erosivity, and subtracting pixel-by-pixel values, the rainfall erosivity change from 1989 to 2009 displayed minimum and maximum values of changes in a range of –59.66 to 55.38 MJ mm/ha h yr, with mean and standard deviation values of 11.99 and 10.99 MJ mm/ha h yr, respectively (Figure 6.9).

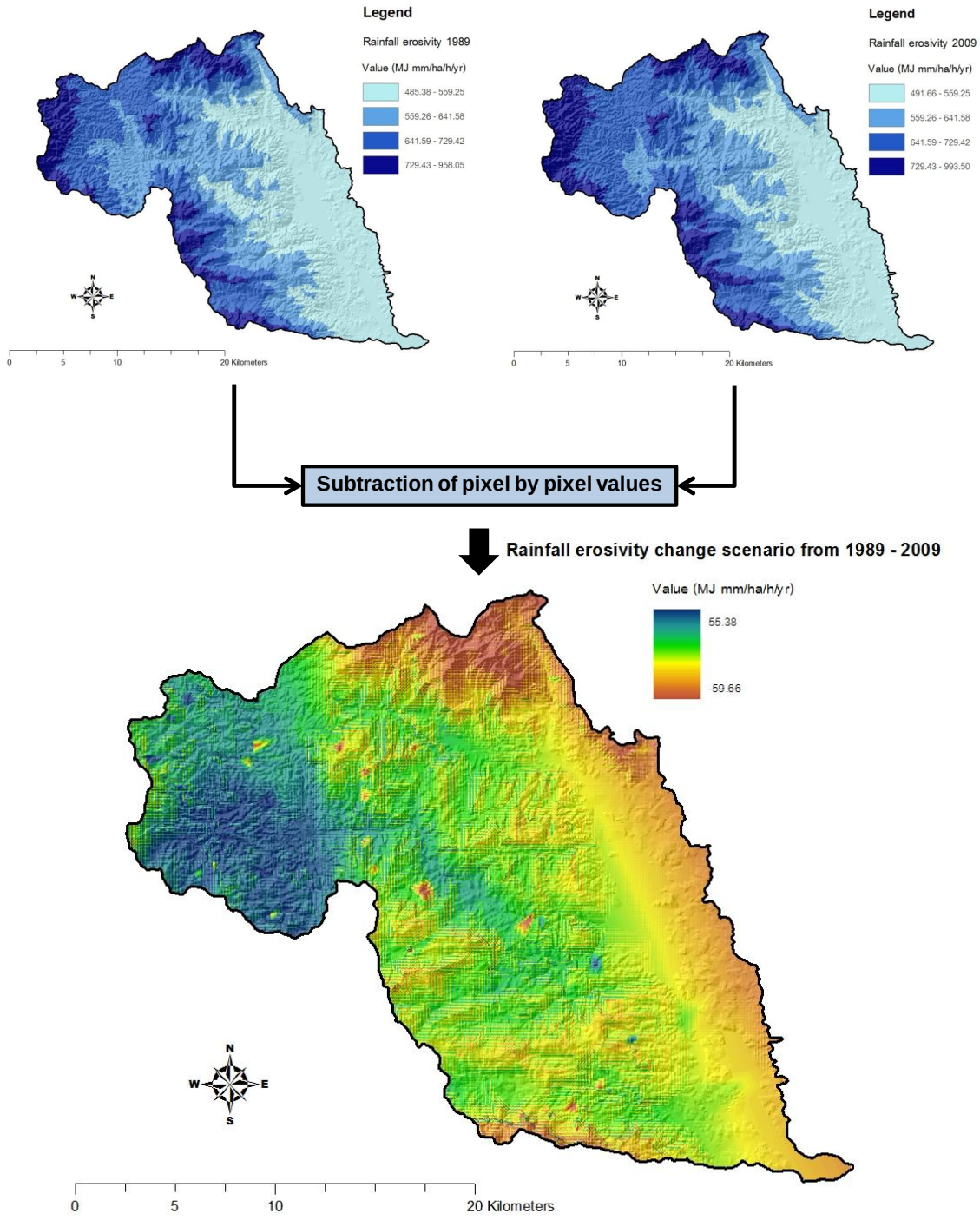

Figure 6.9 Rainfall erosivity change scenario during 1989 – 2009

In addition, the positive pixel values of each scenario indicates that rainfall over the past two decades has increased to 90% of the total area, with only 10% witnessing a decrease (negative pixel values) (Figure 6.10)

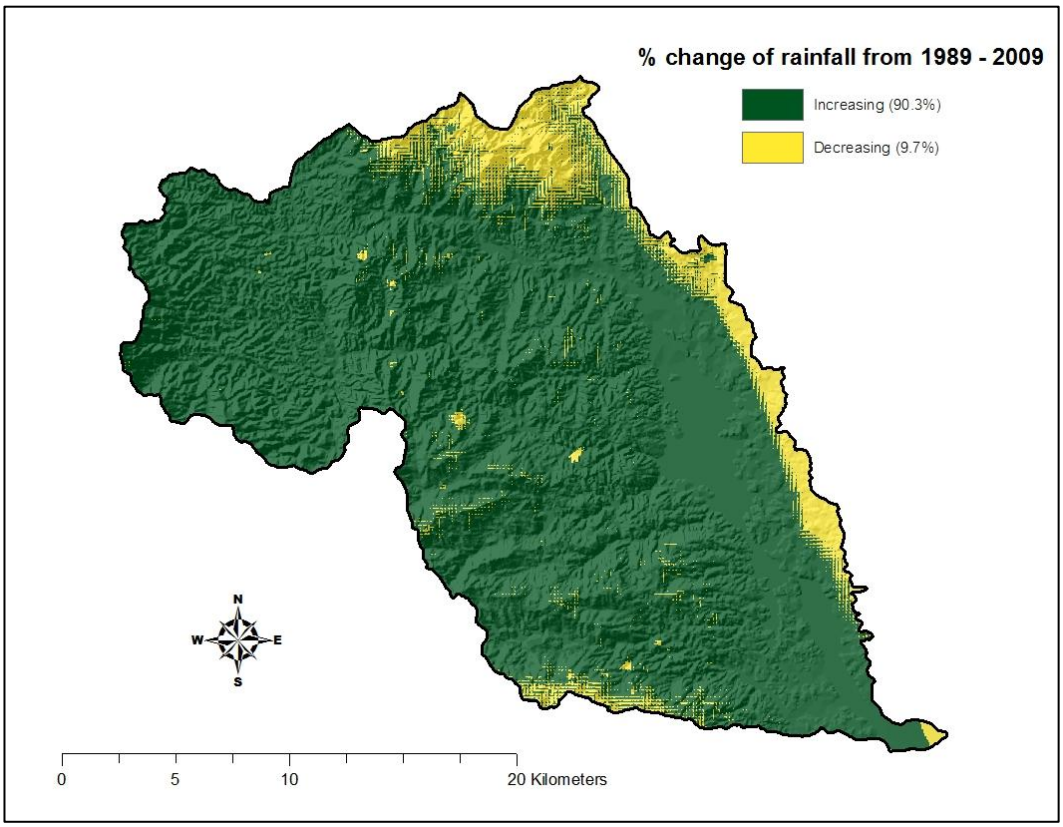

Figure 6.10 Percentage changes of rainfall in the Mae Rim watershed during 1989–2009

(2) Soil erosion change scenario

The spatially-distributed soil erosion map of Mae Rim in 2009, it showed the estimated values of annual soil loss, for the whole watershed, ranging from 0 to 48,049 tonnes ha^{-1} yr^{-1} with the mean annual soil loss of 31.11 tonnes ha^{-1} yr^{-1} (see also Figure 4.22). A new soil erosion map for 1989 was built up. The RUSLE-GIS-based model also computed annual soil loss rates for 1989,

ranging from 0 – 29,798 tonnes ha^{-1} yr^{-1}, while the mean annual soil loss and standard deviation were 26.96 and 173.69 tonnes ha^{-1} yr^{-1}, respectively (Figure 6.11).

Moreover, after combining two different time period maps of soil erosion (i.e. 1989 and 2009) to generate a soil erosion change scenario, the output indicated that mean annual soil loss rate in the Mae Rim watershed had increased at the rate of 15.4% since 1989. In addition, results obtained from subtracting pixel-by-pixel between maps showed the minimum and maximum value of its differentiated annual soil loss, varying from –17,766 to 43,351 tonnes ha^{-1} yr^{-1}, including mean and standard deviation values as 4.19 and 256.97 tonnes ha^{-1} yr^{-1}, respectively. All calculated positive (+) and negative (–) values referred to increasing and decreasing changes in soil erosion from 1989 to 2009 while zero (0) value referred to the fact there was no change in soil erosion in this study area.

Figure 6.12 shows areas of soil erosion increased from 1989 to 2009, covering 277 km^2 or 54% of total watershed area, while areas of 56 km^2 or 11% of total watershed area were covered by decreased soil erosion. The residual areas of 35% of total watershed area (182 km^2) showed unchanged soil erosion because of being locations of built-up areas and water bodies, which have no effect on the changing soil.

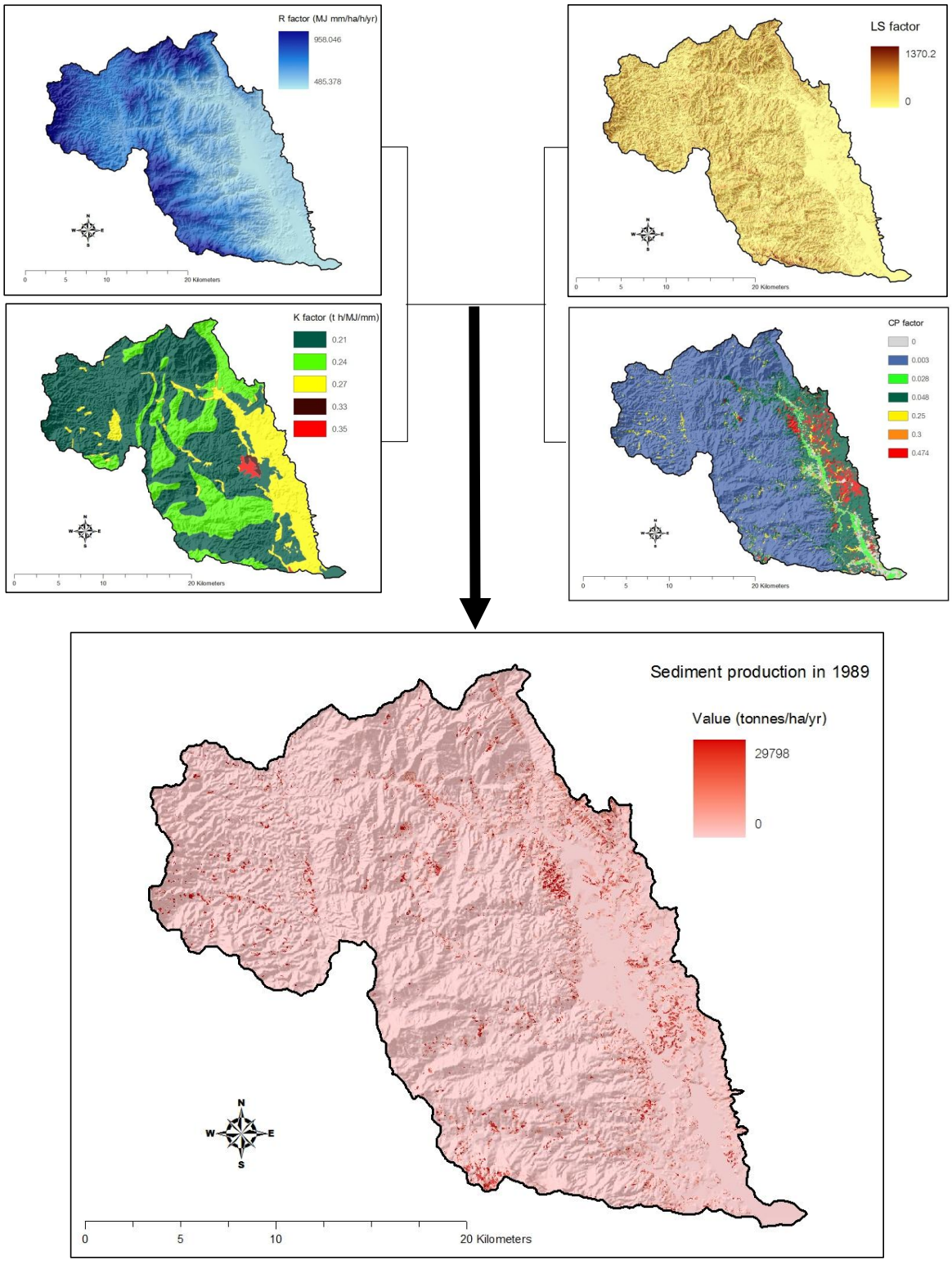

Figure 6.11 Annual soil loss map in 1989 of the Mae Rim watershed, NW Thailand, generated based on RUSLE equation [4.1], i.e. A = R•K•LS•CP

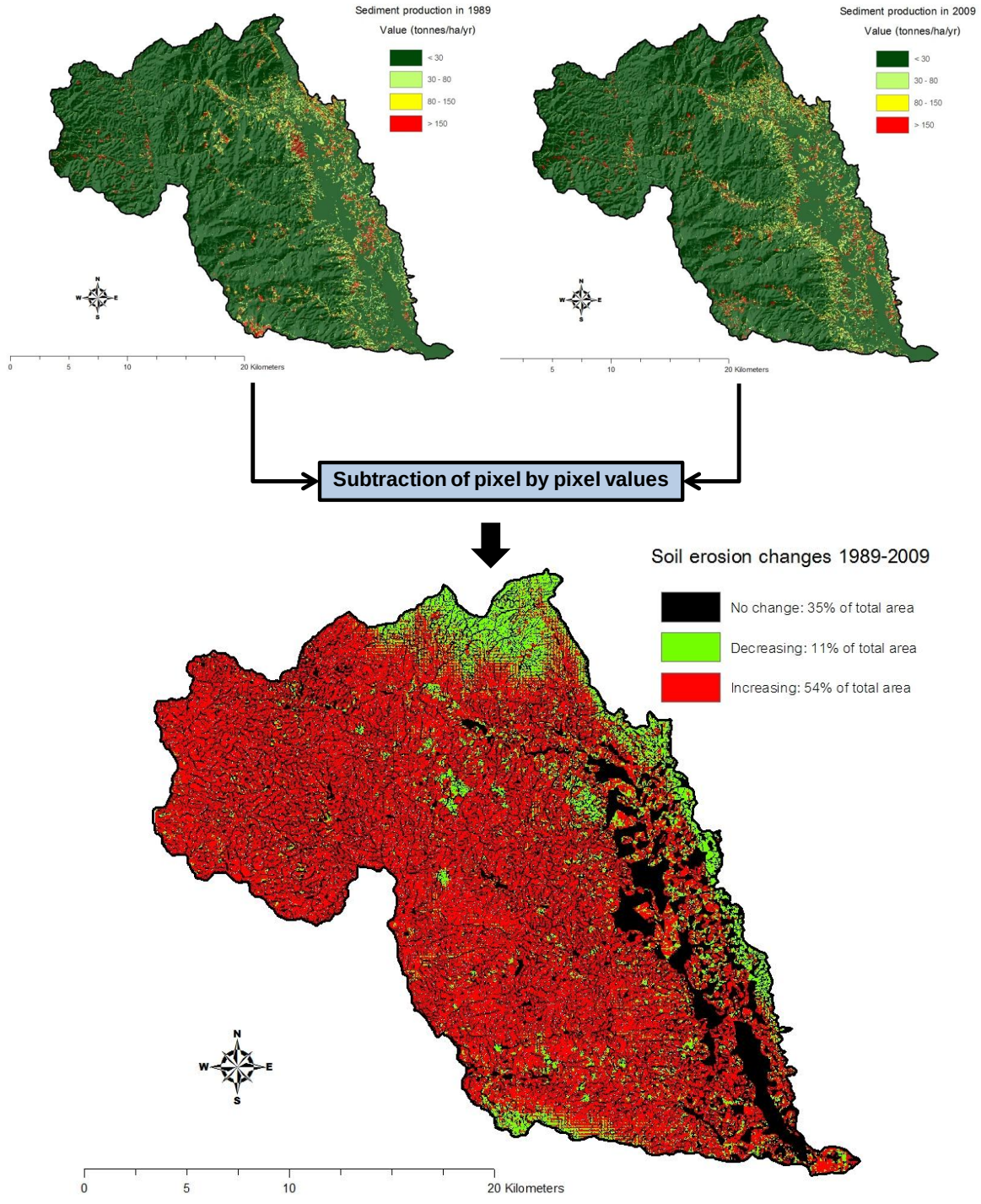

Figure 6.12 Soil erosion changes scenario from 1989 to 2009

(3) Spatial relationship between changes of rainfall erosivity and soil erosion

Results derived from overlaying maps between rainfall erosivity change and soil erosion change during 1989–2009 by using GIS, illustrated the spatial relationship between rainfall erosivity and soil erosion changes in the Mae Rim watershed (Figure 6.13). It can be concluded that there were two direct relationships, two inverse relationships and no relationship at all between rainfall erosivity change and soil erosion change in the Mae Rim watershed.

The direct relationships include: (1) rainfall increased (RI) and soil erosion increased (SI) or 'RI-SI correlation'; (2) rainfall decreased (RD) and soil erosion decreased (RD) or 'RD-SD correlation'. More than half of the Mae Rim watershed (53.4% of total area) is a RI-SI correlation. Table 6.7 and Figure 6.14 reveal that the increased rainfall has a greater effect on the increased soil erosion. This relationship has resulted in 16.8 tonnes ha^{-1} yr^{-1} increase in magnitude of mean annual soil erosion from 1989 to 2009. Also, for the RD-SD correlation, the decreased rainfall has significantly caused a –12.5 tonnes ha^{-1} yr^{-1} decrease in magnitude of mean annual soil erosion, covering 6% of total area (3,095 ha).

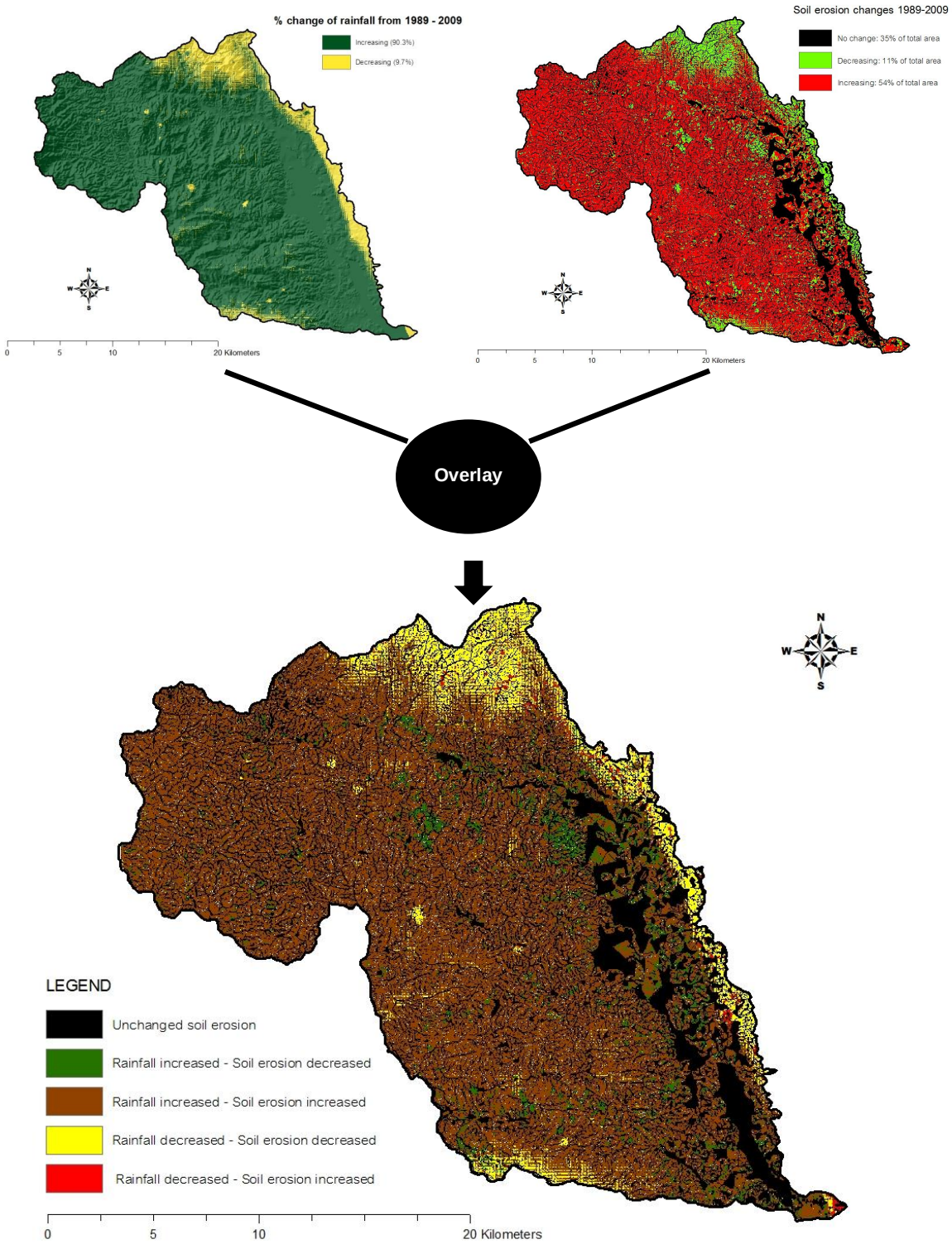

Figure 6.13 Map of spatial correlation between rainfall erosivity and soil erosion changes in the Mae Rim watershed.

Table 6.7 Soil erosion magnitudes varying according to different spatial correlations of rainfall change and soil erosion change during 1989 – 2009

Rainfall-soil erosion correlations	Area (ha)	Mean annual soil erosion 1989 (tonnes ha^{-1} yr^{-1})	Mean annual soil erosion 2009 (tonnes ha^{-1} yr^{-1})	Differentiation
Unchanged soil erosion	18,152	0.21	0.22	0.01
Rainfall increased-Soil erosion decreased	2,510	5.13	1.05	–4.08
Rainfall increased-Soil erosion increased	27,482	7.50	24.29	16.79
Rainfall decreased-Soil erosion decreased	3,095	13.63	1.17	–12.46
Rainfall decreased-Soil erosion increased	261	0.49	4.38	3.89
Total	51,500	26.96	31.11	4.15

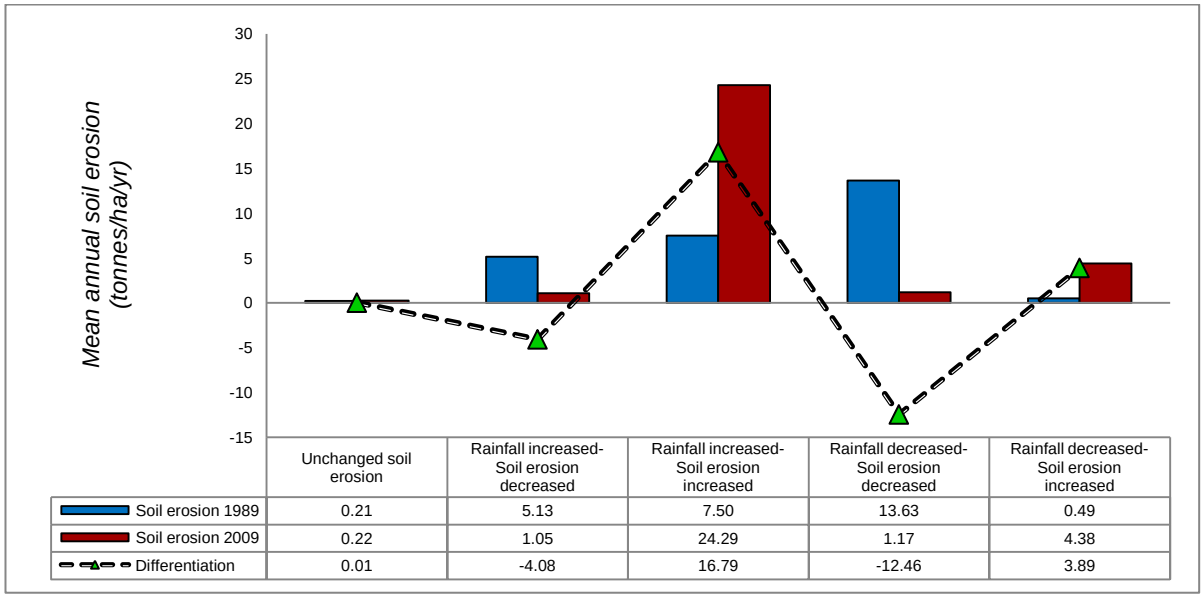

Figure 6.14 Soil erosion variations under changing rainfall from 1989 to 2009

The inverse relationships include: (1) rainfall increased (RI) and soil erosion decreased (SD) or 'RI-SD correlation'; (2) rainfall decreased (RD) and soil erosion increased (SI) or 'RD-SI correlation'. The RI-SD correlation in particular

shows more inversely affected soil erosion than the RD-SI correlation, by covering 5% of total area (2,510 ha), resulting in a decrease of –4.1 tonnes ha^{-1} yr^{-1} mean annual soil erosion from 1989 to 2009. The latter correlation (RD-SI) has occurred in the smallest area of the watershed (i.e. only 261 ha or 0.5% of total area), resulting in an increase of 3.9 tonnes ha^{-1} yr^{-1} mean annual soil erosion (Table 6.7 and Figure 6.14). .

However, because 35.2% of total watershed area (18,152 ha) was mostly covered by perennial rivers and lakes as well as permanent built-up areas, there were no effects associated with both increase and decrease in rainfall on soil erosion. As a result, soil erosion change in such areas has hardly taken place over the 20 year study period. According to Table 6.7, a very slight increase has been found of only 0.01 tonnes ha^{-1} yr^{-1} variation in the mean annual soil erosion rate from 1989 to 2009 (Table 6.7 and Figure 6.14).

(4) Spatial effects of rainfall erosivity against soil erosion relations in combination with land use change scenario

Results obtained from effects of rainfall erosivity change and soil erosion changes in combination with land use change scenario were summarised as below (Table 6.8).

Table 6.8 Spatial relations of rainfall change - soil erosion change - land use change

A. Rainfall increased (RI) – Soil erosion increased (SI)	**Area (ha)**	**% of total area**
1. Evergreen forest (not changed)	20,299.55	39.42
2. Deciduous forest (not changed)	2,886.57	5.60
3. Evergreen forest to Deciduous forest	1,469.10	2.85
4. Deciduous forest to Field crops	550.87	1.07
B. Rainfall decreased (RD) – Soil erosion decreased (SD)	**Area (ha)**	**% of total area**
1. Evergreen forest (not changed)	2,030.29	3.94
2. Deciduous forest (not changed)	611.09	1.19
3. Deciduous forest to Evergreen forest	100.98	0.20
4. Field crops to Deciduous forest	85.54	0.17
C. Rainfall increased (RI) – Soil erosion decreased (SD)	**Area (ha)**	**% of total area**
1. Deciduous forest to Evergreen forest	640.42	1.24
2. Field crops to Deciduous forest	440.38	0.86
3. Bare land/ fallow to Evergreen forest	183.77	0.36
4. Mixed orchards to Evergreen forest	151.24	0.29
D. Rainfall decreased (RD) – Soil erosion increased (SI)	**Area (ha)**	**% of total area**
1. Deciduous forest to Field crops	63.51	0.12
2. Evergreen forest to Deciduous forest	56.29	0.11
3. Evergreen forest to Bare land/ fallow	23.85	0.05
4. Deciduous forest to Bare land/fallow	22.57	0.04

Table 6.8 clearly delineates that rainfall erosivity change affecting soil erosion change in terms of direct relationships (i.e., RI-SI and RD-SD correlations) has largely taken place in both virgin (unchanged) evergreen forest (39.4% and 3.94% of total area) and deciduous forest (5.6% and 1.2% of total area), respectively. In addition, areas of conversion from evergreen forest to deciduous forest and deciduous forest to field crops are in the top third and fourth orders of 2.9% and 1.1% of total area, respectively, responding to the

positive direct relation of rainfall erosivity and soil erosion, while areas of conversion from deciduous forest to evergreen forest and field crop lands to deciduous forest of 0.2% and 0.17% of total area are in the top third and fourth orders responding vice versa.

Regarding inverse relations of rainfall erosivity and soil erosion, i.e. rainfall increased and soil erosion decreased (RI-SD correlation), and rainfall decreased and soil erosion increased (RD-SI correlation), they have mostly taken place only in small proportions of total area. This is particularly the case in patches of conversion from deciduous forest to evergreen forest (1.24% of total area) which have mostly reacted with the RI-SD relationship, while patches of conversion from deciduous forest to field crops (0.12% of total area) and evergreen forest to deciduous forest (0.11% of total area) have mainly responded to the RD-SI relationship. Under these circumstances, it can generally be concluded that the reversions of other land uses to forestlands (particularly evergreen forest) over the past 20 years have caused soil erosion to decrease despite an increase in rainfall erosivity (e.g., as illustrated in Table 6.8C). Meanwhile, the conversions from virgin forestlands to other land uses and land covers have caused soil erosion to increase despite a decrease in rainfall erosivity (e.g., as illustrated in Table 6.8D).

6.3.3 Sensitivity analysis of soil erosion risk scenarios

This section involves testing the driving forces (i.e., rainfall and land use changes), to investigate the impact of changes to soil erosion events in the Mae Rim watershed, and also to examine the response of a variety of different future scenarios under expected assumptions to the few key variables associated with rainfall erosivity change and land use change.

The 23 different soil erosion sensitivity scenarios are developed by varying rainfall erosivity and land use (Figure 6.15). In addition to providing the estimated mean annual soil erosion for assessing relative variations compared with the main scenario (i.e., current soil erosion 2009), the calculated erosive magnitudes in each scenario are also classified along different severity levels (based on FAO, 2006). As such, the results obtained from sensitivity analysis are shown in Table 6.9

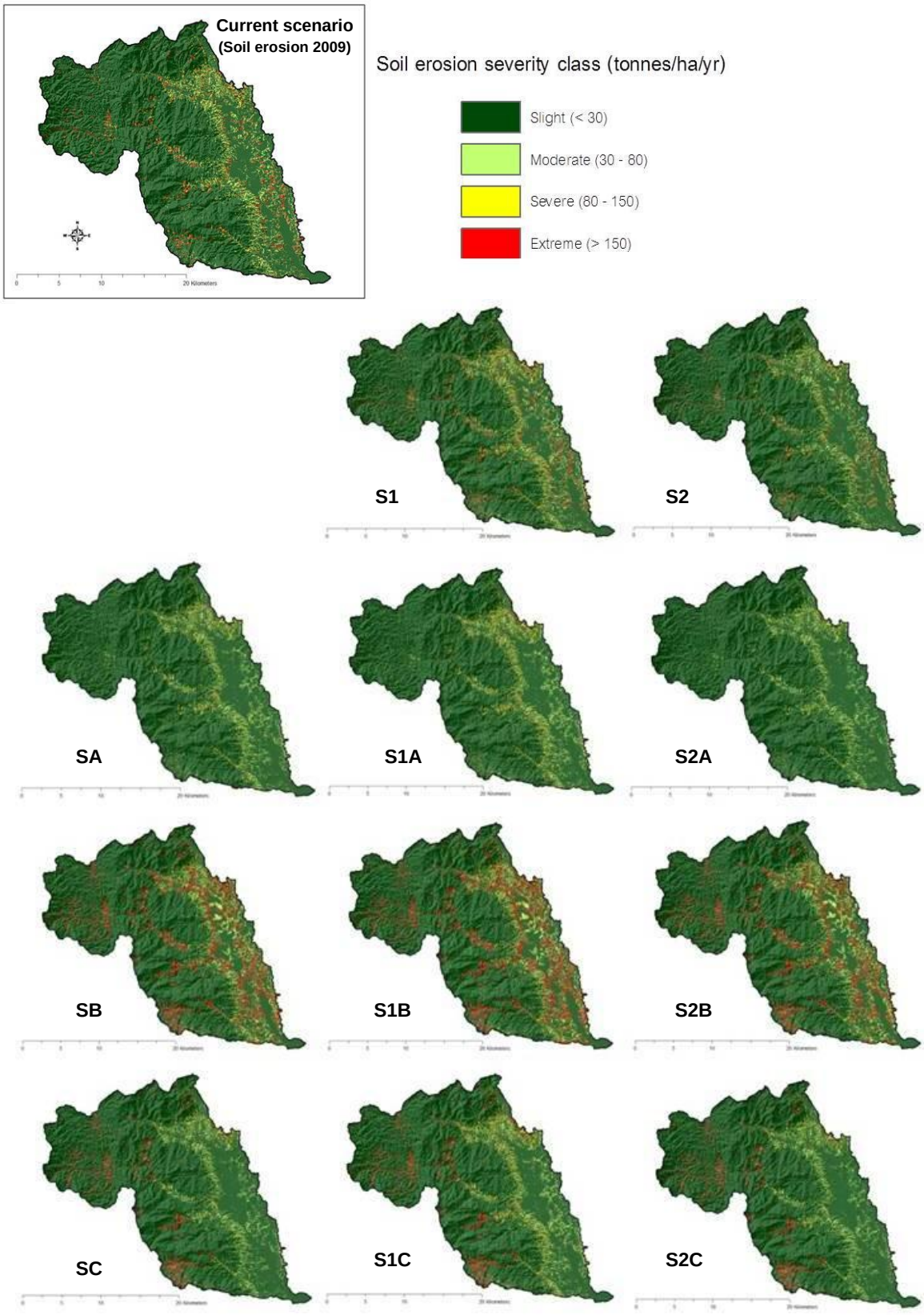

Figure 6.15 Illustration of various soil erosion risk scenarios in sensitivity analysis, by changing R and C, based on assumptions regarding expected future events

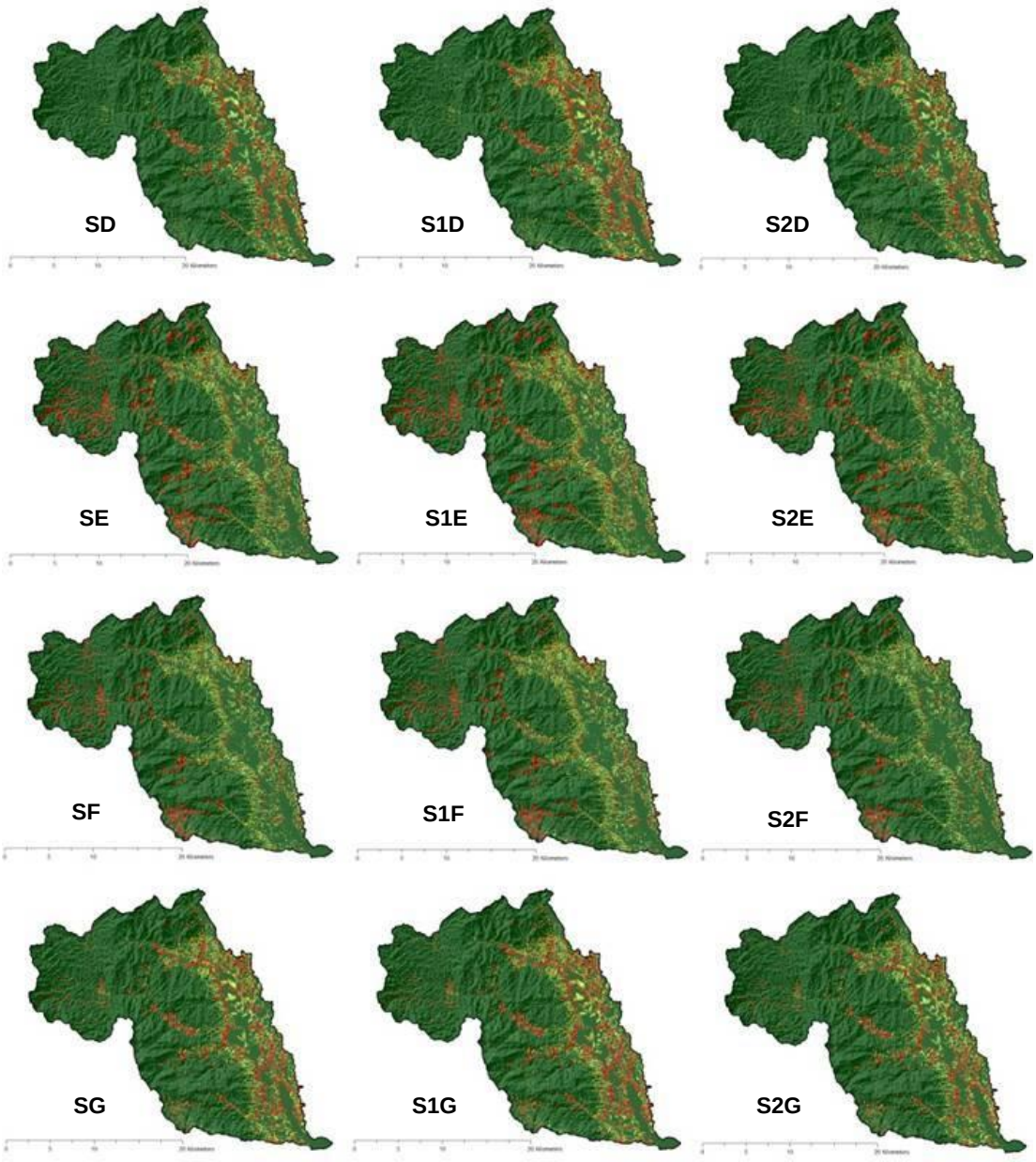

Figure 6.15 (Cont.): Illustration of various soil erosion risk scenarios in sensitivity analysis, by changing R and C, based on assumptions regarding expected future events

Table 6.9 Sensitivities of model sediment prediction relative to changes in inputs for the various future scenarios under assumption of changing rainfall and land use variables

Scenario	% of total area affected by ***SE***				Mean ***SE*** (tonnes ha^{-1} yr^{-1})	Differentiation of mean ***SE*** (tonnes ha^{-1} yr^{-1})	Variation (%)
	Severity class (tonnes/ha/yr)						
	0–30	30–80	80–150	>150			
Soil erosion 2009 (main scenario)	88.17	5.82	2.43	3.58	31.11	0	0
S1	86.98	6.05	2.84	4.13	37.33	6.22	+20
S2	89.56	5.46	1.95	3.03	24.89	–6.22	–20
SA	90.71	6.09	2.10	1.10	13.51	–17.6	–57
SB	83.31	5.09	2.76	8.84	80.63	49.52	+159
SC	88.22	5.92	2.04	3.81	45.97	14.86	+48
SD	86.16	5.24	2.78	5.82	46.88	15.77	+51
SE	84.22	5.47	2.61	7.71	57.08	25.97	+83
SF	86.48	5.67	2.32	5.52	57.04	25.93	+83
SG	85.02	5.23	2.84	6.92	55.42	24.31	+78
S1A	89.41	6.44	2.62	1.53	16.21	–14.9	–48
S1B	82.31	5.17	2.95	9.58	96.75	65.64	+211
S1C	86.94	6.28	2.54	4.24	55.16	24.05	+77
S1D	85.13	5.32	3.00	6.55	56.25	25.14	+81
S1E	83.11	5.65	2.86	8.38	68.5	37.39	+120
S1F	85.30	5.92	2.72	6.06	68.45	37.34	+120
S1G	83.99	5.30	3.04	7.67	66.51	35.40	+114
S2A	92.22	5.53	1.49	0.75	10.81	–20.3	–65
S2B	84.45	5.00	2.54	8.00	64.5	33.39	+107
S2C	89.69	5.37	1.50	3.43	36.77	5.66	+18
S2D	87.34	5.14	2.50	5.03	37.5	6.39	+21
S2E	85.52	5.19	2.37	6.93	45.67	14.56	+47
S2F	87.84	5.30	1.89	4.97	45.63	14.52	+47
S2G	86.18	5.15	2.59	6.08	44.34	13.23	+42

Note: SE*= Soil erosion per year;* ***S****= Scenario;* ***1****= Changing rainfall erosivity (+20%);* ***2****= Changing rainfall erosivity (–20%);* ***A****= All bare lands and field crop lands are reverted to forested land;* ***B****= All bare lands and field crop lands are expanded (3 times of pixel);* ***C****= Upland field crops are only expanded;* ***D****= Lowland field crops are only increased;* ***E****= Bare lands are only expanded, all field crop lands remain the same as 2009;* ***F****= Bare lands and upland field crops are expanded, lowland field crops remain the same as 2009;* ***G****= Bare lands and lowland field crops are expanded, upland field crops remain the same as 2009.*

In Table 6.9, the overview results of 23 scenario sensitivities reflect clearly that the most important variable is not rainfall, but rather that the land use change variable is more significant than changing rainfall. For example, despite the fact that a 20% rainfall erosivity is increased, S1A still has a lower sensitivity in the mean annual soil erosion rate (16.21 tonnes ha^{-1} yr^{-1}) with its variation of –48%, compared to the current soil erosion 2009 (mean annual soil erosion magnitude = 31.11 tonnes ha^{-1} yr^{-1}). This is because, for S1A, all bare lands and field crop lands are assumed to revert to forestland throughout the watershed. Thus, the plant canopies in the forestland can protect soil from erosion caused by raindrop impacts. Moreover, in spite of a 20% decrease in rainfall erosivity, the scenario sensitivities like S2B, S2C, S2D, S2E, S2F and S2G demonstrate that their magnitudes of mean annual soil erosion of 64.5, 36.8, 37.5, 45.7, 45.6 and 44.3 (unit: tonnes ha^{-1} yr^{-1}), respectively, are significantly higher than that of the current soil erosion 2009. Such results indicate that a 20% decrease in rainfall erosivity cannot lower the magnitude of mean annual soil erosion below that of the current soil erosion 2009, if the bare land and field crops are increasingly expanded from their existing patches.

Furthermore, the scenario sensitivities of S1B, SB and S1E are respectively most sensitive to the extremely severe area of soil erosion (erosive magnitude > 150 tonnes ha^{-1} yr^{-1}); whilst the predicted mean soil erosion rates of S1B, SB and S1E are 96.8, 80.6 and 68.5 tonnes ha^{-1} yr^{-1} with their variations of +211%, +159% and +120%, respectively. Results of these scenario sensitivities obviously indicate a need for concern regarding the danger of soil erosion in the

study area, which may take place if bare land and field crop land, as well as rainfall erosivity, increase in the future.

However, the reversion to forest from patches of bare land and field crops, including decreased rainfall erosivity, demonstrate clearly that the area of extremely severe soil erosion is reduced in the study area. As evidenced in scenario S2A, it reveals that there are reductions of soil erosion in the extremely severe areas (0.75% of total area) and a magnitude of mean annual soil erosion (10.8 tonnes ha^{-1} yr^{-1}), with its variation of –65% (compared to that of the current soil erosion 2009). In addition to S2A, the scenarios' sensitivities of SA, S1A and S2 have also estimated the magnitude of mean annual soil erosion below that of the main scenario 2009, i.e. 13.5, 16.2 and 24.9 tonnes ha^{-1} yr^{-1} and their variations of –57%, –48% and –20%, respectively. Interestingly, the results of S1A show that although rainfall erosivity has increased to 20% in the watershed area, the magnitude calculated and percentage variation of the mean annual soil erosion can be lower than that of S2 (only change in rainfall erosivity by –20%). This is because there is an increase in the percentage of forested lands from bare land and field crop lands.

6.4 Discussion

It would appear that the mountainous watersheds in NW Thailand have encountered changes in use throughout history up until the present time, and that these have not only been rapid, but also radical (Suraswadi *et al*., 2005). The findings from this research elucidate clearly that the changing rainfall

erosivity and land use change have had substantial effects on the soil erosion of the Mae Rim watershed in NW Thailand over the past 20 years (from 1989–2009). In particular, land use change displays a greater influence on soil erosion than changing rainfall erosivity in this study area. This is consistent with previous work by Ward *et al.* (2009), whose study confirmed that land use change has much greater effect than rainfall erosivity change within the range of climate variability simulated over the late Holocene in Meuse catchment, NW Europe. Moreover, according to the results of this research, soil erosion in the Mae Rim watershed reveals an increasing change in the mean annual soil erosion rate from 26.96 tonnes ha^{-1} yr^{-1} (in 1989) to 31.11 tonnes ha^{-1} yr^{-1} (in 2009), at a relative variation rate of 15.4%. Between 1989 and 2009, there is a slight increase in average annual rainfall erosivity. Results obtained from GIS map overlaying illustrate that soil erosion is affected by a rainfall erosivity variation of 2% (i.e., mean annual rainfall erosivity in 1989 has increased from 610.85 MJ mm $ha^{-1}h^{-1}$ yr^{-1} to 622.92 MJ mm ha^{-1} h^{-1} yr^{-1} in 2009), while the residue (98% of relative variation) could probably be affected because of human interference, such as logging, clearing and burning land for agriculture and/or even developing rural road networks into the local villages on steep slopes in the highland areas (Ziegler *et al*., 2000; Crozier, 2010).

It should be noted that the rainfall erosivity change is different from rainfall change, especially in units (i.e., MJ mm ha^{-1} yr^{-1} is a unit of rainfall erosivity, whereas mm is a unit of rainfall). Thus, the amounts between them are not equal.

However, the rainfall erosivity increasing from 1989 to 2009, according to thesis result, should be involved with a trend of total annual rainfall at such period. From a statistical data of total annual rainfall measured in Chiang Mai City centre (16 km distance from the Mae Rim watershed), it demonstrates that there is an increase of its trend line of about 28% from 1989 to 2009 (Figure 6.16).

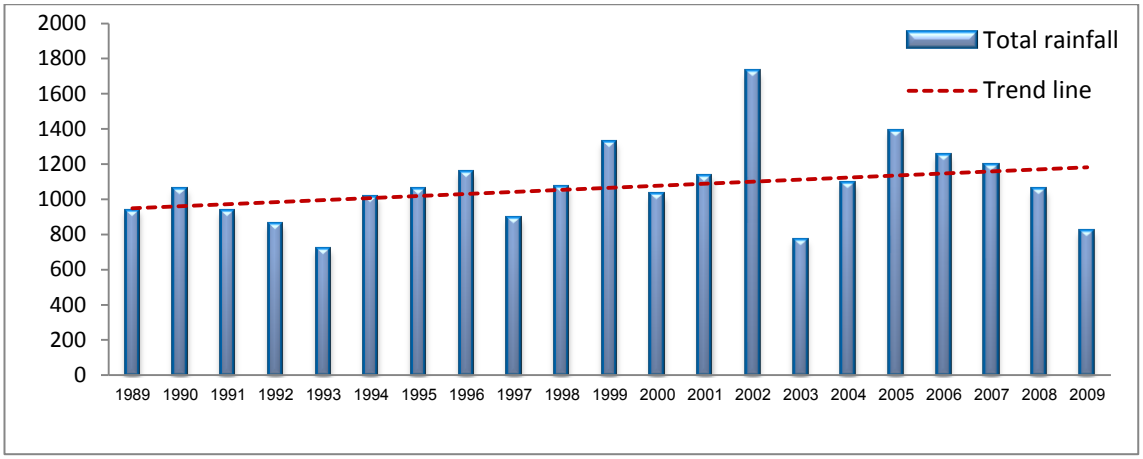

Figure 6.16 Total annual rainfall (mm), from 1989 to 2009, measured at the city centre of Chiang Mai. (Source: The Meteorological Department, Thailand, 2011)

Land use change is not only predominant over the rainfall erosivity change in most tropical climatic zones in terms of forcing soil erosion (Verburg *et al.,* 2006; Hartter *et al.,* 2008), but changing land use in the temperate climatic zone also played a part, as a highly distinctive effect on soil loss, and exceeds changing climate. Notebaert *et al.* (2011) estimated that soil erosion in the Dijle catchment in Belgium has increased since the early Holocene (~4800 BCE) to current (~1990 CE) by only 9% because of climatic changes, and by 6000% due to land use changes. Similar to Ward *et al.* (2009), their results show that

sediment yield in the study area on a very long time scale (between 4000-3000 BP and 20th Century) was increased only 9% by rainfall erosivity change, while there was a 198% increase in sediment yield brought about by changing land use.

6.4.1 Land use change effect on soil erosion

Results from overlaying maps between the spatially-distributed soil erosion risk 2009 (generated by using RUSLE-GIS-based model) and the land use change scenario from 1989 to 2009 (interpreted and classified based on Remote Sensing processes) indicates that the conversion from deciduous forest to field crop areas causes extremely severe soil erosion (erosive magnitude > 150 tonnes ha^{-1} yr^{-1}) in the Mae Rim watershed over the past two decades (between 1989 and 2009). The finding illustrates that the agricultural patch expanding in the forested land can become an area vulnerable to drastic soil erosion. This result is supported by earlier work of Wichitkosum (2012) who studied the effect of land use change between 1990 and 2010 on the Pa Deng sub-district in the west of Thailand. Her result revealed that the area of very high soil erosion risk (erosive magnitude > 125 Mg ha^{-1} yr^{-1}) emerged due to the conversion from forest to agriculture. In addition, Schiettecatte *et al.* (2008) also points out that the area with a very high erosion risk sees soil erosion rise to 12% as a result of conversion from forest into arable land over the period 1985 – 2000 in Cuyaguateje watershed (Cuba).

However, when determining the overall hazard areas of soil erosion by combining extreme and severe soil erosion risk classes, the result clearly shows that the (unchanged) deciduous forest is the area with the highest risk of soil erosion, and could have serious effects on the Mae Rim watershed. The high risk of deteriorated areas in the deciduous forest is supported by Weyerhäuser (2001). The tropical deciduous forest is the forested area most prone to disturbance by humans and is increasingly under threat from illegal logging or encroachment, as well as being sacrificed to urban and industry development. Typically, the tropical deciduous forest in Thailand is normally located at an altitude of between 50 and 1000 m a.s.l. (Thanapakpawin *et al*., 2006; Chaiyo *et al.*, 2011). Because it is situated adjacent to human habitation, especially in lowland areas (below 600 m a.s.l.), it is not possible for it to avoid being threatened or used by humans. Moreover, wildfire and expansion of slash-and-burn agriculture are also significant issues and put deciduous forest even more at risk of soil erosion. Consistently, Teranova *et al*. (2009) insist that the magnitude of soil erosion has been increased by wildfire severity. When a wildfire occurs, much ash is generated as well as the soil structure being damaged. The superficial pore clogging by the thick ash layers, and the reduction of soil porosity, as a consequence of serious fire, can increase runoff and erosion. For deciduous forest in Northwest Thailand, wildfires have been taking place due to the leaf shedding of the trees which is the major component in biomass fuels (Chaiyo *et al.*, 2011). According to Elliot *et al.* (2003), the wildfires can be set off by both natural or anthropogenic causes and frequently

affect deciduous forest every year, especially during the hot-dry season (February–April).

6.4.2 Rainfall erosivity change effect on soil erosion

Outputs obtained from the GIS overlaying method of maps, between rainfall erosion change and soil erosion change from 1989 – 2009, reveal that there are four different relationships taking place in this area (i.e., RI-SI, RD-SD, RI-SD and RD-SI correlations). The RI-SI and RD-SD correlations indicate that when rainfall increased, soil erosion increased and, also, when rainfall decreased, soil erosion decreased. These correlations can generally be called 'direct relationships'. In addition, the RI-SD and RD-SI correlations indicate that when rainfall increased, soil erosion decreased and, also, when rainfall decreased, soil erosion increased. These correlations can be known as 'inverse or indirect relationships'

The direct relationships have been mostly displayed in this area (see Table 6.7). Particularly in the RI-SI correlation, 39.4% of watershed area occurred in the virgin (unchanged) evergreen forest. Despite the fact that the evergreen forest relates to the cause of soil erosion increasing with rising rainfall, it does not mean, however, that increasing soil erosion will be serious for the evergreen forest. According to the result in Figure 6.8(c), it clearly shows that the soil erosion risk is only moderate (0 – 30 tonnes ha^{-1} yr^{-1}) in the evergreen forest. The most important thing that makes the evergreen forest secure from severe soil erosion is due to the fact that dense canopies of evergreen forest trees can

help to reduce the intensity of rainfall. As Chang (1993, p.63) remarks ‘forests intercept a higher fraction of raindrops on the soil surface through the protective layer on the forest floor’.

However, increased rainfall erosivity does not imply that it will always result in increased soil erosion and, in turn, the increased rainfall erosivity can cause the soil erosion decrease as well. All the above-mentioned are inverse relationships between rainfall erosivity and soil erosion that took place in the study area over the past 20 years (see also Table 6.8). The RI-SD correlation has emerged because of reversions to forested land. Mostly, a 1.2% of total area (640 ha) has been converted from deciduous forest to evergreen forest. An achievement of forest restoration by planting native tree species in the degraded deciduous forest is the key to accelerate recovery of evergreen forest (Elliot *et al*., 2003).

For RD-SI correlation, although it has occurred in a small proportion of the watershed area, it is considered important to investigate the coherent impacts of two driving forces (i.e., land use change and rainfall erosivity change) on soil erosion. Results from this study indicate that soil erosion has increased despite rainfall decrease. It is due to the results of transitional conversions of natural (virgin) forest to other land uses. For example, there are the conversions of: (1) deciduous forest to field crop land (0.12% of total area or 64 ha), (2) evergreen forest to deciduous forest (0.11% of total area or 56 ha) and (3) evergreen forest to bare land (0.05% of total area or 24 ha). These changes can probably lead to extremely severe soil erosion or deteriorated areas if there is a lack of

effective soil conservation practices on the areas concerned. However, the RD-SI correlation may occur not only as a result of changes in natural virgin forest. As in the previous work of Zhang and Nearing (2005), they found that the greater variability in daily precipitation distribution can cause soil erosion to increase in spite of the predicted annual precipitation decrease in arable land.

6.4.3 Scenario sensitivity analyses

The overview results reflected in the 23 experimented scenarios, which are controlled by changing rainfall erosivity and land use (i.e., focusing on field crop and bare land) under various expected assumptions, can be summarised in brief as follows:

(1) Increase in rainfall erosivity can significantly increase soil erosion (i.e., S1) and will exacerbate severe soil erosion if the cultivated areas on both lowland and upland areas are also increasingly expanded (i.e., S1B – S1G) when compared to the baseline value (predicted mean annual soil erosion) of current soil erosion 2009 (see also Table 6.9). In scenario sensitivity S1, it shows that a 20% increase in rainfall erosivity can lead to a 20% increase in soil erosion in the Mae Rim watershed for the period between 1989 and 2009. This result is fairly close to that deduced by Kim *et al.* (2009). They use the Climate Generator (CLIGEN) and the Water Erosion Projection Project (WEPP) to analyse the relationship between climate and soil erosion. Their result reveals that an increase in precipitation parameters of 20% can increase soil erosion of 27% in the Jeon-Ju plains in Korea for the period between 1966 and 2005. In addition, Lee *et al.* (1996) study sensitivity of the US Corn Belt by using the

Erosion Productivity Impact Calculator (EPIC) and they also calculate that a 20% increase in precipitation can cause soil erosion to increase by 37%.

Based on expected assumptions (see also Table 6.4), however, when testing the model by increasing three-fold field crop land and bare land from their current existing patches, including increasing rainfall erosivity of 20%, the results of scenario sensitivities (i.e., S1B – S1G) show very high variations from the baseline ranging between +77% and +211. These high values of percentage variations in the predicted mean annual soil erosion rates clearly reinforce and prove the previous results that land use change has a greater impact on soil erosion than rainfall erosivity change. Similar to Ward *et al.* (2009), they use WATEM/SEDEM to simulate sediment yield and also test two sensitivity analyses including rainfall erosivity change and the conversion of forest to arable land. The result indicates that the sediment yield has changed to +207% due to effects of climate and land use changes between 4000 – 3000 BP and 1000 – 2000 AD.

(2) A decrease in rainfall erosivity cannot reduce soil erosion below the baseline value of the current soil scenario 2009 if the expansion of the field crop lands and bare lands continuously increase on both lowland and upland areas (i.e., S2B – S2G). Also, reversal of forestlands from all upland and lowland field crop areas and bare lands can considerably reduce soil erosion below the baseline of the current soil scenario 2009 (i.e., SA, S1A and S2A). This is in agreement with the conclusion from Nearing *et al.* (2005) that soil erosion should increase

or decrease, depending upon how much protection there is of the soil surface, and if the forested lands are clear-cut for purposes of expanding cultivated land, an increase in rainfall erosivity will exacerbate the soil erosion problem.

(3) The lowland field crop area (< 600 m a.s.l.) is a little bit more vulnerable to soil erosion than the upland field crop area (> 600 m a.s.l.). Results from comparing sensitivity scenarios indicate that expansions of the field crop farming in lowlands result in changes in absolute values of predicted mean annual soil erosion more than in the uplands, i.e., SD (47 tonnes ha^{-1} yr^{-1}) > SC (46 tonnes ha^{-1} yr^{-1}), S1D (56 tonnes ha^{-1} yr^{-1}) > S1C (55 tonnes ha^{-1} yr^{-1}) and S2D (38 tonnes ha^{-1} yr^{-1}) > S2C (37 tonnes ha^{-1} yr^{-1}). These results are consistent with Forsyth and Walker (2008) that most cultivation still occurs on the flatter lowland slopes in northern Thailand and poses the biggest threat to the soil erosion problem due to repeated cultivation. Tingting *et al.* (2008) applied the IMAGE\LDM to assess the soil erosion risk in northern Thailand, their result identifies that the soil erosion risk is the highest in the transitional zone of forest and agriculture at altitudes ranging from 100 – 400 m a.s.l. (lowlands), as a result of the uplands being covered by forest more than in the lowlands, soil erosion risk in a high altitude area is lower than in a low altitude area.

6.5 Conclusion

This research has delineated the effects of changing land use and rainfall erosivity on soil erosion over the past two decades (between 1989 and 2009), and also tested sensitivity analysis on the effect of controlling variables in each soil erosion risk scenario under various assumed conditions.

The land use change map can be generated based on remote sensing processes. The two different periods of Landsat imageries captured in 1989 and 2009 has been interpreted and classified by using Maximum Likelihood method, and the overall accuracies of land use classifications are 89% and 87%, respectively.

The rainfall erosivity change map from 1989 to 2009 can be generated by overlaying and subtracting values pixel-by-pixel in the raster data. The output displays the values ranging between –59.66 and 55.38 MJ mm/ha h yr. The mean and standard deviation values are 11.99 and 10.99 MJ mm/ha h yr, respectively.

The soil erosion map for 1989 can be generated by using the RUSLE-GIS-based model. To produce the soil erosion change scenario during 1989–2009, the different periods of soil erosion maps have been overlaid, and pixel values subtracted. As a result, the minimum and maximum values show the differentiated annual soil loss, varying between –17,766 and 43,351 tonnes ha^{-1}

yr^{-1}, including mean and standard deviation values as 4.19 and 256.97 tonnes ha^{-1} yr^{-1}, respectively.

According to the results of this study, soil erosion in the Mae Rim watershed has increased in mean annual soil erosion rate from 26.96 tonnes ha^{-1} yr^{-1} (in 1989) to 31.11 tonnes ha^{-1} yr^{-1} (in 2009), with a relative variation of 15.4%.

From the effect of land use change on soil erosion over the past 20 years, it can be concluded that most areas of conversion from deciduous forest to field crops (364 ha) are those more vulnerable to extremely severe soil erosion (erosive magnitude >150 tonnes ha^{-1} yr^{-1}), while the overall hazard areas of soil erosion by combining extreme and severe soil erosion risk classes have responded to the (unchanged) deciduous forest.

The effect of rainfall erosivity change on soil erosion, among transition dynamics of rainfall, land use and soil surface between 1989 and 2009, indicates that rainfall erosivity change affecting soil erosion mostly occurs in the virgin evergreen forest. In other words, it means that soil erosion increased when rainfall increased in most areas of evergreen forest, but not seriously. Whereas the deciduous forest converted to field crop land seems to be very serious for soil erosion, the result indicates that it has an inverse relationship in such transitional zone; resulting to increase in soil erosion despite a decrease in rainfall erosivity.

The sensitivity analysis method is used to test the key controlling variables of RUSLE modelling, such as rainfall erosivity (R) and vegetation covers (C), under various assumptions that are expected to occur in the future. The outputs from analyses clearly show a higher sensitivity in changing land use than changing rainfall erosivity. The S1B, SB and S1E are the most sensitive to the extremely severe area of soil erosion (erosive magnitude >150 tonnes ha^{-1} yr^{-1}), and the predicted mean soil erosion rates are 96.8, 80.6 and 68.5 tonnes ha^{-1} yr^{-1} with the relative variations of +211%, +159% and +120%, respectively. As a result, these scenario sensitivities obviously reflect the fact that the soil erosion hazard in this study area may take place if bare land and field crop land, as well as rainfall erosivity, are increased in the future.

6.6 Chapter summary

This chapter has shown that soil erosion in the Mae Rim watershed is most dependent upon land use change, rather than rainfall erosivity change. Moreover, the conversion from deciduous forest to field crop land can lead to increase soil erosion at an extremely high level. The 23 soil erosion sensitivity scenarios have been simulated under various assumptions that are expected to occur in the future, and found that the soil erosion hazard in this study area may take place if bare land, field crop land and rainfall erosivity are increased simultaneously in the future. In the final chapter (Chapter 7), the thesis's key findings and recommendations from the work are discussed.

CHAPTER 7: CONCLUSIONS

7.1 Introduction

Soil erosion is one type of land degradation that is a serious threat to sustainability of cultivation in Thailand. About 17.4 million ha or 34% of the cultivated area is classified as vulnerable to soil erosion, especially in the more rugged terrain of northwest Thailand (GMS Environment Operations Centre, 2007). Moreover, much of the eroded soil originates and are transported from upland areas, and are deposited on the lower hill slopes, lowlands, or in lakes and reservoirs. This leads to critical environmental problems, such as sediment deposition in the riverbeds and subsequent increased flooding potential, reduced reservoir storage capacity and degradation of aquatic ecosystems from increased water turbidity, and mobilisation of contaminants. Currently, climate and land use change impacts have also been linked to an increase in soil erosion by water (Asselman *et al*., 2003; Li *et al*., 2009; Ward *et al.,* 2009; Maeda *et al.,* 2010). In the most tropical mountainous watershed of Thailand, there is very high rainfall erosivity taking place, especially in the rainy season. In addition, there is increasing encroachment of agricultural activities on steeply sloping land, without effective land management practice. These are the major causes that contribute to soil erosion and land degradation problems.

Mae Rim watershed (515 km^2) is a tropical mountainous watershed in northwest Thailand, which was chosen as a case study area for this thesis. This watershed is not only an important water supplier, but can also be a sediment

supplier, which needs to be assessed to guide management practice. However, the factors that cause soil erosion in the Mae Rim watershed are poorly understood. Prior to this research, it was not clear whether the sediment transport capacity or the spatially distributed sediment delivery ratio concept is best when used in conjunction with RUSLE and applied in the context of the tropical mountainous watersheds in Northwest Thailand. Knowledge and understanding of processes involved with the rainfall and land use change impacts on soil erosion dynamics are still limited in this watershed. Thus, this thesis has set out the original research objectives as follows:

I. Identify the spatial variation of soil erosion risk and the key controls which interact to generate the extremely high soil erosion rates in the study area. This work could help as an evaluation tool to plan for future appropriate land use planning

II. Compare and verify the sediment yield predictions, derived from RUSLE-GIS-based modelling in conjunction with two different approaches of Sediment Transport Capacity (STC) and Spatial Interpolation of Sediment Delivery Ratio (SISDR).

III. Assess the sensitivity of soil erosion to scenarios of land use and climate change on soil erosion in the study area.

This concluding chapter summarises the major findings of the thesis undertaken and links these to the original research objectives above and assesses how the objectives were achieved. Sections 7.2.1–7.2.3, respectively, explain key findings in Chapters 4–6 and which are linked to objectives I–III. The significant contributions to watershed soil erosion studies are also evaluated; the recommendations and future research needs are advanced.

7.2 Key findings

The key findings from this thesis can be concluded based on three result chapters as follows:

7.2.1 Spatial variation on soil erosion risk by using RUSLE-GIS-based model

(1) Rainfall erosivity factor (R factor) evaluated by taking latitude and longitude including altitude into account, provides a higher correlation coefficient (r = 0.787) than using a single altitude (r = 0.771), both altitude and latitude (r = 0.772) and both altitude and longitude (r = 0.780). This result clearly indicates that the rainfall erosivity in the Mae Rim watershed is not only influenced by altitude, but also depends on the geographical coordinates of the location (i.e., latitude and longitude). This is an alternative method for calculating the R factor that is recommended from this thesis for generating the improved spatially distributed rainfall erosivity map.

(2) The computed soil erosion in the Mae Rim watershed is found to be between 0 and 48,089 tonnes ha^{-1} yr^{-1}; the mean erosion rate is estimated

about 31 tonnes ha^{-1} yr^{-1}. This implies that the predicted mean erosion rate of the Mae Rim watershed is in the range of the actual mean erosion rates (from field measurements) in South East Asia, which normally lies between 0 and 40 tonnes ha^{-1} yr^{-1} (cited from Dubber and Hedbom, 2008, p.41). For the predicted maximum value of 48,049 tonnes ha^{-1} yr^{-1} of this watershed, which falls in only one pixel, covering about 625 m^2 (0.0625 ha); probably resulting from an extreme value in the LS factor, which is a result of the challenges in DEM extrapolation.

(3) The spatial distribution of soil erosion risk in the Mae Rim watershed, especially in extreme severe soil erosion source (erosive magnitude >150 tonnes ha^{-1} yr^{-1}) seems to be associated with bare land (44%), field crop land (27%) and high steep slope (16%), respectively.

(4) The higher value of rainfall erosivity (R >750 MJ mm/ha h yr) does not associate with extreme severe soil erosion in this watershed. This is due to the fact that heavy rain usually occurred over the dense forest, where generally grew up on upland slope and mountainous areas over 1,000 m a.s.l. The canopy of the evergreen forest trees can help to reduce the energy of rainfall intensity when it dropped to the ground.

(5) A strong relationship between land use/land cover factor (CP factor) and slope length-steepness factor (LS factor) are proven by Pearson's correlation coefficient test (significance level 0.01). According to Hopkin's scale of magnitude (cited from Kotrlik and Williams, 2003, p.5), which indicates that the CP factor and LS factor have 'moderate correlations' (i.e., r = 0.3 and r = 0.26, respectively) with soil erosion generation, whereas the erosivity (R-factor)

and erodibility (K-factor) seem to be insubstantial correlations with soil erosion generation in the Mae Rim watershed. These imply that if there are any changes taking place in land use/cover, slope length or slope gradient, they could possibly affect soil erosion changes in the Mae Rim watershed more than the changes in rainfall erosivity and soil types.

7.2.2 Sediment yield assessment using sediment rating curve and RUSLE-GIS-based model

(1) Regarding the annual suspended sediment yield estimation, this study employs the sediment rating curve method to derive the power equation, basing on equation [5.3], for estimating the suspended sediment load of eight watersheds in Upper Ping River Basin. As a result, the best-fit regression relationships provide the coefficient of determination (r^2) of SSC_{RC}–Q at all eight watersheds range between 0.23 and 0.58; *p*-value < 0.001. In addition, results obtained from the the SSC_{RC}–Q relationship analysis show an estimated annual sediment load of the Middle Mae Ping watershed in the top rank; it creates total suspended sediment loads of 5,279,900 tonnes/ yr in 2009. Whereas the Upper Mae Ping and Upper Mae Wang watersheds followed in second and third positions with amounts of 3,738,400 and 1,951,000 tonnes/ yr, respectively. The amount of annual suspended sediment load in the Mae Rim watershed was the smallest, at only 375,400 tonnes/ yr.

(2) To investigate among the eight sub-watersheds of the Upper Ping River Basin, the Upper Mae Wang watershed is the only site of Northwest Thailand that produces a mean annual suspended sediment yield (SSY) over

5,000 tonnes km^{-2} yr^{-1} (in 2009). In addition, its mean annual SSY is around 42 times and 21 times greater than the global (120 tonnes km^{-2} yr^{-1}) and Asian mean annual SSY values (242 tonnes km^{-2} yr^{-1}), respectively. In comparison to the other watersheds recorded across the world, the given SSY value of the Upper Mae Wang watershed is still 11 times smaller than the world's highest rate of mean annual SSY at China's Huangfushuan watershed, which recorded, in 1980, a mean annual SSY exceeding 50,000 tonnes km^{-2} yr^{-1}.

(3) The relationships between the mean annual SSY and drainage basins in the eight sub-watersheds of the Upper Ping River Basin illustrate the strong inverse correlation (r = –0.794; p-value = 0.019), based on the rating curve plotted in this study. This implies that these watershed areas of the Upper Ping River Basin are dominated by local conditions (e.g., topography, lithology and vegetation cover), rather than gully erosion, riverbank erosion and mass movement.

(4) The predicted mean annual SSY value of the Mae Rim watershed (an experimental case study), for the water year 2009, derived from the coupled RUSLE-STC, is 646 tonnes km^{-2} yr^{-1}, whereas the coupled RUSLE-SISDR predicts the mean annual SSY value as 742 tonnes km^{-2} yr^{-1}. These predicted values are underestimate and slightly overestimate (i.e., −11% and 2%, respectively) when assessing the percentage difference from the actual measured value (729 tonnes km^{-2} yr^{-1}).

(5) In comparison of model efficiency between the coupled RUSLE-STC (sediment transport capacity) and RUSLE-SISDR (spatial interpolation of sediment delivery ratio), it can be concluded that the RUSLE-SISDR can predict

mean annual rate of SSY more accurately than the RUSLE-STC. This is because both the Nash and Sutcliffe's model efficiency (NSME) and the Relative Root Mean Square Error (RRMSE) provide better values of model efficiency and performance than the RUSLE-STC, i.e., $NSME_{RUSLE\text{-}SISDR}$ = 0.99 is closer to '1' than $NSME_{RUSLE\text{-}STC}$ = 0.92, and $RRMSE_{RUSLE\text{-}SISDR}$ = 0.02 is closer to '0' than $RRMSE_{RUSLE\text{-}STC}$ = 0.11.

7.2.3 Land use and rainfall erosivity change impacts on soil erosion

(1) From 1989 to 2009, soil erosion in the Mae Rim watershed has increased in mean annual soil erosion rate, from 26.96 tonnes/ha/yr (in 1989) to 31.11 tonnes ha^{-1} yr^{-1} (in 2009), with a relative variation of 15.4%. Within such a period of change, the increased soil erosion was affected by a rainfall erosivity variation of 2%, while the residue (98% of relative variation) could probably be affected because of human interference such as logging, clearing and burning land for agriculture, and/or even developing rural road networks into the local villages on the steep slope in the distant highland areas.

(2) Results from overlaying maps between the current soil erosion risk (in 2009) and the land use change map (during 1989–2009), indicates that the conversion from deciduous forest to field crop areas is the major cause of extremely severe soil erosion (erosive magnitude >150 tonnes ha^{-1} yr^{-1}) in the Mae Rim watershed over the past two decades. However, when determining the overall hazardous areas of soil erosion by combining extreme and severe soil erosion risk classes, the result clearly shows that the (unchanged) deciduous forest is the key area vulnerable to soil erosion. Therefore, illegal

logging, wildfire and expansion of slash-and-burn agriculture in this watershed are significant issues, and put deciduous forest even more at risk of soil erosion.

(3) Among transition dynamics of rainfall, land use and soil surface between 1989 and 2009, indicates that rainfall erosivity change affecting soil erosion mostly occurs in the virgin evergreen forest. In other words, it means that soil erosion increased when rainfall increased in most areas of evergreen forest, but not seriously. Whilst the conversion from deciduous forest to field crop land seems to be very serious for soil erosion, the result indicates that this transitional area relates to the inverse relationship; resulting in soil erosion increase despite reduced rainfall.

(4) The sensitivity analysis method is applied to test the key controlling variables of RUSLE modelling, i.e., rainfall erosivity (R) and vegetation covers (C), under various assumptions that are expected to occur in the future. The outputs from analyses clearly show a higher sensitivity in changing land use than changing rainfall erosivity. In addition, these scenario sensitivities obviously reflect the fact that the soil erosion hazard in this study area may take place if bare land and field crop land, as well as rainfall erosivity, are increased simultaneously in the future.

7.3 Significant contributions to watershed soil erosion studies

The improved methods and key findings in this thesis can contribute to knowledge, and understanding the current studies of watershed soil erosion as following conclusions:

7.3.1 Soil erosion modelling

This thesis demonstrates that there are improvements on applying the RUSLE-GIS based model for better estimating soil erosion and sediment yield in the Mae Rim watershed.

Particularly in generation of rainfall erosivity factor (R factor), it was introduced to improve a technique for better evaluation by assigning the estimated R factor into each grid cell or pixel based on digital elevation model (DEM), instead of the conventional method that generates the rainfall surface by spatial interpolation from the measured points (weather stations). A new proposed method of this thesis is to take into consideration the altitude, latitude and longitude in order to assess the value of rainfall erosivity for the Mae Rim watershed. The result obtained from multiple regression analysis obviously illustrates that the rainfall erosivity considered by incorporating altitude, latitude and longitude have a strong correlation than other tests. This is a new or an alternative method suggested for producing the rainfall erosivity values that is more detailed and realistic (i.e., rainfall pattern is affected by local topography and geographical locations) than by smooth surface interpolation.

In terms of estimating suspended sediment yield, this thesis has employed two different concepts, i.e., the sediment transport capacity (STC) and the sediment delivery ratio (SDR), by combining with the RUSLE model. Particularly regarding the improved SDR concept, this research introduces an innovative technique regarding spatial interpolation of sediment delivery ratio (SISDR), based on the concept of William and Berndt (1972) that the slope gradient of the main river is more significant than other parameters to sediment production, and also provides the spatially extrapolated SDR values to every cell within the watershed.

Furthermore, results from comparative studies of model efficiency between the coupled RUSLE-STC and RUSLE-SISDR can conclude that the RUSLE-SISDR should be suggested for estimating suspended sediment yield because of providing a reasonable validation of the model, while another one is unsuccessful in prediction of suspended sediment yield in the Mae Rim watershed. Consequently, the innovative RUSLE-SISDR modelling could be utilised by other researchers who are interested in sediment yield prediction. The strength of this model not only provides a better SSY prediction result, as well as being easy to conduct between the data input and the model, but also depicts the spatial distribution of the SDR. However, the limitation of the RUSLE-SISDR is that it is unable to predict the sediment deposition. Depending on the purpose, if the researchers need to pay more attention to the processes of soil erosion, the RUSLE-STC should be recommended.

7.3.2 Soil erosion under land use and rainfall changes in the tropical mountainous watershed

With high-magnitude storms, especially in the rainy season and rapid changes of land use take place over the past two decades in the tropical mountainous watershed have caused concern about soil erosion and land degradation. Moreover, research on soil erosion impacted by the rainfall and land use changes in this zone (e.g., northwest Thailand) are rare. Therefore, the results from this thesis can contribute to insight into the processes involved with the rainfall and land use changes in the tropical mountainous watershed.

The research results have clearly indicated that soil erosion in the Mae Rim is subject to land use change, rather than rainfall change. Despite high rainfall erosivity in this watershed, most heavy rainfall usually occurs on upland areas that have been covered by dense forest trees and vegetations, resulting in mild soil erosion.

In addition, the results from comparing scenarios between rainfall erosivity change and soil erosion change based on land use change, during the past 20 years in the Mae Rim watershed, revealed that there are four spatial correlations:

(1) Rainfall increased – Soil erosion increased correlation (RI-SI)

(2) Rainfall decreased – Soil erosion decreased correlation (RD-SD)

(3) Rainfall increased – Soil erosion decreased correlation (RI-SD)

(4) Rainfall decreased – Soil erosion increased correlation (RD-SI)

The spatial correlations of RI-SI and RD-SD are considered under the normal conditions. Both relationships appear on the most unchanged land uses. Particularly from the research, it indicates that soil erosion increased by rainfall increases (RI-SI correlation) are not a serious problem. This is because such correlation appears on the most undisturbed (unchanged) tropical evergreen forest, which is a slight degree of soil erosion (0 – 30 tonnes ha^{-1} yr^{-1}).

Most interesting issues of this study are both latter correlations (i.e., RI-SD and RD-SI), since these spatial correlations are considered under specific conditions from the land use changes in the Mae Rim watershed. As the result of this thesis, it has been clearly shown that the conversion from deciduous forest to field crop land can lead to increase soil erosion at an extremely severe level (erosive magnitude >150 tonnes ha^{-1} yr^{-1}), despite rainfall erosivity decrease.

On the other hand, due to the fact that deciduous forest and bare land have reconverted to evergreen forest, soil erosion has decreased despite rainfall erosivity increase. These findings can be lead to a significant insight into the spatial interaction processes between rainfall erosivity, land use and soil erosion changes on the tropical mountainous watershed, and also being useful for planners or decision makers in management of land use and soil conservation practices.

7.4 Recommendations and future research needs

Results of the research clearly show that an anthropogenic factor is more important than a physiographic factor. However, the anthropogenic factor is controllable and manageable through mechanism of government policy, and is a means of strengthening knowledge of soil conservation to farmers based on a technical basis. In particular, the upland minority farmers or hill tribes are still lacking proper knowledge on soil management. Although the government has recently encouraged upland farmers to cultivate cash crops (e.g., cabbage soybean, maize) instead of opium production, soil erosion and land degradation problems still exist. Consequently, agricultural zoning is important, as well as an earnest contribution in natural resource conservation measures by the government. These factors will be able to alleviate severity of soil erosion that might occur in the future. In addition, replacing bare fallow lands by planting trees is something that should be achieved, so that trees and canopies can help to protect the soil against the raindrop impact.

With respect to applying a new approach of integrated RUSLE-SISDR modelling to estimate the suspended sediment yield, uncertainty is still present in the case of an application to the different site conditions, even though this thesis illustrated a good prediction result for the experimented area. Therefore, this research presents a further challenge, as well as to experiment and improve the performance of the new approach of modelling for assessing suspended sediment yields in several worldwide catchments or watersheds.

Finally, the higher multispectral sensor of satellite images, e.g., IKONOS with a spatial resolution of 4 m. and QuickBird with a spatial resolution of 2.44 m. (Vrieling, 2006), could be additionally used to study soil erosion, especially when detecting and monitoring gullies. The high-resolution satellite image is a useful tool for obtaining data on the ground, especially in area where direct field survey is difficult (e.g., areas of dense forest and steep slope). It can also provide a better result in terms of soil erosion assessment, than using Landsat Thematic Mapper (TM) / Enhanced Thematic Mapper Plus (ETM+) imageries with a spatial resolution of 30 m. The spectral reflectance from surface water in visible red (wavelength λ = 0.63–0.69 μm) and near infrared (wavelength λ = 0.75–0.90 μm) range of Landsat satellite imagery has a good relationship with suspended sediment concentration (Lodhi *et al.,* 1998; Nas *et al*., 2010). This method can help to quantify the suspended sediment concentrations and fluxes in rivers or other water bodies from space, in cases where a lack of direct measurement exists, especially during large floods (Kilham *et al*., 2012). As such, it is therefore an alternative way that should be recommended for validating soil erosion modelling.

APPENDICES

Appendix I: A worked example of slope calculation

Appendix II: Land use change analysis

Appendix III: Some pictures from fieldwork data collection

Appendix I:

A worked example of slope calculation

The following Figure I-1 is an example of a moving 3x3 window as neighboring operation or D8 method or Horn's method. The actual values of elevation of Mae Rim watershed that ranges between 320 -1780 metres was assigned into each pixel. Then, the slope value of the centre cell of the moving window will be calculated.

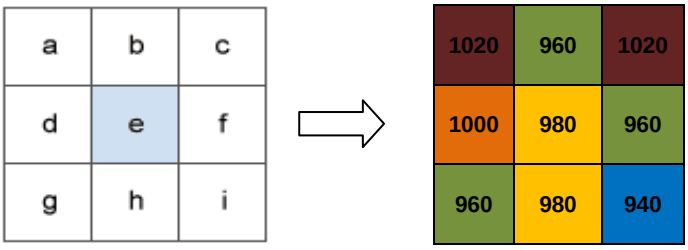

Figure I-1 The example of moving 3x3 window

The cell size is 25 units. The default slope measure of degrees will be used.
The rate of change in the x direction for the centred cell 'e' i

The cell size is 25 units. The default slope measure of degrees will be used.

The rate of change in the x direction for the centred cell 'e' is:

[dz/dx] = ((c + 2f + i) - (a + 2d + g)) / (8 * x_cell_size)

= ((1020 + 1920 + 940) - (1020 + 2000 + 960)) / (8 * 25)

= (3880 - 3980) / 200

= -0.5

The rate of change in the y direction for cell '*e*' is:

[dz/dy] = ((g + 2h + i) - (a + 2b + c)) / (8 * y_cell_size)

= ((960 + 1960 + 940) - (1020 + 1920 + 1020)) / (8 * 25)

= (3860 - 3960) / 200

= -0.5

Taking the rate of change in the x and y direction, the slope for the center cell '*e*' is calculated using:

rise_run = $\sqrt{}$ ($[dz/dx]^2 + [dz/dy]^2$)

= $\sqrt{}$ ($(-0.5)^2 + (-0.5)^2$]

= $\sqrt{}$ [0.25 + 0.25]

= 0.707

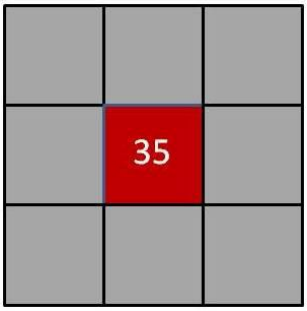

Figure I-2 The result of calculated slope

slope_degrees = ARCTAN (rise_run)

= ARCTAN (0.707)

= 35.26

Thus, the integer slope value for cell '*e*' is '35 degrees' (Figure I-2). **Ans**

Appendix II:

Land use change analysis

VALUE	COUNT	LULC1989	LULC2009	Area (ha)	Des_1989	Des_2009
80	7	1	1	1	Water body	Urban area
67	424	2	1	38	Urban area	Urban area
69	205	3	1	18	Field crops	Urban area
42	604	4	1	54	Deciduous forest	Urban area
63	184	5	1	17	Mixed orchards	Urban area
57	200	6	1	18	Villages	Urban area
52	513	7	1	46	Paddy fields	Urban area
37	87	8	1	8	Bare land	Urban area
22	98	9	1	9	Evergreen forest	Urban area
82	2	1	2	0	Water body	Evergreen forest
7	102	2	2	9	Urban area	Evergreen forest
14	906	3	2	81	Field crops	Evergreen forest
3	14892	4	2	1338	Deciduous forest	Evergreen forest
9	194	5	2	17	Mixed orchards	Evergreen forest
17	128	6	2	12	Villages	Evergreen forest
78	2	7	2	0	Paddy fields	Evergreen forest
6	4811	8	2	432	Bare land	Evergreen forest
1	357185	9	2	32093	Evergreen forest	Evergreen forest
46	50	1	3	4	Water body	Deciduous forest
56	972	2	3	87	Urban area	Deciduous forest
30	12090	3	3	1086	Field crops	Deciduous forest
8	72300	4	3	6496	Deciduous forest	Deciduous forest
23	1295	5	3	116	Mixed orchards	Deciduous forest
39	1536	6	3	138	Villages	Deciduous forest
49	571	7	3	51	Paddy fields	Deciduous forest
20	2869	8	3	258	Bare land	Deciduous forest
12	26041	9	3	2340	Evergreen forest	Deciduous forest
74	7	1	4	1	Water body	Field crops
31	1135	2	4	102	Urban area	Field crops
40	5966	3	4	536	Field crops	Field crops
26	14387	4	4	1293	Deciduous forest	Field crops
27	903	5	4	81	Mixed orchards	Field crops
28	1091	6	4	98	Villages	Field crops
59	1517	7	4	136	Paddy fields	Field crops
5	2700	8	4	243	Bare land	Field crops
10	2344	9	4	211	Evergreen forest	Field crops
44	191	1	5	17	Water body	Water body
72	45	2	5	4	Urban area	Water body
68	53	3	5	5	Field crops	Water body
41	407	4	5	37	Deciduous forest	Water body
76	18	5	5	2	Mixed orchards	Water body
77	11	6	5	1	Villages	Water body
81	38	7	5	3	Paddy fields	Water body
71	81	8	5	7	Bare land	Water body
34	268	9	5	24	Evergreen forest	Water body
73	4	1	6	0	Water body	Mixed orchards
33	1029	2	6	92	Urban area	Mixed orchards
66	496	3	6	45	Field crops	Mixed orchards
16	1965	4	6	177	Deciduous forest	Mixed orchards
62	476	5	6	43	Mixed orchards	Mixed orchards
32	852	6	6	77	Villages	Mixed orchards

64	884	7	6	79	Paddy fields	Mixed orchards
21	333	8	6	30	Bare land	Mixed orchards
19	331	9	6	30	Evergreen forest	Mixed orchards
58	1	1	7	0	Water body	Bare land
51	94	2	7	8	Urban area	Bare land
50	656	3	7	59	Field crops	Bare land
24	2633	4	7	237	Deciduous forest	Bare land
25	104	5	7	9	Mixed orchards	Bare land
55	120	6	7	11	Villages	Bare land
61	159	7	7	14	Paddy fields	Bare land
15	2719	8	7	244	Bare land	Bare land
2	4431	9	7	398	Evergreen forest	Bare land
79	26	1	8	2	Water body	Paddy fields
65	805	2	8	72	Urban area	Paddy fields
70	456	3	8	41	Field crops	Paddy fields
45	2158	4	8	194	Deciduous forest	Paddy fields
47	727	5	8	65	Mixed orchards	Paddy fields
54	815	6	8	73	Villages	Paddy fields
53	6446	7	8	579	Paddy fields	Paddy fields
36	952	8	8	86	Bare land	Paddy fields
35	140	9	8	13	Evergreen forest	Paddy fields
75	5	1	9	0	Water body	Villages
38	1711	2	9	154	Urban area	Villages
43	762	3	9	68	Field crops	Villages
18	4742	4	9	426	Deciduous forest	Villages
29	639	5	9	57	Mixed orchards	Villages
48	2596	6	9	233	Villages	Villages
60	730	7	9	66	Paddy fields	Villages
13	665	8	9	60	Bare land	Villages
11	2090	9	9	188	Evergreen forest	Villages
	573182			51500		

Table III-1 Cross tabulation of land use and land cover classes between 1989 and 2009 (area in ha)

	2009									
1989	Bare land	Deciduous forest	Evergreen forest	Field crops	Mixed orchards	Paddy fields	Urban area	Local villages	Water body	Total (ha)
Bare land	244	258	432	243	30	86	8	60	7	1367
Deciduous forest	237	6496	1338	1293	177	194	54	426	37	10251
Evergreen forest	398	2340	32093	211	30	13	9	188	24	35304
Field crop areas	59	1086	81	536	45	41	18	68	5	1940
Mixed orchards	9	116	17	81	43	65	17	57	2	408
Paddy fields	14	51	0	136	79	579	46	66	3	976
Urban area	8	87	9	102	92	72	38	154	4	568
Local villages	11	138	12	98	77	73	18	233	1	660
Water body	0	4	0	1	0	2	1	0	17	26
Total (ha)	981	10577	33983	2700	572	1125	209	1252	100	51500

Appendix III:

Some pictures from fieldwork data collection

Figure IV-1: The Royal Irrigation Department (RID)'s sediment laboratory, Chiang Mai, Thailand (visit on 21 August 2010).

Figure IV-2: Gully erosion survey in the Mae Rim watershed (26 July 2010)

Figure IV-3: Suspended sediment collection demostrated by RID's staffs at station P21 (Mae Rim River, Mae Rim watershed, NW Thailand)

Figure IV-4: Suspended sediment collection demostrated by RID's staffs at station P84

(Mae Wang River, Mae Wang watershed, NW Thailand)

REFERENCES

Abaci, O. and Papanicolaou, A.N. (2008) Evaluating the performance of water erosion prediction project (WEPP) model for large watershed. *World Environmental and Water Resources Congress 2008 Ahupua'a*, pp. 1–10.

Abu Hammad, A. (2011) Watershed erosion risk assessment and management utilising revised universal soil loss equation-geographic information systems in the Mediterranean environments. *Water and Environment Journal*, 25(1): 1–14.

Achite, M. and Ouillon, S. (2007) Suspended sediment transport in a semiarid watershed, Wadi Abd, Algeria (1973–1995). *Journal of Hydrology*, 343(3–4): 187–202.

Aflizar, Saidi, A., Husnain, Indra, R., Darmawan, Harmailis, Somura, H., Wakatsuki, T. and Masunaga, T. (2010) Soil erosion characterization in an agricultural watershed in West Sumatra, Indonesia. *Tropics*, 19(1): 29–42.

Ahmad, A. and Quegan, S. (2012) Analysis of maximum likelihood classification on multispectral data. *Applied Mathematical Sciences*, 6(129): 6425–6436.

Aksoy, H. and Kavvas, M.L. (2005) A review of hillslope and watershed scale erosion and sediment transport models. *Catena*, 64(2–3): 247–271.

Alatorre, L.C. and Begueria, S. (2009) Identification of eroded areas using remote sensing in a badlands landscape on Marls in the Central Spanish Pyrenees. *Catena*, 76(3): 182–190.

Alexander, D. (1999) *Natural Disasters.* Massachusetts: Kluwer Academic Publishers.

Ali, K.F. and de Boer, D.H. (2003) Construction of sediment budgets in large-scale drainage basins: the case of the upper Indus River. In: *Erosion Prediction in Ungauged Basins: Integrating Methods and Techniques* (Proceedings of symposium HS01 held during IUGG2003 at Sapporo. July 2003). IAI-IS Publ. no. 279, pp. 206–215.

Allen, T.L., Wilhelm, M.B., Heldmann, J.L. and Allen, S.J. (2008) Correlation of regional topography and Martian Gully orientation. *Workshop on Martian Gullies: Theories and Tests.*

Allison, R.J. and Thomas, D.S.G. (1993) “The sensitivity of landscapes.” In Thomas, D.S.G and Allison, R.J. (eds.) *Landscape Sensitivity.* Chichester, West Sussex: John Wiley & Sons, pp. 1–5.

Amore, E., Modica, C., Nearing, M.A. and Santoro, V.C. (2004) Scale effect in USLE and WEPP application for soil erosion computation from three Sicilian Basins. *Journal of Hydrology,* 293(1–4): 100–114.

Anderson, J. R., Hardy, E.E., Roach, J.T. and Witmer, R.E. (1976) *A land use and land cover classification system for use with remote sensor data.* U.S. Geological Survey Professional Paper 964, Washington, DC: US Government Printing Office.

Angima, S.D., Stott, D.E., O’Neill, M.K., Ong, C.K. and Weesies, G.A. (2003) Soil erosion prediction using RUSLE for central Kenyan highland conditions. *Agriculture Ecosystems and Environment,* 97(1–3): 295–308.

Anhonditsis, G., Koulouri, M., Giourga, C. and Loumou,A. (2002) Quantitative assessment of agricultural runoff and soil erosion using mathematical modelling: applications in the Mediterranean region. *Environmental Management,* 30(3): 434–453.

Anoldus, H. (1980) “An approximation of the rainfall factor in the Universal Soil Loss Equation.” In De Booth, M. and Gabrields, D. (eds). *Assessment of Erosion*, John Wiley and Sons.

Arekhi, S., Bolourani, A.D., Shabani, A., Fathizad, H. and Ahamdy-asbchin, S. (2012) Mapping soil erosion and sediment yield susceptibility using RUSLE, Remote Sensing and GIS (Case study: Cham Gardalan Watershed, Iran). *Advances in Environmental Biology*, 6(1): 109–124.

Arekhi, S., Niazi, Y. And Kalteh, A.M. (2010) Soil erosion and sediment yield modeling using RS and GIS techniques: a case study, Iran. *Arabian Journal of Geosciences,* 5(2): 285–296.

Ashiq, M.W., Zhao, C., Ni, J. and Akhtar, M. (2010) GIS-based high-resolution spatial interpolation in mountain-plain areas of Upper Pakistan for regional climate change impact studies. *Theoretical and Applied Climatology,* 99(3–4): 239–253.

Asian Disaster Preparedness Center. (2002) *Overview of Disaster Risk Management and Approaches for Mitigation of the Impacts*. Bangkok: ADPC.

Asselman, N.E.M. (2000) Fitting and interpretation of sediment rating curves. *Journal of Hydrology*, 234(3–4): 228–248.

Asselman, N.E.M., Middelkoop, H. and van Dijk, P.M. (2003) The impact of changes in climate and land use on soil erosion, transport and deposition of suspended sediment in the River Rhine. *Hydrological Processes*, 17(16): 3225–3244.

Babel, M.S., Najim, M.M.M. and Loof, R. (2004) Assessment of Agricultural NonPoint Source Model for a Watershed in Tropical Environment. *Journal of Environmental Engineering,* 130(9): 1032–1041.

Baigorria, G.A. and Romero, C.C. (2007) Assessment of erosion hotspots in a watershed: Integrating the WEPP model and GIS in a case study in the Peruvian Andes. *Environmental Modelling & Software*, 22(8): 1175–1183.

Baird, W.F. (2007) *Sebewaing River Sediment Transport Modelling Study*: *Final Report*, Detroit District: USACE, 97p.

Baker, M.M., Govers, G., van Doom, A., Quetier, F., Chouvardas, D. and Rounsevell, M. (2008) The response of soil erosion and sediment export to land-use change in four areas of Europe: the importance of landscape pattern. *Geomorphology,* 98(3–4): 213-226.

Balamurugan, G. (1991) Sediment balance and delivery in a humid tropical urban river basin: the Kelang River, Malaysia. *Catena*, 18(3–4): 271–278.

Bazzoffi, P. (2009) Soil erosion tolerance and water runoff control: minimum environmental standards. *Regional Environmental Change*, 9(3): 169–179.

Beasley, D.B., Huggins, L.F., and Monke, E.J. (1980) ANSWERS: a model for watershed planning. *Transactions of American Society of Agricultural Engineers*, 23(4): 938–944.

Beskow, S., Mello, C.R., Norton, L.D., Curi, N., Viola, M.R. and Avanzi, J.C. (2009) Soil erosion prediction in the Grande River Basin, Brazil using distributed modelling. *Catena,* 79(1): 49–59.

Bettinger, P. and Wing, M.G. (2004) *Geographic Information Systems: Application in Forestry and Natural Resources Management*. New York: McGraw-Hill.

Bhattarai, R. and Dutta, D. (2007) Estimation of soil erosion and sediment yield using GIS at catchment scale. *Water Resources Management,* 21(10): 1635–1647.

Bhuyan, S.J., Kalita, P.K., Janssen, K.A. and Barnes, P.L. (2002) Soil loss predictions with three erosion simulation models. *Environmental Modelling & Software*, 17(2): 137–146.

Boardman, J. (2006) Soil erosion sciences: reflections on the limitations of current approaches. *Catena*, 68(2–3): 73–86.

Boer, R., Fletcher, D.J. and Campbell, L.C. (1993) Rainfall patterns in a major wheat-growing region of Australia. *Australian Journal of Agricultural Research,* 44: 609–624.

Bogen, J. (1996) "Erosion and sediment yield in Norwegian Rivers." In Walling, D.E. and Webb, B.W. (eds.) *Erosion and Sediment Yield: Global and Regional Perspectives* (Proceedings of the Exeter Symposium July 1996). IAHS Publ. no. 236, pp. 73–84.

Bonan, G. (2008) *Ecological Climatology: Concepts and Applications.* 2nd edition, Cambridge: Cambridge University Press.

Boochabun, K., W. Tych, N. A. Chappell and P. A. Carling (2004) Statistical modelling of rainfall and river flow in Thailand. *Journal Geological Society of India*, 64, pp. 503–515.

Boonprakorb, K. and Hattirat, S. (2006) *Crisis or Opportunity: Climate Change and Thailand.* Bangkok: Greenpeace Southeast Asia.

Bosco, C., Rusco, E., Montanarella, L. and Panagos, P. (2009) Soil erosion in the Alpine area: risk assessment and climate change. *Studi Trentini di Scienze Naturali*, 85, pp. 117–123.

Bou Kheir, R., Abdallah, C. and Khawlie, M. (2008) Assessing soil erosion in Mediterranean Karst landscapes of Lebanon using remote sensing and GIS. *Engineering Geology*, 99(3–4): 239–254.

Bou Kheir, R., Cerdan, O. and Abdallah, C. (2006) Regional erosion risk mapping in Lebanon. *Geomorphology*, 82(3–4): 347–359.

Bridge, J.S. (2003) *River and Floodplains: Forms, Processes, and Sedimentary Record.* Massachusetts: Blackwell Publishing.

Bryan, R.B. (2000) Soil erodibility and processes of water erosion on hillslope. *Geomorphology*, 32(3–4): 385–415.

Bryan, R.B., Govers, G. and Poesen, J. (1989) The concept of soil erodibility and some problems of assessment and application. *Catena,* 16(4–5): 393–412.

Burrough, P. A. and McDonell, R. A. (1998) *Principles of Geographical Information Systems*. New York: Oxford University Press.

Buss, S., Cai, Z., Cardenas, B., Fleckenstein, J., Hannah, D., Heppell, K., Hulme, P., Ibrahim, T., Kaeser, D., Krause, S., Lawler, D., Lerner, D., Mant, J., Malcolm, I., Old, G., Parkin, G., Pickup, R., Pinay, G., Porter, J., Rhodes, G., Richie, A., Riley, J., Robertson, A., Sear, D., Shields, B., Smith, J., Tellam, J. and Wood, W. (2009) *Using Science to Create a Better Place: The Hyporheic Handbook.* Bristol: Integrated Catchment Science Programme, Environment Agency.

Candela, L., Elorza, F.J., Jiménez-Martínez, J. and von Igel, W. (2012) Global change and agricultural management options for groundwater sustainability. *Computers and Electronics in Agriculture,* 86, pp. 120–130.

Cannon, T. (1994) "Vulnerability analysis and the explanation of natural disasters." In Blaikie, P.M., Cannon, T., Davis, I., Wisner, B. (eds.), *At Risk: Natural Hazards, People's Vulnerability and Disasters*. London: Routledge, pp. 13-30.

Cebecauer, T. and Hofierka, J. (2008) The consequences of land-cover changes on soil erosion distribution in Slovakia. *Geomorphology*, 98(3–4): 187–198.

Chaiyo, U., Garivait, S. and Wanthongchai, K. (2011) Carbon storage in above-ground biomass of tropical deciduous forest in Ratchaburi Province, Thailand. *World Academy of Science, Engineering and Technology,* 58, pp. 636–641.

Chakela, Q. and Stocking, M.A. (1988) An improved methodology for erosion hazard mapping: part II application to Lesotho. *Geografiska Annaler,* 70(3): 181–189.

Chang, J.H. (1993) “Hydrology in humid tropical Asia.” In Bonell, M., Hufschmidt, M.M. and Gladwell, J.S. (eds.) *Hydrology and Water Management in the Humid Tropics: Hydrological Research Issues and Strategies for Water Management.* Cambridge, Cambridge University Press, pp. 55–66.

Charlton, R. (2008) *Fundamentals of Fluvial Geomorphology.* New York: Routledge.

Chen, C., Tsai, C. and Tai, C. (2006) Simulation of sediment yield from watershed by physiographic soil erosion-deposition model. *Journal of Hydrology,* 327(3–4): 293–303.

Chen, Z., Chen, W., Leblanc, S.G. and Henry, G.H.R. (2010) Digital photograph analysis for measuring percent plant cover in the Arctic. *Arctic,* 63(3): 315–326.

Childs, C. (2004) Interpolating surfaces in ArcGIS Spatial Analyst. *ArcUser*, 7(3): 32–35.

Cohen, M.J., Shepherd, K.D. and Walsh, M.G. (2005) Empirical reformulation of the universal soil loss equation for erosion risk assessment in a tropical watershed. *Geoderma*, 124(3–4): 235–252.

Cohn, T.A., DeLong, L.L., Gilroy, E.J., Hirsch, R.M. and Wells, D.K. (1989) Estimating constituent loads. *Water Resources Research*, 25(5): 937–942.

Coleman D.J. and Scatena F.N. (1986) “Identification and evaluation of watershed sediment sources.” In Hadley, R.F. (ed.), *Drainage Basin Sediment Delivery*, IAHS Publication 159, pp. 3–18.

Congalton, R.G. (1991) A review of assessing the accuracy of classifications of remotely sensed data. *Remote Sensing of Environment*, 37(1): 35–46.

Costa, M.H. and Foley, J.A. (2000) Combined effects of deforestation and doubled atmospheric CO_2 concentrations on the climate of Amazonia. *Journal of Climate,* 13(1): 18–34.

Coulthard, T.J., Hancock, G.R. and Lowry, J.B.C. (2012) Modelling soil erosion with a downscaled landscape evolution model. *Earth suface processes and landforms,* 37(10): 1046–1055.

Coulthard, T.J., Macklin, M.G. and Kirkby, M.J. (2002) A cellular model of Holocene upland river basin and alluvial fan evolution. *Earth Surface Processes and Landforms,* 27(3): 269–288.

Coulthard, T. J., Ramirez, J., Fowler, H. J. and Glenis, V. (2012) Using the UKCP09 probabilistic scenarios to model the amplified impact of climate change on drainage basin sediment yield. *Hydrology and Earth System Sciences*,16(11): 4401–4416.

Crozier, M.J. (2010) Deciphering the effect of climate change on landslide activity: a review. *Geomorphology,* 124(3–4): 260–267.

Cunningham, W.P., Cunningham, M.A. and Saigo, B.W. (2007) *Environmental Science: A Global Concern.* Nine edition, New York: McGraw-Hill.

Dale, V.H. (1997) The relationship between land-use change and climate change. *Ecological Applications,* 7(3): 753–769.

De Aragao, R., Srinivasan, V.S., Suzuki, K., Kadota, A., Orugo, M. and Sakata, Y. (2005) "Evaluation of Physical-Based Model to Simulate the Runoff and Erosion Processes in a Semiarid Region in Brazil." In IAHS-AISH Publication 292, Wallingford: *International Association of Hydrological Sciences*, pp. 85–93.

De Asis, A.M. and Omasa, K. (2007) Estimation of vegetation parameter for modelling soil erosion using linear spectral mixture analysis of Landsat ETM data. *Journal of Photogrammetry & Remote Sensing*, 62(4): 309–324.

De Jong, S.M., Paracchini, M.L., Bertolo, F., Folving, S., Megier, J. and De Roo, A.P.J. (1999) Regional assessment of soil erosion using the distributed model SEMMED and remotely sensed data. *Catena,* 37(3–4): 291–308.

De Roo, A.P.J. and Offermans, R.J.E. (1995) "LISEM: a physically-based hydrological and soil erosion model for basin-scale water and sediment management." In *Modelling and Management of Sustainable Basin-Scale Water Resource Systems*, IASH Publ. No. 231, pp. 399–407 (Proceedings of a Boulder Symposium, July 1995).

De Vente, J. and Poesen, J. (2005) Predicting soil erosion and sediment yield at the basin scale: Scale issues and semi-quantitative models. *Earth-Sciences Reviews,* 71(1–2): 95–125.

De Vente, J., Poesen, J. and Verstraeten, G. (2005) The application of semi-quantitative methods and reservoir sedimentation rates for the prediction of basin sediment yield in Spain. *Journal of Hydrology,* 305(1–4): 63–86.

De Vente, J., Poesen, J., Arabkhedri, M. and Verstraeten, G. (2007) The sediment delivery revisited. *Progress in Physical Geography*, 31(2): 155–178.

De Vente, J., Poesen, J., Govers, G. and Boix-Fayos, C. (2009) The implications of data selection for regional erosion and sediment yield modelling. *Earth Surface Processes and Landforms,* 34(15): 1994–2007.

De Vente, J., Poesen, J., Verstraeten, G., Van Rompaey, A. and Govers, G. (2008) Spatially distributed modelling of soil erosion and sediment yield at regional in Spain. *Global and Planetary Change*, 60(3–4): 393–415.

Demirci, A. and Karaburun, A. (2012) Estimation of soil erosion using RUSLE in a GIS framework: a case study in the Buyukcekmece Lake watershed, Northwest Turkey. *Environmental Earth Sciences*, 66(3): 903–913.

Derose, R.C., Gomes, B., Marden, M., Trustrum, N.A. (1998) Gully erosion in Mangatu Forest, New Zealand, estimated from digital elevation models. *Earth Surface Processes and Landforms*, 23(11): 1045–1053.

Desmet, P.J.J. and Govers, G. (1995) GIS-based simulation of erosion and deposition patterns in an agricultural landscapes: a comparison of model results with soil map information. *Catena*, 25(1–4): 389–401.

Desmet, P.J.J. and Govers, G. (1996) A GIS procedure for automatically calculating the USLE LS factor on topographically complex landscape units. *Journal of Soil and Water Conservation*, 51(5): 427–433.

Dickinson, W.T. (1981) “Accuracy and precision of suspended sediment loads.” In *Erosion and Sediment Transport Measurement,* IAHS Publ. no. 133, pp. 195-202 (Proceedings of the Florence Symposium, June 1981).

Ding, J. and Richards, K. (2009) Preliminary modelling of sediment production and delivery in the Xihanshui River basin, Gansu, China. *Catena,* 79(3): 277–287.

Diodato, N. (2006) Modelling net erosion response to enviroclimatic changes recorded upon multisecular timescales. *Geomorphology*, 80(3–4): 164–177.

Diodato, N. and Grauso, S. (2009) An improved correlation model for sediment delivery ratio assessment. *Environmental Earth Sciences,* 59(1): 223–231.

Dlamini, P., Orchard, C., Jewitt, G., Lorentz, S., Titshall, L. and Chaplot, V. (2011) Controlling factors of sheet erosion under degraded grasslands in the sloping lands of KwaZulu-Natal, South Africa. *Agricultural Water Management*, 98(11): 1711–1718.

Donjadee, S., Clemente, R.S., Tingsanchali, T. and Chinnarasri, C. (2010) Effect of vertical hedge interval of vetiver grass on erosion on steep agricultural lands. *Land Degradation & Development,* 21(3): 219–227.

Douglas, I. (1999) "Hydrological investigations of forest disturbance and land cover impacts in South-East Asia: a review." In *Changes and Disturbance in Tropical Rainforest in South-East Asia*. Philosophical Transactions: Biological Sciences, 354(1391): 1725–1738.

Dubber, W. and Hedbom, M. (2008) *Soil Erosion in Northern Lao PDR: an Evaluation of the RUSLE Erosion Model.* Geobiosphere Science Centre, Physical Geography and Ecosystems Analysis, Lund University, Sweden.

Dunne, T. (1974) *Suspended Sediment Data for the Rivers of Kenya*. Nairobi: Rep. to Ministry of Water Development, 108 pp.

Efe, R., Ekici, D. and Cürebal, I. (2008) Erosion analysis of Şahin Creek Watershed (NW of Turkey) using GIS based on RUSLE (3d) method. *Journal of Applied Sciences*, 8(1): 49–58.

Elliot, S., Navakitbumrung, P., Kuarak, C., Zangkum, S., Anusarnsunthorn, V. and Blakesley, D. (2003) Selecting framework tree species of restoring seasonally dry tropical forests in northern Thailand based on field performance. *Forest Ecology and Management,* 185(1–3): 177–191.

Ellis, A.M., Garcia, A.J., Focks, D.A., Morrison, A.C. and Scott, T.W. (2011) Parameterization and sensitivity analysis of a complex simulation model for mosquito population dynamics, dengue transmission, and their control. *The American Journal of Tropical Medicine and Hygiene.* 85(2): 257–264.

ESRI (2012) *Understanding Drainage Systems.* Available from: http://webhelp.esri.com/arcgisdesktop/9.3/printBooks_topics.cfm?pid=6050 [Accessed 8 September 2013]

Evans, R. (2006) Sustainable practice to limit soil erosion: a review and discussion. CAB Reviews: Perspectives in Agriculture. *Veterinary Science, Nutrition and Natural Resources No. 030*, pp. 1–13.

Fang-Fang, Z., Bing, Z., Jun-Sheng, L., Qian, S., Yuan-Feng, W. and Yang, S. (2011) Comparative analysis of automatic water identification method based on multispectral remote sensing. *Procedia Environmental Sciences,* 11(Part C): 1428–1487.

FAO (2006) *Guidelines for Soil Description*. 4th Edition, Rome.

FAO (2011) *Thailand and FAO Achievements and Success stories*. Bangkok: Thai Affairs Section, FAO Regional Office for Asia and the Pacific.

Feng, X., Wang, Y., Chen, L., Fu, B. and Bai, G. (2010) Modeling soil erosion and its response to land-use change in hilly catchments of the Chinese Loess Plateau. *Geomorphology*, 118(3–4): 239–248.

Feng, Z., Wang, Y., Chen, L., Fu, B. and Bai, G. (2009) modeling soil erosion and its response to land-use change in hilly catchments of the Chinese Loess Plateau. *Geomorphology,* 118(3–4): 239–248.

Fentie, B., Yu, B., Silburn, M.D. and Ciesiolka, C.A.A. (2002) Evaluation of eight different methods to predict hillslope runoff rate for a grazing catchment in Australia. *Journal of Hydrology,* 261(1-4): 102–114.

Ferguson R.I. (1987) Accuracy and precision of methods for estimating river loads. *Earth Surface Processes and Landforms*, 12(1): 95–104.

Fernández, C., Vega, J.A. and Vieira, D.C.S. (2010) Assessing soil erosion after fire and rehabilitation treatments in NW Spain: Performance of RUSLE and revised Morgan-Morgan-Finney models. *Land Degradation & Development*, 21(1): 58–67.

Ferro, V. and Porto, P. (2000) Sediment delivery distributed (SEDD) model. *Journal of Hydrologic Engineering,* 5(4): 411–422.

Fistikoglu, O. and Harmancioglu, N.B. (2002) Integration of GIS with USLE in assessment of soil erosion. *Water Resources Research*, 16(6): 447–467.

Fornes, W.L., Whiting, P.J., Wilson, C.G. and Matisoff, G. (2005) Caesium-137 derived erosion rates in an agricultural setting: the effects of model assumptions and management practices. *Earth Surface Processes and Landforms*, 30(9): 1181–1189.

Forsyth, T. (2005) Land use impacts on water resources: science, social and political factors. In Anderson, M. (Ed.), *Encyclopedia of Hydrological Sciences*. Chichester: Wiley.

Forsyth, T. and Walker, A. (2008) *Forest Guardians, Forest Destroyers: The Politics of Environmental Knowledge in Northern Thailand*. Chiang Mai: Silkworm Book.

Foster, G.R., Toy, T.E. and Renard, K.G. (2003) "Comparison of the USLE, RUSLE1.06c, and RUSLE2 for application to highly distributed lands." In Renard, K.G., McIlroy, S.A., Gburek, W.J., Cranfield, H.E. and Scott, R.L. (eds.) *First Interagency Conference on Research in Watersheds.* Washington, DC: USDA-Agricultural Research Service, pp. 154–160.

Fox, J., Krummel, J., Yarnasarn, S., Ekasingh, M. and Podger, N. (1994) "Land use and landscape dynamics in Northern Thailand: Assessing change in three upland watersheds since 1954." In *Spatial Information and Ethnoecology: Case Studies from Indonesia, Nepal, and Thailand. East-West Center Working Paper, Environment Series*, 38, pp. 27–42.

Francke, T., López-Tarazón, J.A. and Schröder, B. (2008) Estimation of suspended sediment concentration and yield using linear models, random forests and quantile regression forests. *Hydrological Processes*, 22(25): 4892–4904.

Fróis, N., Chan, T.Y.W., Kaunisvesi, L.K., Mitterer, M., Omoro, L.M.A., Toronen, A.A.J., Mulyani, Y.A. and Songchan, R. (2008) *Forest Ecosystem in Northern Thailand.* Sixth University of Helsinki Course on Tropical Forest Ecology and Silviculture (ME 451), Helsinki, Finland.

Fu, B., Newham, L.T.H. and Ramos-Scharron, C.E. (2010) A review of surface erosion and sediment delivery models for unsealed roads. *Environmental Modelling &Software*, 25(1): 1–14.

Fu, B., Wang, Y., Lu, Y., He, C., Chen, L., and Song, C. (2009) The effects of land-use combinations on soil erosion: a case study in the Loess Plateau of China. *Progress in Physical Geography,* 33(6): 793–804.

Fu, G., Chen, S. and McCool, D.K. (2006) Modelling the impacts of no-till practice on soil erosion and sediment yield with RUSLE, SEDD, and ArcView GIS. *Soil & Tillage Research*, 85(1–2): 38–49.

Fukushima, M., Kanzaki, M., Hara, M., Ohkubo, T., Preechapanya, P. and Choocharoen, C. (2008) Secondary forest succession after the cessation of swidden cultivation in the montane forest area in Northern Thailand. *Forest Ecology and Management,* 255(5–6): 1994–2006.

Fullen, M.A. (2003) Soil erosion and conservation in Northern Europe. *Progress in Physical Geography,* 27 (3): 331-358.

Gale, N. (2000) The relationship between canopy gaps and topography in western Ecuadorian rain forest. *Biotropica,* 32(4a): 653–661.

Gao, J. (2009) *Digital Analysis of Remotely Sensed Imagery.* New York: McGraw-Hill.

Gao, P. (2008) Understanding watershed suspended sediment transport. *Process in Physical Geography*, 32(3): 243-263.

George A., Pierret A., Boonsaner A., Valentin C., Orange D. and Planchon O. (2009) Potential and limitations of Payments for Environmental Services (PES) as a means to manage watershed services in mainland Southeast Asia. *International Journal of Commons*, 3(1): 16–40.

GMS Environment Operation Center. (2005) *Thailand National Environmental Performance Assessment (EPA) Report.* Bangkok.

GMS Environment Operation Center. (2007) *Environmental Performance Assessment*. Bangkok.

Gover, G. (2011) “Misapplications and misconceptions of erosion models.” In Morgan, R.P.C. and Nearing, M.A. (eds.) *Handbook of Erosion Modelling.* Chichester, West Sussex: Wiley-Blackwell, pp. 117-134.

Graham, S.T., Famiglietti, J.S. and Maidment, D.R. (1999) Five-minute, 1/2°, and 1° data sets of the continental watersheds and river networks for use in regional and global hydrologic and climate system modeling studies. *Water Resources Research,* 35(2): 583-587.

Griffiths, G. A. (1982). Spatial and temporal variability in suspended sediment yields of North Island Basins, New Zealand*. Journal of the American Water Resources Association*, 18(4): 575–584.

Gurnell, A.M., Hodson, A., Clark, M.J., Bogen,J., Hagen, J.O. and Tranter, M. (1994) "Water and sediment discharge from glacier basins: an arctic and alpine comparison." In *Variability in Stream Erosion and Sediment Transport,* IAHS Publ. no. 224, pp. 325–334 (Proceedings of the Canberra Symposium December 1994).

Guyot, J.L., Filizola, N., Quintanilla, J. and Cortez, J. (1996) "Dissolved solids and suspended sediment yields in the Rio Madeira basin, from the Bolivian Andes to the Amazon." In Walling, D.E. and Webb, B.W. (eds.) *Erosion and Sediment Yield: Global and Regional Perspectives*. IAHS Publ. no. 236, pp. 55-63 (Proceedings of the Exeter Symposium July 1996).

Hancock, G. R. (2009) A catchment scale assessment of increased rainfall and storm intensity on erosion and sediment transport for Northern Australia.*Geoderma*, 152 (3): 350–360.

Hancock, G.R. (2012) Modelling stream sediement concentration: An assessment of enhanced rainfall and storm frequency. *Journal of Hydrology,* 430-431(2): 1–12.

Hancock, G.R., Lowry, J.B.C., Coulthard, T.J., Evans, K.G. and Moliere, D.R. (2010) A catchment scale evaluation of the SIBERIA and CAESAR landscape evolution models. *Earth Surface Processes and Landforms,* 35(8): 863–875.

Hardjowitjitro, H. (1981) "Soil erosion as a result of upland traditional cultivation in Java Island." In Tinsangchali, T. and Eggers, H. (eds.) *Proceedings of the Southeast Asian Regional Symposium on Problems of Soil Erosion and Sedimentation.* AIT Bangkok, pp. 173–179.

Haregeweyn, N., Poesen, J., Nyssen, J., Govers, G., Verstraeten, G., De Vente, J., Decker, J., Moeyersons, J. and Haile, M. (2008) Sediment yield variability in Northern Ethiopia: a quantitative analysis of its controlling factors. *Catena*, 75(1): 65–76.

Haregeweyn, N., Poesen, J., Nyssen, J., Verstraeten, G., De Vente, J., Govers, G., Deckers, S. and Moeyersons, J. (2005) Specific sediment yield in Tigray-Northern Ethiopia: Assessment and semi-quantitative modelling. *Geomorphology*, 69(1–4): 315–331.

Hartcher, M.G. and Post, D.A. (2008) The impact of improved landuse cover on the range of modelled sediment yield from two sub-catchments of the Mae Chaem, Thailand. *Mathematics and Computers in Simulation*, 78(2–3): 367–378.

Hartter, J., Lucas, C., Gaughan, A.E. and Aranda, L.L. (2008) Detecting tropical dry forest succession in a shifting cultivation mosaic of the Yucatán Peninsula, Mexico. *Applied Geography,* 28(2): 134–149.

Hekimoglu, M. and Barlas, Y. (2010) “Sensitivity analysis of system dynamics models by behaviour pattern measures.” In *Proceedings of the 28th International Conference of the System Dynamics Society*, pp. 1–31.

Hellweger, F.L., Schlosser, P., Lall, U. And Weissel, J.K. (2004) Use of satellite imagery for water quality studies in New York Harbor. *Estuarine, Coastal and Shelf Science,* 61(3): 437–448.

Hessel, R., Jetten, V.G., Liu, B. and Qiu, Y. (2011) “Evaluating effects of soil and water management and land use change on the Loess Plateau of China using LISEM.” In Morgan, R.P.C. and Nearing, M.A. (eds.) *Handbook of Erosion Modelling.* Chichester, West Sussex: Wiley-Blackwell, pp. 223–248.

Hewitt, K. (1997) *Region of Risk: A Geography Introduction to Disaster.* New York: John Wiley & Sons.

Hickey, R. (2000) Slope angle and slope length solutions for GIS. *Cartography*, 29(1): 1–8.

Hill, K., Botsford, E. and Booth, D.B. (2003) A rapid land cover classification method for use in urban watershed analysis. *Water Resource Series Technical Report No. 173*, Department of Civil and Environmental Engineering, University of Washington, Seattle, Washington.

Hillman, M. and Brierley, G. (2005) A critical review of catchment-scale stream rehabilitation programmes. *Progress in Physical Geography,* 29(1): 50–70.

Horowitz, A.J. (2003) An evaluation of sediment rating curves for estimating suspended sediment concentrations for subsequent flux calculations. *Hydrological Processes*, 17(17): 3387–3409.

Huang, C., Wells, L.K. and Norton, L.D. (1999) Sediment transport capacity and erosion processes: model concepts and reality. *Earth Surface Processes and Landforms,* 24(6): 503–516.

Hui, L., Xiaoling, C., Lim, K.J., Xiaobin, C. and Sagong, M. (2010) Assessment of soil erosion and sediment yield in Liao watershed, Jiangxi Province, China, using USLE, GIS, and RS. *Journal of Earth Science*, 21(6): 941–953.

Iadanza, C and Napolitano, F. (2006) Sediment transport time series in the Tibet River. *Physics and Chemistry of the Earth*, 31(18): 1212–1227.

Irvem, A., Topaloglu, F. and Uygur, V. (2007) Estimating spatial distribution of soil loss over Seyhan River Basin in Turkey. *Journal of Hydrology,* 336(1–2): 30–37.

Jain, M.K. and Das, D. (2010) Estimation of sediment yield and areas of soil erosion and deposition for watershed prioritization using GIS and remote sensing. *Water Resources Management*, 24(10): 2091–2112.

Jain, M.K. and Kothyari, U.C. (2000) Estimation of soil erosion and sediment yield using GIS. *Hydrological Sciences Journal,* 45(5): 771–786.

Jain, M.K., Mishra, S.K. and Shah, R.B. (2009) Identification of sediment source and sink areas in a Himalayan watershed using GIS and remote sensing. *Land Degradation & Development*, 20(6): 623–639.

Jain, S.K., Singh, P., Saraf, A.K. and Seth, S.M. (2003) Estimation of sediment yield for a rain, snow and Glacier Fed River in the Western Himalayan Region. *Water Resources Management*, 17(5): 377–393.

Jakeman A.J., Letcher, R.A., Rojanasoonthon, S., Cuddy, S. and Scott, A. (2005) *Integrating Knowledge for River Basin Management Progress in Thailand*. Canberra: Australian Centre for International Agricultural Research.

Jensen, J.R. (2007) *Remote Sensing of the Environment: An Earth Resource Perspective*. 2nd ed., Upper Saddle River, New Jersey: Pearson Prentice Hall.

Jetten, V.G. and Maneta, M.P. (2011) "Universal soil loss equation and revised universal soil loss equation." In Morgan, R.P.C. and Nearing, M.A. (eds.) *Handbook of Erosion Modelling.* Chichester, West Sussex: Wiley-Blackwell, pp. 33-51.

Jha, M.K. and Paudel, R.C. (2010) Erosion predictions by empirical models in a mountainous watershed in Nepal. *Journal of Spatial Hydrology*, 10(1): 89–102.

Jianjun, P. and Bergsma, E. (1998) Flood hazard prediction from soil properties by remote sensing and geographic information system: a case study of Mae Rim watershed, Chiang Mai Province, Thailand. *Pedosphere,* 8(1): 71–78.

Jones, H. G. and Vaughan, R.A. (2010) *Remote Sensing of Vegetation: Principles, Techniques, and Applications.* Oxford: Oxford University Press.

Jordan, G., Van Rompaey, A., Szilassi, P., Csillag, G., Mannaert, C. and Woldai, T. (2005) Historical land use changes and their impact on sediment fluxes in the Balaton basin (Hungary). *Agricultural, Ecosystems and Environment*, 108(2): 119–133.

Kunta, K. (2009) *Effects of Geographic Information: Quality on Soil Erosion Prediction.* Institute of Geodesy and Photogrammetry, ETH Hönggerberg: Swiss Federal Institute of Technology Zurich, 153p.

Kao, S. and Liu, K. (2001) Estimating the suspended sediment load by using the historical hydrometric record from the Lanyang-Hsi Watershed. *TAO*, 12(2): 401–414.

Kapalanga T.S. (2008) A review of land degradation assessment methods. *Land Restoration Training Programme*, Keldnaholt, 112 Reykjavík, Iceland, pp. 17–68.

Karaburun, A. (2010) Estimation of C factor for soil erosion modelling using NDVI in Buyukcekmece watershed. Ozean Journal of Applied Sciences, 3(1): 77–85.

Karydas, C.G., Sekuloska, T. and Silleos, G.N. (2009) Quantification and site-specification of the support practice factor when mapping soil erosion risk associated with olive plantations in Mediterranean island of Crete. *Environmental Monitoring and Assessment,* 149(1–4): 19–28.

Karvonen, T., Koivusalo, H., Jauhiainen, M., Palko, J., and Weppling, K. (1999) A hydrological model for predicting runoff from different land use areas. *Journal of Hydrology*, 217(3): 253–265.

Kefi, M., Yoshino, K. and Setiawan, Y. (2012) Assessment and mapping of soil erosion risk by water in Tunisia using time series MODIS data. *Paddy and Water Environment*, 10(1): 59–73.

Khosrowpanah, S., Heitz, L.F., Wen, Y., and Park, M. (2007) Develop a GIS-based soil erosion potential model of the UGUM Watershed. *WERI*: Technical Report No. 117.

Kilham, N.E., Roberts, D. and Singer, M.B. (2012) Remote sensing of suspended sediment concentration during turbid flood conditions on the Feather River, California – A modeling approach. *Water Resources Research,* 48, pp. 1–18.

Kim, M.K., Flanagan, D.C., Frankenberger, J.R. and Meyer, C.R. (2009) Impact of precipitation changes on runoff and soil erosion in Korea using CLIGEN and WEPP. *Journal of Soil and Water Conservation,* 64(2): 154–162.

Kim, S.M., Choi, Y., Suh, J., Oh, S., Park, H.D. and Yoon, S.H. (2012) Estimating of soil erosion and sediment yield from mine tailing dumps using GIS: a case study at the Samgwang mine, Korea. *Geosystem Engineering*, 15(1): 2–9.

Kinnell, P.I.A. (2005) Why the universal soil loss equation and the revised version of it do not predict event erosion well. *Hydrological Processes,* 19(3): 851–854.

Kinnell, P.I.A. (2008) Sediment delivery from hill slopes and the Universal Soil Loss Equation: Some perceptions and misconceptions. *Hydrological Processes,* 22(16): 3168–3175.

Kinnell. P.I.A. (2010) Event Soil Loss, Runoff and universal soil loss equation family of models: a review. *Journal of Hydrology*, 385(1–4): 384–397.

Kirkby, M.J., Bracken, L.J. (2009) Gully processes and gully dynamics. *Earth Surface Processes and Landforms*, 34(14): 1841–1851.

Kirkby, M.J., Imeson, A.C., Bergkamp, G. and Cammeraat, L.H. (1996) Scaling up process and models from the field plot to the watershed and regional areas. *Journal of Soil and Water Conservation*, 51(5): 391–396.

Kirkby, M.J., Irvin, B.J., Jones, R.J.A., Gover, G. and PESERA team. (2008) The PESERA coarse scale erosion model for Europe. I. – Model rationale and implementation. *European Journal of Soil Science,* 59(6): 1293–1306.

Kirkwood, V., Dumanski, J., Bootsma, A., Stewart, R.B., and Muma, R. (1989) *The Land Potential Database for Canada: Users' Handbook*. Ontario: Research Branch, Agriculture Canada.

Kisi, O., Karahan, M.E. and Şen, Z. (2006) River suspended sediment modelling using a fuzzy logic approach. *Hydrological Processes*, 20(20): 4351–4362.

Knighton, D. (1998) *Fluvial Form & Processes: a New Perspective*. London: Arnold.

Knisel, W.G. (1980) CREAMS: a field scale model for chemicals, runoff and erosion from agricultural management systems. *USDA Conservation Research Report Vol. 26*, 160 pp.

Kotrlik, J. W. and Williams, H. A. (2003) The Incorporation of effect size in information technology, learning, and performance. *Information Technology, Learning, and Performance Journal*, 21(1): 1–7.

Krishna Bahadur, K.C. (2009) Mapping soil erosion susceptibility using remote sensing and GIS: a case of the Upper Nam Wa Watershed, Nan Province, Thailand. *Environmental Geology,* 57(3): 695–705.

Kutiel, H. (1988). Rainfall variations in the Galilee (Israel), II. Variations in the temporal distribution between 1931–1960 and 1951–1980. *Journal of Hydrology*, 99(1): 179–185.

Laften, J.M., Lane, L.J., and Foster, G.R. (1991) WEPP: a new generation of erosion prediction technology. *Journal of Soil and Water Conservation*, 46(1): 34–38.

Lal, R. (2001) Soil degradation by erosion. *Land Degradation & Development*, 12(6): 519–539.

Lamelas, M.T., Hoppe, A., de la Riva, J. and Marinoni, O. (2009) Modelling environmental variable for georesources assessment to support sustainable land-use decisions in Zaragoza (Spain). *Geomorphology*, 111(1–2): 88–103.

Lane, L.J., Hernandez, M. and Nichols, M. (1997) Processes controlling sediment yield from watershed as functions of spatial scale. *Environmental Modelling & Software,* 12(4): 355–369.

Latrubesse, E. M., Stevaux, J. C. and Sinha, R. (2005) Tropical rivers. *Geomorphology*, 70(3): 187-206.

Lawler, D.M. (1991) “Sediment and solute yield from the Jökulsá á Sólheimasandi glacierized river basin, southern Iceland.” In *Environmental Change in Iceland: Past and Present*. Maizels JK, Caseldine C (eds.), Dordrecht: Kluwer Academic Publishers, pp. 303 – 332.

Lawler, D.M. (2008) Advances in the continuous monitoring of erosion and deposition dynamics: Developments and applications of the new PEEP-3T system. *Geomorphology*, 93(1–2): 17–39.

Lawler, D.M. and Fairchild, I.J. (2010) New developments in process understanding and modelling in geomorphology: introduction and overview. *Earth Surface Processes and Landforms*, 35(10): 1247–1250.

Lawler, D.M., West, J.R., Couperthwaite, J.S. and Mitchell, S.B. (2001) Application of a novel automatic erosion and deposition monitoring system at a channel bank site on the Tidal River Trent, U.K. *Estuarine, Coastal and Shelf Science,* 53(2): 237–247.

LDD. (2000) *Soil loss map of Thailand*. Bangkok: Land Development Department, Ministry of Agriculture and Cooperatives.

Le Bissonnais, Y., Montier, C., Jamagne, M., Daroussin, J. and King, D. (2001) Mapping erosion risk for cultivated soil in France. *Catena*, 46(2–3): 207–220.

Le Gouée, P., Delahaye, D., Bermond, M., Marie, M., Douvinet, J. and Viel, V. (2010) SCALES: a large-scale assessment model of soil erosion hazard in Basee-Normandie (northern-western France). *Earth Surface Processes and Landforms*, 35(8): 887–901.

Lee, J.L., Phillips, D.L. and Dodson, R.F. (1996) Sensitivity of the US Corn Belt to climate change and elevated CO2: II Soil erosion and organic carbon. *Agricultural System,* 52(4): 503–521.

Lesschen, J.P., Kok, K., Verburg, P.H. and Cammeraat, L.H. (2007) Identification of vulnerable areas for gully erosion under different scenarios of land abandonment in Southeast Spain. *Catena*, 71(1): 110–121.

Li, Z., Liu, W.Z., Zhang, X.C. and Zheng, F.L. (2009). Impact of land use change and climate variability on hydrology in an agricultural catchment on the Loess Plateau of China. *Journal of Hydrology,* 377(1–2): 35–42.

Licciardello, F., Govers, G., Cerdan, O., Kirkby, M.J., Vacca, A. and Kwaad, F.J.P.M. (2009) Evaluation of the PESERA model in two contrasting environments. *Earth Surface Processes and Landforms*, 34(5): 629–640.

Lidén, R. (1999) A new approach for estimating suspended sediment yield. *Hydrology and Earth System Sciences*, 3(2): 285–294.

Lillesand, T.M. and Kiefer, R.W. (2002) *Remote sensing and image interpretation*. Fourth edition, New York: John Wiley & Sons.

Lim, K.J., Sagong, M., Engel, B.A., Tang, Z., Choi, J. and Kim, K. (2005) GIS-based sediment tool. *Catena*, 64(1): 61–80.

Lin, C.Y., Lin, W.T. and Chou, W.C. (2002) Soil erosion prediction and sediment yield estimation: the Taiwan experience. *Soil & Tillage Research,* 68(2): 143–152.

Lodhi, M.A., Rundquist, D.C., Han, L. and Kuzila, M.S. (1998) Estimation of suspended sediment concentration in water using integrated surface reflectance. *Geocarto International,* 13(2): 11–15.

Loebis, J. and Taryana, O. (1988) “Erosion-sedimentation study for reservoir siltation control.” In ASEAN-US Watershed Project (ed.), *Proceedings Seminar on Watershed Research and Management Practices.* Laguna, Philippines, pp. 133–142.

Lorsirirat, K. and Maita, H. (2006) “Soil erosion problems in Northeast Thailand: a case study from the view of agricultural development in a rural community near Khon Kaen.” In Marui, H. (ed.) *Disaster Mitigation of Debris Flows, Slope Failures and Landslides*. Niigata: University of Academy Press, pp. 675–686.

Lorz, C., Bukker, F., Fürst, C., Goldbach, A., Roig, L.H. and Makeschin, F. (2010) A planning support tool for sediment management – a case study from Central Brazil. *Landmod*, pp. 1–11.

Loughran, R.J., Campbell, B.L., Shelly, D.J. and Elliott, G.L. (1992) Developing a sediment budget for a small drainage basin in Australia. *Hydrological Processes*, 6(2): 145–158.

Lu, D., Li, G., Valladares, G.S. and Batistella, M. (2004) Mapping soil erosion risk in Rondonia, Brazilian Amazonia: using RUSLE, remote sensing and GIS. *Land Degradation & Development*, 15(5): 499–512.

Lu, H., Moran, C.J. and Prosser, I.P. (2006) Modelling sediment delivery ratio over the Murray Darling Basin. *Environmental Modelling and Software*, 21(9): 1297–1308.

Luk, S., diCenzo, P.D. and Liu, X.Z. (1997) Water and sediment yield from a small catchment in the hilly granitic region, South China. *Catena*, 29(2): 177–189.

Ma, Q., Yu, X., Fu, G. and Liu, Q. (2012) The changing relationship between spatial pattern of soil erosion risk and its influencing factors in Yimeng mountainous area, China 1986–2005. *Environmental Earth Sciences,* 66(5): 1535–1546.

Maeda, E.E., Pellikka, P.K.E., Siljander, M. and Clark, B.J.F. (2010) Potential impacts of agricultural expansion and climate change on soil erosion in the Eastern Arc Mountains of Kenya. *Geomorphology*, 123(3–4): 279–289.

Magellan (2013) *Magellan Tritron 2000.* [online]. Available from: http://www.magellangps.com/Store/Triton [Accessed 9 September 2013]

Maglinao, A.R., Agus, F., Ilao, R.O., Toan, T.D. and Penning De Vries, E., (2002) "Soil erosion management in catchment: indentifying best bet options with famers' participation." In *Proceedings of 12th International Soil Conservation Conference Beijing 2002*, pp. 374–380.

Mango, L.M., Melesse, A.M., McClain, M.E., Gann, D. and Setegn, S.G. (2011) Land use and climate change impacts on the hydrology of the upper Mara River Basin, Kenya: results of a modeling study to support better resource management. *Hydrology and Earth System Sciences*, 15(7): 2245–2258.

Mano, V., Nemery, J., Belleudy, P. and Poirel, A. (2009) Assessment of suspended sediment transport in four alpine watersheds (France): influence of the climatic regime. *Hydrological Processes,* 23(5): 777–792.

Manyatsi, A.M., Ntshangase, N. (2008) Mapping of soil erosion using remotely sensed data in Zombodze South, Swaziland*. Physics and Chemistry of the Earth*, 33(8–13): 800–806.

Mao, D., Zeng, Z., Wang, C. and Lin, W. (2007) "Regional assessment of soil erosion based on the multivariate membership model." In *Fourth International Conference on Fuzzy System and Knowledge Discovery Conference Publication IEEX (Volume: 1*). pp. 208-212 (Haikou, 24-27 August 2007).

Mapiam, P.P. and Sriwongsitanon, N. (2009) Estimation of the URBS model parameters for flood estimation of ungauged catchments in the upper Ping river basin, Thailand. *ScienceAsia*, 35(1): 49–56.

Märker, M., Angeli, L., Bottai, L., Costantini, R., Ferrari, R., Innocenti, L. and Siciliano, G. (2008) Assessment of land degradation susceptibility by scenario analysis: A case study in Southern Tuscany, Italy. *Geomorphology*, 99(1–2): 120–129.

Marquínez, J., Lastra, J. and García, P. (2003) Estimation models for precipitation in mountainous regions: the use of GIS and multivariate analysis. *Journal of hydrology*, 270(1): 1–11.

Martínez-Carreras, N., Soler, M., Hernández, E. and Gallart, F. (2007) Simulating badland erosion with KINEROS2 in a small Mediterranean mountain basin (Vallcebre, Eastern Pyrenees). *Catena,* 71(1): 145–154.

Martínez-Casasnovas, J.A. (2003) A spatial information technology approach for the mapping and quantification of gully erosion. *Catena*, 50(2–4): 293–308.

Marttila, H. and Kløve, B. (2010) Dynamic of erosion and suspended sediment transport from drained peatland forestry. *Journal of Hydrology,* 388(3–4): 414–425.

Mello, C. D., Viola, M. R., Beskow, S., and Norton, L. D. (2013) Multivariate models for annual rainfall erosivity in Brazil. *Geoderma*, 202: 88–102.

Merritt, W.S., Letcher, R.A., Jakeman, A.J., 2003. A review of erosion and sediment transport models. *Environmental Modelling & Software*, 18(8–9): 761–799.

Merritt, W.S., Yu, S.S., Jaiaree, S. and Nongharnpitak, N. (1999) "Soil erosion modelling in the Mae Pan subcatchment in Northern Thailand." In Oxley, L., Scrimgeour, F., Jakeman and MODSIM99, A.J. (eds.), *Proceedings International Congress on Modelling and Simulation,* University of Waikato New Zealand, Vol.3, pp. 871-876. (6–9 December 1999).

Meusburger, M., Konz, N., Schaub, M. and Alewell, C. (2010) Soil erosion modelled with USLE and PESERA using QuickBird derived vegetation parameters in an Alpine Catchment. *International Journal of Applied Earth Observation and Geoinformation*, 12(3): 208–215.

Meusburger, K., Steel, A., Panagos, P., Montanarella, L. and Alewell, C. (2012) Spatial and temporal variability of rainfall erosivity factor for Switzerland. *Hydrology and Earth System Sciences*, 16(1): 167-177.

Miller, G.T. (2006) *Environmental Science: Working with the Earth*. 11th ed. Belmont, CA: Thompson Brook/Cole.

Millward, A.A. and Mersey, J.E. (1999) Adapting the RUSLE to model soil erosion potential in a mountainous tropical watershed. *Catena,* 38(2): 109–129.

Mitasova, H., Brown, W.M. and Johnston, D.M. (2000) *Terrain Modeling and Soil Erosion Simulation: Final Report.* Geographic Modeling Systems Lab, University of Illinois at Urbana-Champaign.

Mitasova, H., Hofierka, J., Zlocha, M. and Iverson, L.R. (1996) Modelling topographic potential for erosion and deposition using GIS. *International Journal of Geographical Information Science,* 10(5): 629–641.

Montenegro, S. and Ragab, R. (2012) Impact of possible climate and land use changes in the semi arid regions: A case study from North Eastern Brazil. *Journal of Hydrology,* 434–435, pp. 55–68.

Morgan, R.P.C. (2001) A simple approach to loss prediction: A revised Morgan-Morgan-Finney model. *Catena,* 44(4): 305–322.

Morgan, P.R.C. (2005) Soil Erosion & Conservation., Third edition, Massachusetts: Blackwell Publishing.

Morgan, P.R.C. (2011) "Modelling development: A users perspective" In Morgan, R.P.C. and Nearing, M.A. (eds.) *Handbook of Erosion Modelling.* Chichester, West Sussex: Wiley-Blackwell, pp. 7–32.

Morgan, R.P.C. and Duzant, J.H. (2008) Modified MMF (Morgan-Morgan-Finney) model for evaluating effects of crops and vegetation cover on soil erosion. *Earth Surface Processes and Landforms*, 32(1): 90–106.

Morgan, R.P.C. and Nearing, M.A. (2011) *Handbook of Erosion Modelling.* Chichester, West Sussex: Wiley-Blackwell.

Morris, G.L. and Fan, J. (1998) *Reservoir Sedimentation Handbook*. New York: McGraw-Hill.

Muklislin, M. and Sukoco. (2011) Utilizing geographic information system for prediction of soil erosion in Sono Sagren catchment area. *American Journal of Engineering and Applied Sciences,* 4(2): 270–275.

Mulligan, M. and Wainwright, J. (2004) "Modelling and model building." In Wainwright, J. and Mulligan, M. (eds.) *Environmental Modelling: Finding Simplicity in Complexity.* London: John Wiley & Sons, Ltd., pp. 7–73.

Mutua, B.M., Klik, A. and Loiskandl, W. (2006) Modelling soil erosion and sediment yield at a catchment scale: The case of Masinga catchment, Kenya. *Land Degradation & Development*, 17(5): 557–570.

Nam, P.T., Yang, D., Kanae, S., Oki, T. and Musiake, K. (2003) Global soil loss estimate using RUSLE model: the use of global spatial datasets on estimating erosive parameters. *Geoinformatics*, 14(1): 49–53.

Nas, B., Ekercin, S., Karabörk, H., Berktay, A. and Mulla, D.J. (2010) An application of Landsat-5TM image data for water quality mapping in Lake Beysehir, Turkey. *Water, Air & Soil Pollution,* 212(1–4): 183–197.

Nearing, M.A. (1998) Why soil erosion models over-predict small soil losses and under-predict large soil losses. *Catana,* 32(1): 15–22.

Nearing, M.A. (2004) "Soil erosion and conservation." In Wainwright, J. and Mulligan, M. (eds.) *Environmental Modelling: Finding Simplicity in Complexity.* London: John Wiley & Sons, Ltd., pp. 277–290.

Nearing, M.A., Jetten, V., Baffaut, C., Cerdan, O., Couturier, A., Hernandez, M., Le Bissonnais, Y., Nichols, M.H., Nunes, J.P., Renschler, C.S., Souchère, V. and van Oost, K. (2005) Modelling response of soil erosion and runoff to changes in precipitation and cover. *Catena,* 61(2–3): 131–154.

Nekhay, O., Arriaza, M. and Boerboom, L. (2009) Evaluation of soil erosion risk using analytic network process and GIS: a case study from Spanish Mountain olive plantation. *Journal of Environmental Management*, 90(10): 3091–3104.

Nigel, R. and Rughooputh, S. (2010) Mapping of monthly soil erosion risk of mainland Mauritius and its aggregation with delineated basin. *Geomorphology*, 114(3): 101–114.

Notebaert, B., Verstraeten, G., Ward, P., Renssen, H. and Van Rompaey, A. (2011) Modelling the sensitivity of sediment and water runoff dynamics to Holocene climate and land use changes at the catchment scale. *Geomorphology,* 126(1–2): 18–31.

Nu-Fang, F., Zhi-Hua, S., Lu, L. and Chen, J. (2011) Rainfall, runoff, and suspended sediment delivery relationships in a small agricultural watershed of the Three Gorges area, China. *Geomorphology,* 135(1–2): 158–166.

Nunes, J.P. and Nearing, M.A. (2011) "Modelling impacts of climatic changes: Case studies using the new generation of erosion models." In Morgan,

R.P.C. and Nearing, M.A. (eds.) *Handbook of Erosion Modelling.* Chichester, West Sussex: Wiley-Blackwell, pp. 289–312.

Ogunlana, E.A., Noomhorm, A. and Silakul, T. (2010) Alley farming in Thailand. *Sustainability,* 2, 2523–2540.

Old, G.H., Lawler, D.M. and Snorrason, A. (2005) Discharge and suspended sediment dynamics during two jökulhlaups in the Skaftá river, Iceland. *Earth Surface Processes and Landforms*, 30(11): 1441–1460.

Oldeman, L.R., Hakkeling, R.T.A. and Sombroek, W.G. (1991) *World Map of the Status of Human Induced Soil Degradation.* Wageningen: ISRIC/UNEP.

Olive, R. J., and Rieger, W. A. (1992) "Stream suspended sediment transport monitoring: why, how, and what is being measured?" In Bogen, J., Walli, D. E., and Day, T. J. (eds.) *Erosion and Sediment Transport Monitoring Programmes in River Basins*, IHAS Publication No. 210: Wallingford, IHAS Press, pp. 245–254.

Ongsomwang, S. and Thinley, U. (2008) Spatial modeling for soil erosion assessment in Upper Lam Phra Phloeng Watershed, Nakhon Ratchasima, Thailand. *Suranaree Journal of Science Technology.* 16(3): 253–262.

Onyando, J.O., Kisoyan, P., Chemelil, M.C. (2005) Estimation of potential soil erosion for River Perkerra catchment in Kenya. *Water Resources Management*, 19(2): 133–143.

Osturk, F. (1996) "Suspended sediment yields of rivers in Turkey." In Walling, D.E. and Webb, B.W. (eds.) *Erosion and Sediment Yield: Global and Regional Perspectives*. IAHS Publ. no. 236, pp. 65–71 (Proceedings of the Exeter Symposium July 1996).

Ouyang, D. and Bartholic, J. (1997) "Predicting sediment delivery ratio in Saginaw Bay watershed." In *Proceedings of the 22nd National Association of Environmental Professionals Conference,* Orlando FL. pp. 659–671 (May 1997).

Palm, C.A., Vosti, S.A., Sanchez, P.A. and Ericksen, P.J. (2005) *Slash-and-Burn Agriculture: The search for Alternatives.* New York: Columbia University Press.

Pandey, A., Mathur, A., Mishra, S.K. and Mal, B.C. (2009) Soil erosion modelling of a Himalayan watershed using RS and GIS. *Environmental Earth Sciences,* 59(2): 399–410.

Paningbatan, E.P., Ciesiolka, C.A., Coughlan, K.J. and Rose, C.W. (1995) Alley cropping for managing soil erosion of hilly lands in the Philippines. *Soil Technology,* 8(3): 193–204.

Parsons, A.J., Wainwright, J., Brazier, R.E. and Powell, D.M. (2006) Is sediment delivery a fallacy? *Earth Surface Processes and Landforms*, 31(10): 1325–1328.

Parsons, A.J., Wainwright, J., Brazier, R.E. and Powell, D.M. (2008) Is sediment delivery a fallacy? Reply. *Earth Surface Processes and Landforms*, 33(10): 1630–1631.

Pahlman, C. (1991) Soil erosion? That's not how we see the problem! *ILEIA Newsletter,* 7(1/2): 24–26.

Panomtarinichigul, M. (2006) "Research on sustainable hill farming in Northern Thailand." In *International Conference on Challenges to Interdisciplinary Collaborative Research.* Institute of Ethnology, Academia Sinica, Taipei, Taiwan.

Patriche, C.V., Capatana, V. and Stoica, D.L. (2006) Aspects regarding soil erosion spatial modelling using the USLE/RUSLE within GIS. *Geographia Technica,* No. 2, pp. 88–97.

Pelacani, S., Märker, M. and Rodolfi, G. (2008) Simulation of soil erosion and deposition in a changing land use: A modelling approach to implement the support practice factor. *Geomorphology,* 99(1–4): 329–340.

Perumal, K. and Bhaskaran, R. (2010. Supervised classification performance of multispectral images. *Journal of Computing,* 2(2): 124–129.

Picouet, C., Hingray, B. and Olivry, J.C. (2001) Empirical and conceptual modelling of the suspended sediment dynamics in a large tropical African river: the Upper Niger River basin. *Journal of Hydrology*, 250 (1–4): 19–39.

Pimentel, D. (1993) *World Soil Erosion and Conservation.* Cambridge: Cambridge University Press.

Pimentel, D. (2006) Soil erosion: A food and environmental threat. *Environmental, Development and Sustainability,* 8(1): 119–137.

Pistocchi, A. (2008) An assessment of soil erosion and freshwater suspended solid estimates for continental-scale environmental modelling. *Hydrological Processes.* 22(13): 2292–2314.

Poesen, J., Nachtergaele, J., Verstraeten, G. and Valentin, C. (2003) Gully erosion and environmental change: importance and research needs. *Catena*, 50(2-4): 91–133.

Polyakov, V.O. and Nearing, M.A. (2003) Sediment transport in rill flow under deposition and detachment conditions. *Catena,* 51(1): 33–43.

Pongsai, S., Schmidt Vogt, D., Shrestha, R.P., Clemente, R.S., and Eiumnoh, A. (2010) Calibration and validation of the Modified Universal Soil Loss Equation for estimating sediment yield on sloping plots: A case study in Khun Satan catchment of Northern Thailand. *Canadian Journal of Soil Science,* 90(4): 585–596.

Porterfield, G. (1972) *Computation of fluvial-sediment discharge*. US Government Printing Office.

Prabhakar, S.V.R.K. (2011) “Climate change impacts in Japan and Southeast Asia: Implications for crop adaptation.” In Yadav, S.S., Redden, R., Hatfield, J.L., Lotze-Campen, H. and Hall, A.J.W. (eds.) *Crop Adaptation to Climate Change.* Chichester, West Sussex: John Wiley & Sons, pp. 131–142.

Prasannakumar, V., Shiny, R., Geetha, N. and Vijith, H. (2011) Spatial prediction of soil erosion risk by remote sensing, GIS and RUSLE approach: a case study of Siruvani river watershed in Attapady valley, Kerala, India. *Environmental Earth Sciences*, 64(4): 965-972.

Prasannakumar, V., Vijith, H., Abinod, S., and Geetha, N. (2012) Estimation of soil erosion risk within a small mountainous sub-watershed in Kerala, India, using Revised Universal Soil Loss Equation (RUSLE) and geo-information technology. *Geoscience Frontiers*, 3(2): 209–215.

Prosser, I.P. and Rustomji, P. (2000) Sediment transport capacity relations for overland flow. *Progress in Physical Geography*, 24(2): 179–193.

Quinton, J.N., Krueger, T., Freer, J., Brazier, R.E. and Bilotta, G.S. (2011) “A case study of uncertainty: Applying GLUE to EUROSEM.” In Morgan, R.P.C. and Nearing, M.A. (eds.) *Handbook of Erosion Modelling.* Chichester, West Sussex: Wiley-Blackwell, pp. 80–97.

Rahman, M. M., Csaplovics, E., Koch, B. and Köhl, M. (2004) “Interpretation of tropical vegetation using Landsat ETM+ imagery.” In Altan, M.O. (ed.) *International Archives of the Photogrammetry, Remote Sensing and Spatial Information Sciences*, Vol. XXXV, Part B-YF, Istanbul, pp. 157–162.

Rahman, Md.R., Shi, Z.H. and Chongfa, C. (2009) Soil erosion hazard evaluation-an integrated use of remote sensing, GIS and statistical approaches with biophysical parameters toward. *Ecological Modelling*, 220(13-14): 1724–1734.

Ramussen, T.J., Ziegler, A.C., Ramussen, P.P. and Stiles, T.C. (2006) The value of continuous turbidity monitoring in TMDL programs. In: *Proceedings of the Eighth Federal Interagency Sedimentation Conference (8thFISC), April2-6, 2006,* Reno, NV, USA: JFIC, pp. 840–847.

Ranzi, R., Le, T.H. and Rulli, M.C. (2012) A RUSLE approach to model suspended sediment load in the Lo River (Vietnam): Effects of reservoirs and land use changes. *Journal of Hydrology*, 422–423, pp. 17–29.

Recha, J., Kapukha, M., Wekesa, A., Shames, S. and Heiner, K. (2014) *Sustainable Agriculture Land Management Practices for Climate Change Mitigation: A training guide for smallholder farmers.* Washington, DC: EcoAgriculture Partners.

Reda A.G., Tripathi, N.K., Soni, P., Tipdecho, T. and Phalke, A. (2013) Temporal climate trend of Ping Basin of Thailand and implications for Mekong Region. Journal of Earth Science Climatic Change, 4(4): 146.

Renard, K. G., Foster, G. R., Weesies, G. A., McCool, D. K. and Yoder, D. C. (1997). *Predicting Soil Erosion by Water: a Guide to Conservation Planning with the Revised Universal Soil Loss Equation (RUSLE).* Agriculture Handbook Number 703, Washington, DC: US Department of Agriculture.

Renard, K.G., Yoder, D.C., Lightle, D.T. and Dabney, S.M. (2011) “Universal soil loss equation and revised universal soil loss equation.” In Morgan, R.P.C. and Nearing, M.A. (eds.) *Handbook of Erosion Modelling.* Chichester, West Sussex: Wiley-Blackwell, pp. 137–167.

Renschler, C.S. and Harbor, J. (2002) Soil erosion assessment tools from point to regional scale-the role of geomorphologist in land management research and implementation. *Geomorphology*, 47(2–4): 189–209.

Rerkasem, B. and Rerkasem, K. (1995) The Mae Sa-Kog Ma biosphere reserves (Thailand). *Working Paper N°3*, Paris: UNESCO.

Rhodes, B.P., Conejo, R., Benchwan, T., Titus, S. and Lawson, R. (2005) Paleocurrents and provenance of the Mae Rim Formation, Northern Thailand: implications for tectonic evolution of the Chiang Mai basin. *Journal of the Geological Society*, 162(1): 51–63.

Richards, J.A., Jia, X. (2006) *Remote sensing digital image analysis: An introduction.* Forth edition, Germany: Springer-Verlag Berlin Heidenberg.

Ricker, M.C., Odhiambo, B.K. and Church, J.M. (2008) Spatial analysis of soil erosion and sediment fluxes: a paired watershed study of two Rappahannock River tributaries, Stafford County, Virginia. *Environmental Management*, 41(5): 766–778.

Rijsdijk, A., (Sampurno) Bruijnzeel, L.A. and Prins, Th.M. (2007) Sediment yield from gullies, riparian mass wasting and bank erosion in the Upper Konto catchment, East Java, Indonesia. *Geomorphology,* 87(1–2): 38–52.

Risse, L.M., Nearing, M.A., Nicks, A.D., Laflen, J.M. (1993) Error assessment in the universal soil loss equation. *Soil Science Society of America Journal*, 57(3): 825–833.

Rode, C.W. and Fredo, H.G. (1999) Testing AGNPS for soil erosion and water quality modelling in agricultural catchments in Hesse (Germany). *Physics and Chemistry of the Earth (B)*, 24(4): 297–301.

Rodriguez, JL.G. and Suárez, MC.G. (2010) Historical review of topographical factor, LS, of water erosion models. *Aqua-LAC*, 2(2): 56–61.

Rogerson, P.A. (2006) *Statistical Methods for Geography: a Student’s Guide*. 2nd edition, London: SAGE.

Romero, M.E.R. (2001) *Modelling the Hydrological Sensitivity to Land Use Change in a Tropical Mountainous Environment*. PhD thesis, Department of Geography, King's College London.

Rooseboom, A. (1992) *Sediment Transport in Rivers and Reservoirs: a South African perspective*. Stellenbosch: Sigma Beta Consulting Engineers.

Roper, L.D. (2011) *Precipitation Rate versus Latitude and Longitude.* [online]. Available from: http://www.roperld.com/science/PrecipLatitude_Longitude.htm [Accessed 20 June 2014]

Royal Irrigation Department (2011) *Monthly and Annual Suspended Sediment in Main River Basins of Thailand*. Chiang Mai: Sediment and Water Quality Group, Royal Irrigation Department (RID) of Thailand.

Royall, D. (2007) A comparison of mineral-magnetic and distributed RUSLE modeling in the assessment of soil loss on a southeastern U.S. cropland. *Catena*, 69(2): 170–180.

RSAC (2013) *What is Remote Sensing?* [online]. Available from: http://www.rsacl.co.uk/rs.html [Accessed 6 September 2013]

Russell, M.A., Walling, D.E. and Hodgkinson, R.A. (2001) Suspended sediment sources in two small lowland agricultural catchments in the UK. *Journal of Hydrology,* 252(1–4): 1–24.

Sadalmelik, I (2007) *The Topographic map of Thailand* [online]. Available from: http://commons.wikimedia.org/wiki/User:Sadalmelik [Accessed 6 September 2013].

Sakurai, K., Kozasa, S., Yuasa, T., Puriyakorn, B., Preechapanya, P., Tanpibal, V., Muangnil, K. and Prachaiyo, B. (1996) Changes in soil properties after land degradation associated with various human activities in Thailand. *Soil science and plant nutrition*, *42*(1): 81-92.

Sang-Arun, J., Mihara, M., Horaguchi, Y. and Yamaji, E. (2006) Soil erosion and participatory remediation strategy for bench terraces in northern Thailand. *Catena,* 65(3): 258–264.

Sangchyoswat, C. (1998) *Geographical Analysis of Landscape in the Wat Chan Watershed, Northern Thailand*. PhD Thesis, University of Hawaii.

Schiettecatte, W., D'hondt, L., Cornelis, W.M., Acosta, M.L., Leal, Z., Lauwers, N., Almoza, Y., Alonso, G.R., Díaz, J., Ruíz, M. and Gabriels, D. (2008) Influence of landuse on soil erosion risk in the Cuyaguateje watershed (Cuba). *Catena,* 74(1): 1–12.

Schmitt, L.K. (2007) Developing and applying a soil erosion model in a data-poor context to an island in the rural Philippines. *Environment, Development and Sustainable*, 11(1): 19–42.

Schumm, S.A. (2005) *River Variability and Complexity.* Cambridge: Cambridge University Press.

Scoccimarro, M., Walker, A., Dietrich, C., Schreider, S., Jakeman, T. and Ross, H. (1999) A framework for integrated catchment assessment in northern Thailand. *Environmental Modelling & Software*, 14(6): 567–577.

Sepaskhah, A. R. and Panahi, J. (2007) Estimating storm erosion index in IR Iran. *Iranian Journal of Science and Technology*, 31(B2): 237–248.

Shalaby, A. and Tateishi, R. (2007) Remote sensing and GIS for mapping and monitoring land cover and land-use changes in the Northwestern coastal zone of Egypt. *Applied Geography,* 27(1): 28–41.

Shamshad, A., Azhari, M.N., Isa, M.H., Wan Hussin, W.M.A. and Parida, B.P. (2008) Development of an appropriate for estimation of RUSLE EI_{30} index and preparation of erosivity maps for Palue Penang in Peninsular Malaysia. *Catena*, 72(3): 423–432.

Shen, Z.Y., Gong, Y.W., Li, Y.H., Hong, Q., Xu, L. and Liu, R.M. (2009) A comparison of WEPP and SWAT modelling soil erosion of the Zhangjiachong Watershed in the Three Gorges Reservoir Area. *Agricultural Water Management,* 98(10): 1435–1442.

Shi, Z.H., Cai, C.F., Ding, S.W., Wang, T.W. and Chow, T.L. (2004) Soil conservation planning at the small watershed level using RUSLE with GIS: a case study in the three Gorge Area of China. *Catena*, 55(1): 33–48.

Sidle, R.C., Ziegler, A.D., Negrishi, J.N., Nik, A.R., Siew, R. and Turkelboom, F. (2006) Erosion processes in steep terrain—Truths, myths, and uncertainties related to forest management in Southeast Asia. *Forest Ecology and Management,* 224(1–2): 199–225.

Sidorchuk, A. (2009) A third generation erosion model: the combination of probabilistic and deterministic components. *Geomorphology*, 110(1–2): 2–10.

Sim, J. and Wright, C.C. (2013) The Kappa statistic in reliability studies: uses, interpretation, and sample size requirements. *Physical Therapy,* 85(3): 257–268.

Sivakumar, B. and Wallender, W.W. (2005) Predictability of river flow and suspended sediment transport in the Mississippi River basin: a non-linear deterministic approach. *Earth Surface Processes and Landforms*, 30(6): 665–677.

Slaymaker, O. (1996) *Geomorphic Hazard*. Chichester: John Wiley & Sons.

Smith, H.G. (2008) Estimation of suspended sediment loads and delivery in an incised upland headwater catchment, south-eastern Australia. *Hydrological Processes*, 22(16): 3135–3148.

Smith, R.E., Quinton, J., Goodrich, D.C. and Nearing, M. (2010) Soil-erosion models: where do we really stand? Short communication (discussion) on the papers by Wainwright *et al.* (2008a, b, c). *Earth Surface Processes and Landforms*, *35*(11): 1344–1348.

Smith, S.J., Williams, J.R., Menzel, R.G., and Coleman, G.A. (1984) Prediction of sediment yield from Southern Plains Grasslands with the modified universal soil loss equation. *Journal of Range Management*, 37(4): 295–297.

Song, Y., Liu, L., Yan, P. and Cao, T. (2005) A review of soil erodibility in water and wind erosion research. *Journal of Geographical Sciences*, 15(2): 167–176.

Sonneveld, B.G.J.S. and Dent, D.L. (2009) How good is GLASOD? *Journal of Environmental Management,* 90(1): 274–283.

Sonneveld, B.G.J.S., Keyzer, M.A. and Stroonijder, L. (2011) Evaluating quantitative and qualitative models: An application for nationwide water erosion assessment in Ethiopia. *Environmental Modelling & Software,* 26(10): 1161–1170.

Srimongkol, K. and Marten, G.G. (1986). “Traditional agriculture in Northern Thailand.” In Marten, G.G. (ed.) *Traditional Agriculture in Southeast Asia: A Human Ecology Perspective*. Boulder, Colorado: Westview Press, pp. 85–102.

Suraswadi, P., Thomas, D.E., Pragtong, K, Preechapanya, P. and Weyerhaeuser, H. (2005) “Northern Thailand: Changing smallholder land use patterns.” In Palm, C.A., Vosti, S.A., Sanchez, P.A. and Ericksen, P.J. (eds.) *Slash-and-Burn Agriculture: The search for Alternatives.* New York: Columbia University Press, pp. 355–384.

Syvitski, J.P.M., Vorosmarty, C.J., Kettner, A.J. and Green, P. (2005) Impacts of humans on the flux of terrestrial sediment to the global coastal ocean. *Sciences*, 308(5720): 376–380.

Tameazyan, G.P. (1989) Global peculiarities and tendencies in river discharge and wash-down of the suspended sediments – the earth as a whole. *Journal of Hydrology,* 107(1–4): 113–131.

Thanapakpawin, P., Richey, J., Thomas, D., Rodda, S., Campbell, B. and Logsdon, M. (2006) Effects of landuse change on the hydrologic regime of the Mae Chaem river basin, NW Thailand. *Journal of Hydrology,* 334(1–2): 215–230.

Tangestani, M.H. (2006) Comparison of EPM and PSIAC models in GIS for erosion and sediment yield assessment in a semi-arid environment: Afzar Catchment, Fars Province, Iran. *Journal of Asian Earth Sciences*, 27(5): 585–597.

Tangtham, N. (2002) *Mathematical Models of Soil Erosion and Sediment Pollution in Watershed.* Bangkok: Faculty of Forestry, Kasetsart University.

Terranova, O., Antronico, L., Coscarelli, R. and Iaquinta, P. (2009) Soil erosion risk scenario in the Mediterranean environment using RUSLE and GIS: an application model for Calabria (Southern Italy). *Geomorphology,* 112(3–4): 228–245.

Thompson, G.R. and Turk, J. (2007) *Earth Science and the Environmnent.* 4th edition, Belmont, USA: Thompson Brooks/Cole.

Thothong, W., Huon, S., Janeau, J.L., Boonsaner, A., de Rouw, A., Planchon, O., Bardoux, G. and Parkpian, P. (2011) Impact of land use change and rainfall on sediment and carbon accumulation in a water reservoir of North Thailand. *Agriculture, Ecosystems and Environment,* 140(3–4): 521–533.

Tingting, L.V., Xiaoyu, S., Dandan, Z., Zhenshan, X., and Jianming, G. (2008) Assessment of soil erosion risk in northern Thailand. *The International Achieves of the Photogrammetry, Remote Sensing and Spatial Information Sciences,* Vol. XXXVIII (88): 703–708.

Tiwari, A.K., Risse, L.M., and Nearing, M. (2000) Evaluation of WEPP and its comparison with USLE and RUSLE. *Transaction of the American Society of Agricultural Engineers,* 43(5): 1129–1135.

TMD (2011) *Rainfall and Severe Flooding over Thailand in 2011*. Available from: http://www.tmd.go.th/en/vent/flood_in_2011.pdf. [Accessed 16 March 2013]

Trabucchi, M., Puente, C., Comin, F. A., Olague, G. and Smith, S. V. (2012) Mapping erosion risk at the basin scale in a Mediterranean environment with opencast coal mines to target restoration actions. *Regional Environmental Change*, 12(4): 675–687.

Tudsri, S. and Kaewkunya, C. (2002) Effect of leucaena row spacing and cutting intensity on the growth of leucaena and three associated grasses in Thailand. *Asian Australasian Journal of Animal Sciences*, 15(7): 986–991.

Turkelboom, F., Poesen, J. and Trébuil G. (2008) The multiple land degradation effects caused by land-use intensification in tropical steeplands: a catchment study from Northern Thailand. *Catena,* 75(1): 102–116.

United Nations Disaster Relief Co-ordinator (UNDRO) (1982) *Natural Disasters and Vulnerability Analysis*. Geneva: Report of Export Group Meeting.

Valentin, C., Agus, F., Alamban, R., Boosaner, A., Bricquet, J. P., Chaplot, de Guzman, T., de Rouw, A., Janeau, J.L., Orange, D., Phachomphonh, K., Phai, D.D., Podwojewski, P., Ribolzi, O., Silvera, N., Subagyono, K., Thiébaux, J.P., Toan, T.D. and Vadari, T. (2008). Runoff and sediment losses from 27 upland catchments in Southeast Asia: Impact of rapid land use changes and conservation practices. *Agriculture, Ecosystems and Environment*, 128(4): 225–238.

Valentin, C., Poesen, J. and Li, Y. (2005) Gully erosion: impacts, factors and control. *Catena,* 63(2–3): 132–153.

Van Rompaey, A., Bazzoffi, P., Jones, R.J.A. and Montanarella, L. (2005) Modeling sediment yields in Italian catchments. *Geomorphology*, 65(1–2): 157–169.

Van Rompaey, A.J.J., Verstraeten, G., Van Oost, K., Govers, G. and Poesen, J. (2001) Modelling mean annual sediment yield using a distributed approach. *Earth Surface Processes and Landforms,* 26(11): 1221–1236.

Verburg, P.H., Overmars, K.P., Huigen, M.G.A., de Groot, W.T. and Veldkamp, A. (2006) Analysis of the effects of land use change on protected areas in the Philippines. *Applied Geography,* 26(2): 153–173.

Vemu, S. and Pinnamaneni, U.B. (2011). Estimation of spatial patterns of soil erosion using remote sensing and GIS: a case study of Indravati catchment. *Natural Hazards,* 59(3): 1299–1315.

Verstraeten, G., Poesen, J., De Vente, J. and Koninckx, X. (2003) Sediment yield variability in Spain: a quantitative and semiqualitative analysis using reservoir sedimentation rates. *Geomorphology*, 50(4): 327–348.

Verstraeten, G., Prosser, I.P. and Fogarty, P. (2007) Prediction the spatial patterns of hillslope sediment delivery to river channels in the Murrumbidgee catchment, Australia. *Journal of Hydrology*, 334(3–4): 440–454.

Vigiak, O., Okoba, B.O., Sterk, G. and Groenenberg, S. (2005) Modelling catchment-scale erosion pattern in the African Highland. *Earth Surface Processes and Landforms*, 30(2): 183–196.

Vrieling, A. (2006) Satellite remote sensing for water erosion assessment: a review. *Catena*, 65(1): 2–18.

Wainwright, J. (2008) Can modelling enable us to understand the rôle of humans in landscape evolution? *Geoforum,* 39(2): 659–674.

Wainwright, J. and Millington, J.D.A. (2010) Mind, the gap in landscape-evolution modelling. *Earth Surface Processes and Landforms,* 35(7): 842–855.

Wainwright, J., Mathys, N. and Esteves, M. (2006) Gully erosion in mountain areas: processes, measurement, modelling and regionalization. *Earth Surface Processes and Landforms,* 31(2): 133–134.

Wainwright, J., Parsons, A. J., Müller, E. N., Brazier, R. E., and Powell, D. M. (2010) Standing proud: a response to 'Soil-erosion models: where do we really stand?' by Smith et al. *Earth Surface Processes and Landforms*, 35(11): 1349–1356.

Walford, N. (2011) *Practical Statistics for Geographers and Earth Scientists.* Chichester, West Sussex: Wiley-blackwell.

Walker, A. (2003) Agricultural transformation and the politics of hydrology in Northern Thailand. *Development and Change*, 34(5): 941–964.

Walker, J.P. and Willgoose, G.R. (1999) On the effect of digital elevation model accuracy on hydrology and geomorphology. *Water Resources Research*, 35(7): 2259–2268.

Walling, D.E. (1977) Assessing the accuracy of suspended sediment rating curves for a small basin. *Water Resources Research*, 13(3): 531–538.

Walling, D.E. (1983) The sediment delivery problem. *Journal of Hydrology*, 65, pp. 209–237.

Walling, D.E. (1984). The sediment yields of African rivers. *IAHS-AISH publication 144*, 265–283.

Walling, D.E. (2005) Tracing suspended sediment sources in catchments and river system. *Science of the Total Environment,* 344(1–3): 159–184.

Walling, D.E. and Fang, D. (2003) Recent trends in the suspended sediment loads of the world's rivers. *Global and Planetary Change*, 39(1–2): 111–126.

Walling, D.E. and Webb, B.W. (1981) The reliability of suspended sediment load data. In: *Proceeding of the Florence Symposium, June 1981.* IAHS Publ. no. 133*,* pp. 177–194.

Walling, D.E. and Webb, B.W. (1996) *Erosion and Sediment Yield: Global and Regional Perspectives*. Exeter: IAHS Publication no. 236.

Walling, D.E., He, Q. and Whelan, P.A. (2003) Using ^{137}Cs measurement to validate the application of the AGNPS and ANSWERS erosion and sediment yield models in two small Devon catchments. *Soil and Tillage Research,* 69(1–2): 27–43.

Wang, G., Gertner, G., Liu, X. and Anderson, A. (2001) Uncertainty assessment of soil erodibility factor for revised universal soil loss equation. *Catena,* 46(1): 1–14.

Wang, X., Zheng, D. and Shen, Y. (2008) Land use change and its driving forces on the Tibetan Plateau during 1990-2000. *Catena,* 72(1): 55–66.

Wangpakapattanawong, P., Kavinchan, N., Vaidhayakarn, C., Schmidt-Vogt, D. and Elliott, S. (2010) Fallow to forest: Applying indigenous and scientific knowledge of swidden cultivation to tropical forest restoration. *Forest Ecology and Management,* 260(8): 1399–1406.

Ward, P.J. (2008) River Meuse suspended sediment yield: a new estimate and past estimates revisited. *Netherlands Journal of Geosciences*, 87(2): 189–193.

Ward, P.J., Van Balen, R.T., Verstraeten, G., Renssen, H. and Vandenberghe, J. (2009) The impact of land use change and climate change on late Holocene and future suspended sediment yield of the Meuse catchment. *Geomorphology,* 103(3): 389–400.

Warren, S.D., Mitasova, H., Hohmann, M.G., Landsberger, S., Iskander, F.Y., Ruzycki, T.S. and Senseman, G.M. (2005) Validation of 3-D enhancement of the Universal Soil Loss Equation for prediction of soil erosion and sediment deposition. *Catena*, 64(2–3): 281–296.

Wei, W., Chen, L. and Fu, B. (2009) Effects of rainfall change on water erosion processes in terrestrial ecosystems: a review. *Progress in Physical Geography,* 33(3): 307–318.

Weltzin, J. F., Loik, M. E., Schwinning, S., Williams, D. G., Fay, P. A., Haddad, B. M., Harte, J., Huxman, T.E., Knapp, A.K., Lin, G., Pockman, W.T., Shaw, M.R., Small, E.E., Smith, M.D., Smith, S.D., Tissue, D.T. and Zak, J. C. (2003) Assessing the response of terrestrial ecosystems to potential changes in precipitation. *Bioscience*, 53(10): 941–952.

West, T.S. (1996) "Approximate dynamic model sensitivity for large, complex space structures." In *MSC 1996 World Users' Conference Proceedings,* pp. 1–20.

Weyerhäuser, H. (2001) *Potential of Semi-Natural Management of Deciduous Forests in Thailand.* Deutsche Gesellschaft für, Eschborn: Tropical Forest Research.

White, S. (2005) Sediment yield prediction and modelling. *Hydrological Processes*, 19(15): 3053–3057.

Wichitkosum, S. (2012) Impacts of land use changes on soil erosion in Pa Deng sub-district, adjacent area of Kaeng Krachan National Park, Thailand. *Soil and Water Research,* 7(1): 10–17.

Wijesekara, N.T.S. and Samarakoon, L. (2001) Extraction of parameters and modelling soil erosion using GIS in a grid environment. *The 22nd Asian Conference in Remote Sensing*, National University of Singapore, 5–9 November, 2001, pp. 34–39.

Wilkie, D.S. and Finn, J.T. (1996) *Remote Sensing Imagery for Natural Resources Monitoring*. New York: Columbia University Press.

Wilkinson, S.N., Prosser, I.P., Rustomji, P. and Read, A.M. (2009) Modelling and testing spatially distributed sediment budgets to relate erosion processes to sediment yields. *Environmental Modelling & Software,* 24(4): 489–501.

Williams, J.R., Renard, K.G. and Dyke, P.T. (1983) EPIC: A new method for assessing erosion's effect on soil productivity. *Journal of Soil and Water Conservation*, 38(5): 381–383.

Wischmeier, W.H. and Smith, D.D. (1978) *Predicting Rainfall-Erosion Loss: Agricultural Research Service Handbook No. 282*, Washington, D.C., USDA, 48 p.

WMO (2012) *Technical Material for Water Resources Assessment*. Geneva: World Meteorological Organization.

Wood, S.H. and Ziegler, A.D. (2008) Floodplain sediment from a 100-year-recurrence flood in 2005 of the Ping River in northern Thailand. *Hydrology and Earth System Sciences*, 12(4): 959–973.

Xu, Y., Shou, X., Kong, X., Peng, J. and Cai, Y. (2008) Adapting the RUSLE and GIS to model soil erosion risk in a mountains karst watershed, Guizhou Province, China. *Environmental Monitoring and Assessment,* 141(1–3): 275–286.

Yang, W., Kanae, S., Oki, T., Koike, T. and Musiake, K. (2003) Global potential soil erosion with reference to land use and climate changes. *Hydrological Processes,* 17(14): 2913–2928.

Yotapakdee, T. and Havrland, B. (2012) The impact assessment of water resource management in rainfed area in the Upper Ping River Basin, Chiang Mai, Thailand. *International Journal of Environmental Science and Development*, 3(2): 99–102.

Young, A. (1989) *Agroforestry for Soil Conservation.* Wallington, UK: CAB International.

Young, R.A., Onstad, C.A., Borsch, D.D. and Anderson, W.P. (1989) AGNPS: a nonpoint-source pollution model for evaluating agricultural watersheds. *Journal of Soil and Water Conservation,* 44(2): 168–173.

Yue-Qing, X., Xiao-Mei, S., Xiang-Bin, K., Jian, P. and Yun-Long, C. (2008) Adapting the RUSLE and GIS to model soil erosion risk in a mountains karst watershed, Guizhou Province, China. *Environmental Monitoring and Assessment,* 141(1–3): 275–286.

Zhang, C. (2007) *Fundamentals of Environmental Sampling and Analysis*. New Jersey: John Wiley & Sons, Inc.

Zhang, X.C. and Nearing, M.A. (2005) Impact of climate change on soil erosion, runoff, and wheat productivity in central Oklahoma. *Catena,* 61(2–3): 185–195.

Zhang, X.C., Liu, W.Z., Li, Z. and Zheng, F.L. (2009) Simulating site-specific impacts of climate change on soil erosion and surface hydrology in southern Loess Plateau of China. *Catena,* 79(3): 237–242.

Zhou, P. (2008) Landscape-scale soil erosion modelling and ecological restoration for a mountainous watershed in Sichuan, China. *Tropical Forestry Reports 35*, University of Helsinki.

Zhou, P., Luukkanen, O., Tokola, T. and Nieminen, J. (2008) Effect of vegetation cover on soil erosion in the mountainous watershed. *Catena*, 75(3): 319–325.

Ziegler, A.D., Giambelluca, T.W., Sutherland, R.A., Nullet, M.A., Yanasarn, S., Pinthong, J., Preechapanya, P. and Jaiaree, S. (2004) Toward understanding the cumulative impacts of roads in upland agricultural watersheds of northern Thailand. *Agriculture, Ecosystems & Environment,* 104(1): 145–158.

Ziegler, A.D., Sutherland, R.A. and Giambelluca, T.W. (2000) Runoff generation and sediment production on unpaved roads, footpaths and agricultural land surfaces in northern Thailand. *Earth Surface Processes and Landforms*, 25(5): 519–534.

Ziegler, A.D., Sutherland, R.A. and Giambelluca, T.W. (2001) Acceleration of Horton overland flow and erosion by footpaths in an upland agricultural watershed in northern Thailand. *Geomorphology*, 41(4): 249–262.

Ziegler, A.D., Thilde, B.B., Guardiola-Claramonte, M., Giambelluca, T.W., Lawrence, D. and Lam, N.T. (2009) Environmental consequences of the demise in swidden cultivation in Montane Mainland Southeast Asia: Hydrology and geomorphology. *Human Ecology,* 37(3): 361–373.

Ziegler, A.D., Xi, L.X. and Tantasarin, C. (2011) “Sediment load monitoring in the Mae Sa catchment in northern Thailand.” In *Sediment Problems and Sediment Management in Asian River Basins*, IAHS Publ. 349, pp. 86–91 (Proceedings of the Workshop held at Hyderabad, India, September 2009).